UNIVERSITY OF PALERMO
PHD JOINT PROGRAM:
UNIVERSITY OF CATANIA - UNIVERSITY OF MESSINA
XXXIV CYCLE

DOCTORAL THESIS

Stationary, Oscillatory, Spatio-Temporal Patterns and Existence of Global Solutions in Reaction-Diffusion Models of Three Species

Author:
Faezeh FARIVAR

Supervisor:
Prof. Marco SAMMARTINO

Co-Supervisor:
Prof. Gaetana Gambino

A thesis submitted in fulfillment of the requirements for the degree of Doctor of Philosophy

in

Mathematics and Computational Sciences

February 5, 2023

Signed:

Date:

"Maryam Mirzakhani"

"The beauty of mathematics only shows itself to more patient followers."

UNIVERSITY OF PALERMO

Abstract

Department of Mathematics and Computer Sciences

Doctor of Philosophy

Stationary, Oscillatory, Spatio-Temporal Patterns and Existence of Global Solutions in Reaction-Diffusion Models of Three Species

by Faezeh FARIVAR

The goal of my Ph.D. research is to analyze three species models in order to describe the behavior of an ecological community. In particular, two reaction-diffusion systems describing different local interactions between three species have been considered to obtain species coexistence, diversity, and distribution patterns. The first analyzed model describes intraguild predation: there are an IG-predator species, an IG-prey species, and a common resource species, which is shared by both of them. The IGP interaction is of Lotka-Volterra type, coupled with nonlinear diffusion, since we assume that the IG-prey moves towards lower density areas of the IG-predator. In this model, the extinction of species has been surveyed. Performing the linear stability analysis in the neighborhood of the coexistence point, the conditions for the occurrence of Hopf instability have been established. Cross-diffusion is able to induce Turing instability for this system, which would not admit this bifurcation in presence of only classical diffusion terms. Moreover, the effect of each parameter on Turing and Turing-Hopf instability has been detected. Numerical solutions of the system have been computed using spectral method, showing the rich dynamics of the model, including the Turing pattern, time oscillation pattern, Turing-Hopf pattern, and chaotic behavior. The weakly nonlinear analysis also has been employed to predict the amplitude of patterned solutions have been compared with numerical spectral solutions of the reaction-diffusion system. Furthermore, we have used multiscale methods to determine normal form of the model around Turing-Hopf codimension-2 points. Finally, by utilizing the fixed point argument and energy estimate, the existence of the global solution to the system has been established, assuming some conditions on initial data. The second three species model describes the dynamics of two predators competing with each other to feed on the same prey. The functional response of predators is the Holling type. This local dynamics has been coupled with linear cross-diffusion terms taking into account the movement of each species towards lower-density areas of the other species. We have applied linear analysis of the system with and without diffusion to obtain the necessary conditions of stability and the occurrence of Hopf and Turing instability. In particular, weakly nonlinear analysis, Turing regions, and maximum growth rate have been investigated. Using a numerical finite elements method, Turing patterns have also been displayed and compared with WNL solutions. Finally, to prove the existence of global in time of the solutions, a rectangular invariant method has been presented for a particular case.

Acknowledgements

In the name of God. As a Ph.D. student who applied abroad to come true dreams cannot deny admission to Italy, particularly in Palermo, supplied the necessary conditions. I appreciate all the graduation office members who respond compassionately to the issues, and I also acknowledge the professors and colleagues at the University of Palermo and the University of Catania. Indeed, they assisted me in extending my mathematics knowledge and fostered me personally. I retrieved a new family at the University of Palermo.

I would like to offer special thanks to my supervisor Prof. Marco Sammartino for their support at every stage of the Ph.D. period. I want to emphasize their hits, comments, and all critics, illuminating the path and advocating for me to improve. I also appreciate their worthwhile suggestions about taking the fascinating " Mathematical Physics" course and introducing immensely helpful and marvelous references. I also thank Prof. Sammartino for their recommendation about taking the " Harmonic Analysis course," participating in the INDAM group, and individual Ravello summer school, and so ones, all of which would remain in my mind as a gold time of my Ph.D. period.

I would like to express my great gratitude to my coordinator Prof. Lombardo who always patiently paid attention to all issues. It was my honor to participate in a course taught by Prof. Lombardo. Prof. Lombardo taught me how to be responsible, accurate, and quick. I am also impressed by her character and ethics.

I extend my sincere thanks to Prof. Gaetana Gambino for their contribution to the thesis and unwavering support. Prof. Gambino, accompanied by professor Sammartino, never ceased assisting me, even during the Pandemic and Lockdown. Prof. Gambino taught and assisted me in discovering my research field. Meeting with Prof. Gambino and Prof. Sammartino always was informative and beneficial. Being their student is my big honor.

I am deeply grateful to Prof. Vincenzo Sciacca for their numerous time's assistance. I also would like to extend my sincere thanks to Professor Sunra Mosconi for presenting a fantastic course, discussing associated problems, and introducing worthwhile references.

I am deeply grateful to Dr. Valeria Giunta, Research associate at The University of Sheffield, for her warm and friendly aid. I especially thank her for being near me like a sister during my pregnancy and after delivery. She always responded to my questions friendly. I have always enjoyed discussing with her.

I am grateful to Dr. Fazel Hadadifard Visiting Assistant Professor at the University of California Riverside, who remotely taught and assisted me in extending my research issue. Working with him was an experience of great value.

I also want to express my most sincere thankfulness to my colleagues. But, mainly, I want to express my sincere gratitude to my colleague and best friend, Dr. Antonella Nastasi, for her friendly accompaniment upon my arrival in Palermo till now.

I want to dedicate my special thanks to my parents, who never gave up advocating but always gave me courage. Indeed, I took advantage of their support in all my life steps. Certainly, my heartly aim to continue studying for my Ph.D. was to appreciate them and make them happy.

In final, I would like to thank my husband for his support. And my special thanks go to my son, who reminded me that I must become stronger daily to support him.

Contents

Abstract **v**

Acknowledgements **vii**

Introduction **1**

1 A Review of Three Species Systems **7**
1.1 General Lotka-Volterra model (**GLV**), and later modified models . . . 7
1.2 Reaction diffusion of Three Species . . . 10

2 A Lotka-Volterra three species model: pattern formation and oscillation **15**
2.1 Intraguild predation(IGP) . . . 16
2.1.1 Intraguild predation models . . . 17
2.2 A diffusive model of three species of Lotka-Volterra with IGP . . . 19
2.3 Extinction of the species . . . 20
2.4 Analysis of the nondimensional system . . . 22
2.5 Turing Instability . . . 26
2.6 Numerical Results . . . 32
2.6.1 Turing Stationary Patterns and chaotic spatial temporal pattern 33
2.6.2 Numerical results of Hopf instability . . . 34
2.6.3 Turing- Hopf Patterns . . . 36
2.7 Weakly Nonlinear Analysis . . . 37
2.7.1 Numerical simulation VS. WNL . . . 41

3 Normal form of Turing-Hopf codimension two of IGP model **45**
3.1 Normal form . . . 45
3.2 Stationary solution of the reduced system . . . 48
3.3 Numerical results . . . 51

4 A diffusive model of one prey and two competitive predators **57**
4.1 Primary Competitive model . . . 59
4.1.1 Line of Equilibria and Zip Bifurcation . . . 61
4.1.2 Positivity and stability condition of Equilibiria . . . 61
4.1.3 Turing and Zip bifurcation in a reaction- diffusion system . . . 63
4.2 Modified Model . . . 64
4.3 Local analysis of modified model . . . 65
4.3.1 Positivity of the coexistence steady state . . . 67
4.3.2 Local stability of the coexistence steady state . . . 67
4.3.3 Hopf Bifurcation . . . 68
4.3.4 Numerical Simulation . . . 68
4.4 Turing Analysis . . . 69
4.4.1 Turing analysis without cross-diffusion (case I: $k_{ij} = 0,\ i \neq j$) . 71
4.4.2 Turing analysis (case II: $k_{1j} = 0, k_{j1} = 0,\ j = 2, 3$) . . . 71

4.4.3 Turing analysis (case III: $k_{j1} = 0,\ j = 2, 3$) . . . 72
4.5 Turing Region . . . 74
4.6 Numerical simulation . . . 78
4.6.1 Numerical Simulations v.s WNL . . . 79
4.7 Maximum growth rate . . . 79
4.8 Global existence in time of solutions by invariant method . . . 81
The dissipativity and balance law conditions . . . 84
Existence of invariant region . . . 86

5 The existence of time global solution of the IGP **89**
5.1 Main Result . . . 89
5.1.1 Strategy towards the existence . . . 89
5.1.2 Preliminaries . . . 90
5.2 Positivity of the solutions . . . 90
5.3 Local Existence . . . 92
5.3.1 Estimates in L^p norms . . . 93
5.3.2 Estimates in L^2 norms . . . 93
5.3.3 Estimates in $\dot{H}^r$ norms . . . 94
5.3.4 Continuity of Q_1, Q_2 and Q_3 . . . 95
5.4 Global Existence of the solutions (s, u_1, u_2) in the space of $L^p \cap H^r$ . . . 95
5.4.1 *Apriori* bounds in L^p spaces . . . 96
5.4.2 *Apriori* bounds in Sobolev spaces . . . 97

Conclusion **101**

A Analysis of marginal stability of curve $F = 0$ **105**

B Weakly nonlinear analysis **111**
B.1 Drivation of quintic- Stuart- Landau equation IGP system . . . 111
B.2 Weakly nonlinear analysis of the system (4.13) . . . 113

C Normal form calculations **117**
C.1 Calculation of coefficients of $O(\varepsilon^2)$ . . . 117
C.2 Calculation of coefficients of $O(\varepsilon^3)$ . . . 119

References **123**

List of Figures

1 Spatio-temporal patterns in niche (dimensional model) of u_1 in niche, $x \in [0\ 500\pi]$ for given parameters: $m_1 = 0.35$, $m_2 = 2.3165$, $K = 2$, $\gamma_1 = 0.18$, $\gamma_2 = 0.3$, $D_1 = 0.1$, $D_2 = 0.4$, $d_1 = 1$, $d_2 = 0.1$ and $d_3 = 0.003$. For this choic of parameters $E^* \simeq (0.25, 0.75, 0.08)$, Hopf threshold $m_2^c = 2.3077$ corresponding to Turing threshold $c_2^c = 51.1529$ and the critical wavenumber $k_c \simeq 2.6$. 4

2 Transient patterns (dimensional model) from Turing-Hopf to Turing instabilities, $x \in [0\ 2\pi]$ and parameters are the same as Figure 1 and $\Gamma = 100$. Figures in A), B) and C) are a close shot of figures D), E) and F). 5

2.1 *(Hsu, Ruan, and Yang, 2015, Fig. 1.1) All possible schematic diagrams of the direct and indirect interactions among three species predator–prey systems. The arrows present the directions of biomass. (A) Food chain; (B) two predators–one prey; (C) one predator–two preys; (D) food chain with omnivory; and (E) food chain with cycle.* 16

2.2 In the plane (γ, δ), the colored regions show where the positive equilibrium E^* exists. The region I corresponds to the case (2.10), the region II corresponds to the case (2.11). Parameters are fixed as $n_1 = 0.5$, $n_2 = 0.7$, $\alpha = 2.5$, $\eta = 0.8$, $d_u = d = d_w = 0$. 24

2.3 In grey the regions of the parameters in the plane (γ, δ) where the equilibrium E^* exists positive and locally stable. The parameter values are $n_1 = 0.5$, $n_2 = 0.7$, $\alpha = 2.5$, $d_u = d = d_w = 0$. In A) $\eta = 0$. In B) $\eta = 0.8$. 26

2.4 In Panel A): the graph of $P_0(k^2)$ in the general case $d_u d_w \neq 0$. In Panel B): typical graph of $P_0(k_m^2)$, where P is the characteristic polynomial and k_m^2 is defined in (2.42). The parameter values are $n_1 = 0.5$, $n_2 = 0.7$, $\alpha = 2.5$, $\eta = 0.8$, $\gamma = 1.2$, $\delta = 0.6$, $d_u = 0.02$, $d_w = 0.04$. 30

2.5 A) Plot of eigenvalues when wavenumbers are in the interval $[k_M^2, k_m^2]$ as critical bifurcation d varies B) Plot of $P(k^2)$ as critical bifurcation parameter d varies. The parameter are given in Figure 2.4. 30

2.6 Hopf and Turing instability regions for increasing values of α. A) $\alpha = 2.5$, B) $\alpha = 5$, C) $\alpha = 0.9$. The other fixed parameter values are $n_1 = 0.5$, $n_2 = 0.7, \eta = 0.8$. 31

2.7 Turing instability regions as the system parameters change. The parameter set is chosen as in Figure 2.2, except for the parameter specified in the legend of each sub figure and $d_u = 0.2$, $d_w = 0.2$. 32

2.8 Numerical simulation in the Turing instability region with $n_1 = 0.5$, $n_2 = 0.7$, $\eta = 0.8$, $\alpha = 5$, $\gamma = 2, \delta = 0.8$, $d_u = 0.01$, $d_w = 0.2$ and $d = 12.2298$. For this parameter choice the equilibrium point is $E^* = (0.21, 0.35, 0.55)$, the critical Turing threshold is $d_c = 8.1532$ and the critical wavenumber is $k_c = 1.0809$. 33

2.9 Numerical simulation in the Turing instability region with $n_1 = 0.5$, $n_2 = 0.7$, $\eta = 0.8$, $\alpha = 5$, $\gamma = 2, \delta = 0.8$, $d_u = 0.01$, $d_w = 0.2$ and $d = 12.2298$. For this parameter choice the equilibrium point is $E^* = (0.21, 0.35, 0.55)$, the critical Turing threshold is $d_c = 8.1532$ and the critical wavenumber is $k_c = 1.0809$. 34
2.10 Numerical simulation in the Turing instability region with $n_1 = 0.5$, $n_2 = 0.7$, $\eta = 0.9067$, $\alpha = 5$, $\gamma = 2.1$. For this parameter choice the equilibrium point is $E^* = (0.21, 0.35, 0.55)$, Hopf threshold $\delta^c = 1.0753$. . . 35
2.11 Numerical simulation in the Turing instability region with $n_1 = 0.5$, $n_2 = 0.7$, $\eta = 0.8$, $\alpha = 5$, $\gamma = 1.5, \delta = 1.51$, $d_u = 0.04$, $d_w = 0.02$ and $d = 10.3$. For this parameter choice the equilibrium point is $E^* = (0.23, 0.23, 0.67)$, the critical Hopf parameter is $\delta_c = 1.0258$. 36
2.12 Numerical simulation in the Turing-Hopf instability region with $n_1 = 0.5$, $n_2 = 0.7$, $\eta = 0.8$, $\alpha = 5$, $\gamma = 1.6, \delta = \delta^c$, $d_u = 0.04$, $d_w = 0.02$ and $d = 35$. For this parameter choice the equilibrium point is $E^* = (0.22, 0.32, 0.58)$, the critical Turing threshold is $d_c = 28.9415$, critical Hopf parameter is $\delta^c = 1.0753$ and the critical wavenumber is $k_c \simeq 0.9$. A) phase portrait for a specific x and $t \in [0\ , T]$. 37
2.13 Numerical simulation in the Turing-Hopf instability region with $n_1 = 0.5$, $n_2 = 0.7$, $\eta = 0.8$, $\alpha = 5$, $\gamma = 1.6$, $\delta = 1.11$, $d_u = 0.04$, $d_w = 0.02$ and $d = 35$. For this parameter choice the equilibrium point is $E^* = (0.22, 0.32, 0.58)$, the critical Turing threshold is $d_c = 28.9415$, critical Hopf parameter is $\delta_c = 1.0753$ and the critical wavenumber is $k_c \simeq 0.9$. A) phase portrait for a specific x and $t \in [500\ , 700]$. 38
2.14 A) Supercritical and subcritical Turing instability regions. The parameter values are $n_1 = 0.5$, $n_2 = 0.7$, $\alpha = 2.5$, $\gamma = 0.8$, $d_u = 0.02$, $d_w = 0.04$. B) Supercritical and subcritical Turing regions when IG predator self-diffusion varies: $d_w = 0$ and $d_w = 0.2$. Other fixed parameters are $n_1 = 0.5$, $n_2 = 0.7$, $\alpha = 2.5$, $\eta = 0.8$, $\gamma = 1.2$, $d_u = 0.02$. . . 42
2.15 Supercritical and subcritical Turing instability regions when basal resource self-diffusion varies: $d_u = 0$ in the left side, $d_u = 0.2$ in the right side. Other fixed parameters are $n_1 = 0.5$, $n_2 = 0.7$, $\alpha = 2.5$, $\eta = 0.8$, $\gamma = 1.2$, $d_w = 0.04$. 42
2.16 Comparison between the weakly nonlinear solution (solid line) and the numerical solution of system (dotted line) in the supercritical case, with different values of ε: we have fixed $\varepsilon = 0.1$ in the simulation shown in the first line and $\varepsilon = 0.05$ in the simulation shown in the second line. The parameter values used in the simulations are: $n_1 = 0.5$, $n_2 = 0.7$, $\alpha = 5$, $\eta = 0.8$, $\gamma = 1.5$, $\delta = 0.8$, $d_u = 0.02$, $d_w = 0.04$. For this parameter set, the bifurcation threshold is $d_c = 10.2872$ and the critical wavenumber is $k_c = 1.04222$. 43

3.1 The region found by amplitude equations (3.21). Given parameters are: $m_1 = 0.5$, $m_2 = 0.7$, $\eta = 0.8$, $\alpha = 5$, $\gamma = 1.6$, $d_u = 0.1$, $d_w = 0.02$, which obtain $E^* = (0.21, 0.33, 0.55)$ and $\delta^c = 1.0753$, $d_c = 43.3325$, Moreover, critical wave number and critical frequency in which Turing and Hopf bifurcation emerge correspondingly are given $k_c^2 = 0.4144$, $\Omega_c = 0.8447$. 51

3.2 It denotes to Turing- Hopf pattern located in the region R_1, the chosen perturbation parameters are $(d^{(2)}, \delta^{(2)}) = (0.02, 0.001)$. Other parameters are fixed as Figure 3.1. B) is a close shot of figure A). In T-H region Coefficients of amplitude equations (3.21), (3.22) are achieved as: $\sigma_1 = -4.0088, \sigma_2 = 2.1642e-04$, $L_1 = 4.7313e+03$, $L_2 = 5.6030$, $\Omega_1 = -5.9146e+05$, $\Omega_2 = -10.1148$,. 52
3.3 It denotes to Turing- Hopf pattern located in the region R_2, the chosen perturbation parameters for the Figure 3.3A are $(d^{(2)}, \delta^{(2)}) = (0.00075, 0.00009)$ such that coefficients of the amplitude equations are $\sigma_1 = -0.3608, \sigma_2 = 2.0716e-05$ and other coefficients are the same as Figure 3.2, and for the Figure 3.3B $(d^{(2)}, \delta^{(2)}) = (0.001, 0.4)$ such that coefficients of the amplitude equations are $\sigma_1 = -1.6035e+03$, $\sigma_2 = 0.0960$ and other parameters and other coefficients are fixed for both figures as Figure 3.1 and Figure 3.2 respectively. 53
3.4 For fixed parameters given in Figure 3.1 Turing-Hopf pattern located in the region R_2, the chosen perturbation parameters for the Figure 3.4A are $(d^{(2)}, \delta^{(2)}) = (0.028, 0.0001)$ such that coefficients of the amplitude equations are achieved $\sigma_1 = -0.4009$, $\sigma_2 = -3.0607e-04$, and for the Figure 3.4B are $(d^{(2)}, \delta^{(2)}) = (0.1, 0.0004)$ and coefficients are $\sigma_1 = -1.6035$, $\sigma_2 = -2.1883e-05$,, and other parameters and other coefficients are fixed for both figures as Figure 3.1 and Figure 3.2 respectively. 53
3.5 It denotes to stability and Turing pattern located in the region R_5, the chosen perturbation parameters for the Figure 3.5A are $(d^{(2)}, \delta^{(2)}) = (0.005, -0.0002)$ such that coefficients of the amplitude equations are achieved $\sigma_1 = 0.8018$, $\sigma_2 = -5.3894e-05$, and for the Figure 3.5B are $(d^{(2)}, \delta^{(2)}) = (0.3, -0.0001)$ such that coefficients of the amplitude equations are achieved $\sigma_1 = 0.4009$, $\sigma_2 = -3.7765e-04$. and other parameters and other coefficients are fixed as Figure 3.1 and Figure 3.2 respectively. 54
3.6 A) It denotes to stability and Turing pattern located in the region R_8, the chosen perturbation parameters are $(d^{(2)}, \delta^{(2)}) = (-0.06, -0.00028)$ such that coefficients of the amplitude equations are achieved $\sigma_1 = 1.1225$, $\sigma_2 = 3.5295e-06$. B) Hopf pattern emerged by chosen parameter close to the negative part of the line $\mathcal{S}_1$ are $(d^{(2)}, \delta^{(2)}) = (-0.094, -0.00003)$ such that coefficients of the amplitude equations are achieved $\sigma_1 = 0.1203$, $\sigma_2 = 1.0361e-04$. and other parameters and other coefficients are fixed for both figures as Figure 3.1 and Figure 3.2 respectively. . . . 55

4.1 Schematic plot of feeding rate. 60
4.2 Zip Bifurcation, black line implies the stability condition, the green point illustrates intersection point $(u_1(K), u_2(K))$, the red line located in equilibria line shows unstable points while blue line demonstrates stable points. 63
4.3 Zip bifurcation arises for fixed K, A) when $K = a_1 + 2\lambda$ all points on the equilibria line are unstable (red line). B) when $K = a_2 + 2\lambda$ all points on the equilibria line are stable since they satisfy condition (4.10) (blue line). 63

4.4 Local stability of the spices when the Hopf parameter is less then critical one. A) Stability of the system for $K = 6 < K_H$. B) Phase portrait of the system of stable spiral. Given parameters are $a_1 = 3.5$, $a_2 = 4.4$, $d_1 = 1.2$, $d_2 = 1.8$, $m_1 = 4.2$, $m_2 = 7$, $\Gamma = 1$, $\gamma = 2$, which lead to $\lambda_1 = 1.4$, $\lambda_2 = 1.5231$, and $u^* = (1.5231, 0.73, 0.65)$, $K_H = a_1 + 2\lambda_2 = 6.5462$ 69
4.5 Hopf bifurcation occurs when $K > K_H$. A) Periodic solutions of the populations as Hopf parameter crosses the critical value K_H. B) Appearance of the limit cycles as $K > K_H$ grows. For $K \simeq 7.5$, $K \simeq 8$ and $K \simeq 8.5$ stabilized limit cycles are depicted. Given parameters are the same as Figure 4.4. 69
4.6 Necessary condition of Turing instability. A) it illustrates $C(\delta^2) < 0$ (black solid line) if $k_{32} > k_{32}^c$. B) this figure shows if $k_{32} > k_{32}^c$ then $\lambda(\delta^2) > 0$ (black solid line) for the range of wave numbers. Given parameters are the same as (4.46) 73
4.7 Turing region (dashed region)in plane (m_1, K), parameters are obtained in . The orange horizontal line demonstrates $K = K_H$, such that the region above the horizontal line and for each m_1 associates with Hopf region. Dashed line, purple and pink lines are associated to positivity, Turing condition II and Turing condition I respectively. $\Gamma = 5$, $\gamma = 2$. $K = 1.48$, $a_1 = 0.64$, $a_2 = 0.6$, $m_1 = 0.8$, $m_2 = 1.15$, $d_1 = 0.4$, $d_2 = 0.6$, $\varepsilon = 0.12, k_{11} = k_{12} = k_{22} = 0.1$, $k_{23} = 0.1; k_{13} = 0.25, k_{33} = 1$. 75
4.8 Turing region (dashed region) in plane (m_1, K), A) $k_{12} = 0.1$ and other parameters are fixed as (4.46). B) $k_{12} = 0.2$ and other parameters are fixed as Figure 4.7. 76
4.9 Turing region (dashed region) in plane (m_1, K), A) $k_{13} = 0.15$ and other parameters are fixed as (4.46). B) $k_{13} = 0.5$ and other parameters are fixed as Figure 4.7. 76
4.10 Turing region (dashed region) in plane (m_1, K), A) $k_{23} = 0.1$ and other parameters are fixed as (4.46). B) $k_{23} = 0.12$ and other parameters are fixed as Figure 4.7. 77
4.11 Turing region (dashed region) in plane (m_1, K), A) $k_{11} = 0.1$ and other parameters are fixed as (4.46). B) $k_{11} = 0.2$ and other parameters are fixed as Figure 4.7. 77
4.12 Turing region (dashed region) in plane (m_1, K), A) $k_{22} = 0.08$ and other parameters are fixed as (4.46). B) $k_{22} = 0.11$ and other parameters are fixed as Figure 4.7. 77
4.13 Turing region in plane (m_1, K), A) $k_{33} = 0.15$ and other parameters are fixed as (4.46). B) $k_{33} = 1$ and other parameters are fixed as Figure 4.7. 78
4.14 Numerical simulation in the Turing instability for given parameters $\Gamma = 5$, $\gamma = 2$. $K = 1.48$, $a_1 = 0.64$, $a_2 = 0.6$, $m_1 = 0.8$, $m_2 = 1.15$, $d_1 = 0.4$, $d_2 = 0.6$, $\varepsilon = 0.12, k_{11} = k_{12} = k_{22} = 0.1$, $k_{23} = 0.1; k_{13} = 0.25, k_{33} = 1$ Hence $\lambda_1 = 0.4$ and $\lambda_2 = 0.6545$. Moreover, the critical bifurcation parameter is $k_{32}^c = 0.8790$ and correspondingly critical wave number is $\delta_c \simeq 5$ and $E^* = (s, u_1, u_2) = (0.6545, 0.8046, 0.5510)$. 78
4.15 A) Comparison of FEM (dashed blue line) with WNL method(solid red line) B) Turing Patterns of the predator u_1. 79

4.16 Maximum growth rate obtained by chosen parameter values: $K = 1.48$, $\gamma = 2, \Gamma = 5$, $a_2 = 0.5$, $a_1 = 0.4$, $a_2 = 0.6 m_2 = 1.15$, $d_1 = 0.4, m_1 = 0.8$, $d_2 = 0.6$, $k_{11} = 0.1$, $k_{12} = 0.1$, $k_{13} = 0.25$, $k_{22} = 0.1$, $k_{23} = 0.1$, $k_{33} = 1$, $\epsilon = 0.12$ which leads to $k_{32}^c = 0.8790$, $\delta_c^2 = 24.96911$. 80

A.1 Graph of the curve $F(\gamma, \delta) = 0$. (a) $B(\bar{\gamma}) > 0$ and $B^2(\gamma) - 4A(\gamma)C(\gamma) > 0$, which corresponds to *Case 1.* and *Case 2.1.* Here, the parameters are fixed as $n_1 = 0.5$, $n_2 = 0.7$, $\alpha = 2.5$, $\eta = 0.8$, $d_u = d = d_w = 0$, corresponding to *Case 1.*. (b) $B(\bar{\gamma}) > 0$ and $B^2(\gamma) - 4A(\gamma)C(\gamma) < 0$ when $\gamma_- < \gamma < \gamma_+$, where $\gamma_{1,2}$ are drawn in black dots. The parameters are fixed as $n_1 = 0.5$; $n_2 = 22.5$, $\alpha = 2.5$, $\eta = 1.1$, $d_u = d = d_w = 0$, which corresponds to *Case 2.2.*. (c) $B(\bar{\gamma}) > 0$ and $B^2(\gamma) - 4A(\gamma)C(\gamma) < 0$ when $\gamma_- < \gamma < \gamma_+$ where $\gamma_{1,2}$ are drawn in black dots. The parameters are fixed as $n_1 = 0.5$, $n_2 = 100$; $\alpha = 2.5$, $\eta = 1.1$, $d_u = d = d_w = 0$, which corresponds to *Case 3.* 109

List of Tables

4.1 parameters appearing in Eqs.(4.2) 60

List of Abbreviations

WNL	**W**eakly **N**on **L**inear
LV	**L**otka **V**olterra
IGP	**I**ntra**g**uild **P**redation
GLV	**G**eneralized **L**otka **V**olterra
SKT	**S**higesada **K**awasaki **T**eramoto
PDE	**P**artial **D**ifferential **E**quation
ODE	**O**rdinary **D**ifferential **E**quation

To my parents

Introduction

Three species models play an important role in ecology and biology. Indeed, a food web in ecology includes of at least three species. Each specie can be associated with a specific trophic level (number of steps that specie eats or is eaten by others). Therefore, in a food web of three species, plenty of models can be established to simulate one part of nature.
It is just to notice in a classification of classical three species Lotka-Volterra model existence of 34 cases of different classes (food chain, one prey-two predators, two preys- one predator and loops) have been determined (Krikorian, 1979). Therefore, there exist abundant three species models consisting of Lotka-Volterra type, and even more with different functional responses that can be taken into account in studies.

Two species models can be almost considered a competition model or predation model, whereas a three species model involves either predation, competition or predation-competition (Holt and Lawton, 1994), (Polis and Holt, 1992), which practically have been proved.

Moreover, the presence of a third specie (can be omnivore - top predator) can destabilize a food web model due to the assumption of the theoretical model (Tanabe and Namba, 2005, Namba, Tanabe, and Maeda, 2008). Thus, the presence of third specie almost creates a chaotic model.

In addition, according to the pioneering Turing's work Turing, 1952 which states "diffusion-driven instability", a reaction-diffusion of three species can include of the emergence of different patterns due to the presence of numerous instabilities such as Turing instability, wave instability, Turing-Hopf instability, etc.

Further, mathematical models in ecology have been used largely to provide a qualitative explanation for patterns in nature (Council et al., 2000), and help examine the environmental and ecological impact of alternative pollution-control and resources-conservation actions, and aid planners or decision-makers in formulating cost-effective management policies (Li et al., 2013).

This is why comprehension, three species models has became one of the biggest challenges in ecology and biology.

It is observed that background studies around three species have been chiefly devoted to three species of food chain model, then competition and predation models. Hence, mathematical point of view, the recent outcomes of the chain food model of three species are refereed in (Sabir, 2022; Zou et al., 2022; Raw and Sarangi, 2022), and some of the latest findings of competition models of three species have been alluded in (Guin, Roy, and Djilali, 2021). And then, the most recent research of predation return to (Rihan and Alsakaji, 2022; Chen and Guo, 2021). Moreover, (Mishra and Wrzosek, 2022) is also considered a recent survey in part of a combination of predation and competition.

However, the latest ecological, and biological improvements around three species problems give rise to the formation of different mathematical models and outcomes that can be listed simultaneously as food chain area (Dang et al., 2021), competition

(Ohba, Terazono, and Takada, 2022), predation (Goodman et al., 2022) and combination of predation and competition (Liang et al., 2022; Anjos, Costa, and Almeida, 2021).

The issue of the present thesis is an investigation of mathematical models of three species.

Generally, this dissertation is allocated to:
1. Presentation of a chemotaxis model of intraguild predation of three species (**IGP Model**).
2. Modification and investigation of a reaction-diffusion model presented in (Farkas, 1984) and (Ferreira, Silva, and Rao, 2019) of two predators competing for one prey with Holling type II functional responses.

Our goal is to survey the necessary conditions for the formation of patterns and exhibit them numerically.

The first chapter of the thesis is assigned to a review of articles around three species models, that have been qualitatively and quantitatively investigated.

This Chapter commences with a background of the appearance of three species from mathematical and ecological points of view. Then it follows the improvements of ODE models until arrives at the investigation of diffusive models in different classes of three species.

The following Chapters express the outcome of our research.

In Chapter 2, we present a diffusive Lotka-Volterra with an intraguild predation system of three species. Indeed, this model is a comprehensive system of (Holt and Polis, 1997) by adding a nonlinear diffusion term. Roughly speaking, the intraguild predation model of three species describes the competition of two predators for a basal resource, whereas one predator (IG predator) eats the intermediate predator (IG prey). The nonlinear term presented in the diffusion part of the IGP model is known as the Chemotaxis term. In fact, the chemotaxis term $\nabla.(v\nabla w)$ is a subclass of cross-diffusion term $\nabla.(\nabla(vw))$ and associated with a positive sign (negative sign) indicates that intermediate predator (v) migrates away from (toward) IG predator (w) respectively.

This chapter contains proof of the extinction of all species gradually over time. To conquer numerous parameters in dimensional form, a non-dimensional form is presented. The new model includes seven parameters instead of sixteen. Consequently, unique coexistence steady state of the model is found, whose positivity conditions provide two different scenarios:
i. The first considers that the mortality rate of IG prey is less than the conversion rate; consequently, IG prey dies out.
ii. Second opposite case i, i.e., it implies the coexistence of all species. Therefore, the rest of the thesis progresses with this assumption. Accordingly, positive regions in the plane of two kinetic parameters are determined following the noticed assumption.

Implementing linear analysis around the coexistence steady state, local stability is obtained. The achieved characteristic polynomial is cubic; this is why we utilize the relation between eigenvalues and coefficients of a cubic polynomial to prove stability conditions and the Hopf threshold.

Subsequently, we investigate Turing analysis using linear analysis in the presence of diffusion. We establish dispersion relation, and then due to the Routh-Hurwitz criterion, we also prove necessary and sufficient conditions for the emergence of the Turing pattern. In addition, by providing dispersion relation, we demonstrate the emergence of Turing instability in four possible cases, which are associated with self-diffusion parameters of prey and IG predator. We prove that in three

cases, Turing can emerge, while one case does not ensure the emergence of the Turing pattern. We demonstrate the reliability of calculations with a numerical spectral method. Further, we illustrate the necessary conditions for the appearance of Turing-Hopf instabilities and exhibit instability regions of the diffusive model concerning kinetic parameters. Moreover, we survey in plane how Turing regions are changed when other kinetic and diffusion parameters increase. Finally, we prove that wave instability cannot occur using linear analysis.

This Chapter is followed by some numerical results of stationary Turing patterns, time oscillation, and Turing-Hopf patterns. We have obtained some numerical results of the dimensional system, which exhibits chaotic behavior and transition of the model.

The final section of this Chapter is allocated to a Weakly nonlinear analysis of the IGP model. Indeed, we utilize WNL, which has equipped with a multiscale method to capture the amplitude of patterns close to the threshold. And correspondingly, we depict supercritical Turing calculations and patterns. And, then we compare numerical simulations with WNL analysis results.

Moreover, we have achieved some numerical results, which are reported here:
i. Numerical behavior of IG prey in the niche for the dimensional model (2.3) when Γ is considerable (see Figure 1) and is regulating the domain. By increasing Γ, we observe the chaotic behavior of the IG prey. Both Figure 1A and Figure 1B have been simulated in the same time interval. In Figure 1B, the chaotic behavior of the IG prey decreases.
ii. Performance of transition from Turing pattern to Turing-Hopf pattern of model (2.3) is reported in Figure 2.
The results presented in Chapter 2 are contained in (Gambino et al. (Preprinting)).

Chapter 3 is devoted to the calculation of the normal form of non-dimension form of the IGP model mentioned in Chapter 2. To calculate normal form we apply a perturbation technique based on multiple scales. Consequently, we drive Amplitude equations that provide necessary conditions for the appearance of Turing, Hopf, and Turing-Hopf patterns and regions concerning coefficients of the amplitude system. Some numerical results are presented which prove the accuracy of obtained reduced system.

Chapter 4 considers a system consisting of two predators competing for one prey. This model is a modified version of the models presented in (Farkas, 1984, Ferreira, Silva, and Rao, 2019) that we call it Zip model. To achieve the modified model, first, we need to present some existing results around the kinetic part of the system. The zip model contains a line segment of the equilibrium point, providing a degenerate system. One needs to add an intraspecific term to one of the predator equations to overcome degeneracy. Moreover, the modified model is coupled with linear diffusion such that cross-diffusion terms regarding the predators are all positive; predators avoid each other. Following the Chapter, we find a unique coexistence of steady state equilibrium whose positive conditions are determined in the next step.

Then we examine the local stability of the system and prove the stability condition. We demonstrate that the system undergoes the Hopf bifurcation due to varying the carrying capacity parameter of prey. Our presented numerical results confirm the reliability of the results. Furthermore, Turing's analysis of the diffusive system is explored. We figure out that in the absence of cross-diffusion parameters, Turing patterns do not perform; however, for two other cases, we establish the necessary conditions for the emergence of Turing instabilities. After that, for one case (case III, the case in which predators diffuse in different directions and ignore diffusing in the order of prey instead), we survey the Turing region. We examine how the Turing

region is changed when diffusion parameters are altered. And finally, for case III, our numerical results are depicted. At last, the numerical results are compared with weakly nonlinear analysis for the case III.

In Chapter 4, we also investigate maximum growth rate for case III. In the emergence of patterns, we answer "when the number of modes is less or greater than the critical mode?" as the critical bifurcation parameter rises. In the last section of this chapter, the invariant method investigates the global existence in the time of solutions of the modified model with a diffusion matrix including only one cross-diffusion. Indeed, the idea behind this method is that under some dissipativity and balance law conditions, a bounded invariant region of ODE can ensure global existence in the time of strong solutions.

Chapter 5 has been established accompanied by Fazel Hadadifard, Visiting Assistant Professor at University of California, Riverside.
This Chapter is devoted to the global solution of the IGP model in 2D. To prove that, first, we explore the positivity of the solutions. Then local existence of the problem is presented due to the fixed point argument, which is complete with some estimations in L^p, L^2, and H^r spaces. In the final section, we prove the existence of a global solution of the model by finding some a priory estimate in L^p and Sobolev spaces, which complete the proof. Out come of this Chapter has been submitted in (Farivar and Hadadifard (submitted)).

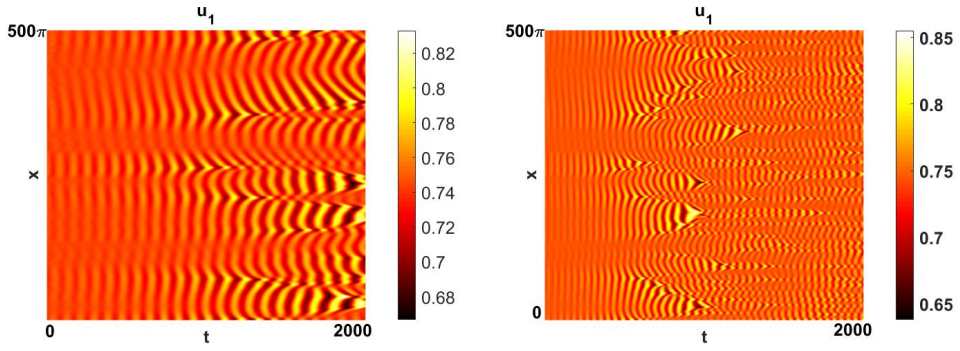

(A) IG prey (u_1) in niche ($\Gamma = 50$).

(B) IG prey (u_1) in niche ($\Gamma = 100$).

FIGURE 1: Spatio-temporal patterns in niche (dimensional model) of u_1 in niche, $x \in [0\ 500\pi]$ for given parameters: $m_1 = 0.35$, $m_2 = 2.3165$, $K = 2$, $\gamma_1 = 0.18$, $\gamma_2 = 0.3$, $D_1 = 0.1$, $D_2 = 0.4$, $d_1 = 1$, $d_2 = 0.1$ and $d_3 = 0.003$. For this choic of parameters $E^* \simeq (0.25, 0.75, 0.08)$, Hopf threshold $m_2^c = 2.3077$ corresponding to Turing threshold $c_2^c = 51.1529$ and the critical wavenumber $k_c \simeq 2.6$.

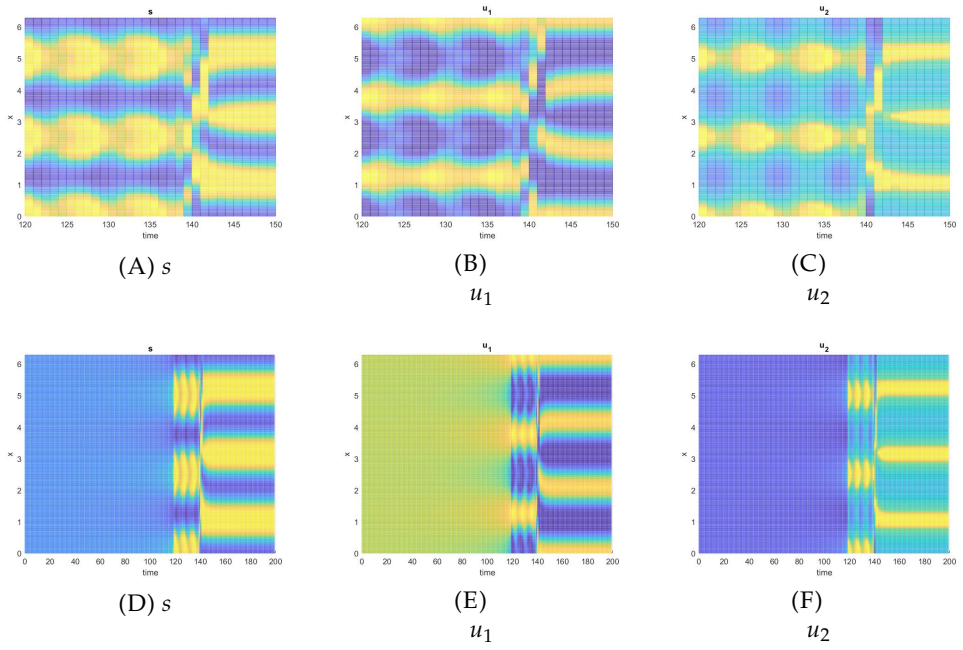

(A) s (B) u_1 (C) u_2

(D) s (E) u_1 (F) u_2

FIGURE 2: Transient patterns (dimensional model) from Turing-Hopf to Turing instabilities, $x \in [0\ 2\pi]$ and parameters are the same as Figure 1 and $\Gamma = 100$. Figures in A), B) and C) are a close shot of figures D), E) and F).

Chapter 1

A Review of Three Species Systems

The introduction of mathematical modeling of biological and ecological systems goes back to the early twentieth century, the attempt of giving a quantitative description of living systems is still a fundamental topic of modern science; the advances in computational sciences, as well the emergence of the new paradigm of "complex systems" have made more urgent (and fruitful) than ever the use of the mathematical methods in the realm of life sciences. Moreover, it is generally acknowledged that a deeper mathematical understanding of biology and ecology can have a groundbreaking impact on subjects like resource management, pollution forecast and control, pattern recognition and control in nature, etc.

In 1910, Lotka was the first to suggest prey-predator model in interpretation of theory of *autocatalytic* chemical reactions. Later, Volterra proposed the use of differential equations to explain differential equation which described the behavior of species in marine ecology. Indeed, he believed that two or three species, sharing the same limited resource, cannot coexist. This idea can be found, in a more general context (Rescigno and Richardson, 1965; Levin, 1970), in more modern literature (see, e.g. (Levins, 2020), and is nowadays expressed as the "*competitive exclusion principle*" proposed by Hardin in the sixties, see (Hardin, 1960). The Lotka-Volterra model was also generalized along another direction: allowing the interaction between species to be described by more complicated functions, other than quadratic ones as in the original **LV** system.

In 1959, to describe the saturation effects of prey consumption (observed at high prey density), Holling introduced modified versions of the **LV** systems. Since then, Holling-type functional response has undergone an extensive investigation by ecologists and mathematical modellers. Indeed, different functional responses were presented by Holling, which was applied by Resenwerg and Mac Arthur (Rosenzweig and MacArthur, 1963) to explain the dynamics exhibited by populations of the predator-prey type, such as Lynx and snowshoe hare. The **LV** system is one of the most extensively studied model of the mathematical literature; it is impossible here to give even a partial account of the relevant papers, and we refer the reader to (Wangersky, 1978).

1.1 General Lotka-Volterra model (GLV), and later modified models

The generalized Lotka–Volterra equations (**GLV**) are a set of equations which are a n-dimensional generalization of the competitive or predator–prey Lotka–Volterra

equations (Hofbauer, Sigmund, et al., 1998). Fundamentally, **GLV** is defined as below to describe the dynamics of biological species $u_1, u_2, \cdots u_n$ as:

$$\frac{du_i}{dt} = u_i f_i(u) \tag{1.1}$$

where $f(u) = r + Au$, where $r, f(u)$ are vectors and and A is community matrix. The vector r describes the intrinsic growth rates of species, A describes the interaction between species in which each entry sign gives different meaning to the system. If:
i. a_{ij}, a_{ji} entries of matrix A are negative, the species i and j are in competition.
ii. a_{ij} and a_{ji} have different signs, then one is predator and the other is the prey. Moreover, the diagonal terms a_{ii} are usually considered negative since each specie hurts itself. Indeed, self-limitation prevents a population from growing indefinitely.

Therefore, the **GLV** systems do not describe typical phenomena like predator preferences, nonlinear responses, and mutualism. On the other hand, **GLV** includes food chain systems, see e.g. (Yang and Fu, 2008), (Chauvet et al., 2002), that are interesting models, both for their practical relevance, and for the variety of the displayed dynamics, ranging from oscillatory behavior up to chaotic behavior.

In 1957, some mathematicians such as Kerner, Hung, and Morowitz (Kerner, 1957), (Huang and Morowitz, 1972), studied the global stability of biological ODEs, however, for the first time in 1977 Goh (Goh, 1976) proved that **GLV** system, describing interactions of n-species which has nontrivial equilibrium has a Lyapunov function and consequently is globally asymptotically stable. After Goh's proof and for the first time in 1979, Gary W. Harrison (Harrison, 1979) applied Goh's theorem to illustrate the global stability of the coexistence equilibrium of a food chain.

In 1975, M. E. Gilpin (Gilpin, 1975) showed that a three-species competitive Lotka-Volterra model may demonstrate population oscillations of a neutral or undamped nature. In truth, if immigration, incomplete overlap, or any other mechanism inhibit extinction, then such a three-species system goes into true limit cycles. Gilpin proposed *"limit cycles are more likely in communities with one odd number of species"*.

An important work to mention is the paper of May and Leonard (May and Leonard, 1975), where the authors studied the classical Gause-Lotka-Volterra system. They showed how the system has bounded non-periodic oscillatory solutions, with ever increasing cycle time, which was an example of *"the complexities that nonlinearities can introduce even into the simplest equations of population biology"*.

Then, in 1977, Freedman and Waltman (Freedman and Waltman, 1977) examined a model of three species including general functional responses for each species. They analyzed equilibria and established stability and boundedness of the equilibria. Moreover, they specifically proved necessary and sufficient conditions for the persistence of species when functional responses are Lotka-Volterra type and mixed Lotka-Volterra with Holling types.

Around 1979 Krikorian (Krikorian, 1979) presented a systematic analysis, showing that, under some restrictions, there are 34 different cases of classical three-species Lotka-Volterra systems [1]. He locally investigated the asymptotic stability of equilibria and global boundedness of all types. Namely, he proved positive critical points of the food chain, two predators-1 prey, and one predator-2 prey systems are globally stable and bounded, whereas, for the loop case, these results are not generally valid.

[1] which are classified as *1) food chains, (nine cases) 2) one predator acting on two preys, (six cases) 3) two predators competing for one prey, (three cases) 4) loops, (sixteen cases)*

In 1986, G. Kirlinger (Kirlinger, 1986) showed that a system of multi-species containing two competing species of logistic **LV** type is stabilized when a predator is introduced to the model. As a result, Kirlinger observed that none of the species become extinct; therefore, the idea of *" No species dies out "* is considered as *Permanence*.

In 1991, Hasting and Powell (Hastings and Powell, 1991) studied a food chain of three species consisting of nonlinear functional responses. They exhibited the existence of chaotic dynamics in long time behavior.

In 1992, Freedman and Ruan (Freedman and Ruan, 1992) investigated a three-species food chain model in which prey perform group defense. They proved that the system underlies a sequence of Hopf bifurcation without delay, and with delay as a Hopf bifurcation parameter, again Hopf bifurcation occurs.

In 1995, MacCann and Yodzis (Mccann and Yodzis, 1995) studied a three-species food chain model containing Holling Type II functional responses. They locally analyzed the model and performed a different set of behavior, including quasi-periodicity, chaos, homoclinic events, and transient chaos. Studying the dynamical behaviors of three species of food chain models continued. For instance, some of them are reported here: Investigation three species with Beddington-DeAngelis functional responses (Naji and Balasim, 2007, Zhao and Lv, 2009), research about the complexity of the three-species model (Lv and Zhao, 2008), Surveying the dynamical behavior of three specie models with Crowley-Martin functional responses (Upadhyay and Naji, 2009). Later, other studies around the local analysis of three species with Holling Type IV (Upadhyay and Raw, 2011, and Parshad et al., 2017) studying around equilibria, stability, and oscillation via Hopf bifurcation in the model of three species consisting of Holling type III were also studied in (Sunaryo, Salleh, and Mamat, 2013).

Some recently specialized models have also alluded to three species models that are followed:

• **Discrete-time model**: this type of model describes a phenomenon in which time is not continuous, and the size of populations is small. This type of model can be applied to non-overlapping generations (see Santra, 2021; Mortuja, Chaube, and Kumar, 2021) and references therein).

• **Fractional model**: For the first time, Ahmed and coauthors investigated fractional Lotka-Volterra models (Ahmed, El-Sayed, and El-Saka, 2007), then generalized Lotka-Volterra model of fractional type was taken into account in (Samardzija and Greller, 1988), two-preys and one predator was also surveyed in (Elettreby, Al-Raezah, and Nabil, 2017). However, one of the recent studies around the fractional three species Lotka-Volterra model utilized the Caputo-Fabrizio operator, a non-singular definition, unlike the Caputo operator found in (Khalighi et al., 2021).

Most of the models reviewed above mentioned either predation or competition in a model. In contrast, according to empirical and theoretical ecologists, cooperation of competition and predation play an essential role in a model. Roughly speaking, killing and eating species by predators while other predators eat some predators is known as "intraguild predation (IGP)," trophic level omnivory", "higher order predation," or "hyperpredation" (superpredator).

One of the role returns to the impact of predation and competition on the presence and exclusion of species in a model. The second role is about the influence of the dynamic behavior of the model. For instance, in a classical Lotak-Volterra model with IGP (which is the simplest model), limit cycles, and chaotic behavior have been exhibited.

For three species with IGP, the shared resource, intermediate predator, and top predator are called prey, IG prey, and IG predator. (Polis and Strong, 1996), (Holt

and Polis, 1997) and references therein. Based on the above, a prey-predator and superpredator model is considered an IGP model.

One excellent local analysis of such these systems can be observed in (Hsu, Ruan, and Yang, 2015), in which authors considered a classical three species Lotka-Volterra model with IGP. They investigated the non-dimensional model and categorized the parameter space into three categories consisting of eight cases. They showed that species of five cases are extinct while the three others can persist. Then for the cases including coexistence, they proved the existence of periodic solutions due to Hopf bifurcation.

In another work, B. Roy and S. K. Roy (Roy and Roy, 2015) considered the prey-predator-superpredator model in which a Holling type II functional response describes the prey interaction with the predator. In contrast, the relationship between prey and predator is given by Holling type III functional response. An example of such a model in ecology is obtained by Diatom (prey), Daphnia (predator), and Channa (superpredator). In addition, in another work, they analyzed (Roy and Roy, 2016) three species of prey predator and superpredator in the mode of fishery model with predator harvesting and prey refuge and migration. They found out that when the model followed by Holling II functional response for prey, it admitted Hopf bifurcation, and they derived the global asymptotic stability of interior equilibrium in the system.

In another model worked recently (Savitri and Panigoro, 2020), authors discussed three species of prey-predator-superpredator, considered consumption of prey-predator by Holling II and predator-superpredator with Holling III. The authors also showed that in the system, equilibria consisting of extinction of prey and predator are unstable, whereas superpredator extinction point and coexistence point are conditionally stable. They proved that two bifurcations, including forward and Hopf bifurcations, occur. In other words, the first occurs around superpredator extinction, while the latter occurs around the model's interior.

Recently, local analysis of three species models containing IGP and emphasizing species features has been widely considered. For example, in a recent attempt, Kumar and Kumari (Kumar and Kumari, 2020) considered a three-species model with fear effect and equipped with Holling type II functional responses. They proved that increasing the fear effect leads to stability of the system, while for the low cost of fear effect the model remains chaotic.

More recently, Cong and coauthors (Cong, Fan, and Zou, 2021) investigated a three-species of IGP. Indeed, they first considered a classical model of three species with IGP, then extracted the predator's functional response due to the classical Holling's time budget argument. They proved how the fear effect could stabilize the system.

We conclude our review of the **GLV** systems, mentioning the role of delay in the emergence of feasible and stable steady states on **GLV**, which contains all possible interaction types (prey-predator, mutualism, competition, and others) considered in (Saeedian et al., 2021). And finally, a large ecosystem (food web) with n species (Lotka-Volterra model) by applying a large random matrix which accounts for the interaction between species was considered by (Akjouj and Najim, 2021).

1.2 Reaction diffusion of Three Species

In reaction-diffusion systems, different types of coherent structures can be observed, like Turing patterns, standing waves, oscillating patterns, spiral waves, and many others.

Turing patterns are considered an important class of structures called self-organization. This class of systems only takes place far from equilibrium. Diffusion plays a vital role in the appearance of self-organization. The worthwhile achievement *" diffusion driven instability"* known as Turing pattern proposed in 1952 (Turing (1952)).

As Levin stated: *Landscapes and seascapes are not homogeneous, but is in general a shifting mosaic of diverse units* (Levin and Segel, 1985). Indeed, in ecology interaction between species can lead to patterns or enhance them, this idea was suggested by some authors (Levin, 1976; Levin, 1981), Whittaker and Levin (Whittaker and Levin, 1977), Paine and Levin (Paine and Levin, 1981).

For the first time in 1972, Segel and Jackson (Segel and Jackson, 1972) proposed that Turing's idea (1952) (Turing (1952)) might work for reaction-diffusion systems in ecology. Indeed they considered the model:

$$\begin{aligned} \frac{dV}{dt} &= V(K + \alpha V - \beta E) + D_v \nabla^2 V, \\ \frac{dE}{dt} &= E(-L + \gamma V - \delta E) + D_E \nabla^2 E, \end{aligned} \tag{1.2}$$

where V, E denoted prey and predator species, and all parameters were considered positive. They proved that the coexistence steady state could be unstable. Then in 1974, Levin (Levin, 1974) figured out the same results for the model above when the sign of parameters δ and α were reversed. In 1976, by employing an approximation method and multiple-time scale theory, Segel and Levin (Segel and Levin, 1976) improved the nonlinear small amplitude theory.

Nevertheless, the presence of diffusion cannot always ensure the emergence of Turing patterns. For example, in a competitive Lotka-Volterra model of two species with self-diffusion, the Turing pattern does not occur. Indeed, self-diffusion explains the tendency of movement of species from high density to low density, while cross-diffusion implies the direction of movement of one species due to the presence of other species.

A milestone in the application of the nonlinear cross-diffusion concept for the explanation of biological and ecological phenomena was represented by the work of Shigesada, Kawasaki and Teramoto (Shigesada, Kawasaki, and Teramoto, 1979). In the formulation of their model, they were motivated by the attempt of explaining the segregation of competing species. Competing species cannot be classified as an activator-inhibitor system and, therefore, classical Turing theory is not able to explain the emergence of coherent structures. In SKT theory, therefore, cross-diffusion arised as an attempt at going beyond Turing theory. The 1979 SKT theory was indeed a success. For example, 1996, Chattopathya and coauthors (Chattopadhyay, Sarkar, and Tapaswi, 1996) showed that, in competitive **LV** system, cross-diffusion is able to cause the emergence of patches. In (Raychaudhuri, Sinha, and Chattopadhyay, 1996), they also investigated the effect of time-varying cross-diffusion. Emergence of Turing patterns and traveling front of the SKT model in 1D and 2D, respectively, were investigated by Gambino and coauthors (Gambino, Lombardo, and Sammartino, 2012), (Gambino, Lombardo, and Sammartino, 2013). Indeed, they first locally investigated the model's coexistence steady state, and they next found necessary conditions for appearance of stationary Turing patterns; they then approximated the amplitude of the patterns by weakly nonlinear analysis.

We now pass to give some account on the work on multispecies (we shall mainly focus on three-species) **LV** systems with diffusion.

In 1982, Kishimoto (Kishimoto, 1982) particularly investigated the presence of

stable spatially non-constant equilibrium in three examples of three species **LV**systems with self-diffusion of all species. He examined three examples including, competitive **LV**, one predator-two competing prey, and two predators-one prey systems. For these specific examples, only one of them admitted necessary conditions of Turing patterns.

And in the following work, Kishimoto and coauthors (Kishimoto, Mimura, and Yoshida, 1983) explored the local stability condition of classical **LV** systems to obtain the Hopf threshold. And using the condition, they proved the existence of stable Spatio-temporal oscillations in classical **LV** systems coupled with self-diffusion of all species.

Simultaneously, Ermentrout and Lewis (Ermentrout and Lewis, 1997) studied the mechanism of formation of spatial patterns in the three species model of **LV** type, consisting of diffusion of only one specie.

In 2000, the role of cross-diffusion in 3×3 Lotka-Volterra competitive model was examined which showed the existence of non-constant steady state (Lou, Martínez, and Ni, 2000).

Later the interest in cross-diffusion systems was motivated by the fact that cross-diffusion has been observed in multi-species systems derived from ecology or biochemistry (Okubo and Levin, 2001; Gurtin, 1974). Furthermore, an investigation of the role of diffusion in the competitive system of Lotka-Volterra for three species was presented in (Martínez, 2003).

B. Spangolo and coauthors (Spagnolo, Fiasconaro, and Valenti, 2003) investigated the time evolution of the Lotka-Volterra model of two preys and one predator with noise phenomena. They found out that for the system of two prey and one predator, the time evolution of the spatial patterns is strongly dependent on the initial conditions of the three species.

A reaction-diffusion system of three species in which the system implied a food chain with prey-dependent and ratio-dependent functional responses and cross-diffusion was considered in (Wang, 2004). Some conditions of local asymptotically stable equilibrium of the system and global existence, bifurcation of non-constant positive steady state, and occurrence of Turing pattern were also obtained. They proved that the stationary patterns' appearance arose solely from the effect of cross-diffusion.

Surveying on strategy and stationary patterns continued for the system of two predators and one prey with cross-diffusion where functional responses were Holling type II (Pang and Wang, 2004). Also, a non-Lotka-Volterra type food chain model with cross-diffusion was presented in (Wang, 2006). In addition, stability and Hopf bifurcation for a delayed prey-predator of two species with the effect of diffusion were studied in (Yan, 2007).

Further, the existence of global solutions for a three-species predator-prey model of Lotka-Volterra type with cross-diffusion was proved in (Pang and Wang, 2008). While bifurcation, chaos, and a traveling wave of a three-species Lotka-Volterra food chain with spatial diffusion and time delay demonstrated in (Cai et al., 2010, Gan et al., 2010), and global and asymptotic stability of positive equilibria of three species Lotka-Volterra mutualism and food chain models with diffusion and time delay analyzed in (Wang et al., 2010, Ma, Li, and Yan, 2012).

Recently, the interaction of three species of the predator-prey system included an impulsive diffusion and Beddington-DeAngelis response was considered, and asymptotic behavior of nonnegative solution for three species and some conditions of permanence and extinction of species were presented (Li, Guo, and He, 2013).

Then, in 2011, a work (Tian, Ling, and Lin, 2011) on a prey-predator mutualist system of three species was investigated. The necessary conditions for performing Turing patterns in cross-diffusion presence were reported.

Moreover, the other work in 2012 authors (Xie, 2012) surveyed the impact of cross-diffusion in a system of three species of food chain model. In addition, the food chain model of three species with diffusion and time delay was considered to investigate the existence of a traveling wave solution (Du and Xu, 2012). Nevertheless, in 2013 (Lv, Yuan, and Pei, 2013), a reaction-diffusion model of the Lotka-Volterra type of generalist predator system of three species with cross-diffusion was taken to prove the appearance of Turing patterns.

In the paper (Tian, Ling, and Lin, 2014), authors considered a food chain model of three species with cross-diffusion to prove the appearance of Turing patterns. While in 2014 (Kuwamura, 2015), the necessary conditions of stationary and oscillatory Turing patterns were investigated in the prey-predator system of two and three species affected by predator dormancy and self-diffusion. In addition, they obtained transient, Spatio-temporal complex patterns. In another three-species food chain system containing Holling II, functional response coupled with cross-diffusion, Turing instability, and limit cycles, and chaos were illustrated (Haile and Xie, 2015).

Recently, the appearance of Hopf bifurcation and Spatio-temporal patterns of three species of food chain model of Lotka-Volterra type in the presence of self and cross-diffusion were studied by (Ma, Li, and Wang, 2017).

Additionally, a model of three species Lotka-Volterra type was considered in which two species are cooperative, and one is competitive with two others. The authors studied the nonlinear stability of traveling wavefronts for the model (Ma, Wu, and Yuan, 2017).

As long as, Rosenweig-MacArthur predator-prey model is well-known as a simple model which exhibits very rich dynamics, diffusive models of these models have been recently investigated, e.g., in 2020, Rosenweig-MacArthur predator-prey models of the food chain of two and three species with self-diffusion were studied; the authors examined stationary and cyclic coexistence steady states of the system and they then obtained how each species' diffusion could affect the ODE system's oscillation and stability (Wang et al., 2021).

More recently, front-Back-Pulse solutions of a three-species competitive Lotka-Volterra model coupled with diffusion systems have been investigated in (Chang and Chen, 2021).

Nevertheless, studies around three specie reaction-diffusion models containing intraguild predation (**IGP**) with different types of ODEs have not been attended to as well as other types. For instance, Mukherjee and coauthors Mukherjee, Ghorai, and Banerjee, 2019 studied a three-species food chain model including IGP, equipped with Holling type II functional responses and coupled with self-diffusion of all species. They employed linear analysis to obtain the Turing threshold. They exhibited grazing patterns of both IG prey and IG predator. Then, using weakly nonlinear analysis, they determined the amplitude of the patterns.

However, one of the latest studies around pattern formation of IGP models can be found in (Han, Dai, and Chen, 2019). In this paper, the authors studied a modified version of the model (Holt and Polis, 1997) with self-diffusion. Indeed, the authors added a nonlocal interaction term to the resource equation. An equation of one specie with nonlocal interactions is defined as:

$$u_t = Du_{xx} + ru(1 - \frac{\Phi_\delta * u}{K}), \quad t > 0 \text{ and } x \in \mathbb{R}, \tag{1.3}$$

where D is the diffusion coefficient, r and K are the intrinsic growth rate and carrying capacity of the resource, and $*$ indicates spatial convolution, and $\int_{-}^{+} \Phi_\delta(y)dy = 1$, (more information can be found in Han, Dai, and Chen, 2019 and references therein). They locally investigated the model and found the Hopf threshold. Employing linear analysis, the necessary conditions of the Turing pattern were obtained. They then studied the influence of nonlocal interaction terms in the emergence of transient patterns from stationary Turing to non-stationary oscillatory patterns and even the appearance of chaotic patterns.

Chapter 2

A Lotka-Volterra three species model: pattern formation and oscillation

The Lotka-Volterra system is the simplest mathematical model of predator-prey interaction as it assumes there is only quadratic interaction between species. For n species it can be written in the following form (Krikorian, 1979):

$$\dot{u_i} = u_r(e_i + \sum_{i=1}^{n} p_{ij}u_j), \quad i, j = 1, 2, ..., n. \tag{2.1}$$

where $u_i(t)$ indicates population densities and $(e_i + \sum_{i=1}^{n} p_{ij}u_j)$ denotes populations growth coefficients, and the following assumptions hold:
i) the dominant term for each species is the birth/death rate, which can be showed by intraspecific interaction;
ii) there is a food chain from an unlimited resource;
iii) if the presence of the population u_i enhances the growth of the population u_j, then the presence of the population u_j inhibits the growth of the population u_i (predator-prey interaction).

The case $n = 2$ has been extensively studied using the theory of monotone dynamical system. For example, (Coste, Peyraud, and Coullet, 1979; Gopalsamy, 1982) studies two species competing Lotka-Volterra models. And also (Křivan, 2007; Deng et al., 2019) can be taken into account as predatory models of **LV** when $n = 2$.

Since 1970's the case $n = 3$ has been addressed (for instance see (Chauvet et al., 2002, Pekalski and Stauffer, 1998, Baek, 2008), classifying the system according to the different possible interactions between the three species.

In specific, in 1979, Krikorian (Krikorian, 1979) classified three species Lotka-Volterra model into four classes consisting of 34 cases:
i) Food chain, (Figure 2.1A)
ii) Two predators- one prey, (Figure 2.1B),
iii) One predator- two preys, (Figure 2.1C),
and Loops,
In which the loop classes were divided into two subclasses (Hsu, Ruan, and Yang, 2015):
iv) Food chain with omnivory, (Figure 2.1D),
v) Food chain with cycle, (Figure 2.1E).
In (Figure 2.1) u_1, u_2, u_3 denotes to species of different trophic levels. Therefore, in the food chain i) there is only one direction between two species of different trophic levels which means that u_1 is resource for primary consumer u_2 and u_3 is a secondary

consumer of u_2. Class (ii) implies two predators (u_2, u_3) of different trophic levels are competing for one resource (u_1). And simultaneously, (iii) indicates that two preys (u_1, u_2) of different trophic levels are resources of one predator (u_3). Class iv describes not only u_2 and u_3 are competing for u_1 but also u_2 is eaten by u_3, hence u_3 is called omnivore, since it eats all existence species. Finally, v implies u_2 eats u_1, and is eaten by u_3 while u_3 is eaten by u_1.

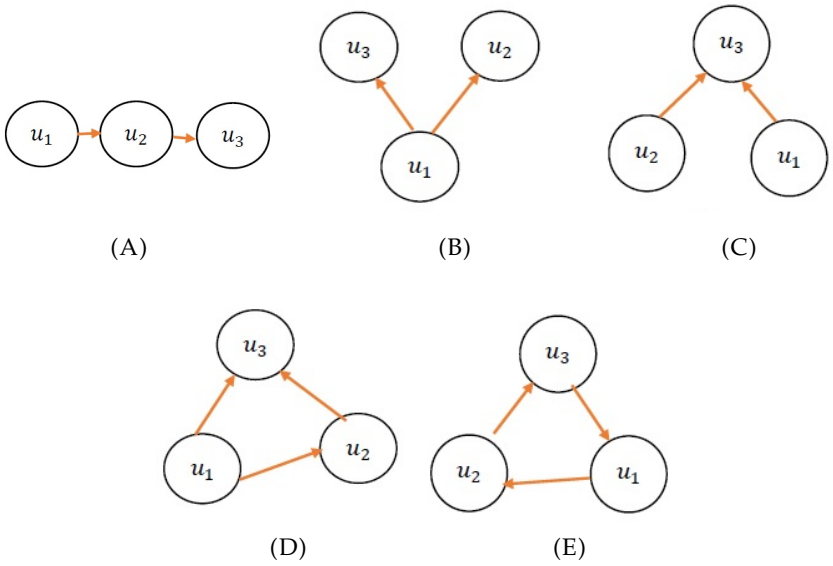

FIGURE 2.1: *(Hsu, Ruan, and Yang, 2015, Fig. 1.1) All possible schematic diagrams of the direct and indirect interactions among three species predator–prey systems. The arrows present the directions of biomass. (A) Food chain; (B) two predators–one prey; (C) one predator–two preys; (D) food chain with omnivory; and (E) food chain with cycle.*

In general, feeding relationships in communities are clarified in three ways: The first is the classical food web which is a schematic description of trophic connections (Krikorian, 1979). The second quantifies energy or mass flow. And finally, intraguild or functional webs experimentally identify strong links. Roughly speaking, to make a simple food web, we only need to recognize "what eats what?". In contrast, we need experimental manipulations or qualitative measurements to construct a food web of interactions or energy flow (Holt and Polis, 1997).

2.1 Intraguild predation(IGP)

In this chapter we will analyze a three species model characterized by intraguild predation. Intraguild predation is a way to consider both competition and predation effect in a community. In this case a predator kills and eats a prey, and also uses the same resource of the prey, so that prey and predator are also competitors for the same prey. Intraguild predation is a particular case of omnivory (Polis and Holt, 1992; Polis, Myers, and Holt, 1989).

According to the (Flynn and Moon, 2011), intraguild predationar models are more possible to take place in lakes. As an example of aquatic intraguild predation, we can consider the food web of *Lake Kinneret* where predatory invertebrates are IG

prey and planktivorous fish is IG predators that both feed on herbivorous zooplankton (basal resource), namely planktivorous fish also eat the predatory invertebrates (Makler-Pick et al., 2017).

The second example denotes a terrestrial IGP model. In particular, in North America, coyotes, gray foxes, and bobcats take into account in the IGP model. Coyotes are considered intraguild predators that feed on gray foxes and bobcats. Indeed, the gray foxes imply an intermediate predator competing with Coyotes for bobcats (Fuller and York, 2000).

Polis and coauthors (Polis, Myers, and Holt, 1989) mentioned that intraguild predation could influence on distribution and evolution of species. This point can be observed in ecology; when wolves insert into the ecosystem (previous example), coyotes become intermediate predators whose mortality increase (Switalski, 2003).

2.1.1 Intraguild predation models

In the last few years, considerable attention has been paid to intraguild predation models.

First, we would like to cite some aquatic and terrestrial studies of three species including IGP. For instance, in 2000 Fedriani and coauthors (Fedriani et al., 2000) studied a terrestrial model of competition and intraguild predation among three sympatric carnivores. Some other terrestrial investigations can be found in (Moser and Obrycki, 2009; Recalde, Breviglieri, and Romero, 2020). And to notice to an aquatic example of three species IGP model, (Irigoien and Roos, 2011) investigated the role of intraguild predation in explanation of fish population, particularly, pelagic fish.

An experimental-ecological model of intraguild predation (Leung et al., 2015) has been presented that includes lionfish as venomous predators (invasive) grouper native species (that share niche with top IG predator(Lionfish) of the Indo-pacific ocean. They proposed a symmetric intraguild predation model to determine whether competition or/and predation have an essential role in the role of lionfish. Recently, another attractive aquatic model containing IGP has also been presented in (Tuckett et al., 2021).

Now, we survey the latest results around the IGP issue mathematical point of view. Although numerous types of three-species models have been investigated, few contain intraguild predation models (IGP). Here we mention some interesting studies around intraguild predation models.
In 2000, Diehl and Feibel (Diehl and Feißel, 2000) studied three species consisting of IGP and analyzed how the population growth of the shared resource influences the food web model. Indeed, they considered the model (2.2) proposed by (Holt and Polis, 1997). The authors analyzed the effect of enrichment (growing carrying capacity of the basal resource) on the food chain model with an omnivore. They approached two steps: in one step, they investigated how increasing carrying capacity could affect the possibilities of coexistence of the species. And in the second step, they comforted some predicted cases with experimental results. They figured out that IG prey may either promote or prevent the omnivore. They also found that, at most, four cases of invasibility and coexistence may occur by enrichment. Additionally, they reported that for stable equilibria of the system, enrichment provides that the basal resource's population density increases while the intermediate predator's population density is decreased.

The existence of chaos in the three-species food web model has been studied in many kinds of literature; Tanabe and Namba (Tanabe and Namba, 2005) investigated the impact of IG predators in destabilizing a system containing IGP. They

contradicted the attitude that a food web model including nonlinear functional responses contains chaotic dynamics since they proved the chaotic behavior of the Lotka-Volterra food web model with intraguild predation (Holt and Polis, 1997). Moreover, in another attempt (Namba, Tanabe, and Maeda, 2008), they found out how increasing diversity of predators consuming IG prey influences stabilizing the food web model.

Recently, in (Kang and Wedekin, 2013), authors considered two IGP models, one containing generalist IG predator and another having specialist IG predator. Moreover, the IGP models consisted Holling Type I functional response between basal resource and intermediate predator and the Holling type III functional response between IG prey and IG predator. They established sufficient conditions of extinction and persistence of all possible cases arising in the food web models.

More recently, Hsu and coauthors (Hsu, Ruan, and Yang, 2015) considered a three spices model of Lotka-Volterra in a food web by omnivory (2.2). Nondimensional form of the model is categorized into 8 cases dependent on the parameters and positivity conditions of equilibria, of which 5 cases are extinct. However, three others contain uniform persistence. They proved the existence of periodic solutions due to Hopf bifurcation and chaotic behavior. They demonstrated the boundary equilibria's global behaviors using Lyapunov and McGehee Lemma. In addition, they studied the boundedness of solutions.

Other studies around the local analysis of IGP models are reported as follows. An investigation of two consumers of one resource coupled with Beddington-DeAngelis functional response in (Hsu, Ruan, and Yang, 2013). Additionally, the other results paid attention to an IG predation model containing intraguild predator with time delay in (Leung et al., 2015) and delay in IG prey in (Shu et al., 2015), a mathematical model of IG predation with prey switching in (Wei, 2019), IGP food web model with strong Allee effect of basal resource (Bai et al., 2021), enhancement of biodiversity and rising complexity in food web due to intraguild predation in (Wang, Brose, and Gravel, 2019). Further, an fast-slow dynamic of intraguild predation with evolutionary effect has been considered (Shen, Hsu, and Yang, 2020). Moreover, uniqueness, boundedness, and non-negativity of solution of fractional order of intraguild predation model containing intraspecific interaction between IG prey and IG Predator have been investigated in (Panja, 2019). And one last investigation returns to studies about the effect of competitive exclusion in an IGP model coupled with Beddington-Deangelis functional response (Ji and Wang, 2022).

Motivated by (Holt and Polis, 1997) we considered the model of three species of Lotka-Volterra in food web containing IGP:

$$\begin{cases} s_t = \Gamma[r(1-\frac{s}{K})s - m_1u_1s - m_2u_2s], \\ u_{1t} = \Gamma[M_1u_1s - D_1u_1 - \gamma_1u_1u_2], \\ u_{2t} = \Gamma[M_2u_2s - D_2u_2 + \gamma_2u_1u_2], \end{cases} \tag{2.2}$$

where, $s(x,t)$, $u_1(x,t)$, $u_2(x,t)$ denote population densities of basal resource, IG prey (intermediate predator), and IG predator (top predator or superpredator). The resource reproduces logistically. All parameters are positive and Γ regulates the domain.

First, we analyzed the species extinction, then to conquer numerous parameters, a nondimensional form of the model has presented. In the nondimensional form, we have employed a linear analysis to explore local stability and instability regions. Further, we have investigated the existence of periodic solutions via Hopf bifurcation.

Within one last decade, more attention concerning diffusive IGP models can be found.

Some results (Durant, 2000, Lucas, Coderre, and Brodeur, 2000) have demonstrated that IG predator tendency is toward a higher density of habitat. In contrast, IG prey runs away created pressure by increasing predation in the higher quality region, and therefore tends to the area of marginal habitat. That is why D. Ryan and R. S. Cantrell (Ryan and Cantrell, 2015) introduced a model which contains IG prey employing a fitness-based dispersion scheme that is adequate for present local resources and reduces predation risk. Therefore their proposed model included Holling-type function responses and a cross-diffusion for IG prey equation to define a fitness-based scheme. Moreover, the existence of a global solution to the model was proved.
Later, Cantrell and coauthors (Cantrell et al., 2017) modified the former model utilizing Beddington-DeAngelis functional responses instead of the Holling type for more than 2D. They proved that this model is more realistic than the former model.

In 2016, a delayed reaction-diffusion consisting of IGP and equipped with functional response II was considered (Han and Dai, 2016). Spatio-temporal behavior and oscillation of the model due to Hopf bifurcation were exhibited.

Recently, a self-diffusion model of IGP containing Beddington-DeAngelis functional response with time delay has reported Spatio-temporal behavior (Han, Dai, and Wang, 2018). Regarding free boundaries, recent work (Zhang and Dai, 2019) investigated a free boundary diffusive IGP model. Moreover, some studies about two and more species of IGP in which local stability and emergence of patterns have investigated cab be found in (see Han, Dai, and Chen, 2019, Lin and Yang, 2018).

Finally, the latest attempt at diffusive IGP models surveyed Spatio-temporal dynamics induced by IG predator (Ji et al., 2022). Indeed they considered a diffusive IGP system. They found that when only IG predator diffuses, the system transformed into a semi-degenerated reaction-diffusion model. They have illustrated the system undergoes to spatially homogeneous oscillations, spatially nonhomogeneous oscillations, chaos, and transition between them.

This chapter is organized as follows: In section 2.2, we describe three species model of intraguild predation in dimensional form. In section 2.3, we prove that species cannot exist for infinite time. In section 2.4, first, the model (2.3) is rescaled. Based on new parameters of the nondimensional model, we determine the coexistence of fixed point and necessary conditions for positive equilibrium. Moreover, the region of existence of stable positive equilibrium is depicted. Further, we established Hopf instability conditions and region. Turing analysis of the IGP model is investigated in section 2.5. Some numerical results confirm the linear analysis of the model in section 2.6. Weakly nonlinear analysis is employed in section 2.7 to obtain amplitude arising in Turing pattern.

2.2 A diffusive model of three species of Lotka-Volterra with IGP

We propose the reaction-diffusion model (2.3). This model is classified in **IGP** models. Namely, this equation not only explains the competition between predator and superpredator for one prey but also the predator (IG prey) is hunted by the superpredator (IG predator). Additionally, the reaction and the diffusion parts both are nonlinear and also the diffusion part includes chemotaxis term. Consider the

PDE model:

$$\begin{cases} s_t = d_1\Delta s + \Gamma[r(1-\frac{s}{K})s - m_1u_1s - m_2u_2s], \\ u_{1t} = d_2\Delta u_1 + c_2\nabla.(u_1\nabla u_2)) + \Gamma[M_1u_1s - D_1u_1 - \gamma_1u_1u_2], \\ u_{2t} = d_3\Delta u_2 + \Gamma[M_2u_2s - D_2u_2 + \gamma_2u_1u_2], \end{cases} \tag{2.3}$$

With homogeneous Neumann boundary conditions, $X \in [0, l] \subset \mathbb{R}^+$ and s, u_1, and u_2 are prey, IG prey and IG predator (superpredator, top predator, or omnivorous) respectively. Moreover, the parameters explaining the food web as:
r: intrinsic birth rate of the prey that is positive and it means the population is able to reproduce.
D_1: is intrinsic death rate of predator and non negative.
D_2: is intrinsic death rate of superpredator and non negative.
D_1 and $D_2 > 0$ denote that the population will reduce unless the appropriate other species are present.
Moreover, other entries of reaction parameters illustrate the interaction between species in such ways:
K: is carrying capacity correspond to resource.
M_1: denotes the effect of the prey on the predator, and it is proportional to the population of the species and the values of M_1.
M_2: denotes prey effect on the superpredator and is proportional to the population of the species as well as the value of the M_2.
Finally, γ_1: implies nonnegative and effect of the superpredator on predator populations and γ_2 nonnegative, and implies is predator effect on superpredator populations. This term explains that superpredators eat both prey and intermediate predator.

In addition, d_1, d_2, d_3 imply correspondingly diffusion parameters of resource, IG prey, and IG predator which are positive. c_2 denotes to a positive cross-diffusion parameter. Further, species segregate in the two dimensions (although here our numerical results are obtained for 1D and only the global solution of the model is investigated in 2D) and reaction coupled with self-diffusion and nonlinear diffusion terms. The nonlinear term is known as the Chemotaxis term. In other words, the diffusion of the populations is explained asymmetrically when a chemotactic term is added to the system. Chemotaxis is described as the oriented migration of organisms under the influence of chemical substances (Hazelbauer, 1979), (Murray, 2001). In fact, in the IG prey equation, the term $\nabla.(u_1\nabla u_2)$ with positive sign explains that intermediate predator (u_1) migrates away from IG predator (u_2). In addition, the chemotaxis term is a sub-term of the cross-diffusion term $\nabla.(\nabla(u_1u_2))$, which states that species u_1 and u_2 move toward their gradient (with a negative sign) or away from their gradient (with a positive sign). The chemotaxis has an attractive effect which leads to agglomeration of particles Gajewski, Zacharias, and Gröger, 1998 that here are members of predators.

2.3 Extinction of the species

The system states (2.2) is type of prey-predator since $sign(\frac{\partial s}{\partial u_i})$, $sign(\frac{\partial u_i}{\partial s})$ and $sign(\frac{\partial u_1}{\partial u_2})$, $sign(\frac{\partial u_2}{\partial u_1})$ are opposite. And since the system includes of $sign(\frac{\partial u_1}{\partial s})$,

$sign(\frac{\partial u_2}{\partial s})$ have the same sign, the system (2.3) considered as competition one. We first show that each coordinate plane is invariant with respect to the system according to the theorem below.

Theorem 2.3.1 *(Chauvet et al., 2002, page 246) Let S be a smooth closed surface without boundary in R^3 and*

$$\begin{aligned} \frac{ds}{dt} &= f_1(s, u_1, u_2), \\ \frac{du_1}{dt} &= f_2(s, u_1, u_2), \\ \frac{du_2}{dt} &= f_3(s, u_1, u_2). \end{aligned} \tag{2.4}$$

where f_1, f_2, f_3, are continuously differentiable. Suppose that $\boldsymbol{n}$ is a normal vector to the surface S at (s, u_1, u_2), and for all $(s, u_1, u_2) \in S$ we have that

$$\boldsymbol{n}.\langle \frac{ds}{dt}, \frac{du_1}{dt}, \frac{du_2}{dt} \rangle = 0,$$

Then S is invariant with respect to the system (2.4).

Here, we apply the method mentioned in Chauvet et al., 2002. Let S be the plane $s = 0$ since the vector $(1, 0, 0)$ is always normal on the plane $s = 0$, we have

$$(1, 0, 0).\langle 0, \frac{du_1}{dt}, \frac{du_2}{dt} \rangle = 0,$$

Thus, similarly it is shown that each coordinates plane is invariant.

Next, we solve each of the three corresponding planar (two variables) systems in the respective coordinate planes. We notice that in absence of prey $s = 0$ the system (2.4) is reduced to

$$\begin{aligned} \frac{ds}{dt} &= 0, \\ \frac{du_1}{dt} &= -D_1 u_1 - \gamma_1 u_1 u_2, \\ \frac{du_2}{dt} &= -D_2 u_2 + \gamma_2 u_1 u_2. \end{aligned} \tag{2.5}$$

In which the only possible fixed point for the system of predator and superpredator is $(0, 0)$ that is stable. Therefore, $\frac{du_2}{dt} \leqslant -D_2 u_2$ gives $u_2 \to 0$ exponentially as $t \to \infty$ and consequently $\frac{du_1}{dt} = -D_1 u_1$, so $u_1 \to 0$ exponentially as $t \to \infty$. That makes sense when in the absence of the prey, the predator and consequently the superpredator extinct.

Moreover, in the plane $u_1 = 0$, the system is

$$\begin{aligned} \frac{ds}{dt} &= \gamma s(1 - \frac{s}{K}) - m_2 u_2 s, \\ \frac{du_1}{dt} &= 0, \\ \frac{du_2}{dt} &= M_2 u_2 s - D_2 u_2. \end{aligned} \tag{2.6}$$

In fact, in this case the system is the same as classical Lotka-Volterra, and it has two equilibrium points $(0,0)$, $\left(\frac{D_2}{M_2}, \frac{\gamma}{m_2}(1 - \frac{D_2\gamma}{KM_2})\right)$. Then

$$\frac{ds}{dt} \leqslant \gamma s(1 - \frac{s}{K}),$$

while in the case of equality there is Bernoli DE whose answer is

$$s(t) = \frac{K}{Kce^{-\gamma t} + 1},$$

for all constant c, so

$$s(t) \leqslant \frac{K}{Kce^{-\gamma t} + 1},$$

then $s \to K$ as $t \to \infty$, that shows s is bounded. In following, we have $\frac{du_2}{dt} \leqslant u_2(M_2 s - D_2)$, hence $u_2(t) \leqslant u_2(0)\exp(M_2 K - D_2)t$ which states that if $M_2 K - D_2 < 0$, then $u_2(t) \to 0$ exponentially as $t \to \infty$. It means that when there is not predator, the superpredator gradually extincts under this condition. Similar arguments obtained for the plane $u_2 = 0$. In summary, in this system all species eventually extinct.

2.4 Analysis of the nondimensional system

Consider the model (2.3), where we again emphasize that all parameters are positive and $X \in [0, l]$, s, u_1, u_2 are population densities of species, how s is basal resource, u_1 is an intermediate consumer and u_2 is omnivorous predator. We rescale the system (2.3) with:

$$X = \sqrt{\frac{d_2}{\Gamma r}}x, \quad t = \frac{1}{\Gamma r}\tau, \quad s = Ku, \quad u_1 = \frac{r}{m_1}v, \quad u_2 = \frac{r}{\gamma_1}w,$$

to obtain the following non dimensional form:

$$\begin{cases} \frac{du}{d\tau} = d_u \frac{\partial^2 u}{\partial x^2} + u(1 - u - v - \eta w), \\ \frac{dv}{d\tau} = \frac{\partial^2 v}{\partial x^2} + d(\frac{\partial v \partial w}{\partial x \partial x} + v\frac{\partial^2 w}{\partial x^2}) + v(-n_1 + \alpha u - w), \\ \frac{dw}{d\tau} = d_w \frac{\partial^2 w}{\partial x^2} + w(-n_2 + \gamma u + \delta v), \end{cases} \tag{2.7}$$

where:

$$\eta = \frac{m_2}{\gamma_1}, \quad n_1 = \frac{D_1}{r}, \quad n_2 = \frac{D_2}{r}, \quad \alpha = \frac{KM_1}{r}, \quad \gamma = \frac{KM_2}{r}, \quad \delta = \frac{\gamma_2}{m_1},$$

and:

$$d_u = \frac{d_1}{d_2}, \quad d_w = \frac{d_3}{d_2}, \quad d = \frac{c_2 r}{d_2 \gamma_1},$$

System (2.7) admits the trivial equilibrium, $E_0 = (0,0,0)$, and three non-negative semi-trivial equilibria: $E_u = (1,0,0)$, $E_{uv} = (\frac{n_1}{\alpha}, \frac{\alpha - n_1}{\alpha}, 0)$ when $\alpha > n_1$, $E_{uw} = (\frac{n_2}{\gamma}, 0, \frac{\gamma - n_2}{\gamma\eta})$ when $\gamma > n_2$. System (2.7) also admits the coexistence point $E^* = (u^*, v^*, w^*)$, with:

$$u^* = \frac{n_1\delta\eta + (\delta - n_2)}{\delta(\alpha\eta + 1) - \gamma}, \quad v^* = \frac{(n_2 - \gamma) - \eta(\gamma n_1 - \alpha n_2)}{\delta(\alpha\eta + 1) - \gamma}, \quad w^* = \frac{\delta(\alpha - n_1) + (\gamma n_1 - \alpha n_2)}{\delta(\alpha\eta + 1) - \gamma}, \tag{2.8}$$

Before discussing the positivity of the equilibrium E^*, it can be proven that, if the mortality rate n_1 is greater than the conversion rate α, then the species v becomes extinct for any positive initial condition (u_0, v_0, w_0) (see Hsu, Ruan, and Yang, 2015, Prop. 2.4). Since we are interested in scenarios supporting the coexistence of all three species, from now on we will assume:

$$\alpha > n_1, \tag{2.9}$$

which implies that $\alpha > 0$. Under the assumption in (2.9), we now discuss the positivity of the equilibrium E^*. By imposing that numerator and denominator of u^*, v^* and w^*, given in (2.8), are both positive or both negative, one gets:

i) If $n_1 < \alpha$, one of the following systems must be satisfied:

$$i.b) \begin{cases} \delta > \dfrac{\gamma}{1 + \alpha\eta}, \\ \delta > \dfrac{n_2}{1 + n_1\eta}, \\ \gamma < \dfrac{n_2(1 + \alpha\eta)}{1 + n_1\eta}, \\ \delta > \dfrac{-n_1\gamma}{\alpha - n_1} + \dfrac{\alpha n_2}{\alpha - n_1}, \end{cases} \tag{2.10}$$

$$i.a) \begin{cases} \delta < \dfrac{\gamma}{1 + \alpha\eta}, \\ \delta < \dfrac{n_2}{1 + n_1\eta}, \\ \gamma > \dfrac{n_2(1 + \alpha\eta)}{1 + n_1\eta}, \\ \delta < \dfrac{-n_1\gamma}{\alpha - n_1} + \dfrac{\alpha n_2}{\alpha - n_1}, \end{cases} \tag{2.11}$$

In order to display the conditions given in (2.10), and (2.11) in the plane (γ, δ), we define the following lines:

$$\begin{aligned} s_d: &\quad \delta = \frac{\gamma}{1+\alpha\eta}, \\ s_u: &\quad \delta = \frac{n_2}{1+n_1\eta}, \\ s_v: &\quad \gamma = \frac{n_2(1+\alpha\eta)}{1+n_1\eta}, \\ s_w: &\quad \delta = \frac{-n_1\gamma}{\alpha-n_1} + \frac{\alpha n_2}{\alpha-n_1}, \end{aligned} \tag{2.12}$$

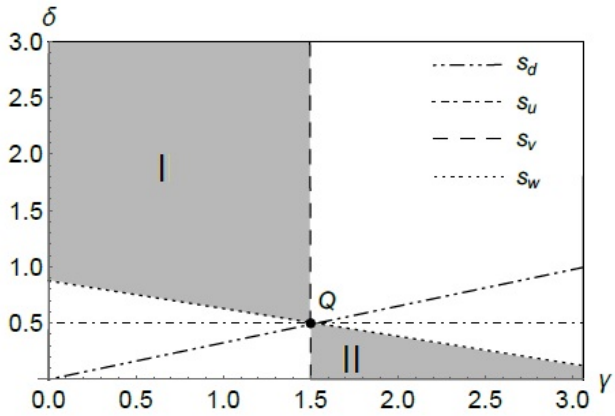

FIGURE 2.2: In the plane (γ, δ), the colored regions show where the positive equilibrium E^* exists. The region I corresponds to the case (2.10), the region II corresponds to the case (2.11). Parameters are fixed as $n_1 = 0.5$, $n_2 = 0.7$, $\alpha = 2.5$, $\eta = 0.8$, $d_u = d = d_w = 0$.

which intersect at the point

$$Q \equiv (\gamma_Q, \delta_Q) = \left(\frac{n_2(1+\alpha\eta)}{1+n_1\eta}, \frac{n_2}{1+n_1\eta}\right). \tag{2.13}$$

In case *i)*, both the systems in *i.a)* and *i.b)* are compatible: in particular, the solution of the system in *i.a)* corresponds to region I in (Figure 2.2) and the solution of the system in *i.b)* corresponds to region II in (Figure 2.2). Notice that the boundaries of regions I and II are just the lines s_v and s_w for any parameters choice. We therefore state:

Proposition 2.4.1 *Let the conditions* (2.10) *or* (2.11) *hold. Then, the system* (2.7) *admits the positive steady state* E^* *defined in* (2.8).

We now analyze the stability of E^* under the conditions of Proposition 2.4.1. The system (2.7), linearized in the neighborhood of E^*, is:

$$\dot{\mathbf{w}} = K\mathbf{w} + D\frac{\partial^2 \mathbf{w}}{\partial x^2}, \quad \mathbf{w} = \begin{bmatrix} u-u^* \\ v-v^* \\ w-w^* \end{bmatrix}, \tag{2.14}$$

where:

$$K = \begin{bmatrix} -u^* & -u^* & -\eta u^* \\ \alpha v^* & 0 & -v^* \\ \gamma w^* & \delta w^* & 0 \end{bmatrix}, \quad D = \begin{bmatrix} d_u & 0 & 0 \\ 0 & 1 & dv^* \\ 0 & 0 & d_w \end{bmatrix}, \tag{2.15}$$

We first investigate the local stability of the positive equilibrium E^* when $d_u = d = d_w = 0$. The characteristic polynomial of the matrix K, given in (2.15), reads:

$$\begin{aligned} &\mathcal{P}(\lambda) = \lambda^3 + P_2\lambda^2 + P_1\lambda_1 + P_0, \\ &P_2 = u^*, \quad P_1 = \alpha u^* v^* + \delta v^* w^* + \gamma\eta u^* w^*, \quad P_0 = ((1+\alpha\eta)\delta - \gamma)u^* v^* w^*, \end{aligned} \tag{2.16}$$

We can express the coefficients of the characteristic polynomial $\mathcal{P}(\lambda)$ in terms of the eigenvalues λ_i, $i = 1, 2, 3$, as follows (Brooks, 2006):

$$P_2 = -(\lambda_1 + \lambda_2 + \lambda_3), \tag{2.17}$$
$$P_1 = \lambda_1\lambda_2 + \lambda_2\lambda_3 + \lambda_1\lambda_3, \tag{2.18}$$
$$P_0 = -\lambda_1\lambda_2\lambda_3, \tag{2.19}$$

We shall show that:
1. E^* is unstable in region II, therefore E^* can be stable only in region I;
2. in region I there may exist a curve along which E^* loses its stability via Hopf bifurcation.

According to the Routh-Hurwitz criterion, E^* is locally stable if

$$P_2, P_0 > 0, \text{ and } P_2P_1 - P_0 > 0, \tag{2.20}$$

where:

$$P_2P_1 - P_0 = -(\lambda_1 + \lambda_2)(\lambda_2 + \lambda_3)(\lambda_1 + \lambda_3), \tag{2.21}$$

P_2 is always greater than zero from its expressions in (2.16), therefore E^* can lose stability if $P_0 < 0$ or $P_2P_1 - P_0 < 0$. Since $P_1 > 0$ by (2.16), the two conditions $P_0 < 0$ and $P_2P_1 - P_0 < 0$ cannot hold together. The coefficient P_0 is negative below the line s_1 (and in particular in region II) and positive above the line s_1 (and in particular in region I), therefore E^* is unstable in region II and it can be stable in region I. The point 1. is thus proved.

In region I the equilibrium E^* is stable when $P_2P_1 - P_0 > 0$ and it is unstable when $P_2P_1 - P_0 < 0$. We now show that $P_2P_1 - P_0 = 0$ is the curve along which Hopf bifurcation occurs.

Using (2.19), the condition $P_0 > 0$ implies that the characteristic polynomial has at least one real negative root, which we denote λ_1, and the other two roots, λ_2 and λ_3, can be either real with the same sign or complex conjugate. Moreover, since $P_2 > 0$, using (2.17), $-\lambda_1 > \lambda_2 + \lambda_3$, therefore it follows that neither $\lambda_1 + \lambda_2$ nor $\lambda_1 + \lambda_3$ can be zero. Thus, by (2.21) we have that $P_2P_1 - P_0 = 0$ if and only if $(\lambda_2 + \lambda_3) = 0$, from which it follows that λ_2 and λ_3 are purely imaginary roots of the characteristic polynomial. This implies that $P_2P_1 - P_0 = 0$ is the condition for the occurrence of Hopf instability, the real part of λ_2 and λ_3 change from positive (when $P_2P_1 - P_0 < 0$) to negative (when $P_2P_1 - P_0 > 0$). The condition $P_2P_1 - P_0 > 0$ for the linear stability of E^* can be written as follows in terms of the system parameters:

$$F = u^*(\alpha v^* + \eta\gamma w^*) + (\gamma - \alpha\eta\delta)v^* w^*, \tag{2.22}$$

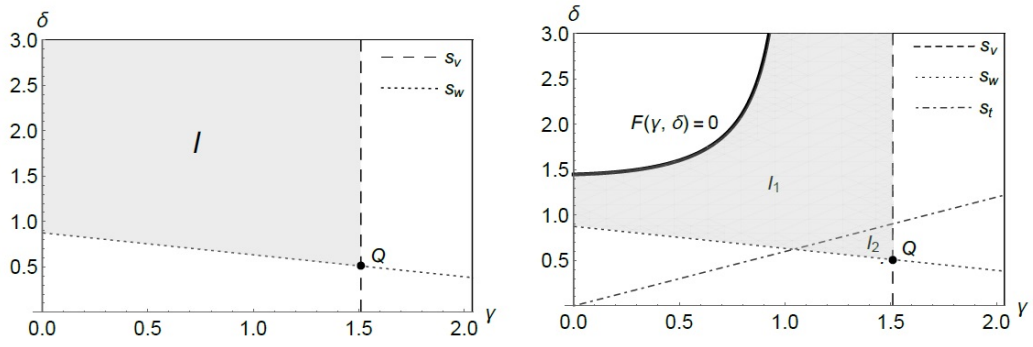

(A) $\eta = 0$ (B) $\eta \neq 0$

FIGURE 2.3: In grey the regions of the parameters in the plane (γ, δ) where the equilibrium E^* exists positive and locally stable. The parameter values are $n_1 = 0.5$, $n_2 = 0.7$, $\alpha = 2.5$, $d_u = d = d_w = 0$. In A) $\eta = 0$. In B) $\eta = 0.8$.

Recalling that $\alpha > 0$, the condition $F > 0$ given by (2.22) is always satisfied when $\eta = 0$, then Hopf bifurcation cannot occur and E^* is locally stable in the entire region I of Figure 2.2. We also observe that, when η is different from zero, the condition (2.22) is always verified below the line:

$$s_t : \quad \delta = \frac{\gamma}{\alpha\eta}, \tag{2.23}$$

Since the line s_t is above the line s_d, in the triangle region I_2, bounded by the lines s_d and s_t and shown in Figure 2.3B, Hopf bifurcation cannot occur and E^* is always locally stable. In Appendix A, we perform a detailed analysis of the Hopf instability curve $F = 0$ in the plane (γ, δ). Through this analysis, we show that only a branch of the curve $F(\gamma, \delta) = 0$ lies in the region I_1, as reported in Figure 2.3B. Moreover, in region I_1 the stability condition (2.22) is satisfied below this branch. We summarize the results of the above discussion in the following Propositions.

Proposition 2.4.2 *(Stability conditions). The coexistence equilibrium point E^*, whose coordinates are given in (2.8), is linearly stable when:*
1. $\eta = 0$ and conditions (2.10) hold (corresponding to region I in Figure 2.3A,
2. $\eta \neq 0$, conditions (2.10) hold and $F > 0$ hold, with F defined in (2.22) (corresponding to the regions I_1 and I_2 in Figure 2.3B.

Proposition 2.4.3 *(Hopf bifurcation). Let $\eta \neq 0$. The positive coexistence steady state E^*, whose coordinates are given in (2.8), loses its stability via a Hopf bifurcation along $F = 0$, with F defined in (2.22). In the plane (γ, δ) the Hopf bifurcation locus corresponds to the solid branch $F(\gamma, \delta) = 0$ in region I_1 shown in Figure 2.3B.*

2.5 Turing Instability

In this Section, we analyze the condition for the Turing instability in the neighborhood of E^*, which occurs when the locally stable equilibrium point becomes unstable due to the effect of the diffusion terms.

Looking for solutions of system (2.14) of the form $e^{ikx+\lambda t}$ leads to the following dispersion relation, which gives the eigenvalue λ as a function of the wavenumber

k:

$$\lambda^3 + P_2(k^2)\lambda^2 + P_1(k^2)\lambda + P_0(k^2) = 0, \tag{2.24}$$

where

$$\begin{aligned} P_2(k^2) &= k^2 tr(D) - tr(K), \\ P_1(k^2) &= (d_u + d_u d_w + d_w)k^4 + (u^*(1 + d_w) + dv^*w^*)k^2 + \alpha u^* v^* + \delta v^* w^* + \gamma\eta u^* w^*, \\ P_0(k^2) &= det(K + k^2 D) = p_3 k^6 + p_2 k^4 + p_1 k^2 + p_0, \end{aligned} \tag{2.25}$$

with

$$\begin{aligned} p_3(k^2) &= d_u d_w, \\ p_2(k^2) &= d_w u^* + \delta d_u d v^* w^*, \\ p_1(k^2) &= (d_u \delta v^* w^* + \gamma\eta u^* w^* + d_w \alpha u^* v^* + d(\delta - \gamma)u^* v^* w^*, \\ p_0(k^2) &= ((\alpha\eta + 1)\delta - \gamma)u^* v^* w^*, \end{aligned} \tag{2.26}$$

Spatial patterns arise in correspondence of those modes k for which $\mathcal{R}(\lambda) > 0$. Being $P_2(k^2); P_1(k^2) > 0$, according to the Routh-Hurwitz criterion the only way to have $\mathcal{R}(\lambda) > 0$ for some $k \neq 0$ in Figure (2.24) is when $P_0(k^2) < 0$. The coefficients p_3 and p_2 are positive. Being E^* stable for the kinetics, the conditions in proposition hold and then the coefficient p_0 is positive. In the following we compute the bifurcation threshold $d = d_c$ and the corresponding most unstable wavenumber k_c.

Case $\mathbf{d_u = d_w = 0}$. P_0 is the following linear polynomial in k^2:

$$P_0(k^2) = p_1 k^2 + p_0, \tag{2.27}$$

where $p_1 = \gamma\eta u^* w^* + d(\delta - \gamma)u^* v^* w^*$ and p_0 is as in (2.26). Since $p_0 > 0$, in order to have $P_0(k^2)$, for some $k > 0$, p_1 must be negative, which leads to the following conditions:

$$\begin{aligned} &\gamma > \delta, \\ &d > d_c := \frac{\gamma\eta}{w^*(\gamma - \delta)}, \end{aligned} \tag{2.28}$$

Therefore, if (2.27) and (2.28) are satisfied, then Turing instability occurs for all k such that:

$$k > k_c := \sqrt{\frac{((\alpha\eta + 1)\delta - \gamma)v^*}{\gamma\eta + d(\gamma - \delta)v^*}}, \tag{2.29}$$

However, conditions (2.28) and (2.29) do not ensure the formation of a Turing pattern because an infinite range of unstable wavenumbers is admitted. Namely, only diffusion and even cross-diffusion of the IG prey cannot guarantee to perform of the Turing pattern.

Case $\mathbf{d_w \neq 0}$ and $\mathbf{d_u = 0}$: $P_0(k^2)$ is the following second order polynomial in k^2:

$$\begin{aligned} & P_0(k^2) = p_2k^4 + p_1k^2 + p_0, \\ \text{where} \quad & p_2 = d_w u^*, \\ & p_1 = \gamma\eta w^* u^* + d_w \alpha u^* v^* + d(\delta - \gamma)u^* v^* w^*, \end{aligned} \tag{2.30}$$

and p_0 is as in (2.26). The minimum of P_0 is attained when:

$$k^2 = k_c^2 := \frac{-p_1}{2p_2}, \tag{2.31}$$

which requires $p_1 < 0$ and therefore from (2.30) we obtain the following conditions

$$\begin{aligned} & \gamma > \delta, \\ & d > \bar{d} := \frac{\gamma\eta w^* + d_w \alpha v^*}{(\gamma - \delta)v^* w^*}, \end{aligned} \tag{2.32}$$

which are necessary for Turing instability to occur.
Defining the quantities a and b as:

$$a = (\gamma - \delta)u^* v^* w^*, \quad b = \gamma\eta u^* w^* + d_w \alpha u^* v^*, \tag{2.33}$$

then $p_1 = -ad + b$. Introducing $d = \dfrac{b}{a} + \xi$ in P_0 one gets:

$$-\frac{\xi^2}{2p_2} + p_0 = 0, \tag{2.34}$$

whose positive roots ξ^+ gives the only critical value of the parameter d:

$$d_c = \frac{b}{a} + \xi^+, \tag{2.35}$$

Therefore Turing instability occurs for all $d > d_c$ given in (2.35). It means that when IG predator diffuses as well as IG prey, the model undergoes Turing instability.

Case $\mathbf{d_w = 0}$ and $\mathbf{d_u \neq 0}$. $P_0(k^2)$ is the following second order polynomial in k^2:

$$\begin{aligned} & P_0(k^2) = p_2k^4 + p_1k^2 + p_0, \\ \text{where} \quad & p_2 = \delta d d_u v^* w^*, \\ & p_1 = \delta d_u v^* w^* + \gamma\eta w^* u^* + d(\delta - \gamma)u^* v^* w^*,, \end{aligned} \tag{2.36}$$

and p_0 is as in (2.26). The minimum of P_0 is attained when:

$$k^2 = k_c^2 := \frac{-p_1}{2p_2}, \tag{2.37}$$

which requires $p_1 < 0$ and therefore from (2.36) we obtain the following conditions

$$\begin{aligned} & \gamma > \delta, \\ & d > \bar{d} := \frac{d_u \delta v^* + \gamma\eta u^*}{(\gamma - \delta)v^* u^*}, \end{aligned} \tag{2.38}$$

which are necessary for Turing instability to occur.

Defining the quantities a and b as:

$$a = (\gamma - \delta)u^*v^*w^*, \quad b = d_u\delta v^*w^* + \gamma\eta u^*w^*, \tag{2.39}$$

then $p_1 = -ad + b$. Introducing $d = \frac{b}{a} + \xi$ in P_0 one gets:

$$-\frac{\xi^2}{2p_2} + p_0 = 0, \tag{2.40}$$

whose positive roots ξ gives the only critical value of the parameter d:

$$d_c = \frac{b}{a} + \xi^+, \tag{2.41}$$

Therefore Turing instability occurs for all $d > d_c$ given in (2.41). In other words when the resource diffuses as well as IG prey, the model undergoes Turing instability.

Case $\mathbf{d_u d_w \neq 0}$. $P_0(k^2)$ is the third order polynomial in k^2 defined in (2.26). If $p_2^2 - 3p_3p_1 > 0$, then P_0 admits the following critical points:

$$k_M^2 = \frac{-p_2 - \sqrt{p_2^2 - 3p_3p_1}}{3p_3}, \quad k_m^2 = \frac{-p_2 + \sqrt{p_2^2 - 3p_3p_1}}{3p_3} \tag{2.42}$$

which are a local maximum and a local minimum, respectively. Notice that k_M^2 is always negative. For $P_0(k^2) < 0$, for some k, we must require $k_m^2 > 0$, which is satisfied if $p_1 < 0$. From the explicit expression of p_1 given in (2.26) we therefore derive the following two necessary conditions:

$$\begin{aligned} &\gamma > \delta, \\ &d > \bar{d} := \frac{d_u\delta v^*w^* + \gamma\eta u^*w^* + d_w\alpha u^*v^*}{(\gamma - \delta)v^*u^*w^*}, \end{aligned} \tag{2.43}$$

Under condition (2.43), the quantity $p_2^2 - 3p_3p_1$ is greater than zero and the typical graph of the curve $P_0(k^2)$ is given in Figure 2.4. Thus, the condition for the marginal stability is:

$$min(P_0(k_c^2)) = 0, \tag{2.44}$$

and the minimum of P_0 is attained when:

$$k_c^2 = k_m^2, \tag{2.45}$$

From conditions (2.44) and (2.45), both the bifurcation value $d = d_c$ and the corresponding most unstable wavenumber k_c can be computed.

Since (2.44), under (2.45), is a cumbersome expression in terms of d, we numerically solve the equation $P_0(k_m^2) = 0$ with respect to d. We have found that just two positive roots $d_1 < d_2$ satisfy the equation. However, via numerical inspection we have observed that only d_2 satisfies condition (2.43). Therefore, there exists only one Turing critical threshold $d = d_2 = d_c$, see Figure 2.4. In Figure 2.5 it is observed that how eigenvalues become positive and $P_0(k^2) < 0$ as wave number and bifurcation parameter d increase respectively.

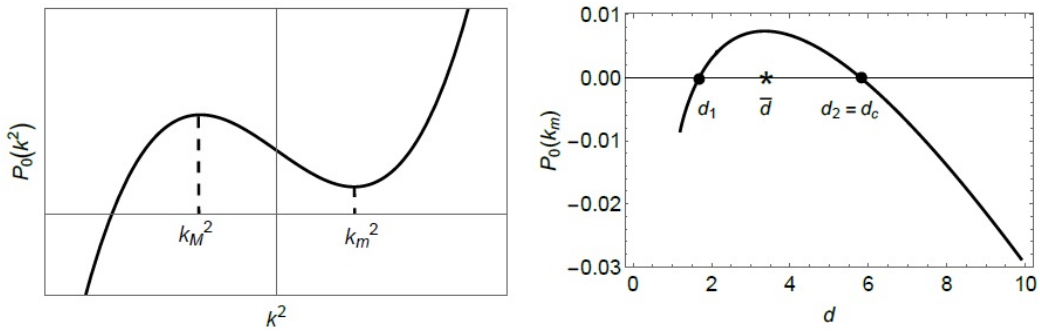

(A) (B) $P_0(k^2)$

FIGURE 2.4: In Panel A): the graph of $P_0(k^2)$ in the general case $d_u d_w \neq 0$. In Panel B): typical graph of $P_0(k_m^2)$, where P is the characteristic polynomial and k_m^2 is defined in (2.42). The parameter values are $n_1 = 0.5$, $n_2 = 0.7$, $\alpha = 2.5$, $\eta = 0.8$, $\gamma = 1.2$, $\delta = 0.6$, $d_u = 0.02$, $d_w = 0.04$.

Remark 2.5.1 *$p_1 < 0$ is a necessary condition for Turing instability. In absence of the cross-diffusion term ($d = 0$) the coefficient p_1 is always positive and Turing instability cannot occur. The only destabilizing effect is therefore the cross-diffusion $d > 0$. Hence, we will adopt d as the bifurcation parameter.*

Remark 2.5.2 . *If $\eta = 0$, condition (2.43) does not hold in region I_2, due to the first inequality in (2.10). Therefore, Turing instability cannot occur.*

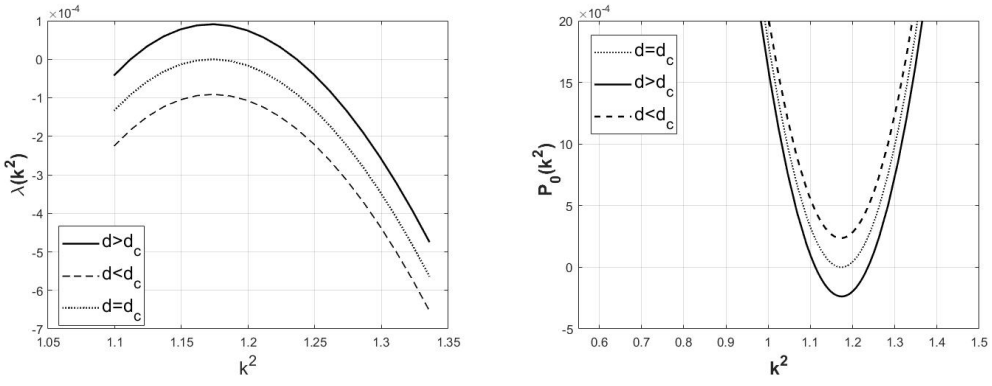

(A) $\lambda(k^2)$ (B) $P_0(k^2)$

FIGURE 2.5: A) Plot of eigenvalues when wavenumbers are in the interval $[k_M^2, k_m^2]$ as critical bifurcation d varies B) Plot of $P(k^2)$ as critical bifurcation parameter d varies. The parameter are given in Figure 2.4.

Remark 2.5.3 . *If $\eta \neq 0$, condition (2.43) can be satisfied in region I_2. In particular, when $\alpha\eta > 1$, the line $\delta = \gamma$ is above the line s_t and the condition (2.43) is satisfied in all the region I_2 implying that Turing instability can occur when the bifurcation parameter d is suitably chosen as we will discuss below.*

Remark 2.5.4 *If $\alpha\eta \leqslant 1$, Turing-Hopf instability cannot occur, in fact the line $\delta = \gamma$ is below the line s_t : $\delta = \dfrac{\gamma}{\alpha\eta}$ and the curve $F = 0$, lying in region I_1, cannot intersect $\delta = \gamma$*

and the necessary condition (2.43) *is not satisfied (see Figure 2.6C). Therefore, necessary condition for Turing-Hopf instability is* $\alpha\eta > 1$ *(see Figure 2.6B).*

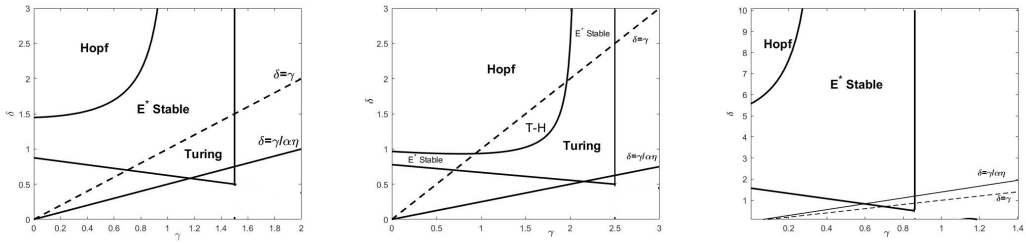

(A) (B) (C)

FIGURE 2.6: Hopf and Turing instability regions for increasing values of α. A) $\alpha = 2.5$, B) $\alpha = 5$, C) $\alpha = 0.9$. The other fixed parameter values are $n_1 = 0.5$, $n_2 = 0.7$, $\eta = 0.8$.

In the following, we analyze the dependence of Turing instability region with respect to all the system parameters.

In the Figure 2.7, the parameters are fixed as Figure 2.2 while only n_1 is varying in Figure 2.7A. It is observed that the Turing region is moving to the right side when the parameter n_1 is decreasing, i.e increase of death rate of the predator v deals to a large unstable area. However the Turing regions decline by rising up the parameter n_2 and it is also moved to the right side Figure 2.7B which means that enhancement of death rate of Predator w make a system more stable.

Another side, the growth rate of the predator concerning the prey varies such that by increasing the parameter value, the Turing region is decreased and shrieked (see Figure 2.7C). Similarly, the system's Turing region declines when the parameter η is enhanced (see Figure 2.7D). Simultaneously, as self-diffusion parameters d_u, d_w rise up Turing regions decreased in Figure 2.7E, Figure 2.7F.

In addition, Figure 2.6 demonstrates the stability and instability regions in parameter plane (γ, δ) such that the Turing region is displayed while the parameter α is varying and the Turing region is confined between two lines $\delta = \gamma$ and $\delta = \dfrac{\gamma}{\alpha\eta}$. It is obvious that Turing region is obtained when $\alpha\eta \geqslant 1$ Figure 2.6A, Figure 2.6B. There is Turing region when the slop of the line $\delta = \gamma$ is greater than the slop of the $\delta = \dfrac{\gamma}{\alpha\eta}$ and the Turing region is greater when the parameter α is increased. But there is no Turing region for $\alpha\eta < 1$ since the necessary condition $\gamma > \delta$ is not satisfied.

Remark 2.5.5 *For the sake of completeness, it remains to prove that* $P_2P_1 - P_0 > 0$ *in* (2.24). *Indeed if this condition were violated the system would admit a* ***Wave instability****. By simple calculations it is possible to show that the condition* $P_2P_1 - P_0 > 0$ (2.24) *and* (2.26) *is also true thanks to the stability conditions* $P_2P_1 - P_0 > 0$ *in* (2.21), *and then there is* ***No Wave Instability*** *without cross-diffusion terms.*

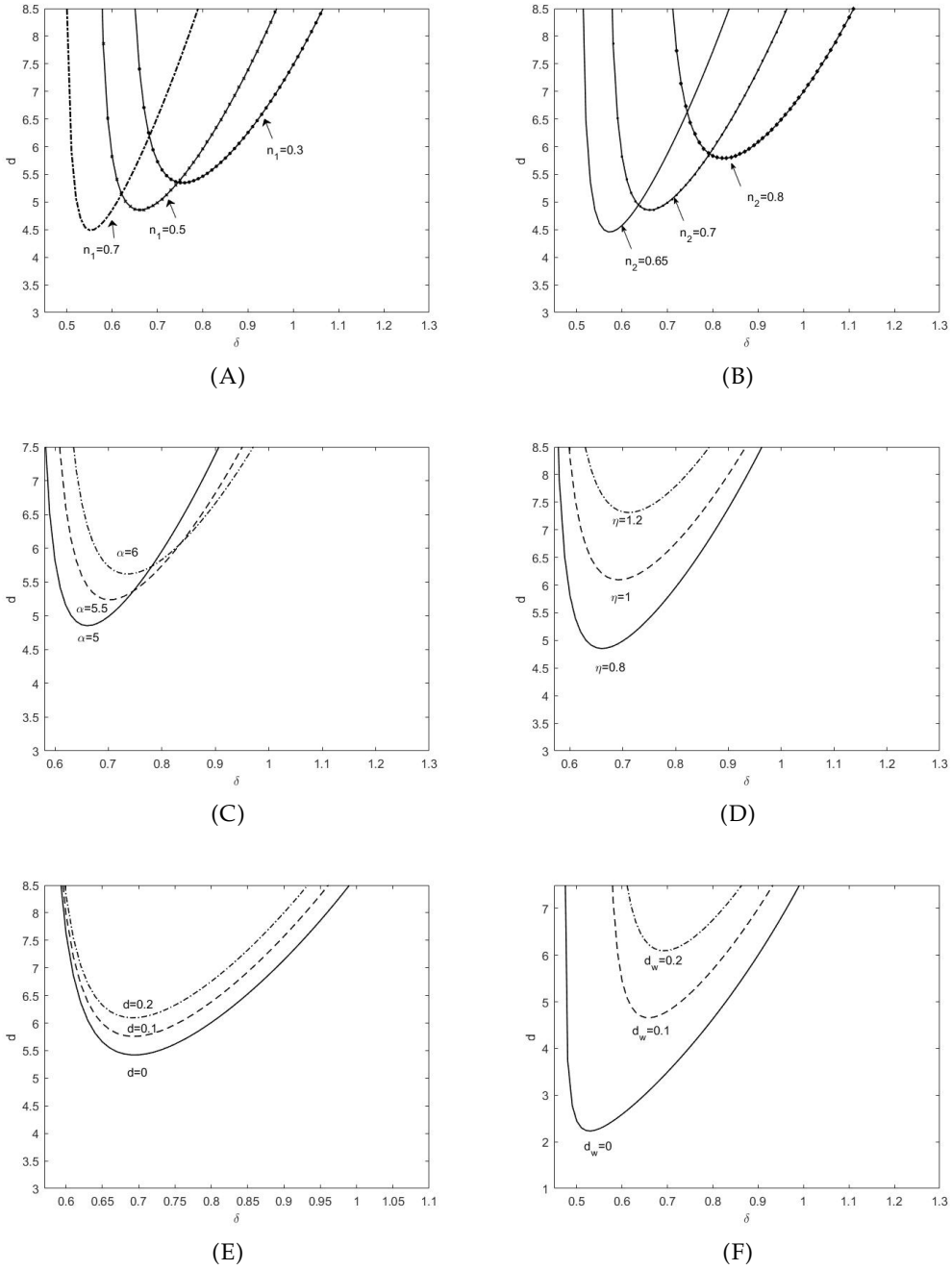

FIGURE 2.7: Turing instability regions as the system parameters change. The parameter set is chosen as in Figure 2.2, except for the parameter specified in the legend of each sub figure and $d_u = 0.2$, $d_w = 0.2$.

Remark 2.5.6 *Also in this case, the stability condition* (2.21) *implies that* $P_2P_1 - P_0 > 0$, *and then the inclusion of the cross-diffusion term is not able to generate* ***Wave Instability.***

2.6 Numerical Results

In this part, we depict numerical results operated on the nondimensional system (2.7) associated with Turing stationary patterns, Hopf pattern, and Turing-Hopf

pattern. In space discretization, we have used Fourier Spectral method with 256 or 512 modes, and in the time integration, we have utilized the second-order explicit Runge-Kutta method.

2.6.1 Turing Stationary Patterns and chaotic spatial temporal pattern

Here, by considering a set of parameters admitted in the instability region of

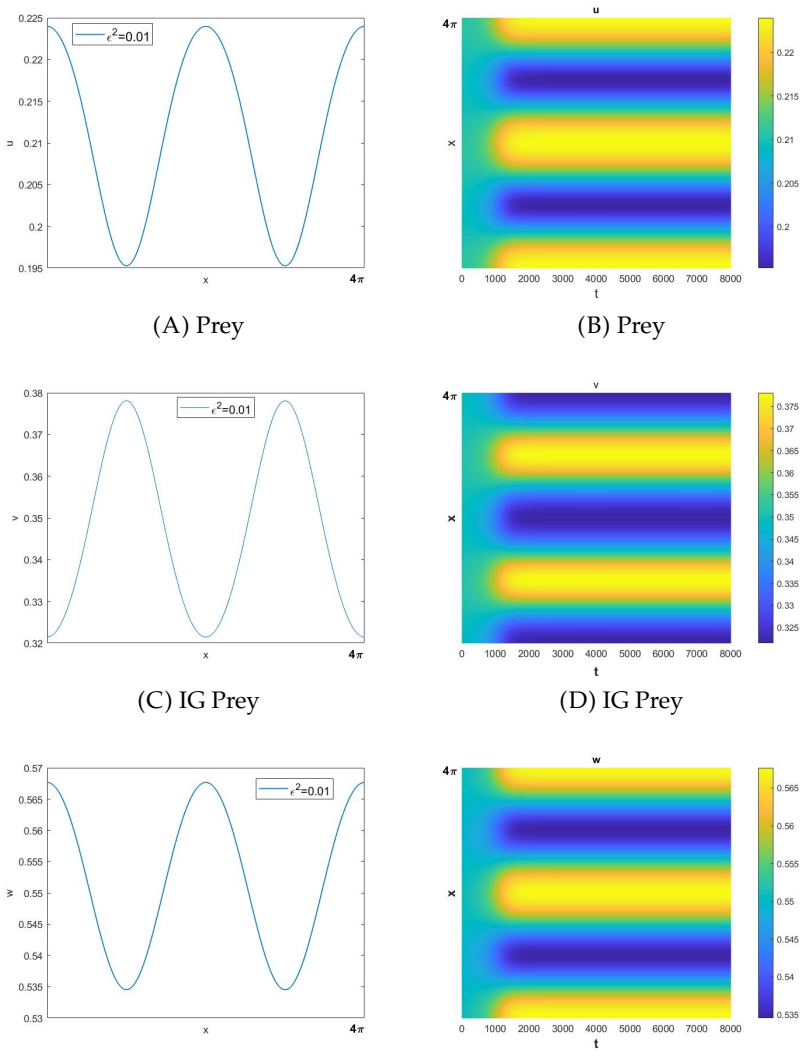

(A) Prey (B) Prey

(C) IG Prey (D) IG Prey

(E) IG Predator (F) IG Predator

FIGURE 2.8: Numerical simulation in the Turing instability region with $n_1 = 0.5$, $n_2 = 0.7$, $\eta = 0.8$, $\alpha = 5$, $\gamma = 2, \delta = 0.8$, $d_u = 0.01$, $d_w = 0.2$ and $d = 12.2298$. For this parameter choice the equilibrium point is $E^* = (0.21, 0.35, 0.55)$, the critical Turing threshold is $d_c = 8.1532$ and the critical wavenumber is $k_c = 1.0809$.

Figure 2.6, and located in the Turing region, the Turing stationary patterns performed in Figure 2.8.

The results of Figure 2.8 has been plotted in the domain $[0\ ,\ 4\pi]$ since for given parameters, the critical wave mode is $k_c \simeq 1$ in $[0\ ,\ 2\pi]$. For chosen parameters,

the critical Turing bifurcation parameter is achieved $d_c = 8.1532$. Therefore, by a little enhancement of d, the coexistence steady state E^* becomes unstable, and string Turing patterns in 1D are formed (see Figure 2.8 left sides). Moreover, from an ecological point of view, these numerical results also recall that direction of diffusion of the resource (prey) and IG predator (top predator or superpredator) are always in phase while IG prey (intermediate predator), whom IG predator eats, is out of phase (see Figure 2.8 right sides). Roughly speaking, the IG predator and IG prey are chasing resources. In contrast, the IG prey runs away from the IG predator since IG prey diffusion is influenced by chemotaxis term with a positive sign.

We have also observed the chaotic behavior of the system (2.7). For this case, we considered the same set of parameters of Figure 2.8 while the critical Turing parameter admits $d = 12.2298$. It is illustrated by a few increasing the cross-diffusion parameter d, the system goes to the Turing instability, however by going more beyond the cross-diffusion parameter, not only the number of modes is increased, but also the chaotic time behavior are taken place (see Figure 2.9).

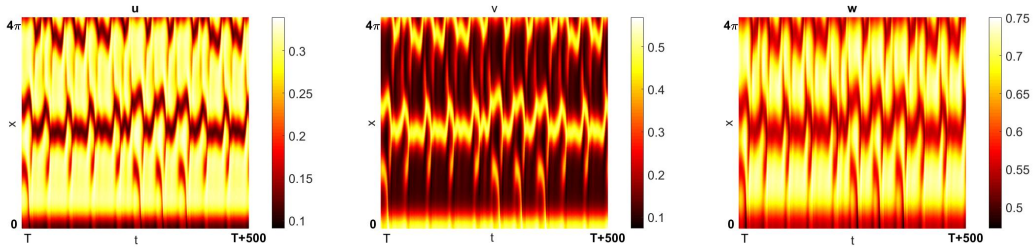

(A) Prey (B) IG Prey (C) IG Predator

FIGURE 2.9: Numerical simulation in the Turing instability region with $n_1 = 0.5$, $n_2 = 0.7$, $\eta = 0.8$, $\alpha = 5$, $\gamma = 2, \delta = 0.8$, $d_u = 0.01$, $d_w = 0.2$ and $d = 12.2298$. For this parameter choice the equilibrium point is $E^* = (0.21, 0.35, 0.55)$, the critical Turing threshold is $d_c = 8.1532$ and the critical wavenumber is $k_c = 1.0809$.

2.6.2 Numerical results of Hopf instability

This section presents some numerical results when the system goes to Hopf instability. As we calculated under the conditions (2.22), we can find the Hopf threshold due to

$$F(\delta)|_{\delta=\delta^c} = 0, \quad \frac{\partial F}{\partial \delta}|_{\delta=\delta^c} \neq 0. \tag{2.46}$$

By numerical results, we found that if $\delta > \delta^c$, the stable equilibrium point E^* undergoes the periodic solutions. While if $\delta < \delta^c$, the system keeps its local stability.

Indeed, Figure 2.10 explains the system's behavior when δ is varying. For these figures, we investigated numerical solution on (2.2) to obtain the time oscillations. As a result, Figure 2.10A and Figure 2.10B show that when $\delta < \delta^c$, E^* is a stable spiral, i.e., for any initial values, the population densities tend to be stable at coexistence steady state.

Another side, as the Hopf bifurcation parameter δ crosses the threshold and increases, the equilibrium becomes unstable and periodic solutions emerge. As the

δ increases, the limit cycles become larger and periodic solution become stable; see Figure 2.10C and Figure 2.10D.

Figure 2.11 describes the local instability of the system when reaction parameter δ crosses the threshold. For these figures, we applied the spectral method on the system (2.7) for other chosen and fixed parameters, while only δ increases. Simultaneously, as the feeding rate of IG predators associated with IG prey rises, the system starts oscillating in time. These oscillations illustrate that population densities of resource and IG prey rise as the population density of IG predator is declined (Figure 2.11B).

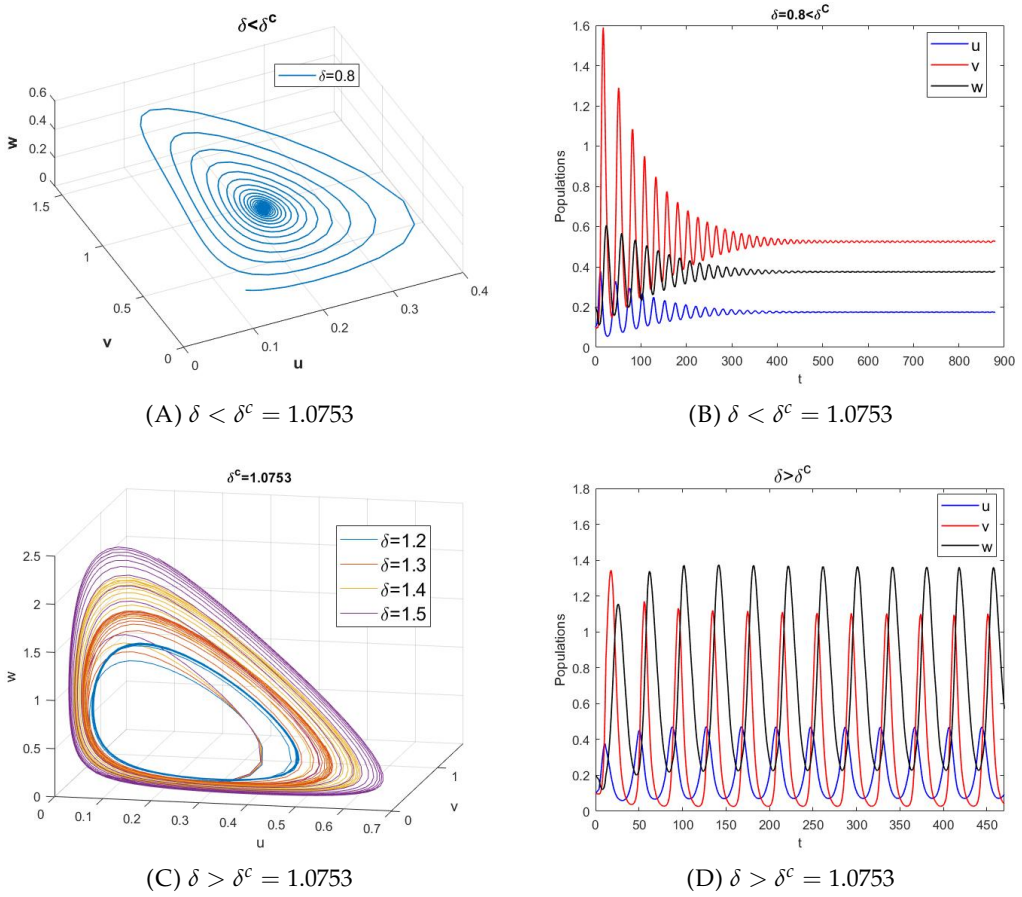

(A) $\delta < \delta^c = 1.0753$ (B) $\delta < \delta^c = 1.0753$

(C) $\delta > \delta^c = 1.0753$ (D) $\delta > \delta^c = 1.0753$

FIGURE 2.10: Numerical simulation in the Turing instability region with $n_1 = 0.5$, $n_2 = 0.7$, $\eta = 0.9067$, $\alpha = 5$, $\gamma = 2.1$. For this parameter choice the equilibrium point is $E^* = (0.21, 0.35, 0.55)$, Hopf threshold $\delta^c = 1.0753$.

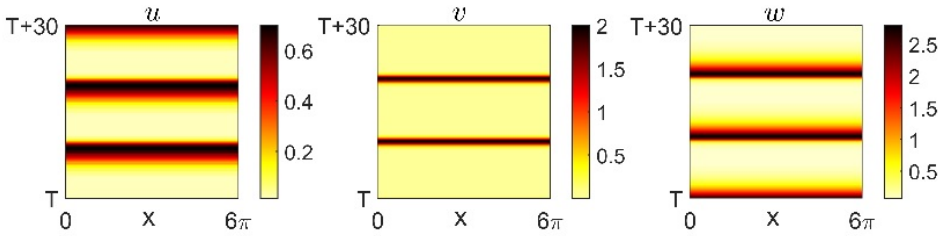

(A)

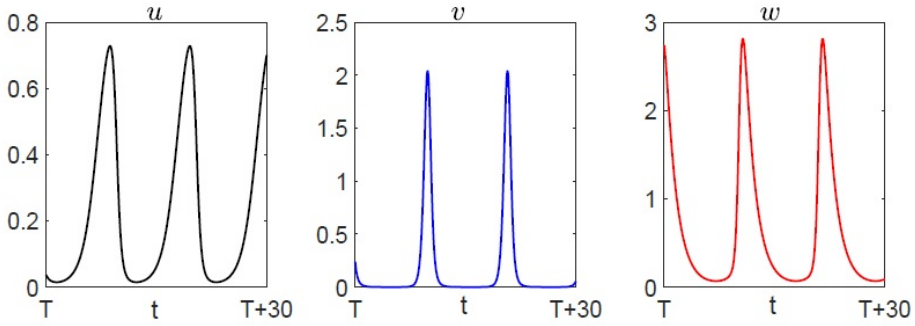

(B)

FIGURE 2.11: Numerical simulation in the Turing instability region with $n_1 = 0.5$, $n_2 = 0.7$, $\eta = 0.8$, $\alpha = 5$, $\gamma = 1.5, \delta = 1.51$, $d_u = 0.04$, $d_w = 0.02$ and $d = 10.3$. For this parameter choice the equilibrium point is $E^* = (0.23, 0.23, 0.67)$, the critical Hopf parameter is $\delta_c = 1.0258$.

2.6.3 Turing- Hopf Patterns

In this numerical results section, we obtain figures in which Turing bifurcation undergoes to Hopf instability. In fact, for given parameters, one needs to find critical Hopf parameter δ_c, then for the founded Hopf threshold, we find crucial Turing bifurcation d_c. As mentioned in previous sections, the system goes to Turing for $d > d_c$ and faces the Hopf if $\delta > \delta_c$. Moreover, in Remark 2.5.4, we mentioned the necessary condition of performing Turing-Hopf instability.

To determine Turing-Hopf patterns for obtained parameters; first we choose, $d > d_c$ while $\delta < \delta^c$, i.e just we expect Turing pattern. As the numerical simulation in Figure 2.8, we expect only emergence of Turing pattern. Then for fixed $d > d_c$, as δ crosses the threshold, Turing-Hopf patterns begin to appear see (Figure 2.12 and Figure 2.13).

Figure 2.12 depicts how the system accepts the Turing- Hopf pattern. In fact, in the figure $\delta = \delta^c$ while $d > d_c$. Figure 2.12A explain phase portrait of the system of Turing faced to threshold Hopf. Figure 2.12B , Figure 2.12C, and Figure 2.12D, illustrate the patterns correspond to the resource u and predators v, w.

Figure 2.13 demonstrates more instability of the system when δ increases from $\delta^c = 1.0753$. It shows that for little increase, i.e $\delta = 1.11$, Spatio-temporal patterns appear. Indeed, phase portrait in the Figure 2.13A of the system state the point clearly. Moreover, in the figures of Figure 2.13 it is obvious that IG predator w oscillate with amplitude bigger than IG prey v and resource u. It means that spatial instability of the IG- predator goes to bigger instability if the larger number of the predator v are eaten by predator w, i.e $\delta \geq \delta^c$.

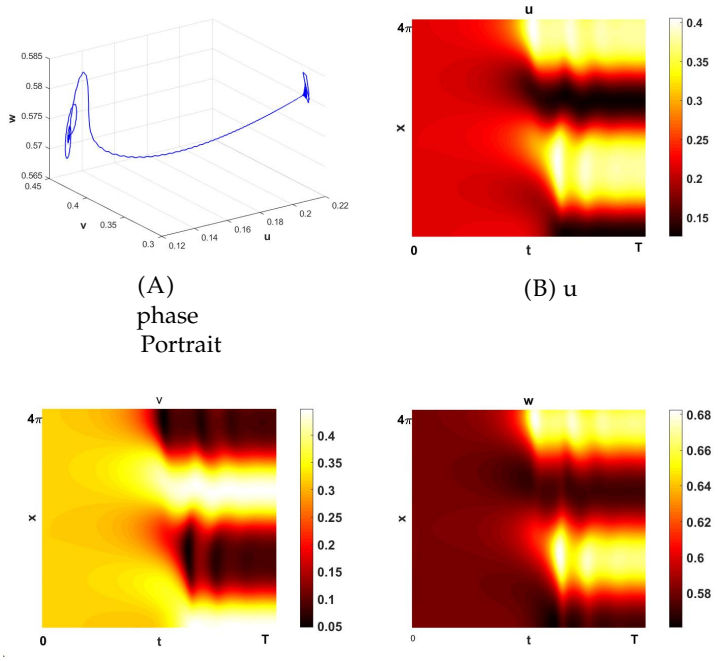

(A) phase Portrait (B) u (C) v (D) w

FIGURE 2.12: Numerical simulation in the Turing-Hopf instability region with $n_1 = 0.5$, $n_2 = 0.7$, $\eta = 0.8$, $\alpha = 5$, $\gamma = 1.6, \delta = \delta^c$, $d_u = 0.04$, $d_w = 0.02$ and $d = 35$. For this parameter choice the equilibrium point is $E^* = (0.22, 0.32, 0.58)$, the critical Turing threshold is $d_c = 28.9415$, critical Hopf parameter is $\delta^c = 1.0753$ and the critical wavenumber is $k_c \simeq 0.9$. A) phase portrait for a specific x and $t \in [0\ , T]$.

2.7 Weakly Nonlinear Analysis

In this section we perform a weakly nonlinear analysis to predict the amplitude of the pattern near the Turing threshold. The weakly nonlinear analysis is based on the multiple scale methods. Since near to the bifurcation the amplitude of the pattern (diffusion-driven instability) has slow temporal scale, then a new temporal scale is defined.

The solution of the original system is written as a weakly nonlinear expansion in the small control parameter ε. We choose $\varepsilon^2 = \dfrac{d - d_c}{d_c}$.

The slow scale is obtained from the linear analysis: it is easy to prove that $\lambda \sim \varepsilon^2$ and, since the growth rate of the perturbation is proportional to the $exp(\lambda t)$, the slow time scale T is order ε^2. Therefore, close to the threshold we separate the fast time t and slow time $T = \varepsilon^2 t$, so that time derivative is obtained as $\partial_t \to \partial_t + \varepsilon^2 \partial_T$.

We separate the linear part from the nonlinear part:

$$\partial_t \mathbf{w} = \mathcal{L}^{d_c}\mathbf{w} + \frac{1}{2}\mathcal{Q}_K(\mathbf{w}, \mathbf{w}) + \nabla.\mathcal{Q}_D^{d_c}(\mathbf{w}, \nabla\mathbf{w}), \qquad \mathbf{w} = \exp\left(i\delta^2 x + \lambda t\right), \tag{2.47}$$

and linear operator is defined as $\mathcal{L}^{d_c} = \Gamma K + D^{d_c}\nabla^2$,
where D and K are defined in (2.15) and nonlinear operators $\mathcal{Q}_K(\mathbf{x}, \mathbf{y})$, $\mathcal{Q}_D^{d_c}(\mathbf{x}, \mathbf{y})$ are introduced as: $\mathbf{x} = (x_u, x_v, x_w)$, $\mathbf{y} = (y_u, y_v, y_w)$.

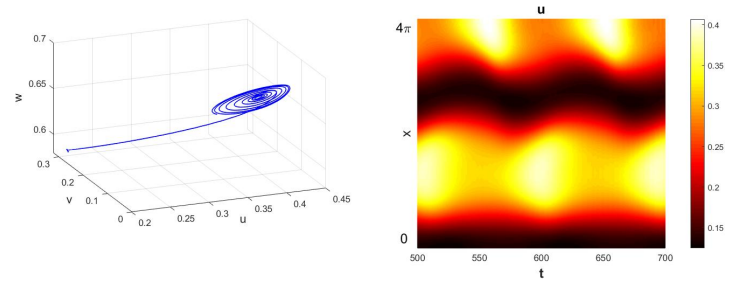

(A) Phase portrait (B) u

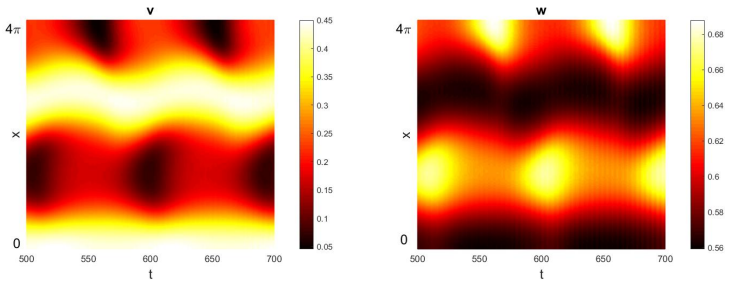

(C) v (D) w

FIGURE 2.13: Numerical simulation in the Turing-Hopf instability region with $n_1 = 0.5$, $n_2 = 0.7$, $\eta = 0.8$, $\alpha = 5$, $\gamma = 1.6$, $\delta = 1.11$, $d_u = 0.04$, $d_w = 0.02$ and $d = 35$. For this parameter choice the equilibrium point is $E^* = (0.22, 0.32, 0.58)$, the critical Turing threshold is $d_c = 28.9415$, critical Hopf parameter is $\delta_c = 1.0753$ and the critical wavenumber is $k_c \simeq 0.9$. A) phase portrait for a specific x and $t \in [500\ , 700]$.

$$\mathcal{Q}_K(\mathbf{x},\mathbf{y}) = \begin{bmatrix} -2x_s y_s - m_1(x_u y_v + x_v y_u) - m_2(x_u y_w + x_w y_u) \\ \alpha(x_u y_v + x_v y_u) - (x_v y_w + x_w y_v) \\ \gamma(x_u y_w + x_w y_u) + \delta(x_v y_w + x_w y_v) \end{bmatrix}, \tag{2.48}$$

$$\mathcal{Q}_D(\mathbf{x},\mathbf{y}) = \begin{bmatrix} 0 \\ d x_v y_w \\ 0 \end{bmatrix}, \tag{2.49}$$

and moreover the bifurcation parameter and solution are expanded asymptotically

$$d = d_c + \varepsilon^2 d^{(2)} + O(\varepsilon^4),$$

$$\mathbf{w} = \varepsilon \mathbf{w}_1 + \varepsilon^2 \mathbf{w}_2 + \varepsilon^3 \mathbf{w}_3 + O(\varepsilon^4),$$

The linear and nonlinear terms are expanded as follows:

$$\mathcal{L}^d = \mathcal{L}^{d_c} + \nabla^2 \varepsilon^2 d^{(2)} \begin{bmatrix} 0 & 0 & 0 \\ 0 & 0 & v^* \\ 0 & 0 & 0 \end{bmatrix},$$

$$\mathcal{Q}_K(\mathbf{w},\mathbf{w}) = \varepsilon^2\mathcal{Q}_K(\mathbf{w}_1,\mathbf{w}_1) + 2\varepsilon^3\mathcal{Q}_K(\mathbf{w}_1,\mathbf{w}_2) + \varepsilon^4\{\mathcal{Q}_K(\mathbf{w}_2,\mathbf{w}_2) + 2\mathcal{Q}_K(\mathbf{w}_1,\mathbf{w}_3)\} + O(\varepsilon^5),$$

$$\nabla.\mathcal{Q}_D^d(\mathbf{w},\nabla\mathbf{w}) = \varepsilon^2\nabla.\mathcal{Q}_D^{d_c}(\mathbf{w}_1,\nabla\mathbf{w}_1) + \varepsilon^3\{\nabla.\mathcal{Q}_D^{d_c}(\mathbf{w}_1,\nabla\mathbf{w}_2) + \nabla.\mathcal{Q}_D^{d_c}(\mathbf{w}_2,\nabla\mathbf{w}_1)\} + \varepsilon^4\{\nabla.\mathcal{Q}_D^{d_c}(\mathbf{w}_2,\nabla\mathbf{w}_2) + \nabla.\mathcal{Q}_D^{d_c}(\mathbf{w}_1,\nabla\mathbf{w}_3) + \nabla.\mathcal{Q}_D^{d_c}(\mathbf{w}_3,\nabla\mathbf{w}_1)\} + O(\varepsilon^5),$$

Now we replace all expansion in (2.47) and sort according to the order of ε. At $O(\varepsilon)$,we obtain the following linear problem:

$$\mathcal{L}^{d_c}\mathbf{w}_1 = 0, \quad \mathbf{w}_1 = A(T)\rho\cos(k_c x),$$

such that satisfying the homogeneous boundary conditions where ρ belongs to the $ker(\Gamma K - k_c^2 D^{d_c})$. In this stage the $A(T)$, the amplitude of the pattern is arbitrary and the vector ρ is considered constant such whose normalization is

$$\rho = \begin{pmatrix} 1 \\ \rho_2 \\ \rho_{3,} \end{pmatrix}, \tag{2.50}$$

with

$$\begin{aligned} \rho_2 &= -\frac{d_u d_w k_c^4 + d_w k_c^2 u^* + u^* w^* \gamma\eta}{d_w k_c^2 u^* + u^* w^* \delta\eta}, \\ \rho_3 &= -\frac{u^* w^*(\gamma-\delta) - w_u^* k_c^2}{d_w k_c^2 u^* + u^* w^* \delta\eta}, \end{aligned} \tag{2.51}$$

where k_c^2 are replaced by is obtained by using Equation (2.45). We observe that ρ_2 is always negative. Also, we point out that the condition $d_c > \bar{d}$ (2.43) ensures that ρ_3 is always positive. Therefore, u and v always oscillate out of phase and u and w always oscillate in phase.

Moreover, at $O(\varepsilon^2)$ there is this linear equation which must be solved:

$$\mathcal{L}^{d_c}\mathbf{w}_2 = \mathbf{F},$$

According to the Fredholm alternative theorem, this equation has a solution if and only if $\langle \mathbf{F}, \psi\rangle = 0$, where ψ^* is defined at

$$\psi = \begin{pmatrix} 1 \\ R_1^* \\ R_2^* \end{pmatrix}\cos(k_c x) = \psi^*\cos(k_c x),$$

and $\langle .,. \rangle$ implied the scalar product in $\mathbf{L}^2(0, \frac{2\pi}{k^c})$ and $\psi^* \in Ker(\Gamma K - k_c^2 D^{d_c})^\dagger$ where $\dagger$ shows transpose of complex conjugate of the matrix.

In particular, $\mathbf{F} = -\frac{1}{4}A^2\sum_{i=0,2}\mathcal{M}_i(\rho,(\rho)\cos(ik_c x)$, in which $\mathcal{M}_i(\rho,\rho) = \mathcal{Q}_K(\rho,\rho) - i^2k_c^2\mathcal{Q}_D^{d_c}(\rho,\rho)$. Hence, the vector $\mathbf{w}_2$ is defined as

$\mathbf{w}_2 = A^2(\mathbf{w}_{20} + \mathbf{w}_{22}\cos(2k_c x))$ so that $\mathbf{L}_i^{d_c}\mathbf{w}_{2i} = -\frac{1}{4}\mathcal{M}_i(\rho,\rho)$, $i = 0,2$ and $\mathbf{L}_i = \Gamma K - i^2k_c^2 D^{d_c}$.

In following, at $O(\varepsilon^3)$ we obtain the linear problem

$$\mathcal{L}^{d_c}\mathbf{w}_3 = \mathbf{G}, \tag{2.52}$$

where $\mathbf{G} = \left(\frac{dA}{dT}\rho + A\mathbf{G}_1^{(1)} + A^3\mathbf{G}_1^{(3)}\right)\cos(k_c x) + A^3\mathbf{G}_3\cos(3k_c x)$, in which

$\mathbf{G}_1^{(1)} = k_c^2 d^{(2)} \begin{bmatrix} 0 & 0 & 0 \\ 0 & 0 & v^* \\ 0 & 0 & 0 \end{bmatrix} \rho,$

$\mathbf{G}_1^{(3)} = -\mathcal{M}_1(\mathbf{w}_{20}, \rho) - \frac{1}{4}\mathcal{M}_2(\rho, \mathbf{w}_{22}) - \frac{1}{4}\{\mathcal{Q}_k(\rho, \mathbf{w}_{22}) + 2k_c^2\mathcal{Q}_D^{d_c}(\mathbf{w}_{22}, \rho)\},$

$\mathbf{G}_3 = -\frac{1}{2}\mathcal{Q}_k(\rho, \mathbf{w}_{22}) + 3k_c^2\mathcal{Q}_D^{d_c}(\rho, \mathbf{w}_{22}) + \frac{3}{2}k_c^2\mathcal{Q}_D^{d_c}(\mathbf{w}_{22}, \rho),$

Finally, by applying the solvability condition, we obtain the Stuart-Landau equation for the amplitude

$$\frac{\partial A}{\partial T} = \sigma A - LA^3,$$

In addition, solvability of the equation (C.2) depends on $\langle \mathbf{G}, \psi \rangle = 0$, whose coefficients are given by

$$\sigma = -\frac{\langle \mathbf{G}_1^{(1)}, \psi \rangle}{\langle \rho, \psi \rangle}, \quad \mathbf{L} = \frac{\langle \mathbf{G}_1^{(3)}, \psi \rangle}{\langle \rho, \psi \rangle},$$

.

In the Stuart-Landau equation the coefficient σ is always positive while L could be either negative or positive, corresponding to a subcritical or supercritical bifurcation.

The nontrivial solution of the amplitude equation is

$$\mathbf{A}_\infty = \sqrt{\frac{\sigma}{L}}, \tag{2.53}$$

which requires $L > 0$, and therefore the result of this analysis is valid only for supercritical bifurcations.

Therefore, the asymptotic behavior of the solution is given by weakly nonlinear analysis of $O(\varepsilon^3)$ is:

$$\mathbf{W} = \varepsilon A\rho cos(k_c x) + \varepsilon^2 A^2[\mathbf{w}_{20} + \mathbf{w}_{22} cos(2k_c x)] + O(\varepsilon^3). \tag{2.54}$$

Generally, a fully scaled amplitude equation from which all parameters have been removed is the form of

$$\partial_T A = \pm A + \partial_X^2 A - |A|^2 A,$$

that is known as Ginzburg-Landau Equation and the positive sign for the first term on the right-hand side corresponds to the above threshold and the negative sign to the below threshold. The Landau-Stuart equation is one type of Ginzburg-Landau equation in which only time scale bifurcation is considered; therefore, there is no middle term. Moreover, in our model, instability occurs when $d > d_c$, i.e., the critical bifurcation parameter is above the threshold, hence the $\sigma > 0$ in the Landau-Stuart equation.

Derivation of quintic Stuart-Landau equation

As far as, we found in previous section in Landau- Stuart equation the coefficient σ is always positive while L could be either negative or positive with respect to subcritical or supercritical bifurcation.

In fact, in subcritical case, the system is not able to capture the time revolution of the pattern, and the system need another time scale which makes more precise approximation (Gambino, Lombardo, and Sammartino, 2012; Gambino, Lombardo, and Sammartino, 2013). This part of calculation is found in B.1.

2.7.1 Numerical simulation VS. WNL

In this section, first we employ WNL to figure out how much big amplitudes vary in Turing regions. Therefore, we determine numerically superciritical and subcritical regions in planes $(\gamma,\ \delta)$ and $(\delta,\ d)$. Then we compare numerical results of stationary Turing pattern with weakly nonlinear analysis.

Figure 2.14A implies to subcritical and supercritical Turing region in the instability regions located in the plane $(\gamma,\ \delta)$. Figure 2.14B indicates as diffusion parameter d_w increases Turing regions decline. We observe that in absence of self-diffusion of IG predator, the system undergoes only supercritical bifurcation. While as IG predator diffuses IG prey has to move away from IG predator faster (i.e d increases) and the system underlies supercritical or subcritical bifurcation.

Furthermore, Figure 2.15 demonstrates when a basal resource does not diffuse ($d_u = 0$), the system faces Turing instability such that instability occurs with small amplitude due to supercritical bifurcation (i.e population densities vary smaller). Indeed, in absence of diffusion of prey, if IG predator eats much more IG prey (for greater values of a constant δ), population densities go to instability very close to equilibrium, however for less than the constant value δ population densities vary with big amplitude via subcritical bifurcation. It is observed in this case, that the subcritical region is smaller than the supercritical region.

Nevertheless, Figure 2.15 right side, indicates as prey moves (d_u increases) the system faces to instabilities. A large part of the Turing region allocates to the subcritical region. In the other words, there is again a constant value of δ such that for less than this value the population densities change with big amplitude, while when δ is bigger than the constant value(IG predator eats more IG prey), the system undergoes supercritical regions and populations vary smaller.

Figure 2.16 demonstrates a comparison of numerical solution of the system (2.7) with weakly nonlinear analysis, for supercritical case when $\varepsilon = 0.1$ and $\varepsilon = 0.05$. Indeed, Weakly nonlinear analysis releases that in the Landau-Stuart equation σ and L are positive. According to the L^2-norm of distances, numerical and weakly nonlinear results depict nice agreements which are consistent with $O(\varepsilon^3)$.

However, in the case $L < 0$ -subcritical case- the amplitude equation (2.53) cannot approximate the solution, therefore we apply higher order of the approximate via quintic Stuart- Landau. equation mentioned in Appendix B.1. Although we employ the fifth order in the approximation of the amplitude equations, the results do not have good agreement with numerical results. Indeed, this failure occurs since approximated A is in $O(\varepsilon^{-1})$, which is not able to capture the amplitude as well as the supercritical case.

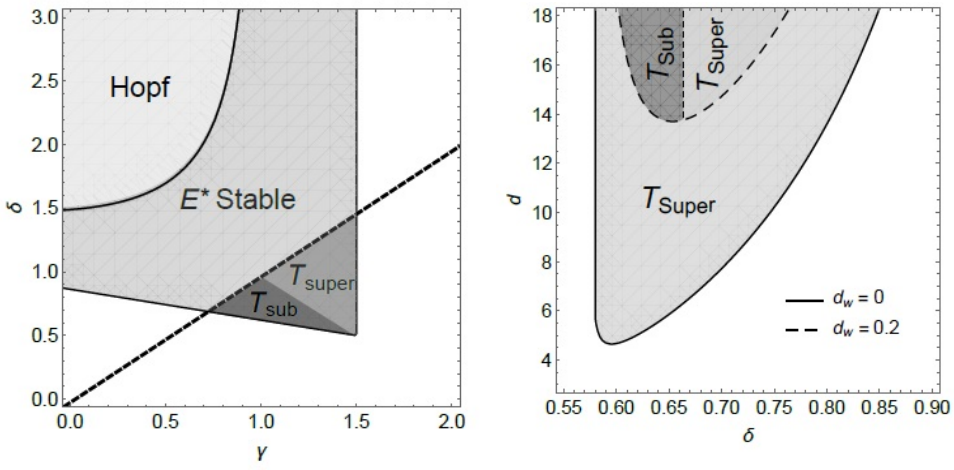

(A) Sub- and super-Turing in plane (γ, δ).

(B) Sub- and super-Turing in plane (δ, d).

FIGURE 2.14: A) Supercritical and subcritical Turing instability regions. The parameter values are $n_1 = 0.5$, $n_2 = 0.7$, $\alpha = 2.5$, $\gamma = 0.8$, $d_u = 0.02$, $d_w = 0.04$. B) Supercritical and subcritical Turing regions when IG predator self-diffusion varies: $d_w = 0$ and $d_w = 0.2$. Other fixed parameters are $n_1 = 0.5$, $n_2 = 0.7$, $\alpha = 2.5$, $\eta = 0.8$, $\gamma = 1.2$, $d_u = 0.02$.

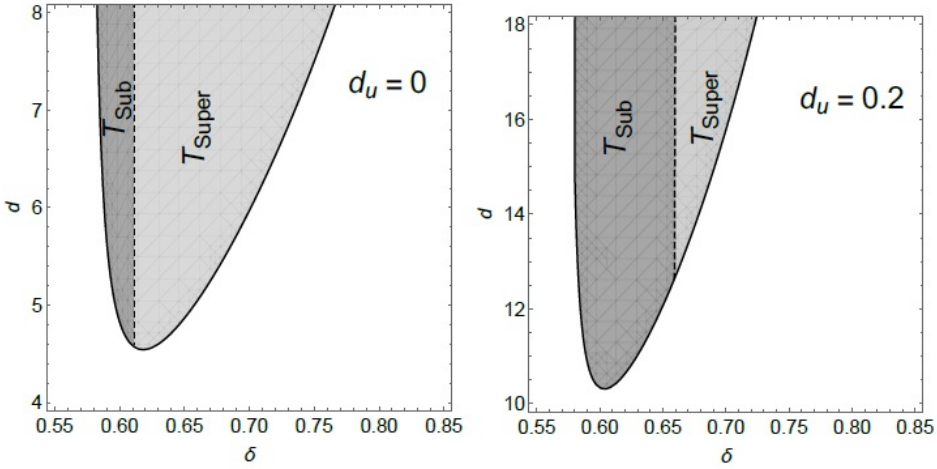

FIGURE 2.15: Supercritical and subcritical Turing instability regions when basal resource self-diffusion varies: $d_u = 0$ in the left side, $d_u = 0.2$ in the right side. Other fixed parameters are $n_1 = 0.5$, $n_2 = 0.7$, $\alpha = 2.5$, $\eta = 0.8$, $\gamma = 1.2$, $d_w = 0.04$.

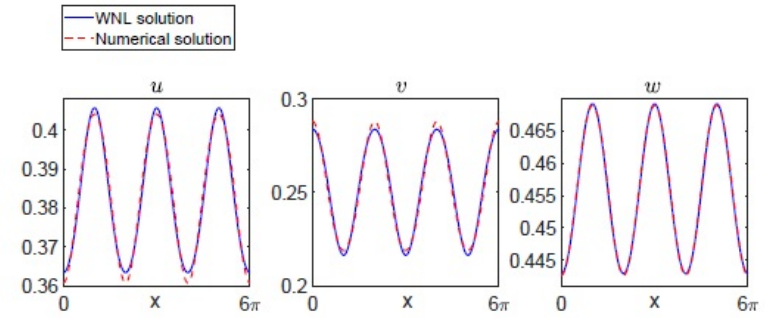

(A) $\varepsilon = 0.1$

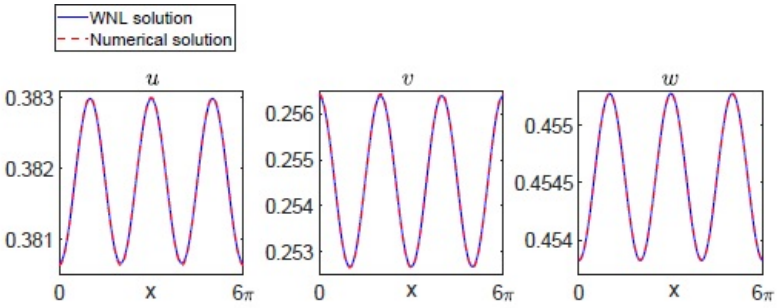

(B) $\varepsilon = 0.05$

FIGURE 2.16: Comparison between the weakly nonlinear solution (solid line) and the numerical solution of system (dotted line) in the supercritical case, with different values of ε: we have fixed $\varepsilon = 0.1$ in the simulation shown in the first line and $\varepsilon = 0.05$ in the simulation shown in the second line. The parameter values used in the simulations are: $n_1 = 0.5$, $n_2 = 0.7$, $\alpha = 5$, $\eta = 0.8$, $\gamma = 1.5$, $\delta = 0.8$, $d_u = 0.02$, $d_w = 0.04$. For this parameter set, the bifurcation threshold is $d_c = 10.2872$ and the critical wavenumber is $k_c = 1.04222$.

Chapter 3

Normal form of Turing-Hopf codimension two of IGP model

We recall that onset of Hopf instability in absence of the diffusion is characterized by a pair of complex conjugate eigenvalues crossing the imaginary axis so that a limit cycle appears out of an unstable equilibrium. The Hopf bifurcation occurs when:

$$Im(\lambda(k)) \neq 0, \quad Re(\lambda(k)) = 0, \quad \text{at } k = 0. \tag{3.1}$$

in marginal state of Hopf, the cubic polynomial has two purely imaginary eigenvalues while the other eigenvalue remains in the left half plane such that the two purely imaginary crosses the origin to the right half plane due to varying critical Hopf bifurcation parameter. Thank to algebraic relation between eigenvalues of cubic polynomial mentioned in Brooks, 2006 and applying on the characteristic function above we can determine eigenvalues of the threshold explicitly as follow:
1. Since $P_2 > 0$ due to (2.17) it is confirmed that $\lambda_1 < 0$. and 2. The two other eigenvalues of the threshold are complex conjugate so $\lambda_{2,3} = \pm i\Omega_c$, thus (2.18) gives $\Omega_c^2 = P_1$ where $P_1 > 0$, consequently

$$\Omega_c = \sqrt{P_1}. \tag{3.2}$$

In the previous chapter we obtained Turing and Hopf instability regions and we found the region and some conditions (see (2.22), (2.43)) such a ways Turing instability faces to Hopf bifurcations. Further, numerical simulation associated with each region and instability were depicted.

3.1 Normal form

In this section, we will use a perturbation technique, based on the method of multiple scales Kidachi, 1980 to compute the normal form of the reaction- diffusion system ((2.7)) in the proximity of the Turing- Hopf codimension-2 bifurcation point. Near the threshold different time scales $T_j = \varepsilon^j t$ and spatial scales $X_j = \varepsilon^j x$ with $j = 0, 1, 2, ...$ can be distinguished. Then, the derivative decouples as follows:

$$\begin{aligned}
\frac{\partial}{\partial t} &= \frac{\partial}{\partial T_0} + \varepsilon\frac{\partial}{\partial T_1} + \varepsilon^2\frac{\partial}{\partial T_2} + \varepsilon^3\frac{\partial}{\partial T_3} + \dots \\
\frac{\partial}{\partial x} &= \frac{\partial}{\partial X_0} + \varepsilon\frac{\partial}{\partial X_1} + \varepsilon^2\frac{\partial}{\partial X_2} + \varepsilon^3\frac{\partial}{\partial X_3} + \dots \\
\frac{\partial^2}{\partial x^2} &= \frac{\partial^2}{\partial X_0^2} + \varepsilon\frac{2\partial^2}{\partial X_0 X_1} + \varepsilon^2(\frac{\partial^2}{\partial X_1^2} + \frac{2\partial^2}{\partial X_0 X_2}) + \varepsilon^3(\frac{2\partial^2}{\partial X_0 X_3} + \frac{2\partial^2}{\partial X_1 X_2}) + \dots
\end{aligned} \tag{3.3}$$

Here we have d and δ as control parameters correspond to the Turing critical parameter and Hopf threshold correspondingly. Both the solutions of the original system ((2.7)) and the control parameters are written as nonlinear expansions in ε as follows :

$$\begin{aligned}
u &= \varepsilon u_1 + \varepsilon^2 u_2 + \varepsilon^3 u_3 + O(\varepsilon^4), \\
v &= \varepsilon v_1 + \varepsilon^2 v_2 + \varepsilon^3 v_3 + O(\varepsilon^4), \\
w &= \varepsilon w_1 + \varepsilon^2 w_2 + \varepsilon^3 w_3 + O(\varepsilon^4), \\
\mathbf{W} &= \varepsilon \mathbf{W_1} + \varepsilon^2 \mathbf{W_2} + \varepsilon^3 \mathbf{W_3} + O(\varepsilon^4), \\
\delta &= \delta^c + \varepsilon\delta^{(1)} + \varepsilon^2\delta^{(2)} + \varepsilon^3\delta^{(3)} + O(\varepsilon^4), \\
d &= d_c + \varepsilon d^{(1)} + \varepsilon^2 d^{(2)} + \varepsilon^3 d^{(3)} + O(\varepsilon^4).
\end{aligned} \tag{3.4}$$

where $\mathbf{W} = [u - u^*, v - v^*, w - w^*]$.
All the expansion coefficients $\mathbf{W_i}, \mathbf{i} = \mathbf{1, 2, 3}, \dots$ depends on the time and spatial scales $T_j, X_j, j = 0, 1, 2, \dots$. By replacing all expansion mentioned above in (3.3),(3.4) into the system (2.7)

$$\dot{\mathbf{W}} = K(u^*)\mathbf{W} - k_c^2 D(u^*)\Delta\mathbf{W}$$

and collecting all the terms at each order in ε, one then gets a sequence of differential system for the $\mathbf{w_i}, i = 1, 2, 3, \dots$.
Here we introduce the following linear operator:

$$\mathcal{L}^c = \frac{\partial}{\partial T_0} - D^{d_c}\frac{\partial^2}{\partial X_0^2} - K^{\delta^c}$$

where K^{δ^c} andD^{d_c} are given in (2.15) computed at the codimension 2 bifurcation point (δ^c, d_c). At the lowest order in ε we recover the following linear problem for the asymptotic coefficient $\mathbf{W_1}$:

$$\mathcal{L}^c\mathbf{W_1} = 0, \tag{3.5}$$

whose solution is given by:

$$\mathbf{W}_1 = \varphi_1(T_k, X_k)e^{i\Omega_c T_0}\mathbf{e_1} + \varphi_2(T_k, X_k)e^{i\delta_c X_0}\mathbf{e}_2 + c.c, \tag{3.6}$$

where the fields φ_1, φ_2 depending on the time and spatial scales $T_k, X_k, k = 1, 2, \dots$ lie on the center manifolds and $c.c$ implies the complex conjugate counterpart. The real numbers Ω_c, δ_c are given by (3.2) and (2.43) respectively, evaluated at the Turing-Hopf singularity. The vectors $\mathbf{e_1} \in Ker(K^{\delta^c} - iI\Omega_c)$ and $\mathbf{e_2} \in Ker(K^{\delta^c} - k_c^2 D^{d_c})$ are

chosen as follows:

$$\mathbf{e_1} = \begin{pmatrix} 1 \\ \dfrac{K_{21}^{\delta^c}(K_{33}^{\delta^c} - i\Omega_c) - K_{31}^{\delta^c}K_{23}^{\delta^c}}{K_{32}^{\delta^c}K_{23}^{\delta^c} - (K_{33}^{\delta^c} - i\Omega_c)(K_{22}^{\delta^c})} \\ \dfrac{K_{32}^{\delta^c}K_{21}^{\delta^c} - K_{31}^{\delta^c}(K_{22}^{\delta^c} - i\Omega_c)}{-K_{32}^{\delta^c}K_{23}^{\delta^c} + (K_{33}^{\delta^c} - i\Omega_c)(K_{22}^{\delta^c})} \end{pmatrix},$$
$$\mathbf{e_2} = \begin{pmatrix} 1 \\ \dfrac{(K_{21}^{\delta^c} - k_c^2 D_{21}^{d_c})(K_{33}^{\delta^c} - k_c^2 D_{33}^{d_c}) - (K_{31}^{\delta^c} - k_c^2 D_{31}^{d_c})(K_{23}^{\delta^c} - k_c^2 D_{23}^{d_c})}{(K_{32}^{\delta^c} - k_c^2 D_{32}^{d_c})(K_{23}^{\delta^c} - k_c^2 D_{23}^{d_c}) - (K_{33}^{\delta^c} - k_c^2 D_{33}^{d_c})(K_{22}^{\delta^c} - k_c^2 D_{22}^{d_c})} \\ \dfrac{(K_{32}^{\delta^c} - k_c^2 D_{32}^{d_c})(K_{21}^{\delta^c} - k_c^2 D_{21}^{d_c}) - (K_{31}^{\delta^c} - k_c^2 D_{31}^{d_c})(K_{22}^{\delta^c} - k_c^2 D_{22}^{d_c})}{-(K_{32}^{\delta^c} - k_c^2 D_{32}^{d_c})(K_{23}^{\delta^c} - k_c^2 D_{23}^{d_c}) + (K_{33}^{\delta^c} - k_c^2 D_{33}^{d_c})(K_{22}^{\delta^c} - k_c^2 D_{22}^{d_c})} \end{pmatrix}, \tag{3.7}$$

where $D_{ij}^{d_c}, K_{ij}^{\delta^c}$ are the i,j-entries of the matrices of D^{d_c}, K^{δ^c}. At $O(\varepsilon^2)$ one gets the linear equation for $\mathbf{W_2}$:

$$\mathcal{L}^c \mathbf{W_2} = -\mathcal{L}^1 \mathbf{W_1} + \mathbf{F}, \tag{3.8}$$

where:

$$\mathcal{L}^1 = \frac{\partial}{\partial T_1} - D^{d^{(1)}} \frac{\partial^2}{\partial X_0^2} - 2D^{d^c} \frac{\partial^2}{\partial X_0 \partial X_1} - K^{\delta^{(1)}}, \tag{3.9}$$

such that

$$\mathbf{F} = \begin{pmatrix} -(u_1)^2 - u_1 v_1 - \eta w_1 u_1 \\ \alpha v_1 u_1 - v_1 w_1 \\ \gamma w_1 u_1 + \delta^c v_1 w_1 \end{pmatrix} + d_c \begin{pmatrix} 0 \\ \dfrac{\partial v_1}{\partial X_0}\dfrac{\partial w_1}{\partial X_0} + v_1 \dfrac{\partial^2 w_1}{\partial X_0^2} \\ 0 \end{pmatrix} \tag{3.10}$$

and

$$D^{d^{(1)}} = d^{(1)} \begin{pmatrix} 0 & 0 & 0 \\ 0 & 0 & v^* \\ 0 & 0 & 0 \end{pmatrix}, \quad K^{\delta^{(1)}} = \delta^{(1)} \begin{pmatrix} 0 & 0 & 0 \\ 0 & 0 & 0 \\ 0 & w^* & 0 \end{pmatrix} \tag{3.11}$$

the equation (3.8) admits a solution if and only if the Fredholm alternative is satisfied. To suppress seculart terms appearing in the source term of (3.8), we impose $T_1 = 0$ and $\delta^{(1)} = d^{(1)} = 0$ in such way that the compatibility condition is automatically satisfied (see details in Appendix C.1).

At order ε^3, one recovers the following linear problem for $\mathbf{W_3}$:

$$\mathcal{L}^c \mathbf{W_3} = -\mathcal{L}^1 \mathbf{W_2} - \mathcal{L}^2 \mathbf{W_1} + \mathbf{G}, \tag{3.12}$$

where

$$\mathcal{L}^2 = \frac{\partial}{\partial T_2} - D^{d^{(2)}} \frac{\partial^2}{\partial X_0^2} - D^{d_c}\left(\frac{\partial^2}{\partial X_1^2} + 2\frac{\partial^2}{\partial X_0 X_2}\right) - \delta^{(2)} \begin{pmatrix} 0 & 0 & 0 \\ 0 & 0 & 0 \\ 0 & w^* & 0 \end{pmatrix}, \tag{3.13}$$

$$\mathbf{G} = \begin{pmatrix} -2u_1u_2 - (u_1v_2 + u_2v_1) - \eta(u_1w_2 + u_2w_1) \\ \alpha(v_1u_2 + u_1v_2) - (v_1w_2 + v_2w_1) \\ \gamma(u_1w_2 + u_2w_1) + \delta^c(v_1w_2 + v_2w_1) \end{pmatrix} + \mathbf{G}_0, \tag{3.14}$$

with

$$D^{d^{(2)}} = d^{(2)} \begin{pmatrix} 0 & 0 & 0 \\ 0 & 0 & v^* \\ 0 & 0 & 0 \end{pmatrix} \tag{3.15}$$

and

$$\mathbf{G}_0 = d_c \begin{pmatrix} 0 \\ \dfrac{\partial v_1}{\partial X_0}\dfrac{\partial w_2}{\partial X_0} + \dfrac{\partial v_2}{\partial X_0}\dfrac{\partial w_1}{\partial X_0} + (v_1\dfrac{\partial^2 w_2}{\partial X_0^2} + v_2\dfrac{\partial^2 w_1}{\partial X_0^2}) \\ 0 \end{pmatrix}, \tag{3.16}$$

Secular terms appear into equation (3.12) and the solvability condition leads to the following system of equations for the fields ϕ_1 and ϕ_2:

$$\frac{\partial \varphi_1}{\partial T_2} = \tilde{\sigma}_1\varphi_1 - \tilde{L}_1|\varphi_1|^2\varphi_1 + \tilde{\Omega}_1|\varphi_2|^2\varphi_1 + \tilde{\delta}_1\frac{\partial^2\varphi_1}{\partial X_1^2}, \tag{3.17}$$

$$\frac{\partial \varphi_2}{\partial T_2} = \tilde{\sigma}_2\varphi_2 - \tilde{L}_2|\varphi_2|^2\varphi_2 + \tilde{\Omega}_2|\varphi_1|^2\varphi_2 + \tilde{\delta}_2\frac{\partial^2\varphi_2}{\partial X_1^2}, \tag{3.18}$$

where the explicit expressions of the coefficients $\tilde{\sigma}_i, \tilde{L}_i, \tilde{\Omega}_i, \tilde{\delta}_i$ with $i = 1, 2.$ are given in (C.16). Notice that the coefficients of equation (3.17) are complex while the coefficients of equation (3.18) are real. Moreover, the coefficient $\tilde{\sigma}_1$ is linearly dependent on $b^{(2)}$ (see (C.16) and (C.7)) and $\tilde{\sigma}_2$ is linearly dependent on $b^{(2)}$ and $d^{(2)}$ (see (C.16) and (C.8)), which are the second order deviation from the bifurcation values. All the other coefficients do not depend on $b^{(2)}$ and $d^{(2)}$ (see (C.17) and (C.9)-(C.13)). Once substituted $\mathbf{W}_2$ in the linear equation (3.12 at $O(\varepsilon^3)$ the source term has the following expression:

$$\mathbf{H}^{(\mathbf{1})}e^{i\Omega_c T_0} + \mathbf{H}^{(\mathbf{2})}e^{i\delta_c X_0} + c.c + \mathbf{H}^*, \tag{3.19}$$

where H^* does not contain secular terms. The quantity $\mathbf{H}^{(\mathbf{i})}$ are determined in Appendix C.2.

3.2 Stationary solution of the reduced system

To survey stationary solution of the reduced system, we apply defined functions below as solution of the system:

$$\varphi_1 = \rho_1 e^{i(\vartheta_1 + QX_1)}, \quad \varphi_2 = \rho_2 e^{i(\vartheta_2 + QX_2)}, \tag{3.20}$$

where $\rho_j(X_1, T_2)$ and $\vartheta_j(T_2), j = 1, 2$. In particular, we investigate only the stability of branches of the solutions to (3.20) against disturbances with $Q = 0$. For this purpose we analyze the stability of the equilibrium of the following normal form:

$$\frac{\partial \rho_1}{\partial T_2} = \rho_1(\sigma_1 - L_1\rho_1^2 + \Omega_1\rho_2^2), \tag{3.21}$$

$$\frac{\partial \rho_2}{\partial T_2} = \rho_2(\sigma_2 - L_2\rho_2^2 + \Omega_1\rho_1^2), \tag{3.22}$$

$$\frac{\partial \vartheta_1}{\partial T_2} = (\sigma_1' - L_1'\rho_1^2 + \Omega_1'\rho_2^2), \tag{3.23}$$

$$\frac{\partial \vartheta_2}{\partial T_2} = 0, \tag{3.24}$$

where $\sigma_j = Re(\tilde{\sigma_j})$, $L_j = Re(\tilde{L_j})$, $\Omega_j = Re(\tilde{\Omega_j})$, $j = 1,2, \sigma_1' = Im(\tilde{\sigma_j})$, $L_1' = Im(\tilde{L_1})$, $\Omega_1' = Re(\tilde{\Omega}_1$. Hence, the system admits four stationary solutions:

$$O \ : \ \rho_1 = \rho_2 = 0, \tag{3.25}$$

$$H \ : \ \rho_1^2 = \frac{\sigma_1}{L_1}, \ \ \rho_2 = 0, \vartheta_1 = \sigma'_1 - L'_1\rho'^2_1; \tag{3.26}$$

$$T \ : \ \rho_1 = 0, \ \ \rho_2^2 = \frac{\sigma_2}{L_2}, \vartheta_2 = 0; \tag{3.27}$$

$$TH \ : \ \rho_1^2 = \frac{\sigma_1 L_2 + \sigma_2 L_1}{L_1 L_2 - \Omega_1\Omega_2}, \ \ \rho_2^2 = \frac{\sigma_2 L_1 + \sigma_1 L_2}{L_1 L_2 - \Omega_1\Omega_2}, \tag{3.28}$$

$$\vartheta_1 = \sigma'_1 - L'_1{\rho'_1}^2 + \Omega'_1\rho'^2_2, \tag{3.29}$$

Indeed, these stationary equilibrium points are classified in following. O is origin as stationary solution which corresponds to the uniform solution to the original system (2.7). The Hopf bifurcation solution has been demonstrated by (3.26) in which the system oscillates in time by frequency ϑ_1.
The solution (3.27) states Turing bifurcation solution that it does not have oscillation in time ($\vartheta_2 = 0$). And finally, Turing- Hopf bifurcation solution has been obtained by (3.28) that states there are spatial and time oscillation by frequency ϑ_1. To find out necessary conditions of existence and stability of the reduced system, we apply linear analysis, applied in Kidachi, 1980. Indeed we apply linear analysis in order to determine the conditions for the existence and the stability of the equilibrium in (3.25)- (3.28) and construct the associated bifurcation diagram in the plane $(d^{(2)}, \delta^{(2)})$. The eigenvalues of the jacobian matrix associated to the system (3.21) in the trivial point are straightforwardly obtained; the equilibrium state O is stable if the following conditions hold:

$$\sigma_j < 0, \ \ \texttt{for } j = 1,2. \tag{3.30}$$

The eigenvalues of the jacobian matrix computed at the point H are $\lambda_1^H = -2\sigma$ and $\lambda_2^H = \sigma_2 + \sigma_1\Omega_2/L_1$. Therefore, the conditions for the existence and stability of the stationary point H and, consequently, of a uniform oscillating solution for the system (2.7), are:

$$L_1 > 0, \tag{3.31}$$

$$\sigma_1 > 0, \tag{3.32}$$

$$\sigma_2 + \frac{\sigma_1\Omega_2}{L_1} < 0. \tag{3.33}$$

Then, along the line S_1, defined as follows:

$$\sigma_1 = 0, \quad \sigma_2 < 0. \tag{3.34}$$

The equilibrium O loses its stability and bifurcates into a solution H. This corresponds to a Hopf bifurcation and therefore to an oscillating in time solution for the reaction- diffusion system (2.7). Notice that $\mathcal{S}_1$ in (3.34) is a horizontal line in the plane $(d^{(2)}, \delta^{(2)})$ as σ_1 is linearly dependent only on $\delta^{(2)}$.
Analogously, the existence and stability of the solution T in (3.27) are obtained when:

$$L_2 > 0, \tag{3.35}$$
$$\sigma_2 > 0, \tag{3.36}$$
$$\sigma_1 + \frac{\sigma_2 \Omega_1}{L_2} < 0, \tag{3.37}$$

and along the critical line $\mathcal{S}_2$

$$\sigma_2 = 0, \quad \sigma_1 < 0. \tag{3.38}$$

the equilibrium O loses its stability and bifurcates into a solution T. This corresponds to a Turing bifurcation for the original system (2.7) so that a stationary pattern develops. Notice that $\mathcal{S}_2$ is a line in the plane $(d^{(2)}, \delta^{(2)})$ as σ_1 is linearly dependent only on $d^{(2)}$ and $\delta^{(2)}$.
Finally, the characteristic polynomial computed at the point TH given in (3.28) reads $\lambda^2 - t\lambda + d$, where:

$$t = 2(L_1\rho_1^2 + L_2\rho_2^2), \quad d = 4\rho_1^2\rho_2^2(L_1L_2 - \Omega_1\Omega_2), \tag{3.39}$$

The stability for TH occurs when $t < 0$ and $d > 0$. Taking into account the expression of the coordinate of TH given in (3.28), the point TH exists stable when the following conditions hold:

$$\sigma_1 L_2 + \sigma_2 \Omega_1 > 0, \tag{3.40}$$
$$\sigma_2 L_1 + \sigma_1 \Omega_2 > 0, \tag{3.41}$$
$$L_1 L_2 - \Omega_2 \Omega_1 > 0, \tag{3.42}$$
$$\sigma_1 L_2(\Omega_2 + L_1) + \sigma_2 L_1(\Omega_1 + L_2) > 0, \tag{3.43}$$

From the conditions (3.31)-(3.33) and (3.41) one recovers that, along the line $\mathcal{S}_3$, defined as follows:

$$\sigma_2 L_1 + \sigma_1 \Omega_2 = 0, \quad L_1 > 0, \sigma_1 > 0, \tag{3.44}$$

the solution H bifurcates into a TH solution. Correspondingly the system (2.7) undergoes a Turing-Hopf bifurcation and a mixed limit cycle-mode and spatial pattern mode solution is admitted. $\mathcal{S}_3$ in (3.44) is a line in the plane $(d^{(2)}, \delta^{(2)})$, as L_1 and Ω_2 are independent on $d^{(2)}$ and $\delta^{(2)}$ and σ_j, $j = 1, 2$ are linearly dependent on $d^{(2)}$ and $\delta^{(2)}$.
Analogously, from the conditions (3.35)-(3.37) and (3.40), we define the following line $\mathcal{S}_4$:

$$\sigma_1 L_2 + \sigma_2 \Omega_1 = 0, \quad L_2 > 0, \sigma_2 > 0, \tag{3.45}$$

Upon crossing $\mathcal{S}_4$ the equilibrium T loses its stability bifurcating into a TH solution, which corresponds to a mixed limit cycle-mode and spatial pattern mode solution for the reaction-diffusion system (2.7): Again notice that $\mathcal{S}_4$ in (3.45) is a line in the plane $(d^{(2)}, b^{(2)})$, as L_2 and Ω_1 are independent on $d^{(2)}$ and $\delta^{(2)}$ and $\sigma_j, \quad j = 1, 2$ are linearly dependent on $d^{(2)}$ and $\delta^{(2)}$.

3.3 Numerical results

This section presents the normal form results around Turing- Hopf codimension-2 bifurcation point, whose analysis was obtained in the previous section. To numerically investigate normal form analysis for a set of parameters, we have received region and figures below:

$$m_1 = 0.5, \quad m_2 = 0.7, \quad \eta = 0.8, \quad \alpha = 5, \quad \gamma = 1.6, \quad d_u = 0.1, \quad d_w = 0.02, \tag{3.46}$$

which obtain $E^* = (0.21, 0.33, 0.55)$ and $\delta^c = 1.0753$, $d_c = 43.3325$, Moreover, critical wave number and critical frequency in which Turing and Hopf bifurcation emerge correspondingly are $k_c^2 = 0.4144$, $\Omega_c = 0.8447$.

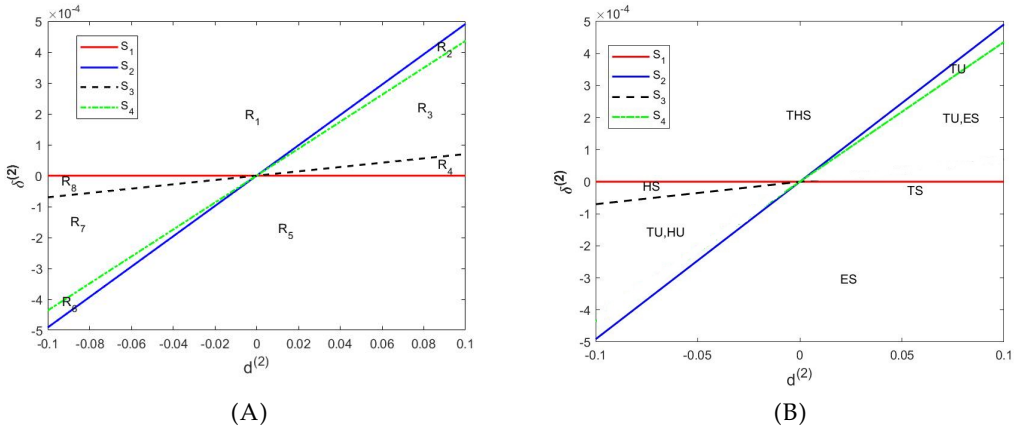

(A) (B)

FIGURE 3.1: The region found by amplitude equations (3.21). Given parameters are: $m_1 = 0.5, \quad m_2 = 0.7, \quad \eta = 0.8, \quad \alpha = 5, \quad \gamma = 1.6, \quad d_u = 0.1, \quad d_w = 0.02$, which obtain $E^* = (0.21, 0.33, 0.55)$ and $\delta^c = 1.0753$, $d_c = 43.3325$, Moreover, critical wave number and critical frequency in which Turing and Hopf bifurcation emerge correspondingly are given $k_c^2 = 0.4144$, $\Omega_c = 0.8447$.

The lines $\mathcal{S}_i$ mentioned in (3.34)- (3.38), (3.44), (3.45) are plotted in Figure 3.1. Indeed, the Figure 3.1A demonstrates the lines which divided the plane $(d^{(2)}, \delta^{(2)})$ into the eight regions $R_i, \ i = 1, 2, ..., 8$. However, the lines $\mathcal{S}_3$, $\mathcal{S}_4$ are defined as $d^{(2)} < 0$, $d^{(2)} > 0$ respectively. In the other words, the region $R_3 = R_4$ and $R_6 = R_7$ which are also proved numerically. Hence in general there are six regions. In addition Figure 3.1B obtains which type of instability each region contains. Therefore, in next we investigate how each region includes of instability.

From the Figure 3.1A, we choose the point $(d^{(2)}, \delta^{(2)}) = (0.02, 0.001) \in R_1$. Linear analysis of the system (3.21) determines that the region R_1 has five equilibria

which are $(0,0)$, and $(\pm 0.0053, \pm 0.0031)$. That means that the original system (2.7) has a saddle point origin and four stable coexistence steady states, which imply to Turing-Hopf instability. Numerical solution of the original system (2.7) also reports Turing-Hopf pattern when $d = d_c + \varepsilon d^{(2)}$ and $\delta = \delta^c + \varepsilon\delta^{(2)}$ where $\varepsilon d^{(2)} = 0.02$, and $\varepsilon^2\delta^{(2)} = 0.001$ in Figure 3.2.

In addition, the Figure 3.2A illustrates that there is a bistability since the Turing patterns switches to Turing- Hopf pattern. The Figure 3.2B is its close shot.

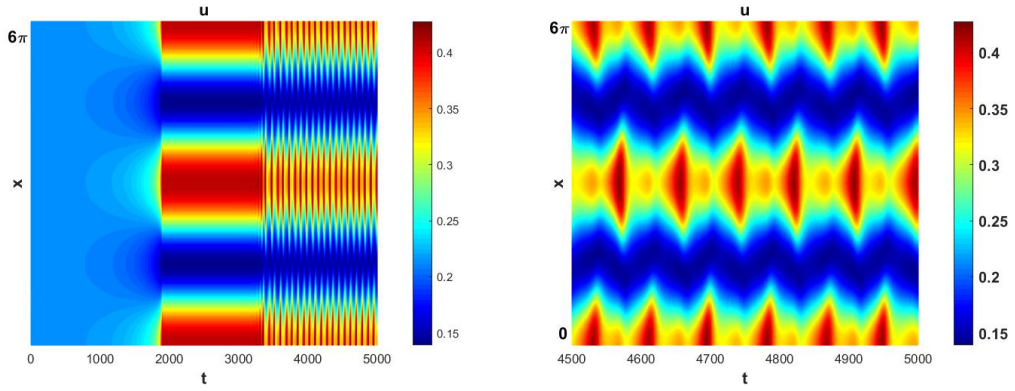

(A) $(d^{(2)}, \delta^{(2)}) \in R_1$ (B) $(d^{(2)}, \delta^{(2)}) \in R_1$

FIGURE 3.2: It denotes to Turing- Hopf pattern located in the region R_1, the chosen perturbation parameters are $(d^{(2)}, \delta^{(2)}) = (0.02, 0.001)$. Other parameters are fixed as Figure 3.1. B) is a close shot of figure A). In T-H region Coefficients of amplitude equations (3.21), (3.22) are achieved as: $\sigma_1 = -4.0088, \sigma_2 = 2.1642e-04$, $L_1 = 4.7313e+03$, $L_2 = 5.6030$, $\Omega_1 = -5.9146e+05$, $\Omega_2 = -10.1148$,.

In region R_2, for chosen parameters $(d^{(2)}, \delta^{(2)}) = (0.06, 0.00028)$ there are seven equilibria $(0,0)$, that notices to the stable origin, $(0, \pm a)$ associated to unstable Turing pattern and coexistence steady states $(\pm a, \pm b)$ that have eigenvalues with negative real parts. Numerical results are mentioned in Figure 3.3.

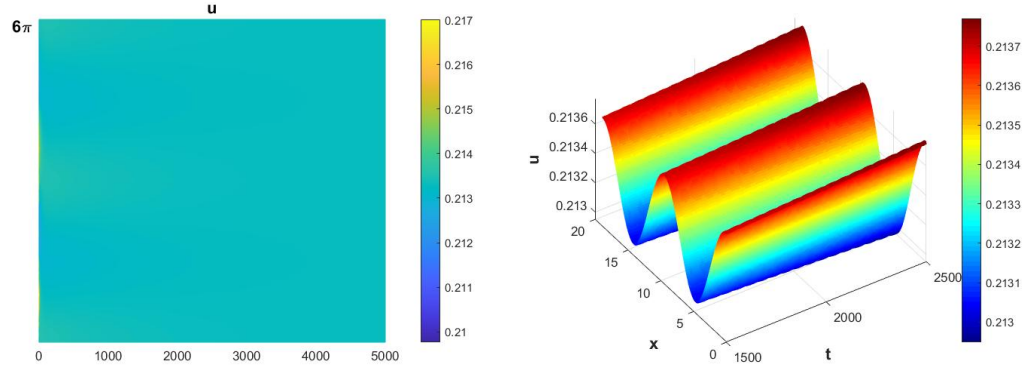

(A) $(d^{(2)}, \delta^{(2)}) \in R_2$ (B) $(d^{(2)}, \delta^{(2)}) \in R_2$

FIGURE 3.3: It denotes to Turing- Hopf pattern located in the region R_2, the chosen perturbation parameters for the Figure 3.3A are $(d^{(2)}, \delta^{(2)}) = (0.00075, 0.00009)$ such that coefficients of the amplitude equations are $\sigma_1 = -0.3608, \sigma_2 = 2.0716e-05$ and other coefficients are the same as Figure 3.2, and for the Figure 3.3B $(d^{(2)}, \delta^{(2)}) = (0.001, 0.4)$ such that coefficients of the amplitude equations are $\sigma_1 = -1.6035e+03$, $\sigma_2 = 0.0960$ and other parameters and other coefficients are fixed for both figures as Figure 3.1 and Figure 3.2 respectively.

In region $R_3 = R_4$, the system (3.21) has three equilibria in which the origin $(0, 0)$ is stable and $(0, \pm c)$ are nodal sources and unstable. That means the system (2.7) contains a constant steady state solution and two unstable solutions, which imply the unstable Turing pattern. See the Figure 3.4.

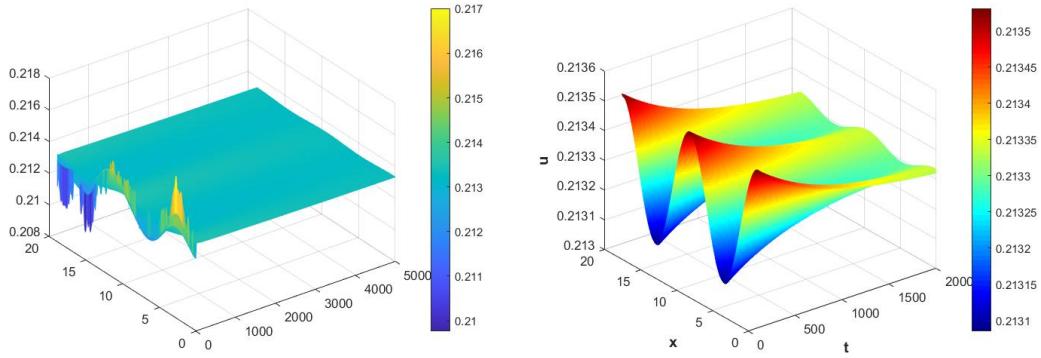

(A) $(d^{(2)}, \delta^{(2)}) \in R_3$ (B) $(d^{(2)}, \delta^{(2)}) \in R_3$

FIGURE 3.4: For fixed parameters given in Figure 3.1 Turing-Hopf pattern located in the region R_2, the chosen perturbation parameters for the Figure 3.4A are $(d^{(2)}, \delta^{(2)}) = (0.028, 0.0001)$ such that coefficients of the amplitude equations are achieved $\sigma_1 = -0.4009$, $\sigma_2 = -3.0607e-04$, and for the Figure 3.4B are $(d^{(2)}, \delta^{(2)}) = (0.1, 0.0004)$ and coefficients are $\sigma_1 = -1.6035$, $\sigma_2 = -2.1883e-05$,, and other parameters and other coefficients are fixed for both figures as Figure 3.1 and Figure 3.2 respectively.

In region R_5 the numerical results are interpreted as: The system (3.21) admits

seven equilibria unstable origin $(0,0)$, two stable point $(\pm e,0)$ and two nodal sources $(0,\pm f)$ where given parameters are $(d^{(2)},\delta^{(2)}) = (0.005,-0.0002)$ (see Figure 3.5A) and $(d^{(2)},\delta^{(2)}) = (0.3,-0.0001)$ (see Figure 3.5B).

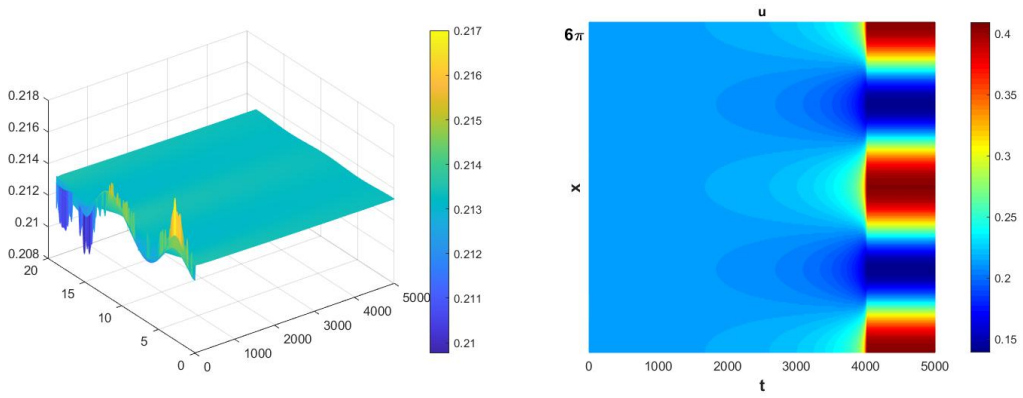

(A) $(d^{(2)},\delta^{(2)}) \in R_5$ (B) $(d^{(2)},\delta^{(2)}) \in R_5$

FIGURE 3.5: It denotes to stability and Turing pattern located in the region R_5, the chosen perturbation parameters for the Figure 3.5A are $(d^{(2)},\delta^{(2)}) = (0.005,-0.0002)$ such that coefficients of the amplitude equations are achieved $\sigma_1 = 0.8018$, $\sigma_2 = -5.3894e-05$, and for the Figure 3.5B are $(d^{(2)},\delta^{(2)}) = (0.3,-0.0001)$ such that coefficients of the amplitude equations are achieved $\sigma_1 = 0.4009$, $\sigma_2 = -3.7765e-04$. and other parameters and other coefficients are fixed as Figure 3.1 and Figure 3.2 respectively.

Furthermore, the region R_6 contains the equilibria unstable origin $(0,0)$ and nodal sink $(\pm g,0)$ which denotes unstable Hopf patterns (see Figure 3.6A). Moreover, the region $R_7 = R_8$ includes of unstable origin, and two nodal sinks $(\pm h,0)$ when $(\delta^{(2)},d^{(2)}) = (-0.05,-0.0001)$. Around and very close to the negative side of the line $\mathcal{S}_1$ we found Hopf pattern for given parameters $(\delta^{(2)},d^{(2)}) = (0.0003,-0.94)$ (See Figure 3.6).

Here we notice that a,b,c,d,e,f denote symbolic numbers.

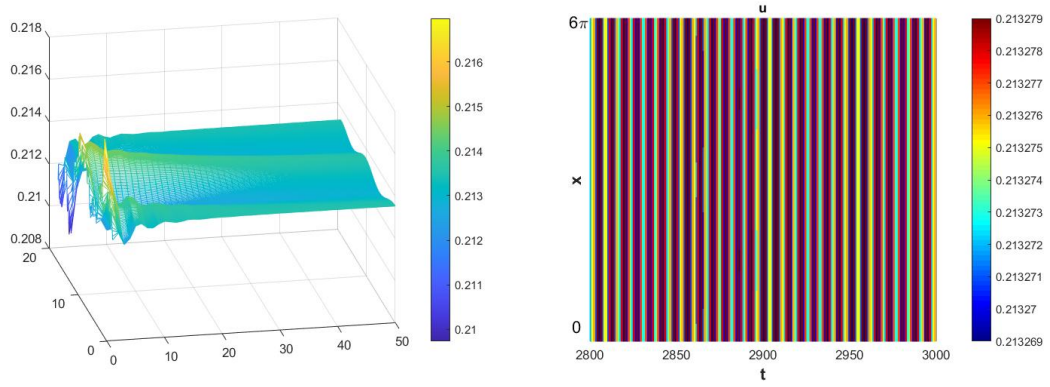

(A) $(d^{(2)}, \delta^{(2)}) \in R_8$ (B) $(d^{(2)}, \delta^{(2)}) \in R_8$

FIGURE 3.6: A) It denotes to stability and Turing pattern located in the region R_8, the chosen perturbation parameters are $(d^{(2)}, \delta^{(2)}) = (-0.06, -0.00028)$ such that coefficients of the amplitude equations are achieved $\sigma_1 = 1.1225$, $\sigma_2 = 3.5295e - 06$. B) Hopf pattern emerged by chosen parameter close to the negative part of the line $\mathcal{S}_1$ are $(d^{(2)}, \delta^{(2)}) = (-0.094, -0.00003)$ such that coefficients of the amplitude equations are achieved $\sigma_1 = 0.1203$, $\sigma_2 = 1.0361e - 04$. and other parameters and other coefficients are fixed for both figures as Figure 3.1 and Figure 3.2 respectively.

Chapter 4

A diffusive model of one prey and two competitive predators

According to the competitive exclusion principle, two or more competitors cannot coexist obscurely (Freedman, 1980). This principle empirically has been examined by Gause (Gause, 1934), while later Ayala's experiments (Ayala, 1969) on two species of Drosophila illustrated coexistence of competitors on a single prey is possible. Several models were theoretically presented to explain Ayala's results. One of the first ones was introduced by Armstrong and McGehee (Armstrong and McGehee, 1980). They considered the model as:

$$\begin{aligned} \frac{du}{dt} &= ru(1-\frac{u}{K}) - auv - \frac{Auv}{1+Bu}, \\ \frac{dv}{dt} &= v(-d+eu), \\ \frac{dw}{dt} &= w(-D+\frac{Eu}{1+Bu}) \end{aligned} \tag{4.1}$$

where u, v, and w denote prey, and predator population densities respectively. Prey grows logistically in absence of competitors and one predator feeding rate is defined with Holling type II functional responses. Authors explored that for adequate given parameters and initial values the system predicts the coexistence of the two predators via a locally attracting periodic orbit.

Indeed, Hutchinson's studies (Hutchinson, 1964) were endorsed by Armstrong and McGehee's results, since Hutchinson's studies obtained that two competing species *"might oscillate in varying numbers, but persist almost indefinitely"*. Whereas other studies (Loladze et al., 2004) and (Levin, 1970) showed that these types of systems do not contain component-wise positive equilibrium and consequently cannot contain stable equilibrium. Another issue regarding Armstrong and McGehee's model was the coexistence steady state only can weakly persistent, but not persistent, therefore it is not permanent. This model was generalized by Hsu, Hubble and Waltman (Hsu, Hubbell, and Waltman, 1978b; Hsu, Hubbell, and Waltman, 1978a) (see also Butler and Waltman (Butler and Waltman, 1981), Cushing (Cushing, 1984, Farkas Farkas, 1984)) such that both competing predators contain Holling type II

functional responses as follows:

$$\begin{aligned} \dot{s} &= \Gamma[\gamma(1-\frac{s}{K})s - \frac{m_1 u_1 s}{a_1+s} - \frac{m_2 u_2 s}{a_2+s}], \\ \dot{u_1} &= \Gamma[\frac{m_1 u_1 s}{a_1+s} - d_1 u_1], \\ \dot{u_2} &= \Gamma[\frac{m_2 u_2 s}{a_2+s} - d_2 u_2]. \end{aligned} \tag{4.2}$$

In this model, s, and u_1, and u_2 imply prey and two competing predators correspondingly. Prey has logistic growth rate while competitors grow via Holling Type II functional responses.

Significant progress of the model presented by Hsu and coauthors (4.2) over Lotka-Volterra model was that bounded resource for each competitive species was expressed with an equation, while in the competitive **LV** model of two predators for a single common prey, only the number of competing species were considered (Hsu, Hubbell, and Waltman, 1978b). Roughly speaking, in the model (4.2), the outcome of competition of one species in absence of another predator is predictable due to measuring growth parameters of functional responses, however in the **LV** model predicting the outcome of the competition is only possible in presence of both predator species.

For the first time this model was originally rised in micro-organism test tube known as chemostat. *A chemostat (from the chemical environment that is static) is a bioreactor to which fresh medium is continuously added, while culture liquid containing leftover nutrients, metabolic end products, and microorganisms is continuously removed at the same rate to keep the culture volume constant (Novick and Szilard, 1950)* (see also Butler and Waltman, 1981). In addition, every three species that satisfy some theoretical conditions (see Farkas, 1987) can contain the known Phenomenon " *ZiP Bifurcation"* (see alsoFarkas, 1984).
One necessary condition is those boundary parameters of predator species are equal for both predators. This assumption leads structurally to an unstable system that is not able to explain a real ecosystem. That is why in these types of systems one predator would be considered *"r-strategist"* and the other one would be considered *"K- strategist"* (Echeverri, Giraldo, and Zarrazola, 2017). Later Farkas studied Zip bifurcation for the model (4.2) employing generalized Holling type III functional responses (Sáez, Stange, and Szántó, 2006), four-dimensional model raised in economy and politology (Bocsó and Farkas, 2003), and more can be found in references in (Echeverri, Giraldo, and Zarrazola, 2017).

In the modeling of competitive predators for a single prey, researchers have investigated the existence of strong coexistence equilibrium through different factors such as interspecific interference (Vance, 1984, Vance, 1985), spatial heterogeneity (Cantrell and Cosner, 2004), and so on. Moreover, the intraspecific interference factor has also been considered an important factor. Indeed, intraspecific interference causes aggressive dispels, fighting, and other behaviors. Intraspecific interference majorly influences feeding rate. This effect can be modeled by other functional responses Beddington–DeAngelis form. Cantrell and coauthors (Cantrell, Cosner, and Ruan, 2004) investigated the modified model of (4.2) by using Beddington-DeAngelis functional responses for one predator species and Holling type II functional responses for the other one. They proved that the coexistence of two or more consumer species feeding on a single specie is possible.

In 2007 Shigui Ruan (Ruan et al., 2007) and others considered a two-competitor/one-prey model in which both competitors exhibit a general functional response, and

one of the competitors reveals a density-dependent mortality rate. They show that the two competitors can coexist upon a single prey. For example, they considered a two-competitor/one-prey model with a Holling II functional response. And demonstrated that density-dependent mortality in one of the competitors could prevent competitive exclusion.

In 2017, Echeverri and coauthors (Echeverri, Giraldo, and Zarrazola, 2017) presented a model of two competing species over a single common prey. Prey has a logistic growth rate, and a predator's feeding rate is defined with concrete trigonometric functions. They proved that this model exhibited the competitive exclusion principle and confirmed the existence of Zip bifurcation.

To investigate the segregation or aggregation of species in a model, reaction-diffusion models are considered. The system employs self-diffusion to demonstrate the movement of species from higher density to lower density. In studying the movement of the species toward /or away from other species, cross-diffusion is utilized.

Ferreira and coauthors (Ferreira and Oliveira, 2009) considered a diffusive model of (4.2) such that the species have self-diffusion. They considered that zip bifurcation is sustained in this type of reaction-diffusion model.

Recently, Ferreira and coauthors (Ferreira, Silva, and Rao, 2019) considered (4.2) with two diffusive types models consisting cross-diffusion. The authors proved that one model sustained Zip Bifurcation while in the other one Zip Bifurcation vanished due to the appearance of Turing instability. Indeed, in the second diffusive model, authors supposed cross-diffusion that predators chase the prey in the same direction, i.e the cross-diffusion parameters were considered negative.
Here we would investigate the diffusive modified model of (4.2) such that the competitive predators avoid each other as chase the prey specie.

This Chapter is organized as well: In 4.1, we review the ZIP model (4.2), coexistence equilibria, and its stability conditions. We introduce the modified model in 4.2, and we then analyze the coexistence of the species in the modified model, its stability conditions, and necessary conditions of Hopf bifurcation in 4.3, In 4.5, 4.4 Turing regions and Turing instability of reaction-diffusion are investigated, and we perform numerical simulation in 4.6. The growth rate is studied in 4.7, and finally global solution of the model by invariant region is established in 4.8.

4.1 Primary Competitive model

Here we consider the model (4.2) whose parameters are obtained in Table 4.1.

Since competitors do not have the interface, we remind u_1 and u_2 are corresponding population densities of competitive predators feeding on a single prey specie s. Both species have access to the prey and compete only by lowing the population shared prey. As it is evident, the prey has a logistic growth rate by $K > 0$ carrying capacity and $\gamma > 0$, which is the intrinsic rate of the increase of the prey. In addition, $s > K$ means that the number of prey is more significant than its carrying capacity, which makes the prey population density unstable. Moreover, the predators have **Holly type-II** functional response that is also called **saturation model** and also **feeding rate**. This means that the amount of prey consumed per predator is a function of the number of present prey. According to the (Farkas, 1984), saturation occurs when the number of prey is large.

In functional response, $m_i > 0$; the growth rate of predators, and a_i denotes the half-saturation constants, which means that the amount of prey that must be

TABLE 4.1: parameters appearing in Eqs.(4.2)

Parameter Value	Description
Γ	regularizes the domain
γ	intrinsic prey growth rate
K	carrying Capacity with respect to the prey
m_i	birth rate of u_i
d_i	death rate of u_i
a_i	half saturation constant

present for the feeding rate reaches half of its maximum. The increasing function of the feeding rate is given:

$$\text{Feeding Rate} = \frac{m_i s}{a_i + s},$$

It converges to $\frac{m_i}{2}$ as s goes to infinity. In other words, since the feeding rate is an increasing function, as the number of prey rises, the number of prey populations eaten by predator u_i will be greater than the feeding rate correspondingly.

Hence a_i is the half-saturation constant for the $i_t h$ predator which is the prey density at which the functional response of the predator is half maximal (Figure 4.1).

The model (4.2), has been studied by many mathematicians. Hsu, Hubble and Waltman (Hsu, Hubbell, and Waltman, 1978a) proved that the system has a positive octant set with respect to the positive initial conditions. And the necessary condition of survive of the $i-th$ predator is that $0 < \lambda_i < K$ where

$$\lambda_i = \frac{m_i a_i}{m_i - d_i}, \tag{4.3}$$

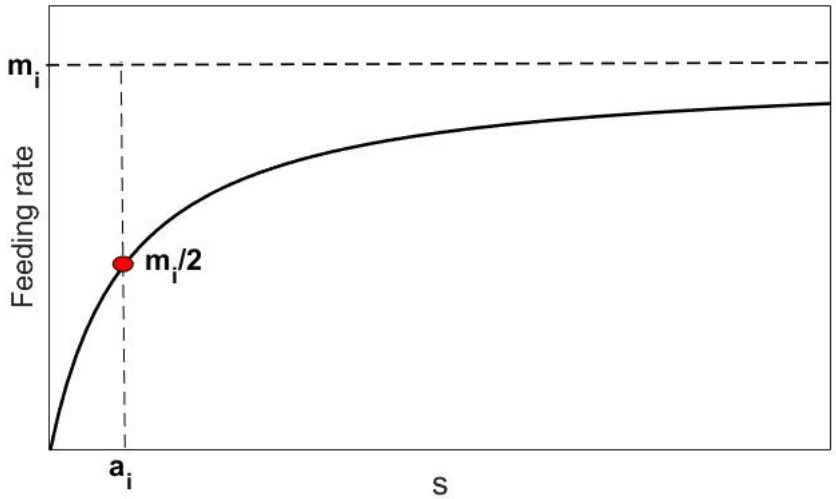

FIGURE 4.1: Schematic plot of feeding rate.

Hsu and coauthors studied the general case in which $\lambda_1 \neq \lambda_2$. Some paper

published (Koch, 1974; Hsu, Hubbell, and Waltman, 1978a) about computer experimental results that show periodic solutions are expected in positive invariant region. Later Smith (Smith, 1982) applied bifurcation theory to prove the existence of periodic solutions in positive octant when the case of $\lambda_1 < \lambda_2$ and the value of $|\lambda_1 - \lambda_2|$ and $K - (a_1 + 2\lambda_1)$ are small enough.

Wilken (Wilken, 1982) considered the particular case $\lambda_1 = \lambda_2 = \lambda$. Moreover, for the case $a_1 = a_2 = a$ the results are summarized as:
I) When $K \leqslant a + 2\lambda$: There is a line segment of stable equilibrium points. II) $K > a + 2\lambda$ then all three species survive and cycle permanently. However, for $a_1 > a_2$, then if
I) $K \geqslant a_1 + 2\lambda$ one of predator species vanishes,
II) $K \leqslant a_1 + 2\lambda$ all species survive and and the solutions tend to some equilibrium point on the line segment.

Indeed, if $\lambda_1 = \lambda_2$ where $a_1 > a_2$, then for $b_i = m_i/d_i$ is $b_1 < b_2$ we have

$$\frac{a_1 d_1}{m_1 - d_1} = \frac{a_2 d_2}{m_2 - d_2}$$

$$a_1 d_1 d_2 (m_1/d_1 - 1) = a_2 d_2 d_1 (m_2/d_2 - 1)$$

thus $b_1 > b_2$ which means that the birth to death ratio of the predator u_1 is greater than predator u_2. Therefore, two different strategies take place. One of them is called $r - strategist$ in which species need more food to survive since the ratio of the birth to death rate and half saturation is higher. The other one is called $k - strategist$, which the predators species of this type need less food to survive when the birth to death rate and half saturation constant are less.

In the next section we consider the model of two predators compete for the same resource, such that this model include of *Zip Bifurcation*.

4.1.1 Line of Equilibria and Zip Bifurcation

In this section we present analysis of the model (4.2) in which $\lambda_1 = \lambda_2 = \lambda$ and a_1 can be different from a_2. Here we suppose $a_1 > a_2$. Indeed, the system accepts equilibria which $(0,0,0), (K,0,0)$ are the trivial equilibria and unstable while there is a line that denotes also the coexistence of the steady state fixed points (Farkas, 1984) $U^* = (s^* = \lambda, u_1^*, u_2^*)$, i.e

$$\frac{m_1 u_1^*}{a_1 + \lambda} + \frac{m_2 u_2^*}{a_2 + \lambda} = \gamma(\frac{K - \lambda}{K}), \tag{4.4}$$

4.1.2 Positivity and stability condition of Equilibiria

Coexistence fixed points (4.4) are positive if

$$s^* = \lambda = \frac{a_i d_i}{m_i - d_i} > 0, \quad i = 1,2 \ \text{ iff } \quad m_i > d_i, \tag{4.5}$$

Since, the two other components u_1^* and u_2^* are located in a line (4.4), to prove that $u_i^*, \quad i = 1,2$ are positive, we need to to show that the two bounds of the segment

line (4.4) are positive, i.e, once we set $u_1^* = 0$ so

$$u_2^* = \frac{\gamma(\frac{K-\lambda}{K})}{\frac{a_2+\lambda}{m_2}}, \tag{4.6}$$

and then $u_2^* = 0$, which gives

$$u_1^* = \frac{\gamma(\frac{K-\lambda}{K})}{\frac{a_1+\lambda}{m_1}}, \tag{4.7}$$

since all parameters are positive (4.7) and (4.6) depict that u_1^* and u_2^* are also positive if

$$K > \lambda, \tag{4.8}$$

Therefore, according to (4.8) and (4.5), and also because of continuity of the line (4.4), we conclude that all equilibria in the line (4.4) are positive.

Linear analysis at U^* implies

$$K(U^*) = \begin{bmatrix} \frac{-\gamma\lambda}{K} + \lambda(\frac{m_1u_1^*}{(a_1+\lambda)^2} + \frac{m_2u_2^*}{(a_2+\lambda)^2}) & \frac{-m_1\lambda}{a_1+\lambda} & \frac{-m_2\lambda_2}{a_2+\lambda} \\ \frac{\beta_1u_1^*}{a_1+\lambda} & 0 & 0 \\ \frac{\beta_2u_2^*}{a_2+\lambda} & 0 & 0 \end{bmatrix} = \begin{bmatrix} f_1 & f_2 & f_3 \\ f_4 & 0 & 0 \\ f_6 & 0 & 0 \end{bmatrix} \tag{4.9}$$

where $\beta_i = m_i - d_i$ and to apply relation we use f_i such that $f_1,\ f_2,\ f_3 < 0$ and $f_4,\ f_6 > 0$.

Theorem 4.1.1 *(Farkas, 1984) The system is locally stable at U^* if $f_1 < 0$, i.e*

$$\frac{m_1u_1^*}{(a_1+\lambda)^2} + \frac{m_2u_2^*}{(a_2+\lambda)^2} < \frac{\gamma}{K}. \tag{4.10}$$

Remark 4.1.1 *In the case $\lambda_1 = \lambda_2 = \lambda$ and $a_1 > a_2$, carrying capacity K is considered as bifurcation parameter, thus for a fixed K and fixed all parameter set there are two lines:*
i. Stability line: for a fixed λ includes all equilibria $U^* = (\lambda, u_1^*, u_2^*)$ such that $u_1^*, u_2^* > 0$, and satisfy

$$\frac{m_1u_1^*}{(a_1+\lambda)^2} + \frac{m_2u_2^*}{(a_2+\lambda)^2} = \frac{\gamma}{K}, \tag{4.11}$$

ii. Equilibrium line(4.4).

Theorem 4.1.2 *(Farkas, 1984) According to the stability condition* (4.10)*, and for bifurcation parameter K, all the points (λ, u_1^*, u_2^*) located in line* (4.4)*:*
a) are stable if $\lambda < K < a_2 + 2\lambda$ (see Figure 4.3B).
b)does not satisfy the inequality (4.10) *and are unstable if $K > a_1 + 2\lambda$ Figure 4.3A.*
c) in the case $a_2 + 2\lambda \leqslant K \leqslant a_1 + 2\lambda$, for a fixed K the two line mentioned in Remark

4.1.1 *intersect at* $(u_1(K), u_2(K))$ *such that the line* (4.4) *divided into two parts. One part includes of stable points which satisfy* (4.11)*, an the other part contains unstable points (see Figure 4.2).*

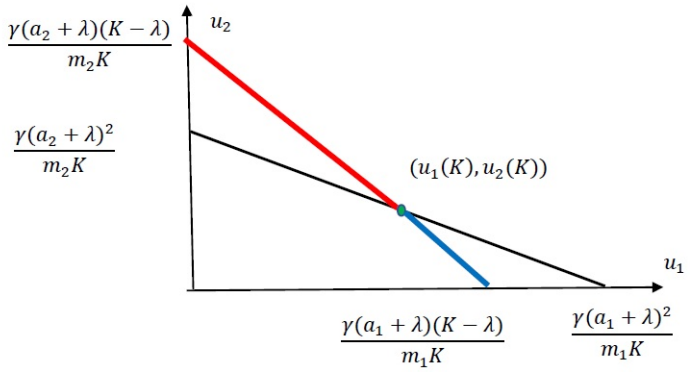

FIGURE 4.2: Zip Bifurcation, black line implies the stability condition, the green point illustrates intersection point $(u_1(K), u_2(K))$, the red line located in equilibria line shows unstable points while blue line demonstrates stable points.

Definition 4.1.1 *(Farkas, 1984) In the case c) mentioned in the Theorem 4.1.2 as K increases from* $a_2 + 2\lambda$ *up to* $a_1 + 2\lambda$ *the point* $(\lambda, u_1(K), u_2(K))$ *moves along the equilibriua line continuously from* $(\lambda, 0, \frac{\gamma(a_2+\lambda)^2}{m_2(a_2+2\lambda)})$ *to* $(\lambda, \frac{\gamma(a_1+\lambda)^2}{m_1(a_1+2\lambda)}, 0)$ *so that the point left behind become unstable (see Figure 4.2), this phenomena is called* ***Zip bifurcation****.*

Remark 4.1.2 *In addition, M. Farkas proved that the problem* (4.9) *goes to supercritical Hopf bifurcation if for a fixed K,* $K = a_i + 2\lambda$, $i = 1, 2$ *(Farkas, 1984).*

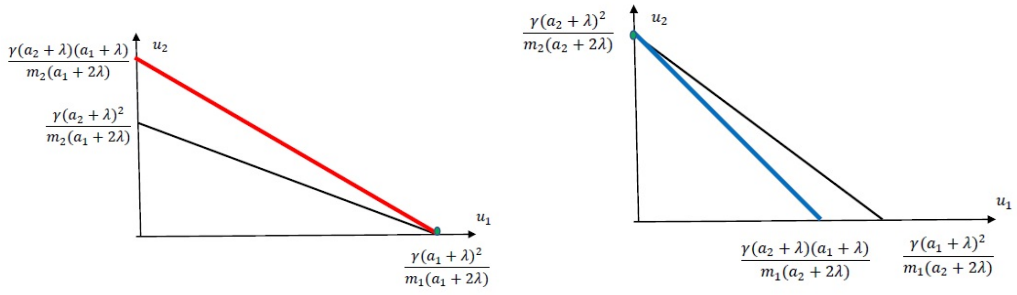

(A) $K = a_1 + 2\lambda$ (B) $K = a_2 + 2\lambda$

FIGURE 4.3: Zip bifurcation arises for fixed K, A) when $K = a_1 + 2\lambda$ all points on the equilibria line are unstable (red line). B) when $K = a_2 + 2\lambda$ all points on the equilibria line are stable since they satisfy condition (4.10) (blue line).

4.1.3 Turing and Zip bifurcation in a reaction- diffusion system

The model of segregation phenomena of the system (4.9) included of self and cross- diffusion investigated by J. D. Ferreira and coauthors. (Ferreira, Silva, and

Rao, 2019) presented as

$$\begin{cases} s_t &= \Delta(k_{11}s + k_{12}u_1 + k_{13}u_2) + \Gamma[\gamma(1-\frac{s}{K})s - \frac{m_1u_1s}{a_1+s} - \frac{m_2u_2s}{a_2+s}], \\ u_{1t} &= \Delta(k_{21}s + k_{22}u_1 + k_{23}u_2) + \Gamma[\frac{m_1u_1s}{a_1+s} - d_1u_1], \\ u_{2t} &= \Delta(k_{31}s + k_{32}u_1 + k_{33}u_2) + \Gamma[\frac{m_2u_2s}{a_2+s} - d_2u_2], \end{cases} \tag{4.12}$$

where the Jacobian matrix of the system (4.2) at one point of the equilibria line is (4.9).

Ferreira and coauthors (Ferreira, Silva, and Rao, 2019) claimed when diffusion matrix above added to the system, segregation phenomena yields Turing patterns while Zip bifurcation vanishes. Indeed, they surveyed diffusion matrix when k_{12}, $k_{13} > 0$, $k_{ii} > 0$ for $i = 1, 2, 3$ while $k_{31},\ k_{21}, k_{23},\ k_{32} < 0$.

Since the system is degenerated, weakly nonlinear analysis cannot be applied. In the next section, we introduce the modified model of the system (4.2) such that the system accepts only one coexistence steady state.

4.2 Modified Model

A modified model of the system (4.2) is introduced here. Indeed, this model is also explaining the competition of two predators for one resource while there is intraspecific interaction between the predator u_1 too, i.e the predator populations u_1 not only decrease due to death but also the interaction between congeners. Moreover, it is obvious that when ε tends to zero, this model returns to the model (4.2). We are aiming to investigate this model locally and also we analyze emergence of patterns. So we consider the diffusion part of the second diffusive model coming form (Ferreira, Silva, and Rao, 2019). The system is introduced as:

$$\begin{cases} s_t &= \Delta(k_{11}s + k_{12}u_1 + k_{13}u_2) + \Gamma[\gamma(1-\frac{s}{K})s - \frac{m_1u_1s}{a_1+s} - \frac{m_2u_2s}{a_2+s}], \\ u_{1t} &= \Delta(k_{21}s + k_{22}u_1 + k_{23}u_2) + \Gamma[(\frac{m_1u_1s}{a_1+s} - \varepsilon u_1^2) - d_1u_1], \\ u_{2t} &= \Delta(k_{31}s + k_{32}u_1 + k_{33}u_2) + \Gamma[\frac{m_2u_2s}{a_2+s} - d_2u_2], \end{cases} \tag{4.13}$$

with homogeneous Neumann boundary conditions in 1D, and where all parameters are defined as the system (4.12), except $\varepsilon > 0$ is added to the system as a intraspecific coefficients of the predator u_1.

Remark 4.2.1 *The reaction of predator u_1 states when the population density of prey s is very large, predator u_1 grows logistically with intrinsic growth rate m_1 and carrying capacity $\frac{m_1}{\varepsilon}$, which means that it cannot grow unbounded.*

Proposition 4.2.1 *To conquer degeneracy of the system (4.12), and have a unique coexistence steady state, one needs $\lambda_1 \neq \lambda_2$, where λ_i have been defined in (4.3)*

In zip model (4.2), both predators interact with prey with Holling type II functional response. According to the competitive exclusion principle (Gause's law) only one species will survive in a niche. That is why previous authors Ferreira, Silva, and Rao, 2019 proposed r- and K-strategies to avoid extinction.

Moreover, self-diffusion parameters $k_{ij} > 0$ for $i = j$, $i = 1, 2, 3$ are self diffusion parameters and k_{ij} for $i \neq j$ are cross- diffusion parameters, so that $k_{12}, k_{13} > 0$.

Remark 4.2.2 *According to the cross-diffusion parameters k_{32} and k_{23} two types of strategies can be evolved as below: i) first strategy is $k_{32}, k_{23} < 0$ that implies predators are chasing prey in the same direction. ii) and second strategy denotes $k_{32}, k_{23} > 0$ which states that predators avoid each other.*

Therefore for the first strategy, and for parameter $k_{1j} > 0$ states that the part $-k_{12}\nabla u_1 - k_{13}\nabla u_2$ of the flux s is directed towards decreasing population density of u_j that the prey runs away from predators. On the other hand, the conditions $k_{2j} < 0$ for $j = 1, 3$, implies that the part $-k_{21}\nabla s - k_{23}\nabla u_2$ of the flux of u_1 is directed towards increasing population density of s and u_2 which means that the predator u_1 moves in anticipation of the predator u_2 and the defense switching behavior of the preys. That is u_1 changes the prey, s. The fluxes for k_{3j} when $j = 1, 2$ are similarly explained.

Nevertheless, second strategy is about predators who are chasing prey in different directions, or in the other word they avoid each other, so diffusion parameters $k_{32}, k_{23} > 0$. Thus the part $-k_{21}\nabla s - k_{23}\nabla u_2$ denotes of flux of u_1 is directed toward decreasing population density of u_2 and increasing population density of s which demonstrates that predator u_1 moves against direction of predator u_2, while it is chasing prey. Rigorously, the flux of k_{3j} in the second strategy is interpreted.

However, we investigate some necessary conditions of emergence of Turing patterns when diffusion is considered as second strategy, and we try to consider a system which can be contained Turing with less diffusion parameters, thus we set $k_{31} = k_{21} = 0$. In fact, to have Turing instability, the necessity of cross-diffusion is surveyed. First, we analyze local stability of the modified system.

4.3 Local analysis of modified model

In this section, first due to the Theorem 2.3.1 we know each coordinate plane is invariant. Now we investigate extinction of species. So we apply the method mentioned in (Chauvet et al., 2002). In absence of prey the system is given:

$$\begin{aligned} \frac{du_1}{dt} &= -d_1 u_1 - \varepsilon u_1^2, \\ \frac{du_2}{dt} &= -d_2 u_2, \end{aligned} \tag{4.14}$$

This is system has one nonnegative equilibrium $(0, 0)$ which is stable. Therefore, $\frac{du_2}{dt} \leqslant -d_2 u_2$ gives $u_2 \to 0$ exponentially as $t \to \infty$. While

$$\frac{du_1}{dt} \leqslant -d_1 u_1 + \varepsilon u_1^2,$$

In case of equality, it is a Bernoulli DE. whose solution explicitly is

$$u_1 = \frac{1}{ce^{-d_1 t} + \varepsilon/d_1},$$

therefore $u_1 \to d_1/\varepsilon$ as $t \to \infty$. Indeed, it is observed that in the absence of the prey the predator u_2 is only extinct. Similarly, when $u_1 = 0$ then

$$\begin{aligned} \frac{ds}{dt} &= \gamma s(1 - \frac{s}{K}) - \frac{m_2 u_2 s}{a_2 + s}, \\ \frac{du_2}{dt} &= \frac{m_2 u_2 s}{a_2 + s} - d_2 u_2, \end{aligned} \tag{4.15}$$

This system has an unstable coexistence steady state $\left(\lambda_2, \frac{(K-\lambda_2)(a_2+\lambda_2)}{Km_2}\right)$. Indeed, $\frac{ds}{dt} \leqslant \gamma s(1 - \frac{s}{K})$ such that $\frac{ds}{dt} \leqslant \frac{K}{Kce^{-\gamma t} + 1}$, thus $s \to K$ as $t \to \infty$, consequently $\frac{du_2}{dt} \leqslant \frac{m_2 u_2 K}{a_2 + K}$ that Granwall's inequality implies u_2 is bounded for each positive initial value $u_2(0)$, i.e $u_2 \leqslant u_2(0)\left(e_0^{\int t} \frac{m_2 K}{a_2 + K} ds\right)$.

Moreover, if we set $u_2 = 0$ then the system (4.9) reduces to

$$\begin{aligned} \frac{ds}{dt} &= \gamma s(1 - \frac{s}{K}) - \frac{m_2 u_2 s}{a_2 + s}, \\ \frac{du_1}{dt} &= \frac{m_1 u_1 s}{a_1 + s} - d_1 u_1 - \varepsilon u_1^2, \end{aligned} \tag{4.16}$$

hence $s \to K$ as $t \to \infty$, so

$$\frac{du_1}{dt} \leqslant u_1\left(\frac{m_1 K}{a_1 + K} - d_1 - \varepsilon u_1\right) = u_1\left(\bar{M}/\varepsilon - u_1\right),$$

which denotes that $u_1 \to \frac{\bar{M}_1}{\varepsilon}$ as $t \to \infty$, and where $\bar{M} = \frac{m_1 K}{a_1 + K} - d_1$.

Therefore, in the absence of predator u_1, both prey and predator u_2 survive. And similarly in the absence of predator u_2, both prey and predator u_1 survive.

Consider the modified competitive model (4.13) and suppose $a_1 \neq a_2$. So it admits four equilibrium points in form of $(0,0,0)$, $(K,0,0)$, $(\lambda_2, 0, u_2^0)$, $(s^0, u_1^0, 0)$ in which at least one species dies out, and one coexistence steady state $u^* = (s^*, u_1^*, u_2^*)$ as obtained:

$$\begin{aligned} s^* &= \frac{a_2 d_2}{m_2 - d_2} = \lambda_2, \\ u_1^* &= 1/\epsilon(\frac{m_1 s^*}{a_1 + s^*} - d_1), \\ u_2^* &= \frac{a_2 + s^*}{m_2}(\gamma(1 - \frac{s^*}{K}) - \frac{m_1 u_1^*}{a_1 + s^*}), \end{aligned} \tag{4.17}$$

As λ_i, $i = 1, 2$ were defined in previous parts $\lambda_i = \frac{a_i d_i}{m_i - d_i}$, for $i = 1, 2$ and $\lambda_1 \neq \lambda_2$ via Proposition 4.2.1.

Remark 4.3.1 *There exists a unique coexistence steady state if $\lambda_1 \neq \lambda_2$, otherwise the predator specie u_1 ($u_1^* = 0$) will dies out and the coexistence steady state does not survive any more.*

4.3.1 Positivity of the coexistence steady state

Since the system demonstrates an ecological problem, the coexistence steady state must be positive. Hence, the prey species are positive if the birth rate of predator u_2 is greater than its death rate, i.e. $m_2 > d_2$. Moreover, predator u_1^* is always positive if $\lambda_2 > \lambda_1$. On the other side, u_2 is an increasing function if $s > \lambda_2$.

These results and equilibrium point found in (4.17) obtain the necessary positivity conditions of s^*, u_1^*, u_2^* as below:

$$(i) \quad s^* = \lambda_2 > 0 \;\leftrightarrow\; m_2 > d_2 > 0, \tag{4.18}$$

$$(ii) \quad u_1^* = 1/\varepsilon\left(\frac{(m_1 - d_1)(\lambda_2 - \lambda_1)}{a_1 + \lambda_2}\right) > 0 \;\Rightarrow$$

$$(ii_1) \quad m_1 < d_1 \text{ and } \lambda_2 < \lambda_1 \text{ or } (ii_2) \quad m_1 > d_1 \text{ and } \lambda_2 > \lambda_1 \tag{4.19}$$

$$(iii) \quad u_2^* > 0 \;\leftrightarrow\; K > \lambda_2, \;\; \frac{\gamma(K - \lambda_2)\varepsilon(a_1 + \lambda_2)^2 - Km_1(m_1 - d_1)(\lambda_2 - \lambda_1)}{K\epsilon(a_1 + \lambda_2)^2} > 0.$$

Positivity analysis of the predator u_1^* u_2^* determines some different scenarios:

Proposition 4.3.1 *Positivity condition (ii) concludes two results (ii_1), (ii_2) while the first one is failed. Indeed, $m_1 < d_1$ leads to $\lambda_1 < 0$ which consequently leads $\lambda_2 < 0$, however it contradicts positivity condition s^*. Therefore, u_1^* is positive only under condition (ii_2).*

Proposition 4.3.2 *Since K is carrying capacity of prey, thus $s^* = \lambda_2$ illustrates that $K > \lambda_2$, also $\lambda_2 > \lambda_1$ due to positivity condition (ii) so we conclude that $K > \lambda_1$. Further, positivity of u_2^* takes place under two below scenarios:*
a) if $m_1 < d_1$, which means that death rate of predator u_1 is more than its birth rate so in shortage of predator u_1 there are more food for predator u_2, and due to positivity condition (ii_2) u_2^* is definitely positive, while it cannot takes place because of condition (ii) and Proposition 4.3.1.
b) if $m_1 > d_1$, the inequality mentioned in (iii) must be satisfied.

4.3.2 Local stability of the coexistence steady state

To survey stability of the reaction of the modified system, we calculate the Jacobian matrix at $u^* = (s^*, u_1^*, s_2^*)$, that is

$$K(U^*) = \begin{bmatrix} \frac{-\lambda_2\gamma}{K} + \lambda_2\left(\frac{m_1u_1^*}{(a_1+\lambda)^2} + \frac{m_2u_2^*}{(a_2+\lambda)^2}\right) & \frac{-m_1\lambda}{a_1+\lambda} & \frac{-m_2\lambda_2}{a_2+\lambda} \\ \frac{\beta_1u_1^*}{a_1+\lambda} & -\varepsilon u_1^* & 0 \\ \frac{\beta_2u_2^*}{a_2+\lambda} & 0 & 0 \end{bmatrix} = \begin{bmatrix} f_1 & f_2 & f_3 \\ f_4 & f_5 & 0 \\ f_6 & 0 & 0 \end{bmatrix}, \tag{4.20}$$

where $\beta_i = m_i - d_i > 0$, $f_2, f_3, f_5 < 0$ and $f_4, f_6 > 0$,

$$\begin{aligned} |\lambda - K(u^*)| &= \lambda^3 + \lambda^2(-f_1 - f_5) + \lambda(-f_2f_4 + f_1f_5 - f_3f_6) + f_3f_5f_6 \\ &= \lambda^3 + A\lambda^2 + B\lambda + C. \end{aligned} \tag{4.21}$$

Simple calculation illustrates that $C > 0$, while due to Routh-Hurwitz criteria, we needs to have $A, B > 0$, $AB - C > 0$. Obviously, necessary condition of all $A, B >$

$0, AB - C > 0$ is $f_1 < 0$. Thus $k(u^*)$ is stable if $f_1 < 0$, i.e

$$\left(\frac{m_1 u_1^*}{(a_1+\lambda)^2} + \frac{m_2 u_2^*}{(a_2+\lambda)^2}\right) < \frac{\gamma}{K}. \tag{4.22}$$

We next investigate appearance of Hopf bifurcation.

4.3.3 Hopf Bifurcation

Since the reaction has a stability condition mentioned in (4.22), we survey the necessary condition of the appearance of Hopf bifurcation. Hopf occurs when a stable point goes to periodic solutions. Here, we consider carrying capacity K as the Hopf bifurcation parameter. Indeed, as K varies, the system goes to Hopf bifurcation. That means that at threshold K, one eigenvalue remains on the left side of the X-axis while the two other negative eigenvalues transfer to two pure conjugate imaginary eigenvalues.

Therefore, consider the function below

$$F(K) = \frac{m_1 u_1^*}{(a_1+s^*)^2} + \frac{m_2 u_2^*(K)}{(a_2+s^*)^2} - \frac{\gamma}{K}, \tag{4.23}$$

The exciting point of finding the threshold of the modified system is that the critical Hopf bifurcation point of the system (4.23) occurs at $K_{Hopf} = K_H = a_1 + 2\lambda_2$, i.e

$$F(K_H) = 0, \Rightarrow K_H = a_1 + 2\lambda_2, \tag{4.24}$$

such that $F(K)$ is an increasing function, since all parameters are positive and $s^* = \lambda_2 > 0$, i.e

$$F'(K_H) = \frac{\gamma s^*}{(a_2+s^*)K^2} > 0.$$

All results above are confirmed by numerical simulation in the next section.

4.3.4 Numerical Simulation

Consider the parameters below:

$$a_1 = 3.5,\ a_2 = 4.4,\ d_1 = 1.2,\ d_2 = 1.8,\ m_1 = 4.2,\ m_2 = 7,\ \Gamma = 1,\ \gamma = 2, \tag{4.25}$$

which lead to $\lambda_1 = 1.4,\ \ \lambda_2 = 1.5231$, and

$$u^* = (1.5231, 0.73, 0.65), \quad K_H = a_1 + 2\lambda_2 = 6.5462, \tag{4.26}$$

Figure 4.4A), Figure 4.4B) proves that system is stable if $K < K_H$. Figure 4.4B) shows that the equilibrium point is a sink. In addition, Figure 4.4B) demonstrates that if $K > K_H$ the system goes to the periodic solution Figure 4.5A). In fact, by increasing bifurcation parameter K, limit cycles arises such that as K increases, the limit cycles grow in Figure 4.5B).

Moreover, Figure 4.5A) states that for the parameter set amplitude of the periodic solution of the predator species u_1 is less than the other species, since this predator species are affected not only by intraspecific interactions between their population but also natural death.

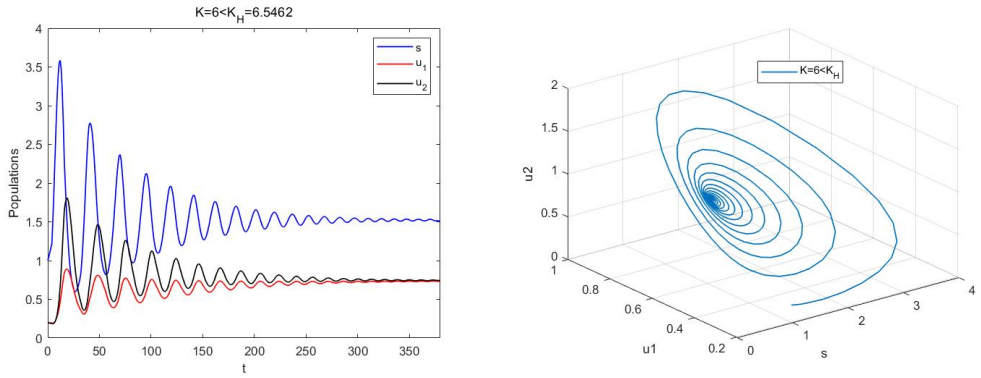

(A) $K < K_H$ (B) $K < K_H$

FIGURE 4.4: Local stability of the spices when the Hopf parameter is less then critical one. A) Stability of the system for $K = 6 < K_H$. B) Phase portrait of the system of stable spiral. Given parameters are $a_1 = 3.5$, $a_2 = 4.4$, $d_1 = 1.2$, $d_2 = 1.8$, $m_1 = 4.2$, $m_2 = 7$, $\Gamma = 1$, $\gamma = 2$, which lead to $\lambda_1 = 1.4$, $\lambda_2 = 1.5231$, and $u^* = (1.5231, 0.73, 0.65)$, $K_H = a_1 + 2\lambda_2 = 6.5462$

However, the resource s take advantages of reduction of population densities of the predator species u_1 and the resource specie oscillates with highest amplitude. In the other words, in Figure 4.5A) periodic solutions produced by Hopf bifurcation state that for a specific time period all species grow and fall down approximately with the same slop (i.e the population densities increase and decrease almost with one speed), though their amplitudes are different, and the least one is associated with predator u_1.

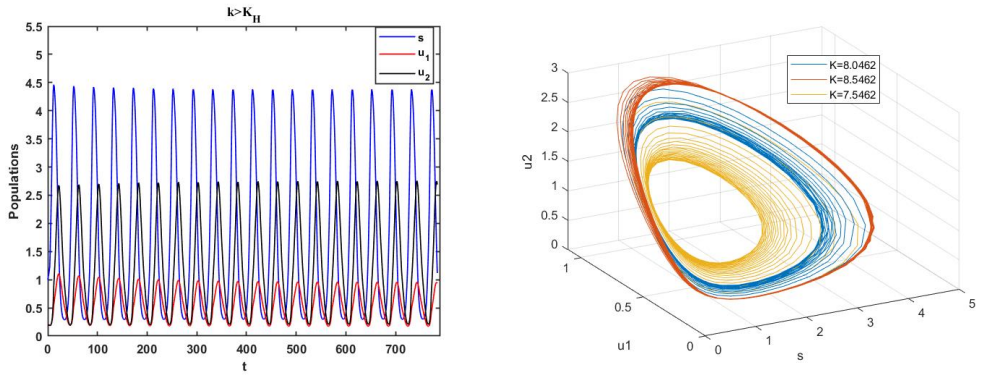

(A) $K > K_H$ (B) $K > K_H$

FIGURE 4.5: Hopf bifurcation occurs when $K > K_H$. A) Periodic solutions of the populations as Hopf parameter crosses the critical value K_H. B) Appearance of the limit cycles as $K > K_H$ grows. For $K \simeq 7.5$, $K \simeq 8$ and $K \simeq 8.5$ stabilized limit cycles are depicted. Given parameters are the same as Figure 4.4.

4.4 Turing Analysis

Here, the existence of Turing bifurcation of (4.13) is analyzed. That is linear analysis leads to the following dispersion relation for kinetic matrix (4.20) and general

diffusion matrix

$$D(u^*) = \begin{bmatrix} k_{11} & k_{12} & k_{13} \\ k_{21} & k_{22} & k_{23} \\ k_{31} & k_{32} & k_{33} \end{bmatrix}, \tag{4.27}$$

where we emphasize that here all diffusion parameters are considered positive.

Consider $W = [s - \lambda_2,\ u_1 - u_1^*\ u_2 - u_2^*]^t$,
then linearized system is achieved as $\dot{\mathbf{W}} = \Gamma K\mathbf{W} + D\Delta\mathbf{W}$ whose solution has the form of $\mathbf{W} = \exp^{i\delta x + \lambda t}$, where δ indicates wave number hence dispersion relation of the equation is obtained by

$$|\lambda I + \delta^2 D - K| = 0,$$

which gives a cubic polynomial of the form of

$$\lambda^3 + A(\delta^2)\lambda^2 + B(\delta^2)\lambda + C(\delta^2) = 0, \quad \text{where} \tag{4.28}$$

$\mathrm{A}(\delta^2) = \delta^2(k_{11} + k_{22} + k_{33}) - f_1 - f_5,$
$B(\delta^2) = \delta^4(k_{11}k_{22} + k_{11}k_{33} - k_{32}k_{23} + k_{22}k_{33} - k_{12}k_{21} - k_{31}k_{13})$
$+ \delta^2(-f_5k_{11} - f_1k_{22} - f_1k_{33} + f_4k_{21} + f_3k_{31} + f_6k_{13} - f_5k_{33})$
$+ f_1f_5 - f_2f_4 - f_3f_6 = b_1\delta^4 + b_2\delta^2 + b_3,$
$\mathrm{C}(\delta^2) = \delta^6(k_{11}k_{22}k_{33} - k_{11}k_{23}k_{32} - k_{12}k_{21}k_{33} + k_{12}k_{31}k_{23} + k_{13}k_{21}k_{32} - k_{13}k_{31}k_{22})$
$+ \delta^4(-f_1k_{22}k_{33} + f_1k_{32}k_{23} + f_2k_{21}k_{33} + f_4k_{12}k_{33} - f_2k_{31}k_{23} - f_6k_{12}k_{23} - f_3k_{21}k_{32}$
$- f_4k_{13}k_{32} + f_3k_{31}k_{22} + f_6k_{13}k_{22} - f_5k_{11}k_{33} + f_5k_{31}k_{13})$
$+ \delta^2(-f_4f_2k_{33} + f_2f_6k_{23} + f_3f_4k_{32} - f_3f_6k_{22} + f_1f_5k_{33} - f_6f_5k_{13} - f_3f_5k_{31})$
$+ f_3f_5f_6 = c_1\delta^6 + c_2\delta^4 + c_3\delta^2 + c_4,$

In following, we look for necessary conditions in which Turing instability can be taken place for some different cases of the presence of self- and cross-diffusion coefficients. In fact, the investigation is presented due to applying Routh-Hurwitz criteria. According to the Turing analysis, in presence of diffusion a stable coexistence steady state with real negative eigenvalues transfer to the real positive eigenvalues which yield to emergence of stationary patterns. Indeed, there is a range of wave numbers $[\delta_1^2\ ,\ \delta_2^2]$ where the system goes to spatial patterns. The critical wave number can be found by the necessary condition $C(\delta^2) < 0$ due to Routh-Hurwitz criteria. Indeed, in the threshold, cubic polynomial $C(\delta_{min}^2) = 0$ where

$$\delta_{Max}^2 = \frac{-c_2 - \sqrt{c_2^2 - 3c_1c_3}}{3c_1}, \quad \delta_{min}^2 = \frac{-c_2 + \sqrt{c_2^2 - 3c_1c_3}}{3c_1}. \tag{4.29}$$

Here, it is reminded that signs of each component of the reaction matrix (4.20) is followed as:

$$\begin{aligned} &f_1 < 0, \quad f_2 < 0, \quad f_3 < 0, \quad f_5 < 0, \\ &f_4 > 0, \quad f_6 > 0. \end{aligned} \tag{4.30}$$

In the strategy of avoidance of predator (i.e positive cross-diffusion k_{32}, k_{23}), k_{32} is critical obtained as bifurcation parameter.

4.4.1 Turing analysis without cross-diffusion (case I: $k_{ij} = 0,\ i \neq j$)

First, we consider the diffusion matrix without all cross-diffusion parameters. In absence of all cross-diffusion parameters, the diffusion matrix of the system (4.13) is

$$D(u^*) = \begin{bmatrix} k_{11} & 0 & 0 \\ 0 & k_{22} & 0 \\ 0 & 0 & k_{33} \end{bmatrix}, \tag{4.31}$$

The kinetic matrix as obtained in (4.20). Dispersion relation (4.28) is reduced to

$$\begin{aligned} A(\delta^2) &= \delta^2(k_{11} + k_{22} + k_{33}) - f_1 - f_5, \\ B(\delta^2) &= \delta^4(k_{11}k_{22} + k_{11}k_{33} + k_{22}k_{33}) + \delta^2(-f_5k_{11} - f_1k_{22} - f_1k_{33} - f_5k_{33}) \\ &\quad + f_1f_5 - f_2f_4 - f_3f_6, \end{aligned} \tag{4.32}$$

$$\begin{aligned} C(\delta^2) &= \delta^6(k_{11}k_{22}k_{33}) \\ &\quad + \delta^4(-f_1k_{22}k_{33} - f_5k_{11}k_{33}) \\ &\quad + \delta^2(-f_4f_2k_{33} - f_3f_6k_{22} + f_1f_5k_{33}) + f_3f_5f_6, \end{aligned} \tag{4.33}$$

Simple computations show that in absence of the cross-diffusion, $A(\delta^2) > 0$, moreover stability condition $f_1 < 0$ leads to $B(\delta^2) > 0,\ C(\delta^2) > 0$ and finally $AB - C > 0$, therefore, so the system is stable and consequently there is **no Turing instability**.

4.4.2 Turing analysis (case II: $k_{1j} = 0, k_{j1} = 0,\ j = 2, 3$)

The diffusion matrix of the system (4.13) is

$$D(u^*) = \begin{bmatrix} k_{11} & 0 & 0 \\ 0 & k_{22} & k_{23} \\ 0 & k_{32} & k_{33} \end{bmatrix}, \tag{4.34}$$

The coefficients of dispersion relation is changed to

$$\begin{aligned} &B(\delta^2) = \delta^4(k_{11}k_{22} + k_{11}k_{33} + k_{22}k_{33} - k_{23}k_{32}) + \delta^2(-f_5k_{11} - f_1k_{22} - f_1k_{33} - f_5k_{33}) \\ &+ f_1f_5 - f_2f_4 - f_3f_6 = b_1\delta^4 + b_2\delta^2 + b_3, \end{aligned} \tag{4.35}$$

$$\begin{aligned} C(\delta^2) &= \delta^6(k_{11}k_{22}k_{33} - k_{11}k_{23}k_{32}) + \delta^4(-f_1k_{22}k_{33} - f_5k_{11}k_{33} + f_1k_{32}k_{23}) \\ &\quad + \delta^2(-f_4f_2k_{33} + f_2f_6k_{23} + f_3f_4k_{32} - f_3f_6k_{22} + f_1f_5k_{33}) + f_3f_5f_6 \\ &\quad = c_1\delta^6 + c_2\delta^4 + c_3\delta^2 + c_4, \end{aligned} \tag{4.36}$$

it needs parameter k_{32} or k_{23} to be chosen as bifurcation parameter to Turing pattern can emerge. We choose k_{32} as bifurcation parameter. Since in (4.41) b_1 and b_3 are positive, to have $B > 0$ we need $b_1 > 0$ too and in addition, due to Routh-Hurwitz $C(\delta^2)$ must be negative. Therefore, to find a positive critical wave number (4.29) and critical bifurcation parameter the steps below must be satisfied:

Step 1: $\mathbf{b_1 > 0}$

$$k_{32} < \frac{k_{11}k_{22} + k_{11}k_{33} + k_{22}k_{33}}{k_{23}} := k_{32}^{(b_1)},$$

Step 2: $c_1 > 0$

$$k_{32} < \frac{k_{22}k_{33}}{k_{23}} := k_{32}^{(1)}, \tag{4.37}$$

Step 3: $c_2 < 0$

$$k_{32} > \frac{(f_1k_{22}k_{33} + f_5k_{11}k_{33})}{f_1k_{23}} := k_{32}^{(2)}, \tag{4.38}$$

It is obvious that denominator and nominator are both negative since $f_1, f_5 < 0$.
Step 4: $c_3 < 0$

$$k_{32} > \frac{f_4f_2k_{33} - f_2f_6k_{23} - f_3f_4k_{32} + f_3f_6k_{22} - f_1f_5k_{33}}{f_3f_4} := k_{32}^{(3)}, \tag{4.39}$$

Where denominator is always negative, though nominator whose sign can be changed, so we choose parameter set such that to have a positive nominator and consequently positive k_{32}.
Finally, to find the positive critical bifurcation parameter k_{32}^c, we put

$$P = max\{k_{32}^{(2)}, k_{32}^{(3)}\},$$

which gives $k_{32} > P$ that indicates $k_{32}^c = P + \eta$ such that η is a positive unknown and all are replaced in (4.29) and (4.4).

4.4.3 Turing analysis (case III: $k_{j1} = 0,\ j = 2, 3$)

In this case, the Kinetic matrix is the same as (4.20), while diffusion matrix is changed to

$$D(u^*) = \begin{bmatrix} k_{11} & k_{12} & k_{13} \\ 0 & k_{22} & k_{23} \\ 0 & k_{32} & k_{33} \end{bmatrix}, \tag{4.40}$$

Indeed, in this case the flux of predator $u_2(u_3)$ is directed against direction of the $u_3(u_2)$ and they are not affected by the flux of prey, therefore $k_{21} = k_{31} = 0$. Hence, the dispersion relation is

$$(\lambda)^3 + A(\delta^2)(\lambda)^2 + B(\delta^2)\lambda + C(\delta^2) = 0,$$

.

The coefficients of dispersion relation is changed to

$$\begin{aligned} B(\delta^2) &= \delta^4(k_{11}k_{22} + k_{11}k_{33} + k_{22}k_{33} - k_{23}k_{32}) \\ &+ \delta^2(-f_5k_{11} - f_1k_{22} - f_1k_{33} - f_5k_{33} + f_4k_{12} + f_6k_{13}) \\ &+ f_1f_5 - f_2f_4 - f_3f_6 = b_1\delta^4 + b_2\delta^2 + b_3, \end{aligned} \tag{4.41}$$

$$\begin{aligned} C(\delta^2) &= \delta^6(k_{11}k_{22}k_{33} - k_{11}k_{23}k_{32}) \\ &+ \delta^4(-f_1k_{22}k_{33} - f_5k_{11}k_{33} + f_1k_{32}k_{23} + f_4k_{12}k_{33} - f_6k_{12}k_{23} - f_4k_{13}k_{32} + f_6k_{13}k_{22}) \\ &+ \delta^2(-f_4f_2k_{33} + f_2f_6k_{23} + f_3f_4k_{32} - f_3f_6k_{22} + f_1f_5k_{33}) + f_3f_5f_6 \\ &= c_1\delta^6 + c_2\delta^4 + c_3\delta^2 + c_4, \end{aligned} \tag{4.42}$$

that $A > 0$ always, however B and C signs are varied by changing parameter k_{32} which is called bifurcation parameter. so we choose the parameter k_{32} as bifurcation parameter. Therefore, similar to the case II, the steps below must be satisfied:

Step 1: $b_1 > 0$

$$k_{32}^{(b_1)} < \frac{k_{11}k_{22} + k_{11}k_{33} + k_{22}k_{33}}{k_{23}} := k_{32}^{(b_1)},$$

Step 2: $c_1 > 0$

$$k_{32}^{(1)} < \frac{k_{22}k_{33}}{k_{23}} := k_{32}^{(1)},$$

Step 3: $c_2 < 0$

$$k_{32}^{(2)} > \frac{(f_1k_{22}k_{33} - f_4k_{12}k_{33} + f_6k_{12}k_{23} - f_6k_{13}k_{22} + f_5k_{11}k_{33})}{f_1k_{23} - f_4k_{13}} := k_{32}^{(2)}, \tag{4.43}$$

It is obvious that denominator is always negative so nominator must be negative too.

Step 4: $c_3 < 0$

$$k_{32}^{(3)} > \frac{f_4f_2k_{33} - f_2f_6k_{23} + f_3f_6k_{22} - f_1f_5k_{33} + f_5f_6k_{13}}{f_3f_4} := k_{32}^{(3)}, \tag{4.44}$$

Where denominator is always negative, though nominator whose sign can be changed, so we choose parameters such that to have a positive nominator and consequently positive k_{32}.

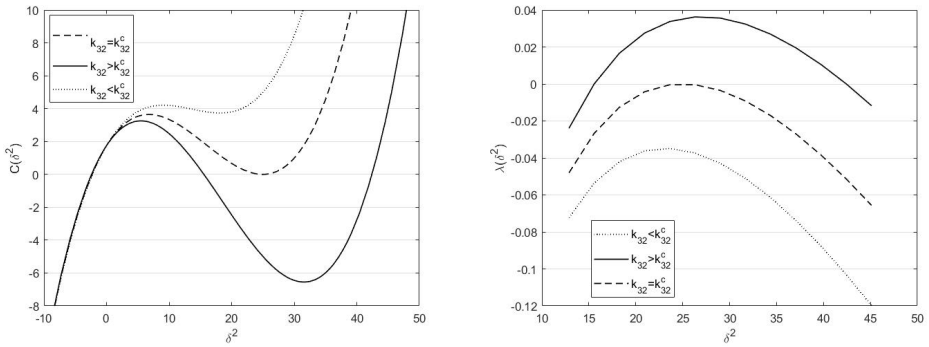

(A) $C(\delta^2)$ (B) $\lambda(\delta^2)$

FIGURE 4.6: Necessary condition of Turing instability. A) it illustrates $C(\delta^2) < 0$ (black solid line) if $k_{32} > k_{32}^c$. B) this figure shows if $k_{32} > k_{32}^c$ then $\lambda(\delta^2) > 0$ (black solid line) for the range of wave numbers. Given parameters are the same as (4.46)

Remark 1: A comparison of step 1 and step 2 implies that step 1 can be ignored. It is emphasized that we are looking for a positive k_{32}^c.

Remark 2: In all cases $A(\delta^2)$ is always positive due to the stability condition.

Remark 3: Routh-Hurwitz criteria state that $B(\delta^2) = b_1\delta^4 + b_2\delta^2 + b_3$ must be positive. Since b_2 and b_3 are positive, it needs $b_1 > 0$.
Remark 4: The sign of c_4 in all cases is positive.
At last, to find the positive critical bifurcation parameter k_{32}^c, we put

$$P = max\{k_{32}^{(2)}, k_{32}^{(3)}\}, \tag{4.45}$$

which $k_{32} > P$ leads to $k_{32}^c = P + \eta$ such that η is a positive unknown and all are replaced in (4.29) and (4.4). Finally, the critical wave number δ_c^2 and critical bifurcation parameter k_{32}^c are found.

Figure 4.6 illustrates necessary conditions $C(\delta^2) < 0, \lambda(\delta^2) > 0$ for Turing instability of the system (4.13) and and for the case **III**.
The parameters have been chosen:

$$\begin{gathered}\Gamma = 5,\ \gamma = 2.\ K = 1.48,\ a_1 = 0.64,\ a_2 = 0.6,\ m_1 = 0.8,\ m_2 = 1.15,\ d_1 = 0.4, \\ d_2 = 0.6,\ \varepsilon = 0.12, k_{11} = k_{12} = k_{22} = 0.1,\ k_{23} = 0.1; k_{13} = 0.25, k_{33} = 1.\end{gathered} \tag{4.46}$$

Hence $\lambda_1 = 0.4$ and $\lambda_2 = 0.6545$. Moreover, the critical bifurcation parameter is $k_{32}^c = 0.8790$ and correspondingly critical wave number is $\delta_c \simeq 5$ and $E^* = (s, u_1, u_2) = (0.6545, 0.8046, 0.5510)$.

Figure 4.6 depicts if the cross-diffusion term $k_{32}^c = 0.8790$, $\delta_c^2 = 24.9691$ then $C(\delta_c^2) = 0$ and consequently $\lambda(\delta_c^2)$ has two negative eigenvalues and one zero eigenvalue. Therefore as the critical parameter k_{32} crosses the k_{32}^c, $C(\delta^2)$ becomes negative. Consequently, $\lambda(\delta_c^2) > 0$, i.e., the dispersion relation has two positive eigenvalues and one negative eigenvalue for a range of modes $[\delta_1^2\ \ \delta_2^2]$ (see Figure 4.6A, Figure 4.6B). In other words, the reaction-diffusion system becomes unstable, and the Turing pattern emerges.

As we found out that Turing instability occurs for as $k_{32} > k_{32}^c$, i.e., the species produce spatial pattern if the flux of predator u_2 associated with predator u_1 increases from critical point (k_{32}^c). It means Turing instabilities take place as much faster as u_2 goes away from predator u_1.

4.5 Turing Region

Turing region of the system (4.13) with diffusion matrix (4.40) is studied. The region is obtained based on the two parameters involved in positivity conditions, stability conditions, and Turing Conditions. Hence, the Turing and positive conditions of fixed points illustrate that we can choose a plane of (m_1, K) as a parameter space. Although, it was mentioned that the system goes to Hopf instability if $K > K_H = a_1 + 2\lambda_2$. Thus in the plane (m_1, K) under conditions (4.22) i.e., $K < K_H = a_1 + 2\lambda_2$ the equilibria are stable, therefore below the horizontal line $K = K_H = a_1 + 2\lambda_2$ the system serves stability of equilibrium points.

First, positivity condition (4.18) is considered in which (ii) and (iii) lead to

$$m_1 > (m_2 - d_2)\frac{a_1 d_1}{d_2 a_2},$$

and gives minimum value of m_1 and

$$m_1 > d_1(1 + \frac{a_1}{K}),$$

presents the relation between parameters K, m_1.

Moreover, conditions (4.38 - Turing condition I) and (4.39- Turing condition II) are Turing conditions, such that both conditions are implicit functions of K, m_1.

Proposition 4.5.1 *(Turing conditions I, II:) Right hand sides of the inequalities* (4.43) *and* (4.44) *are positive if nominators be negative, since denominators are always negative. So the implicit functions*

$$\begin{aligned} F_1 &= f_1k_{22}k_{33} - f_4k_{12}k_{33} + f_6k_{12}k_{23} - f_6k_{13}k_{22} + f_5k_{11}k_{33}, \\ F_2 &= f_4f_2k_{33} - f_2f_6k_{23} + f_3f_6k_{22} - f_1f_5k_{33} + f_5f_6k_{13}, \end{aligned} \tag{4.47}$$

are considered as Turing conditions I, II correspondingly.

Using fixed parameters given in (4.46) Turing region is obtained, where Hopf threshold is determined $K_H \simeq 1.7$ see Figure 4.7.

In following, we study how Turing is influenced by varying self- and cross-diffusion parameters. We remark that Chosen parameters are the same as Figure 4.7.

It is observed that when cross-diffusion k_{12} increases, the Turing region decreases (moving red curves to the left side in Figure 4.8), which means that flux of the resource species that run away from predator species u_1 (i.e. move to lower density) with a greater value of k_{12} makes less chance of instability for a short range of carrying capacity and short range of low birth rate of u_1.

For example in Figure 4.8, as k_{12} grows from 0.1 to 0.2 the system goes to instability (Turing), for the u_1 birth rate range $m_1 \in (0.5,\ 5)$ and the prey carrying capacity $K \in (0.09,\ 0.68)$. Whereas, as $k_{12} = 0.2$, these ranges vary from $m_1 \in (0.5,\ 1.55)$ for prey and $K \in (0.15,\ 0.68)$.

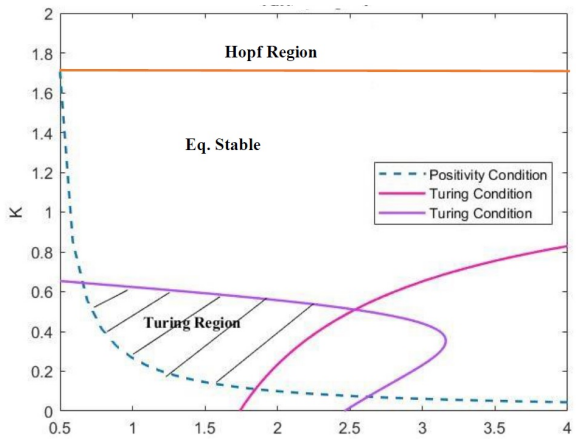

FIGURE 4.7: Turing region (dashed region)in plane (m_1, K), parameters are obtained in . The orange horizontal line demonstrates $K = K_H$, such that the region above the horizontal line and for each m_1 associates with Hopf region. Dashed line, purple and pink lines are associated to positivity, Turing condition II and Turing condition I respectively. $\Gamma = 5,\ \gamma = 2.\ K = 1.48,\ a_1 = 0.64,\ a_2 = 0.6,\ m_1 = 0.8,\ m_2 = 1.15,\ d_1 = 0.4,\ \ d_2 = 0.6,\ \varepsilon = 0.12, k_{11} = k_{12} = k_{22} = 0.1,\ k_{23} = 0.1; k_{13} = 0.25, k_{33} = 1.$

In addition, in this case enhancement and reduction of the cross-diffusion k_{12} does not impact on the Turing condition II, i.e. it is independent of K_{12}.

In Figure 4.9, Turing region varies for different values of cross-diffusion parameter k_{13}, despite k_{12}, by enhancement of cross-diffusion k_{13} Turing region increases.

That confirms that as prey moves to the lower density of predator u_2, the spatial patterns can occur for a wider range of the parameters in the plane (m_1, K). For instance, when $k_{13} = 0.15$, these ranges are $m_1 \in (0.5,\ 1.4)$ and $K \in (1.8,\ 6.5)$. However, these ranges reduce as prey runs away faster from predator u_2, i.e., $m_1 \in (0.5,\ 1.6)$ and $K \in (1.1,\ 6.5)$ Figure 4.9.

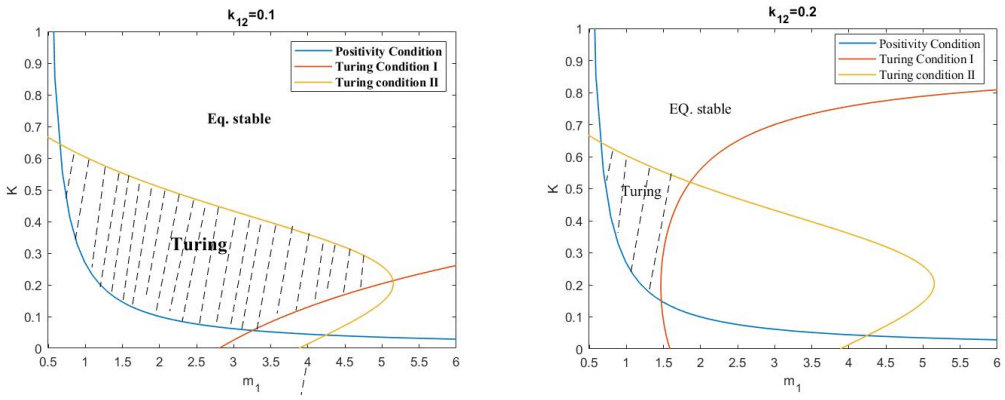

(A) $k_{12} = 0.1$ (B) $k_{12} = 0.2$

FIGURE 4.8: Turing region (dashed region) in plane (m_1, K), A) $k_{12} = 0.1$ and other parameters are fixed as (4.46). B) $k_{12} = 0.2$ and other parameters are fixed as Figure 4.7.

Simultaneously, these results occur in plane of (m_1, K) when k_{23}, k_{33} vary. Figure 4.10 illustrates that as cross- diffusion k_{23} increases Turing region decreases gradually. In the other words, diffusion of predator u_2 against of direction of predator u_2 makes less opportunity of spatial segregation. Figure 4.13, Figure 4.11 indicate that diffusion of s and u_2 (rising up self- diffusion parameters k_{11} and k_{33}) decrease the Turing regions correspondingly , whereas the scenario is reverse when u_2 diffuses faster (i.e k_{22} increases) Figure 4.12.

In summary, simulations of Turing region with respect to varying diffusion parameters demonstrate that diffusion of predator u_1 and moving prey against direction of u_2 make more chance of Turing instability.

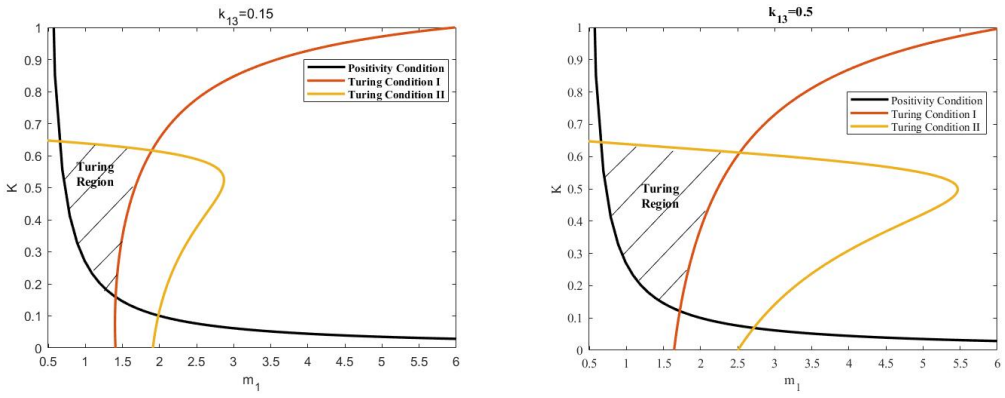

(A) $k_{13} = 0.15$ (B) $k_{13} = 0.5$

FIGURE 4.9: Turing region (dashed region) in plane (m_1, K), A) $k_{13} = 0.15$ and other parameters are fixed as (4.46). B) $k_{13} = 0.5$ and other parameters are fixed as Figure 4.7.

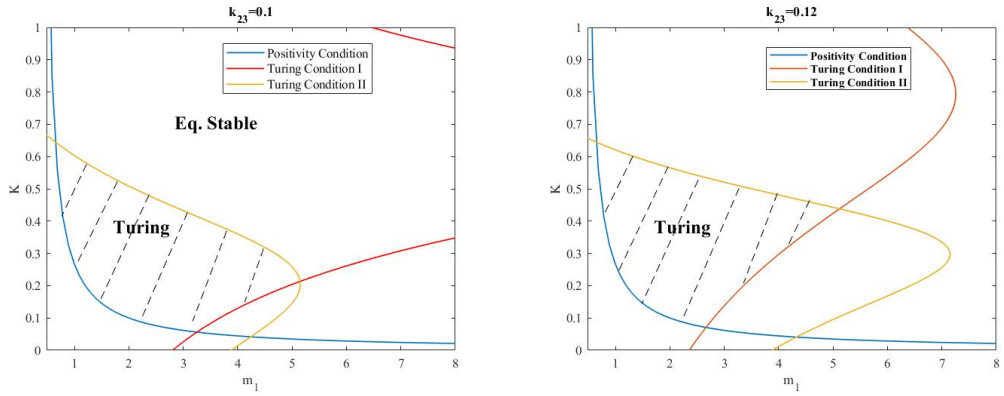

(A) $k_{23} = 0.1$ (B) $k_{23} = 0.12$

FIGURE 4.10: Turing region (dashed region) in plane (m_1, K), A) $k_{23} = 0.1$ and other parameters are fixed as (4.46). B) $k_{23} = 0.12$ and other parameters are fixed as Figure 4.7.

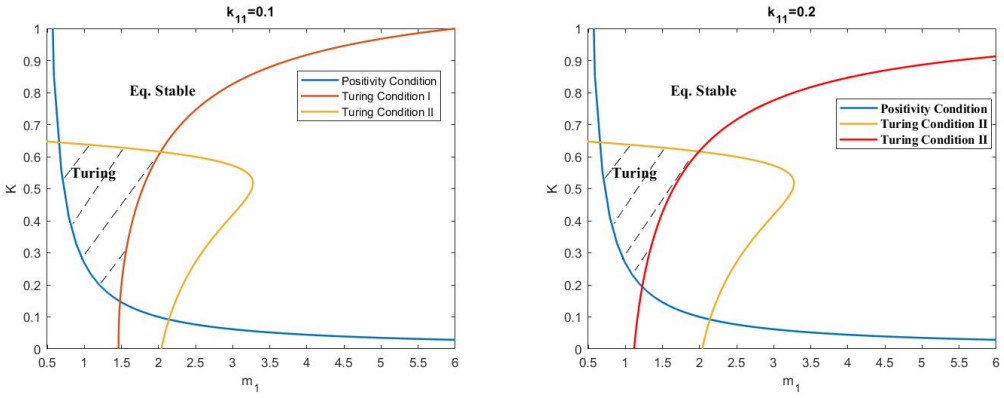

(A) $k_{11} = 0.1$ (B) $k_{11} = 0.2$

FIGURE 4.11: Turing region (dashed region) in plane (m_1, K), A) $k_{11} = 0.1$ and other parameters are fixed as (4.46). B) $k_{11} = 0.2$ and other parameters are fixed as Figure 4.7.

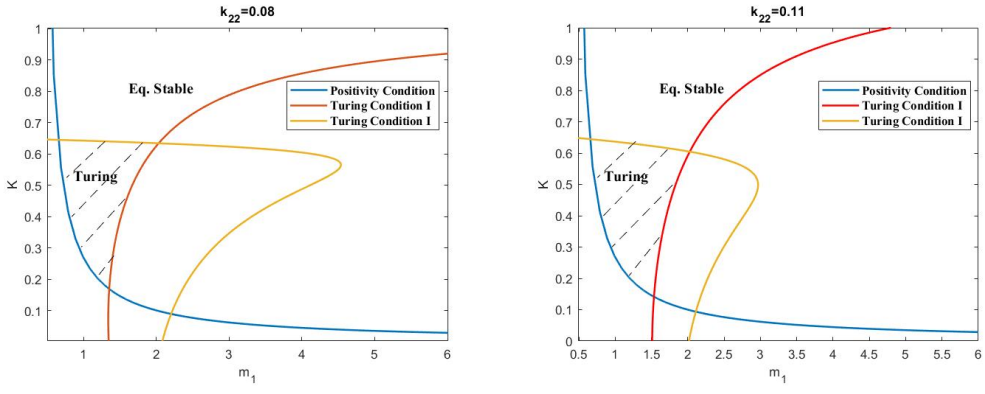

(A) $k_{22} = 0.08$ (B) $k_{22} = 0.11$

FIGURE 4.12: Turing region (dashed region) in plane (m_1, K), A) $k_{22} = 0.08$ and other parameters are fixed as (4.46). B) $k_{22} = 0.11$ and other parameters are fixed as Figure 4.7.

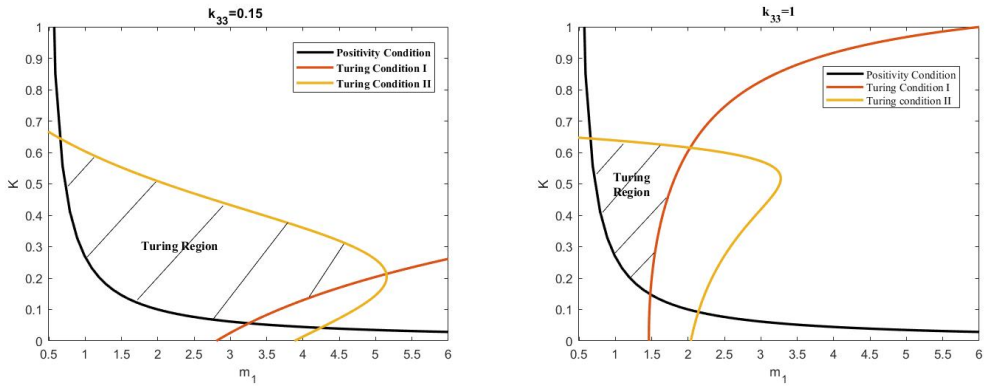

(A) $k_{33} = 0.15$ (B) $k_{33} = 1$

FIGURE 4.13: Turing region in plane (m_1, K), A) $k_{33} = 0.15$ and other parameters are fixed as (4.46). B) $k_{33} = 1$ and other parameters are fixed as Figure 4.7.

4.6 Numerical simulation

Employing the parameters given in (4.46) which leads to $k_{32}^c = 0.8790$ as critical bifurcation parameter, and $\delta \simeq 5$ as critical mode and where the equilibrium point is $E^* = (0.6545, 0.8046, 0.5510)$. Turing patterns have been performed by numerical simulation see Figure 4.14. We applied finite element method which utilizes $\theta -$ *scheme* method for nonlinear systems , in which a weighted average of the time derivative of a dependent variable is approximated at two consecutive time steps by linear interpolation of the values of the variable at the two steps Reddy, 2014. In addition, we applied *Lagrange* $\mathbb{P}_2$ as shape functions .

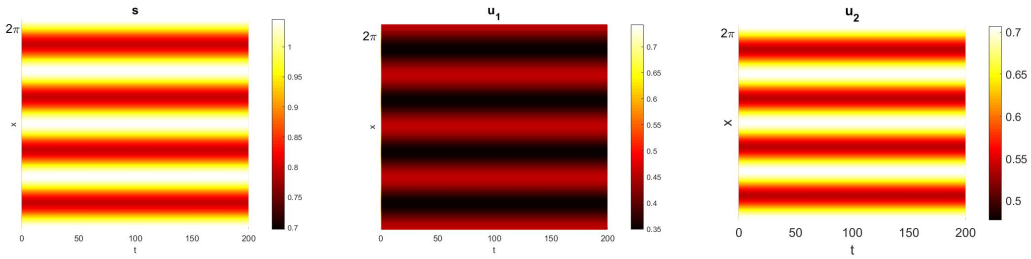

(A) Prey (B) Predator u_1 (C) Predator u_2

FIGURE 4.14: Numerical simulation in the Turing instability for given parameters $\Gamma = 5$, $\gamma = 2$. $K = 1.48$, $a_1 = 0.64$, $a_2 = 0.6$, $m_1 = 0.8$, $m_2 = 1.15$, $d_1 = 0.4$, $d_2 = 0.6$, $\varepsilon = 0.12, k_{11} = k_{12} = k_{22} = 0.1$, $k_{23} = 0.1; k_{13} = 0.25, k_{33} = 1$ Hence $\lambda_1 = 0.4$ and $\lambda_2 = 0.6545$. Moreover, the critical bifurcation parameter is $k_{32}^c = 0.8790$ and correspondingly critical wave number is $\delta_c \simeq 5$ and $E^* = (s, u_1, u_2) = (0.6545, 0.8046, 0.5510)$.

4.6.1 Numerical Simulations v.s WNL

As it has mentioned in (Gambino, Lombardo, and Sammartino, 2012), to capture Turing bifurcation near equilibrium, weakly nonlinear analysis as a multiple scales method is applied. Calculation of these analysis for the system (4.13) has been performed in Appendix B.2. The parameters are the same as parameters applied in (4.46) (correspond to the Figure (4.7)) and $E^* = (0.6545, 0.8046, 0.5510)$. Recall that for those parameters $k_{32} = 0.8878 > k_{32}^c = 0.0.8790$ where $\delta_c^2 = 24.9691$. Moreover, weakly nonlinear computation mentioned in (B.2) shows the case is supercritical due to $\sigma = 3.1255$, $L = 2.0037$. Numerical results of last configuration of u_1 and weakly nonlinear analysis are compared in Figure (4.15).

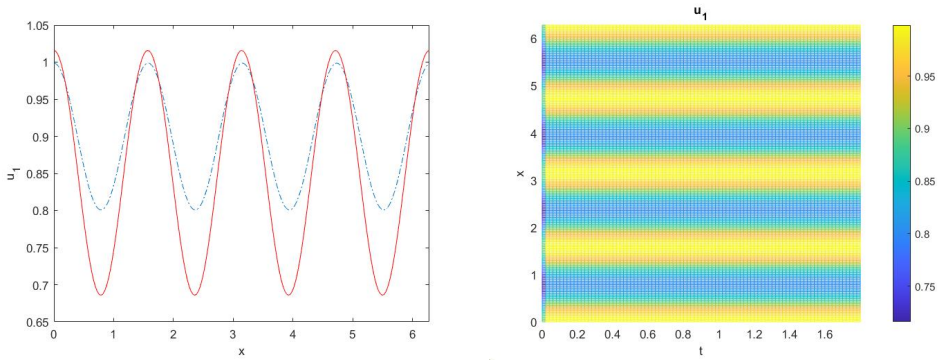

FIGURE 4.15: A) Comparison of FEM (dashed blue line) with WNL method(solid red line) B) Turing Patterns of the predator u_1.

4.7 Maximum growth rate

According to the reference (Murray, 2001, Gambino, Lombardo, and Sammartino, 2012) linear theory can give some clues on the wavelength of the emerging pattern (at least for values of ε that are not exceedingly large). The first factor to be considered is the value δ_m maximizing the growth rate $\lambda(\delta^2)$. Following the reasoning in (Segel, 1984) the value of δ_m can be found by setting:

$$\frac{d\lambda^+}{d\delta^2} = 0, \tag{4.48}$$

where λ^+ is the positive root of the dispersion relation (4.28) (associated with diffusion parameters in case III). Substituting $k_{32} = k_{32}^c(1+\epsilon)$, $\delta_m^2 = \delta_c^2 + \eta$ in (4.48) one can obtain the analytic expression of the curve which gives η as a function of ϵ. The calculations are presented here:

$$A(\delta^2) = a_1\delta^2 + a_2, \tag{4.49}$$

$$B(\delta^2) = b_1\delta^4 + b_2\delta^2 + b_3, \tag{4.50}$$

$$C(\delta^2) = c_1\delta^6 + c_2\delta^4 + c_3\delta^3 + c_4, \tag{4.51}$$

Thus (4.48) determines:

$$\delta_m^2 = \frac{-P_2 + \sqrt{P_2^2 - 4P_1P_3}}{2P_1}, \tag{4.52}$$

where $P_1 = 3c_1$, $P_2 = 2\lambda b_1 + 2c_2$, and $P_3 = a_1\lambda^2 + b_2\lambda + c_3$, such that $c_i,\ \ i = 1,2,3,4$ and $a_i,\ \ i = 1,2$, and $b_i,\ \ i = 1,2,3$ are introduced in (4.41), (4.42). such that $\delta_m^2 = \delta_c^2 + \eta$, hence the results for are follows.

Consider parameters given for the system with diffusion parameter case III in (Figure (4.16)). Indeed, the Figure depicts that δ_m^2 has a root (critical point) which is called ϵ_c. Before, this critical value as ϵ increases the parameter η increases which states that δ_m^2 is bigger than δ_c^2, while after critical value as ϵ rises up η admits negative values which determines that $\delta_m^2 < \delta_c^2$.

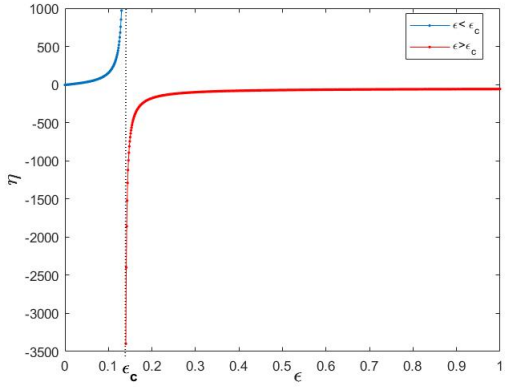

FIGURE 4.16: Maximum growth rate obtained by chosen parameter values: $K = 1.48,\ \gamma = 2, \Gamma = 5,\ a_2 = 0.5,\ a_1 = 0.4,\ a_2 = 0.6m_2 = 1.15,\ d_1 = 0.4, m_1 = 0.8,\ d_2 = 0.6,\ k_{11} = 0.1,\ k_{12} = 0.1,\ k_{13} = 0.25,\ k_{22} = 0.1,\ k_{23} = 0.1,\ k_{33} = 1,\ \ \epsilon = 0.12$ which leads to $k_{32}^c = 0.8790,\ \ \delta_c^2 = 24.96911$.

4.8 Global existence in time of solutions by invariant method

In this section we aim to investigate a positive invariant region of the system (4.13) with diffusion mentioned in (4.61) and conclude global existence in time of solutions. To find a positive invariant solution and prove the existence of the global solution, first, we prove that the system (4.13) containing positive initial values and without diffusion, admits a unique global positive solution. Therefore we prove the below lemma.

Lemma 4.8.1 *The system (4.13) coupled with non-negative initial values $u \in (s^0, u_1^0, u_2^0)$ admits a unique global positive solution.*

Proof: We adapt the method employed in (Hoai Nguyen, Ta, and Viet Ta, 2015). We aim to prove the solution of the system with positive initial values $(s(t), u_1(t), u_2(t)) = u \in \mathbb{R}^3_+$ remains in $\mathbb{R}^3_+$ for $\tau = \infty$. Indeed, the right hand side of the system (4.13) without diffusion contains local Lipschitz continuous functions on $\mathbb{R}^3_+$, so a unique local continuous solution $u = (s, u_1, u_2)$ defined on $[0, \tau)$ exists.

In the first step, we prove $u(t) \in \mathbb{R}^3_+$ for $0 \leqslant t < \tau$. For this reason, we suppose τ be the first time in the interval $[0, \tau)$ such that $u = (s(t), u_1(t), u_2(t))$ touch the boundary $\mathbb{R}^3_+$, i.e

$$\tau_0 = inf\Big\{0 \leqslant t < \tau | s(t)u_1(t)u_2(t) = 0\Big\}, \tag{4.53}$$

Indeed $(s(0), u_1(0), u_2(0)) \in \mathbb{R}^3_+$ results in $s(t) > 0, u_1(0), u_2(0) > 0$, and $0 < t < \tau_0$.

The system (4.13) in absence of diffusion gives

$$\begin{aligned}
s(t) &= s(0)\exp\Big\{\int_0^t \Big[\gamma(1-\frac{s(\nu)}{K}) - \frac{m_1u_1(\nu)}{a_1+s(\nu)} - \frac{m_2u_2(\nu)}{a_2+s(\nu)}\Big]d\nu\Big\}, \ \ 0 \leqslant t < \tau,\\
u_1(t) &= u_1(0)\exp\Big\{\int_0^t \Big[\frac{m_1s(\nu)}{a_1+s(\nu)} - d_1 - \varepsilon u_1(\nu)\Big]d\nu\Big\}, \ \ 0 \leqslant t < \tau,\\
u_2(t) &= u_2(0)\exp\Big\{\int_0^t \Big[\frac{m_2s(\nu)}{a_2+s(\nu)} - d_2\Big]d\nu\Big\}, \ \ 0 \leqslant t < \tau,
\end{aligned} \tag{4.54}$$

u is continuous on $[0, \tau)$ so (4.53), and (4.54) provide $\tau_0 = \tau$. Therefore, $u(t) \in \mathbb{R}^3_+$, for all $0 \leqslant t < \tau$. We need to prove the solution $u(t)$ remains in $\mathbb{R}^3_+$ as $\tau = \infty$. Thus $x(t) \in \mathbb{R}^3_+$ for $0 \leqslant t < \tau$, Eqs in (4.54) leads to

$$\begin{aligned}
0 < s(t) &\leqslant (0)\exp\{\int_0^t \gamma\, d\nu\}, \ \ 0 \leqslant t < \tau,\\
0 < u_i(t) &\leqslant u_i(0)\exp\{\int_0^t m_i\, d\nu\}, \ \ 0 \leqslant t < \tau, \ \ i = 1, 2,
\end{aligned} \tag{4.55}$$

since the coefficients γ and m_i, $i = 1, 2$ are constant and bounded. We obtain that $\lim_{t\to\tau} \|u(t)\| < \infty$, definition of τ concludes $\tau = \infty$. which emphasizes u is a unique global positive solution. □

Definition 4.8.1 *(Kouachi, 2016) A subset $\Sigma \subset (\mathbb{L}^\infty(\Omega))^m$ is called a positively invariant region (or more simply an invariant region) for system (4.62), if all solutions with initial data in Σ remain in Σ for all time in their interval of existence.*

Invariant region can make answer two main questions:
1. when do the solutions of PDE decay to spatially homogeneous function in time?

2. what relationship have spatially homogeneous functions to solutions of ODE? (Conway, Hoff, and Smoller, 1978)

It can be shown that for a set to be invariant for (PDE) it must be a rectangle that is invariant for (ODE) (Conway, Hoff, and Smoller, 1978).

Here we follow the method mentioned in (Kouachi, 2016) whose method is generalized method of the results of (Kuiper, 2000, Kanel and Kirane, 1998). In fact, they have been worked on the system of two species while kouachi (Kouachi, 2016) introduced the method for three and more than three spices.
The diffusion matrix $A = (a_{ij})_{1\leqslant i,j\leqslant 3}$ with real entries is supposed to be diagonalizable with positive eigenvalues $0 < \lambda_1 < \lambda_2 < \lambda_3$, each eigenvalue is of simple multiplicity (general case has been investigated in Kouachi, 2016).
It is supposed that for $|u_1|$ sufficiently large, the reactions in (4.13) satisfy:

1) ***The dissipativity condition (Kouachi, 2016):*** each of function $sf_k(t,x,w)$ does not change sign on $\mathbb{R}^+ \times \mathbb{R}$ that is

$$\sigma_k sf_k(t,x,w) \leqslant 0, \quad \sigma_k = \pm 1, \quad k = 1,2,3, \tag{4.56}$$

2) ***The balance law condition (Kouachi, 2016):*** characteristic $\Phi_{ij}(\sigma|f|)$ of the system are alternate functions with respect to i

$$(-1)^{i+1}\Phi_i(\sigma|f|) \geqslant 0, \tag{4.57}$$

where $\sigma|f| = (\sigma_1|f_1|, \sigma_2|f_2|, \sigma_3|f_3|)$.

Definition 4.8.2 *The set*

$$\Lambda = \cap_{p=1}^{3}\Lambda_p, \tag{4.58}$$

where Λ_p represents the rectangle $\Lambda_p = \{z \in \mathbb{R}^m : \alpha_p \leqslant z_p \leqslant \beta_p\}$, for $p = 1,2,3$ with edges

$$\Lambda_i(\alpha_i) = \{z \in \Lambda_p : z_i = \alpha_i \ (if\ \alpha_i < 0),\ ,\ and\ \ z_i = -\alpha_i \ (if\ \ \alpha_i > 0)\}, p \neq i, \ \ i = 1,2,3. \tag{4.59}$$

and

$$\Lambda_i(\beta_i) = \{z \in \Lambda_p : z_i = \beta_i\}, p \neq i, \ i = 1,2,3. \tag{4.60}$$

In addition we investigate an invariant region of the system (4.13) such that diffusion matrix includes only one cross-diffusion parameter k_{32}, namely,

$$A = \begin{bmatrix} k_{11} & 0 & 0 \\ 0 & k_{22} & 0 \\ 0 & k_{32} & k_{33} \end{bmatrix}, \tag{4.61}$$

Theorem 4.8.1 *(Kouachi, 2016) Consider the system*

$$\frac{\partial w_i(t,x)}{\partial t} - \Sigma a_{ij}\Delta_j(t,x) = f_i(t,x,w), \quad in\mathbb{R}^+ \times \Omega, \tag{4.62}$$

with boundary conditions

$$\frac{\partial w_i(t,x)}{\partial \eta} = g_i(x,w), on \Gamma^N, \quad and \quad w_i(t,x) = \theta_i(x), \quad on \quad \Gamma^D, \tag{4.63}$$

$$\tag{4.64}$$

and initial data $w_i(0,x) = w_i^0(x)$ *in* Ω, *where* Ω *is open bounded domain of class of* $\mathbb{C}^1$ *in* $\mathbb{R}^n$ *with boundary* $\partial\Omega = \Gamma^D \cup \Gamma^N$ *is a disjoint union. In addition, suppose that the diffusion matrix is symmetrizable, then under conditions* (4.56) *and* (4.57), *the region* $\mathcal{S} = X^{-1}(\Lambda)$ *with* Λ *defined by* (4.58) *and* X *contains eigenvectors, the system* (4.69) *is invariant for system* (4.63). *Moreover the solution is global and uniformly bounded on* Ω *for any initial data in* $L_\infty(\Omega)$. *Furthermore, when the conditions are satisfied for all* $w_1 \in \mathbb{R}$, *then*

$$\|w\|_\infty \leqslant \mathcal{C}\|w^0\|_\infty \tag{4.65}$$

where $\mathcal{C}$ *is a positive constant depending only on the diffusion matrix* A *and equal to the unity when* A *is symmetric.*

Before to apply this theorem for the model (4.13) with diffusion matrix (4.61), we remark that the rectangle region defined in Kouachi, 2016 changed to the Definition 4.8, since we are looking for a positively invariant region.

We also remark Kouachi (Kouachi, 2016) supposed that the diffusion matrix of the system (4.63) be symmetrizable to find eigenvalues conveniently. The system (4.13) with the diffusion matrix (4.61) can be diagonalizable and consequently we can find eigenvalues easily. Indeed the diffusion matrix (4.61) consists of the eigenvalues $\lambda_1 = k_{11}, \lambda_2 = k_{22}, \lambda_3 = k_{33}$. In order to have a diagonalizable diffusion matrix, one needs the real positive eigenvalues.

$$0 < k_{11} < k_{22} < k_{33}, \tag{4.66}$$

The eigenvectors correspondingly are

$$x_1 = (1,0,0), \quad x_2 = (0, \frac{-(k_{22}-k_{33})}{k_{32}}, -1), \quad x_3 = (0,0,1), \tag{4.67}$$

We set $Q = \dfrac{k_{22}-k_{33}}{k_{32}}$, due to assumption (4.66) and positivity of all diffusion parameters Q is positive and non-singular. Therefore

$$A = X^{-1}DX,$$

where

$$X = \begin{bmatrix} 1 & 0 & 0 \\ 0 & -Q & 0 \\ 0 & -1 & 1 \end{bmatrix}, \quad X^{-1} = \begin{bmatrix} 1 & 0 & 0 \\ 0 & -\frac{1}{Q} & 0 \\ 0 & -\frac{1}{Q} & 1 \end{bmatrix}, \quad D = \begin{bmatrix} k_{11} & 0 & 0 \\ 0 & k_{22} & 0 \\ 0 & 0 & k_{22} \end{bmatrix}. \tag{4.68}$$

Changing variables $Z = Xw$, where X is matrix of eigenvectors rows $x_i = (x_{i1}, x_{i2}, x_{i3})^t$, the system (4.13) with diffusion (4.61) is equivalent to the following diagonal system:

$$\frac{\partial Z}{\partial t} - D\Delta Z = Xf(t;x,X^{-1}Z), \quad \texttt{in } \mathbb{R}^+ \times \Omega, \tag{4.69}$$

and $\frac{\partial Z}{\partial \eta} = 0;$, and initial condition $Z(0,x) = Z^0(x)$.

Each eigenvector x_i associated to the eigenvalue λ_i corresponds an equation

$$\begin{aligned} \frac{\partial z_i}{\partial t} - \lambda_i \Delta z_i &= F_i(t;x,Z), \quad \texttt{in } \mathbb{R}^+ \times \Omega \\ \frac{\partial z_i}{\partial \eta} &= 0;, \quad z_i(0,x) = z_i^0(x), \end{aligned} \tag{4.70}$$

where

$$w_1 = x_{i,1}^{-1} z_i + \Sigma_{j,\, j\neq i} x_{j,1}^{-1} z_j,$$

$$z_i = \Sigma_{k=1}^{3} x_{i,k} w_k, \tag{4.71}$$

$$F_i(t,x,Z) = \Sigma_{k=1}^{3} x_{i,k} f_k(t,x,X^{-1}Z), \tag{4.72}$$

For each simple eigenvalue, the linear form $\Phi_i(w)$ is defined as

$$\Phi_i(w) = det(A^t - \lambda_i I),$$

by replacing the first row with corresponding component of $w = (w_1, w_2, w_3) \equiv (s, u_1, u_2)$.

$$\Phi_i(w) = \begin{vmatrix} s & u_1 & u_2 \\ k_{12} & k_{22} - \lambda_i & k_{32} \\ k_{13} & k_{23} & k_{33} - \lambda_i \end{vmatrix}, \tag{4.73}$$

Moreover, the new reaction becomes

$$F_i(t,x,Z) = \frac{x_{i,1}}{\Delta_{i,1}} \Phi_i(f(t,x,w)),$$

where $w = X^{-1}Z$.

In order to apply Theorem 4.8.1, conditions (4.56) and (4.57) must be satisfied and a rectangle region must be presented.

The dissipativity and balance law conditions

The dissipativity conditions: we need to prove (4.56) for each reaction.

We set $\sigma_1 = -1$ then $s^2(\gamma(1 - \frac{s}{K}) - \frac{m_1 u_1}{a_1 + s} - \frac{m_2 u_2}{a_2 + s}) \geqslant 0$ which is satisfied if $s < K$.

Moreover we suppose $\sigma_2 = -1$ therefore $s u_1 (\frac{m_1 s}{a_1 + s} - d_1 - \varepsilon u_1) \geqslant 0$ that leads to:

$$\begin{cases} I.\ \ s u_1 \geqslant 0, \ \text{ and } \ \frac{m_1 s}{a_1 + s} - d_1 - \varepsilon u_1 \geqslant 0, \\ \text{or} \\ II.\ \ s u_1 \leqslant 0, \ \text{ and } \ \frac{m_1 s}{a_1 + s} - d_1 - \varepsilon u_1 \leqslant 0, \end{cases} \tag{4.74}$$

Remark 4.8.1 *These two cases are interpreted as:*

a) The first inequality of II denotes that u_1 or s is negative while we are looking for a positive invariant region, therefore it is failed and we ignore to survey the second term in II.

b) Hence we survey the first scenario I. Indeed $su_1 \geqslant 0$ implied that s and u_1 have the same sign. However only we admit positive signs because of the positive invariant region, and also the second term in I is satisfied if

$$u_1 \leqslant \frac{(m_1 - d_1)(s - \lambda_1)}{\varepsilon(a_1 + s)},$$

Since $|s|$ has been considered large enough so

$$u_1 \to \frac{(m_1 - d_1)}{\varepsilon},$$

In final, if $\sigma_3 = 1$, then

$$\begin{cases} I'.\ su_2 \geqslant 0, \ \text{ and } \ \dfrac{m_2 s}{a_2 + s} - d_2 \geqslant 0, \\ \text{or} \\ II'.\ su_2 \leqslant 0, \ \text{ and } \ \dfrac{m_2 s}{a_2 + s} - d_2 \leqslant 0, \end{cases} \tag{4.75}$$

Remark 4.8.2 *The dissipativity condition of the second reaction is interpreted as follows:*

a) The first term in I' denotes s and u_2 have the same sign. Since we need a positive invariant region so only the positive signs are admitted.

b) The second inequality in I' is satisfied if $\dfrac{(m_2 - d_2)(s - \lambda_2)}{a_2 + s} \geqslant 0$ and consequently $s \geqslant \lambda_2$ and $m_2 \geqslant d_2$ or $s \leqslant \lambda_2$ and $m_2 \leqslant d_2$. Positivity conditions of the coexistence steady state mentioned in 4.3.1 leads to $s \geqslant \lambda_2$ and $m_2 \geqslant d_2$. However the dissipativity condition mentioned in (Kouachi, 2016) when $|s|$ is large enough so the second term in I' tends to $\dfrac{(m_2 - d_2)}{a_2}$ which is always satisfied.

c) The first inequality in II' is satisfied if one of the unknowns is negative thus it failed and therefore one does not need to survey the second term in II'.

In following ***The balance law condition*** (4.57) are satisfied as follows:

$$\Phi_1(\sigma|f|) = |f|(k_{22} - k_{11})(k_{33} - k_{11}) \geqslant 0, \tag{4.76}$$

and $\Phi_2(\sigma|f|) = \Phi_3(\sigma|f|) = 0$.

Now we present a positive invariant region. According to $w = X^{-1}Z$, the new variables are $s = z_1$, $u_1 = \dfrac{z_1}{-Q}$, $u_2 = z_3 - \dfrac{z_2}{Q}$. Hence each ODE system is given as

below:

$$\begin{cases} \dfrac{dz_1}{dt} = z_1\left(\gamma(1-\dfrac{z_1}{K}) - \dfrac{m_1 z_2}{-Q_1(a_1+z_1)} - \dfrac{m_2(z_3-\dfrac{z_2}{Q})}{a_2+z_1}\right), \\ \dfrac{dz_2}{dt} = \dfrac{z_2}{((-Q))}\left(\dfrac{m_1 z_1}{a_1+z_1} - d_1 - \dfrac{\varepsilon z_2}{(-Q)}\right), \\ \dfrac{dz_3}{dt} = (z_3 - \dfrac{z_2}{Q})\left(\dfrac{m_2 z_1}{a_2+z_1} - d_2\right), \end{cases} \tag{4.77}$$

In following we find an invariant region of the new system (4.77), the method adapted from (Hoai Nguyen, Ta, and Viet Ta, 2015).

Existence of invariant region

First we find the upper bounds:

$$\begin{aligned} z_2'(t) &= \frac{z_2}{(-Q)}\left(\frac{m_1 z_1}{a_1+z_1} - d_1 - \frac{\varepsilon z_2}{(-Q)}\right) \\ &\leqslant \frac{z_2}{(-Q)}\left((m_1-d_1) - \frac{\varepsilon z_2}{(-Q)}\right) \\ &\leqslant \frac{\varepsilon z_2}{Q^2}\left(\frac{(-Q)}{\varepsilon}(m_1-d_1) - z_2\right), \end{aligned} \tag{4.78}$$

thus $z_2 \leqslant M_{z_2}$ where

$$M_{z_2} = \frac{-Q}{\varepsilon}(m_1-d_1),$$

Moreover, the upper bound of z_3 is obtained as below:

$$\begin{aligned} z_3'(t) &= (z_3 - \frac{z_2}{Q})\left(\frac{m_2 z_1}{a_2+z_1} - d_2\right) \\ &\leqslant z_3\left(\frac{(m_2-d_2)z_1}{a_2+z_1} - \frac{M_{z_2}}{Q}(m_2-d_2)\right) \\ &\leqslant z_3(m_2-d_2) - \frac{M_{z_2}}{Q}(m_2-d_2), \end{aligned} \tag{4.79}$$

which gives $z_3 \leqslant M_{z_3}$ where

$$M_{z_3} = (m_1-d_1) + Ce^{(m_2-d_2)t}, \quad \forall C \geqslant 0,$$

and finally

$$\begin{aligned} z_1' &= z_1\left(\gamma(1-\frac{z_1}{K}) - \frac{m_1 z_2}{-Q(a_1+z_1)} - \frac{m_2(z_3-\frac{z_2}{Q})}{a_2+z_1}\right) \leqslant z_1\left(\gamma(1-\frac{z_1}{K}) + \frac{m_2 z_2}{Q(a_2+z_1)}\right) \\ &\leqslant z_1\left(\gamma(1-\frac{z_1}{K}) + \frac{m_2 M_{z_2}}{Q(a_2+z_1)}\right) \\ &\leqslant z_1\left(\gamma(1-\frac{z_1}{K}) - \frac{m_2(m_1-d_1)}{\varepsilon(a_2+z_1)}\right) \leqslant z_1\left(\gamma(1-\frac{z_1}{K})\right), \end{aligned} \tag{4.80}$$

so based on the comparison theorem $z_1 \leqslant M_{z_1} = K$.

Now we find the lower bound of the invariant region. That is

$$\begin{aligned} z_1' &= z_1\left(\gamma(1-\frac{z_1}{K}) - \frac{m_1 z_2}{-Q(a_1+z_1)} - \frac{m_2(z_3-\frac{z_2}{Q})}{a_2+z_1}\right) \geqslant z_1\left(\gamma(1-\frac{z_1}{K}) - \frac{m_1 M_{z_2}}{a_1} - \frac{m_2 M_{z_3}}{a_2}\right) \\ &\geqslant z_1\left(\frac{\gamma aK - K(m_1 M_{z_2} + m_2 M_{z_3})}{aK} - \frac{\gamma z_1}{K}\right) \\ &\geqslant z_1\frac{\gamma}{K}\left(\frac{\gamma aK - K(m_1 M_{z_2} + m_2 M_{z_3})}{a\gamma} - z_1\right) \\ &\geqslant z_1\frac{\gamma}{K}\left(\frac{K(\gamma a - (m_1 M_{z_2} + m_2 M_{z_3}))}{a\gamma} - z_1\right), \end{aligned} \tag{4.81}$$

where $a = \max\{a_1, a_2\}$, hence the lower bound of z_1 is obtained

$$m_{z_1} = \frac{K(\gamma a - (m_1 M_{z_2} + m_2 M_{z_3}))}{a\gamma} = K\left(1 - \frac{(m_1 M_{z_2} + m_2 M_{z_3})}{\gamma a}\right) < K,$$

Simultaneously, the lower bounds of z_2 and z_3 are given as:

$$\begin{aligned} z_2' &= \frac{z_2}{-Q}\left(\frac{m_1 z_1}{a_1+z_1} - d_1 - \frac{\varepsilon z_2}{-Q}\right) \\ &\geqslant \frac{z_2}{-Q}\left(\frac{(m_1-d_1)m_{z_1} - a_1 d_1}{a_1 + M_{z_1}} - \frac{\varepsilon z_2}{-Q}\right) \\ &\geqslant \frac{z_2\varepsilon}{Q^2}\left(\frac{-Q(m_1-d_1)m_{z_1} - a_1 d_1}{\varepsilon(a_1+M_{z_1})} - z_2\right), \end{aligned} \tag{4.82}$$

therefore comparison theory results in

$$m_{z_2} = \left(\frac{-Q(m_1-d_1)m_{z_1} - a_1 d_1}{\varepsilon(a_1+M_{z_1})}\right),$$

and the lower bound of z_3 is found as

$$\begin{aligned} z_3' &= z_3\left(\frac{m_2 z_1}{a_2+z_1} - d_2\right) - \frac{z_2}{Q}\left(\frac{m_2 z_1}{a_2+z_1} - d_2\right) \\ &\geqslant z_3\left(\frac{(m_2-d_2)m_{z_1} - a_2 d_2}{a_2+M_{z_1}}\right) - \frac{M_{z_2}}{Q}(m_2-d_2) \\ &= z_3\left(\frac{(m_2-d_2)m_{z_1} - a_2 d_2}{a_2+M_{z_1}}\right) - \frac{(m_2-d_2)(m_1-d_1)}{\varepsilon}, \end{aligned} \tag{4.83}$$

comparison theorem obtains

$$z_3(t) \geqslant \frac{B}{A} + Ce^{At}, \quad \forall C \geqslant 0, \quad t \in \mathbf{I},$$

where

$$A = \frac{(m_2-d_2)m_{z_1} - a_2 d_2}{a_2+M_{z_1}}, \quad B = \frac{(m_2-d_2)(m_1-d_1)}{\varepsilon},$$

thus for $C = 0$, $m_{z_3} = \dfrac{m_1-d_1}{\varepsilon}$.

Using the invariant region method mentioned by Smoller (Smoller, 2012), Kuiper

(Kuiper, 1980, Kuiper, 2000), we can complete the proof. Indeed, the region defined by Definition 4.8.2 is invariant if the below conditions are satisfied:

$$F_i(x,t,z) \geqslant 0, \quad \forall z \in \Lambda_i(\alpha_i), \tag{4.84}$$
$$F_i(x,t,z) \leqslant 0, \quad \forall z \in \Lambda_i(\beta_i), \tag{4.85}$$

That is the dissipativity conditions and invariant bounds lead to $\Phi_1(f) > 0$ that

$$F_1(x,t,z) = \frac{x_{1,1}\Phi_1(f)}{\Delta_{1,1}} = \frac{f_1(k_{33}-k_{11})(k_{22}-k_{11})}{(k_{33}-k_{11})(k_{22}-k_{11})} \geqslant 0, \quad \forall z \in \Lambda_i(\alpha_i). \tag{4.86}$$

where $x_{1,1} = 1$, and

$$F_2(x,t,z) = F_3(x,t,z) = 0, \quad \forall z \in \Lambda_i(\alpha_i).$$

and simultaneously due to the dissipativity conditions and invariant bounds mentioned above $\Phi_1(f) < 0$ and

$$F_1(x,t,z) = \frac{x_{1,1}\Phi_1(f)}{\Delta_{1,1}} = \frac{f_1(k_{33}-k_{11})(k_{22}-k_{11})}{(k_{33}-k_{11})(k_{22}-k_{11})} \leqslant 0, \quad \forall z \in \Lambda_i(\beta_i). \tag{4.87}$$

and

$$F_2(x,t,z) = F_3(x,t,z) = 0, \quad \forall z \in \Lambda_i(\beta_i).$$

To conclude, we record that the diffusion matrix (4.61) is diagonalizable with positive eigenvalues, the two systems (4.13) with diffusion matrix (4.61), and (4.69) are parabolic and equivalent. Then if the original system has an invariant region $\Sigma = X^{-1}(\Lambda)$.
Invariant region denotes that $\|Z\| \leqslant \|Z_0\|$ therefore because of $Z = Xu$ we can conclude that

$$\|u\| \leqslant \|X^{-1}Z\| =: \|Z\| \leqslant \|Z_0\| \leqslant Xu_0\| = \|u_0\|,$$

which ends the proof.

The following lemma is stated for the above results.

Lemma 4.8.2 *The region $\mathcal{S} = X^{-1}(\Lambda)$ with Λ found in 4.8 of the system (4.69) is invariant for system (4.13) with diffusion matrix 4.61 and homogeneous Neumann boundary condition. Moreover the solution is global and uniformly bounded on Ω for any initial data in $L_\infty(\Omega)$. Furthermore, when the conditions are satisfied for all $s \in \mathbb{R}$, then*

$$\|u\|_\infty \leqslant \mathcal{C}\|u^0\|_\infty. \tag{4.88}$$

where $\mathcal{C}$ is a positive constant depending only on the diffusion matrix A.

Chapter 5

The existence of time global solution of the IGP

Here we investigate the global solution of the system (2.3). The sections are organized as follows:
In the first section, we demonstrate that the solution with positive initial values of the system remains positive. In section two the existence of the local solution is proved. And finally, energy estimate method employed to present a priory bounds in Sobolev spaces.

5.1 Main Result

Our aim is to show that under certain conditions on the initial values, the $2D$ Prey and Predator model of three species (2.3) admits unique regular global solution for all time $t > 0$. The presence of the constants does not have any major effects on the existence of the solutions, therefore, without loss of generality, one may assume that all constants take the unity value. Hence,

$$\begin{cases} \partial_t s = \Delta s + (1-s)s - u_1 s - u_2 s, \\ \partial_t u_1 = \Delta u_1 + \nabla \cdot (u_1 \nabla u_2) + u_1 s - u_1 - u_1 u_2, \\ \partial_t u_2 = \Delta u_2 + u_2 s - u_2 + u_1 u_2. \end{cases} \tag{5.1}$$

The main result reads:

Theorem 5.1.1 *Let $p : 2 \leq p \leq \infty$, $r \geq 1$ and $T > 0$ is given. Assume $(s^0, u_1^0, u_2^0) \in L^p \cap H^r(\mathbb{R}^2)$ all be positive. Moreover, assume that $\nabla u_1^0 \cdot \nabla (u_2^0)_j > 0$, for $j = 1, 2$. Then the system of equations (5.1) admits unique global solution (s, u_1, u_2) in the space of $L^p \cap H^r(\mathbb{R}^2)$. Moreover, there exists a universal constant $C = C(\|s^0, u_1^0, u_2^0\|_{L^p \cap H^r})$ so that*

$$\|(s, u_1, u_2)\|_{L^p}^p + \int_0^t \|\nabla[|(s, u_1, u_2)|^{\frac{p}{2}}]\|_{L^2}^2 d\tau \leq C, \tag{5.2}$$

$$\|(s, u_1, u_2)\|_{H^r}^2 + \int_0^t \|[(s, u_1, u_2)]\|_{H^{r+1}}^2 d\tau \leq C. \tag{5.3}$$

5.1.1 Strategy towards the existence

The existence argument follows a standard approach. The method consists of two main steps. The local well-posedness is established in the first step: we show that there exists a time interval $[0, T]$ and a space $\mathbb{Y}$ so that the solutions (s, u_1, u_2) exist in the space $\mathbb{Y}$ up to time T (this is done via a fixed point argument). We then continue to see how large this T can be. This is the aim of the second step: we prove

that the blow up is not happening on any finite time interval $[0, T]$. In other words, given any time $T > 0$, the solutions (s, u_1, u_2) remain bounded, in a certain normed space $\mathbb{X}$,

$$\sup_{0\le t\le T} \|(s, u_1, u_2)\|_{\mathbb{X}} < \infty.$$

The two steps together guarantee the existence of global solutions to the system (5.1).

The Chapter is organized as follows. In section 5.1.2 we recall some of the relations which will be used in the sequel. In section 5.2, we demonstrate that the solution with positive initial values remains positive for all time. Sections 5.3 and 5.4 are devoted to the local and global existence of the solutions, respectively. The fixed point argument is used to prove the local existence, and the proof toward the global solutions is taking advantage of the energy estimates on the solutions s, u_1 and u_2 and a bootstrapping process.

5.1.2 Preliminaries

We use standard notation for L^p spaces and Sobolev spaces, namely for $s > 0$, $p \in [1, \infty)$,

$$\begin{aligned} \|f\|_{L^p} &= \left[\int_{\mathbb{R}^2} |f(x)|^2 dx\right]^{\frac{1}{p}}, \\ \|f\|_{H^s} &= \|\Lambda^s f\|_{L^2} + \|f\|_{L^2}. \end{aligned}$$

where $\Lambda^s = (-\Delta)^{\frac{s}{2}}$. In the sequel we make a frequent use of the following well-known relations (Majda, Bertozzi, and Ogawa, 2002).

Lemma 5.1.1 *Assume* $\frac{1}{p} = \frac{1}{p_1} + \frac{1}{q_1} = \frac{1}{p_2} + \frac{1}{q_2}$ *and* $s > 0$ *and* $s_1 \le s \le s_2$. *Then*

(1). Product estimates:

$$\|\Lambda^s(fg)\|_{L^p} \le \|\Lambda^s f\|_{L^{p_1}} \|g\|_{L^{q_1}} + \|f\|_{L^{p_2}} \|\Lambda^s g\|_{L^{q_2}}. \tag{5.4}$$

(1). Gagliardo-Nirenberg estimate:

$$\|\Lambda^s f\|_{L^p} \le \|\Lambda^{s_1} f\|_{L^p}^{\alpha} \|\Lambda^{s_2} f\|_{L^q}^{1-\alpha}, \tag{5.5}$$

where $\frac{1}{r} = \frac{\alpha}{p} + \frac{1-\alpha}{q}$ *and* $s = \alpha s_1 + (1-\alpha)s_2$.

Moreover, we make use of the following semi-group estimates. One may consult (Ji, Yan, and Wu, 2022) for a proof.

Lemma 5.1.2 *Let* $\beta \ge 0$, $\alpha > 0$ *and* $1 \le p \le q \le \infty$. *Then*

$$\|\Lambda^\beta e^{-\nu(-\Delta)^\alpha} f\|_{L^q(\mathbb{R}^d)} \le C t^{-\frac{\beta}{2} - \frac{d}{2\alpha}\left(\frac{1}{q} - \frac{1}{p}\right)} \|f\|_{L^p(\mathbb{R}^d)}. \tag{5.6}$$

5.2 Positivity of the solutions

In this section we show that the solutions of the system (5.1) remain positive, requiring that the initial values be positive, i.e. $s(0,x), u_1(0,x)$ and $u_2(0,x) > 0$. In addition, we assume that $\nabla u_1^0(x) \cdot \nabla u_2^0(x) \ge 0$. These later initial conditions on the derivatives are needed in the existence argument, as the presence of the chemotaxis term $\nabla \cdot [u_1 \nabla u_2]$ in the second equation of (5.1) is challenging, and requires additional assumption.

The positivity argument is based on the following well-known theorem as follows.

Theorem 5.2.1 *Let $\mathcal{L} = L - \partial_t$ be a parabolic operator with continuous coefficients in domain Ω_0:*

$$L\theta = \sum_{i,j=1}^{n} a_{ij}(t,x)\frac{\partial^2\theta}{\partial_i\partial_j} + \sum_{i,j=1}^{m} b_{ij}(t,x)\frac{\partial\theta}{\partial_i} + \sum_{i,j=1}^{n} c(t,x)\theta,$$

and

$$\partial_t\theta = L\theta + f(x,t,\theta,\frac{\partial\theta}{\partial_i},\frac{\partial^2\theta}{\partial_i\partial_j}). \tag{5.7}$$

Assume that

$$|a_{ij}(t,x)| \le M, \quad |b_{ij}(t,x)| \le M(|x|+1), \quad |c_{ij}(t,x)| \le M(|x|^2+1). \tag{5.8}$$

Moreover, assume that $A\theta \ge 0$ in Ω_0 and that

$$\theta(t,x) \ge -B\exp(\beta|x|^2), \tag{5.9}$$

for some positive constants β, B. If $\theta(0,x) \ge 0$ in $\mathbb{R}^n$, then $\theta(t,x) \ge 0$ in Ω.

To apply this theorem to our model, we rewrite the system (5.1) in its vector form

$$\partial_t U = LU + F(x,t,U,\nabla U,\Delta U), \tag{5.10}$$

where

$$U = \begin{pmatrix} s \\ u_1 \\ u_2 \\ \nabla u_1 \\ \nabla u_2 \end{pmatrix}_{5\times 1}, \qquad L := \begin{pmatrix} d_1 & 0 & 0 & 0 & 0 \\ 0 & d_2 & 0 & 0 & 0 \\ 0 & 0 & d_3 & 0 & 0 \\ 0 & 0 & 0 & d_2 & 0 \\ 0 & 0 & 0 & 0 & d_3 \end{pmatrix}_{5\times 5}.$$

Above, We took derivative (gradient) of the second and third equations and add them to the system:

$$\begin{cases} \partial_t(\nabla u_1) = d_2\Delta(\nabla u_1) + F_4(x,t,U,\nabla U,\Delta U), \\ \partial_t(\nabla u_2) = d_3\Delta(\nabla u_2) + F_5(x,t,U,\nabla U,\Delta U). \end{cases} \tag{5.11}$$

The matrix $L = diag(d_1,d_2,d_3,d_2,d_3)$ is positive definite as each $d_i > 0$. Therefore, the conditions of theorem 5.2.1 are satisfied and hence the solutions remain positive for all time, requiring that the initial value $U_i(0,x) > 0$. the above argument is the proof of the following lemma. Generally speaking, starting with positive initial values, the solutions of the system

$$\partial_t U = LU + F(x,t,U,\nabla U),$$

remain positive if the matrix L is positive definite.

Lemma 5.2.1 *Assume $s(0,x) = s^0(x)$, $u_1(0,x) = u_1^0(x)$, $u_2(0,x) = u_2^0(x)$, $\nabla u_1(0,x) = \nabla u_1^0(x)$ and $\nabla u_2(0,x) = \nabla u_2^0(x)$, where the functions $s^0(x), u_1 s^0(x), u_2^0(x), \nabla u_1^0(x)$ and $\nabla u_2^0(x)$ all be positive. Then the solution to the system of equations (5.10) remains positive for all time $t > 0$.*

Note that, this lemma states that, beside the functions s, u_1 and u_2, the derivatives ∇u_1 and ∇u_2 stay positive as well (with some abuse of the notation, since the latest are vectors).

5.3 Local Existence

Proof [Proof of the main theorem 5.1.1] The local existence of the strong solutions in the space of $C([0,T];X)$, $0 < T < 0$ to be determined, is done via a fixed point argument of the integral equations

$$\begin{cases} s(t,x) = e^{(\Delta+1)t}s^0(x) - \int_0^t e^{(\Delta+1)(t-\tau)}\Big[s^2(\tau) + u_1(\tau)s(\tau) + u_2(\tau)s(\tau)\Big]d\tau, \\ u_1(t,x) = e^{(\Delta-1)t}u_1^0(x) + \int_0^t e^{(\Delta-1)(t-\tau)} \\ \Big[\nabla(u_1(\tau)\cdot\nabla u_2(\tau)) + u_1(\tau)s(\tau) - u_1(\tau)u_2(\tau)\Big]d\tau, \\ u_2(t,x) = e^{(\Delta-1)t}u_2^0(x) + \int_0^t e^{(\Delta-1)(t-\tau)}\Big[u_2(\tau)s(\tau) + u_1(\tau)u_2(\tau)\Big]d\tau. \end{cases} \tag{5.12}$$

We define $Q_1(s,u_1,u_2)$, $Q_2(s,u_1,u_2)$ and $Q_3(s,u_1,u_2)$ to be the integrals in the (5.12), respectively. Moreover, we introduce the space $X = L^p \cap H^r$. We then have, by applying lemma 5.1.2 with $q = p$, $\beta = 0$, $\alpha = 1$ and $d = 2$,

$$\begin{aligned} \|e^{(\Delta+1)t}s^0\|_{L^p} &+ \|e^{(\Delta-1)t}u_1^0\|_{L^p} + \|e^{(\Delta-1)t}u_2^0\|_{L^p} \\ &\leq C\Big[e^t\|s^0\|_{L^p} + e^{-t}\|u_1^0\|_{L^p} + e^{-t}\|u_2^0(x)\|_{L^p}\Big] \\ &\leq Ce\Big[\|s^0\|_{L^p} + \|u_1^0\|_{L^p} + \|u_2^0(x)\|_{L^p}\Big]. \end{aligned}$$

Also, by applying lemma 5.1.2 with $q = p = 2$, $\beta = 0$, $\alpha = 1$ and $d = 2$,

$$\begin{aligned} \|e^{(\Delta+1)t}s^0\|_{H^r} &+ \|e^{(\Delta-1)t}u_1^0\|_{H^r} + \|e^{(\Delta-1)t}u_2^0\|_{H^r} \\ &\leq C\Big[e^t\|s^0\|_{H^r} + e^{-t}\|u_1^0\|_{H^r} + e^{-t}\|u_2^0\|_{H^r}\Big] \\ &\leq Ce\Big[\|s^0\|_{H^r} + \|u_1^0\|_{H^r} + \|u_2^0\|_{H^r}\Big]. \end{aligned}$$

Therefore, we define the working space $\mathbb{Y}$ to be

$$\mathbb{Y} = \Big\{(s,u_1,u_2) : \sup_{0\leq t\leq T}\big[\|s\|_X + \|u_1\|_X + \|u_2\|_X\big] \leq 2Ce\big[\|s^0\|_X + \|u_1^0\|_X + \|u_2^0\|_X\big]\Big\} \tag{5.13}$$

We show that $Q_1(s,u_1,u_2)$, $Q_2(s,u_1,u_2)$ and $Q_3(s,u_1,u_2)$ define contraction mapping on the space $\mathbb{Y}$, hence the existence of fixed points (s,u_1,u_2). Through the rest of the proof, we frequently make use of lemma 5.1.2 and the semigroup estimate therein.

5.3.1 Estimates in L^p norms

$$\begin{aligned}
&\|Q_1(s,u_1,u_2)\|_{L^p} \leq \int_0^t \|e^{(\Delta+1)(t-\tau)}[s^2]d\tau\|_{L^p} \\
&+ \int_0^t \|e^{(\Delta+1)(t-\tau)}[u_1 s]\|_{L^p}d\tau + \int_0^t \|e^{(\Delta+1)(t-\tau)}[u_2 s]\|_{L^p}d\tau \\
&\leq \int_0^t (t-\tau)^{-(\frac{2}{p}-\frac{1}{p})} e^{t-\tau}\left[\|s\|_{L^p}^2 + \|s\|_{L^p}\|u_1\|_{L^p} + \|s\|_{L^p}\|u_2\|_{L^p}\right]d\tau \\
&\leq eT^{1-\frac{1}{p}}\left[\sup_{0\leq t\leq T}\|u_1\|_X + \sup_{0\leq t\leq T}\|u_2\|_X\right]\sup_{0\leq t\leq T}\|s\|_X.
\end{aligned}$$

As for the estimate $\|Q_2(s,u_1,u_2)\|_{L^p}$, we first note that taking $\epsilon = \frac{1}{p}$ we have

$$\begin{aligned}
\|e^{(\Delta-1)(t-\tau)}\left[\nabla(u_1\cdot\nabla u_2)\right]\|_{L^p}d\tau &\leq \int_0^t (t-\tau)^{-\frac{1}{2}-(\frac{1+\epsilon}{2}-\frac{1}{p})}\|u_1\cdot\nabla u_2\|_{L^{\frac{2}{1+\epsilon}}}d\tau \\
&\leq \int_0^t (t-\tau)^{-\frac{1}{2}-(\frac{1+\epsilon}{2}-\frac{1}{p})}\|u_1\|_{L^{2p}}\|\nabla u_2\|_{L^2}d\tau.
\end{aligned}$$

Then, by Sobolev as well as the Gagliardo-Nirenberg inequalities

$$\|u_1\|_{L^{2p}} \leq \|(-\Delta)^{\frac{p-1}{2p}}u_1\|_{L^2} \leq \|u_1\|_{L^2}^{\frac{1}{p}}\|\nabla u_1\|_{L^2}^{\frac{p-1}{p}} \leq C\|u_1\|_{L^2} + C\|\nabla u_1\|_{L^2}. \tag{5.14}$$

Hence

$$\begin{aligned}
&\|Q_2(s,u_1,u_2)\|_{L^p} \leq \int_0^t \|e^{(\Delta-1)(t-\tau)}\left[\nabla(u_1\cdot\nabla u_2)\right]\|_{L^p}d\tau + \int_0^t \|e^{(\Delta-1)(t-\tau)}[u_1 s]\|_{L^p}d\tau \\
&+ \int_0^t \|e^{\Delta(t-\tau)}[u_1u_2]\|_{L^p}d\tau \leq \int_0^t (t-\tau)^{-\frac{1}{2}-(\frac{1+\epsilon}{2}-\frac{1}{p})}\left[\left(\|u_1\|_{L^2} + \|\nabla u_1\|_{L^2}\right)\|\nabla u_2\|_{L^2}\right]d\tau \\
&+ \int_0^t (t-\tau)^{-(\frac{2}{p}-\frac{1}{p})}\left[\|s\|_{L^p}\|u_1\|_{L^p} + \|u_1\|_{L^p}\|u_2\|_{L^p}\right]d\tau \\
&\leq T^{\frac{1}{2p}}\left[\sup_{0\leq t\leq T}\|u_1\|_X \sup_{0\leq t\leq T}\|u_2\|_X\right] + T^{1-\frac{1}{p}}\left[\sup_{0\leq t\leq T}\|s\|_X + \sup_{0\leq t\leq T}\|u_2\|_X\right]\sup_{0\leq t\leq T}\|u_1\|_X.
\end{aligned}$$

Moreover,

$$\begin{aligned}
\|Q_3(s,u_1,u_2)\|_{L^p} &\leq \int_0^t \|e^{(\Delta-1)(t-\tau)}[u_2 s]\|_{L^p}d\tau + \int_0^t \|e^{(\Delta-1)(t-\tau)}[u_1u_2]\|_{L^p}d\tau \\
&\leq \int_0^t (t-\tau)^{-(\frac{2}{p}-\frac{1}{p})}e^{-(t-\tau)}\left[\|s\|_{L^p}\|u_2\|_{L^p} + \|u_1\|_{L^p}\|u_2\|_{L^p}\right]d\tau \\
&\leq T^{1-\frac{1}{p}}\left[\sup_{0\leq t\leq T}\|s\|_X + \sup_{0\leq t\leq T}\|u_1\|_X\right]\sup_{0\leq t\leq T}\|u_2\|_X.
\end{aligned}$$

5.3.2 Estimates in L^2 norms

A part of the argument is happening in the space of H^r, and therefore there should be some estimates in L^2. The L^2 estimates are already available through the estimates in L^p spaces (presented above) by taking $p = 2$ in the previous section. So

we have

$$\begin{aligned}
\|Q_1(s,u_1,u_2)\|_{L^2} &\leq T^{\frac{1}{2}}\Big[\sup_{0\leq t\leq T}\|s\|_X+\sup_{0\leq t\leq T}\|u_1\|_X\Big]\sup_{0\leq t\leq T}\|u_2\|_X,\\
\|Q_2(s,u_1,u_2)\|_{L^2} &\leq T^{\frac{1}{4}}\Big[\sup_{0\leq t\leq T}\|u_1\|_X\sup_{0\leq t\leq T}\|u_2\|_X\Big]\\
&+ T^{\frac{1}{2}}\Big[\sup_{0\leq t\leq T}\|s\|_X+\sup_{0\leq t\leq T}\|u_2\|_X\Big]\sup_{0\leq t\leq T}\|u_1\|_X,\\
\|Q_3(s,u_1,u_2)\|_{L^2} &\leq T^{\frac{1}{2}}\Big[\sup_{0\leq t\leq T}\|s\|_X+\sup_{0\leq t\leq T}\|u_1\|_X\Big]\sup_{0\leq t\leq T}\|u_2\|_X.
\end{aligned}$$

5.3.3 Estimates in $\dot{H}^r$ norms

$$\begin{aligned}
&\|Q_1(s,u_1,u_2)\|_{\dot{H}^r}\leq\Big\|\int_0^t(-\Delta)^{\frac{r}{2}}e^{(\Delta+1)(t-\tau)}[s^2]d\tau\Big\|_{L^2}\\
&+\Big\|\int_0^t(-\Delta)^{\frac{r}{2}}e^{(\Delta+1)(t-\tau)}[u_1s]d\tau\Big\|_{L^2}+\Big\|\int_0^t(-\Delta)^{\frac{r}{2}}e^{(\Delta+1)(t-\tau)}[u_2s]d\tau\Big\|_{L^2}\\
&\leq\int_0^t(t-\tau)^{-(1-\frac{1}{2})}\|(-\Delta)^{\frac{r}{2}}s\|_{L^2}\|s\|_{L^2}d\tau\\
&+\int_0^t(t-\tau)^{-(1-\frac{1}{2})}e^{t-\tau}\Big[\|(-\Delta)^{\frac{r}{2}}s\|_{L^2}\|u_1\|_{L^2}+\|s\|_{L^2}\|(-\Delta)^{\frac{r}{2}}u_1\|_{L^2}\Big]d\tau\\
&+\int_0^t(t-\tau)^{-(1-\frac{1}{2})}e^{t-\tau}\Big[\|(-\Delta)^{\frac{r}{2}}s\|_{L^2}\|u_2\|_{L^2}+\|s\|_{L^2}\|(-\Delta)^{\frac{r}{2}}u_2\|_{L^2}\Big]d\tau\\
&\leq CeT^{\frac{1}{2}}\Big[\sup_{0\leq t\leq T}\|s\|_X+\sup_{0\leq t\leq T}\|u_1\|_X+\sup_{0\leq t\leq T}\|u_2\|_X\Big]\sup_{0\leq t\leq T}\|s\|_X.
\end{aligned}\tag{5.15}$$

Above we used the para product estimate, for any $z\geq 0$ and $\frac{1}{p}=\frac{1}{p_1}+\frac{1}{q_1}=\frac{1}{p_2}+\frac{1}{q_2}$,

$$\|(-\Delta)^{\frac{z}{2}}(fg)\|_{L^p}\leq\|(-\Delta)^{\frac{z}{2}}f\|_{L^{p_1}}\|g\|_{L^{q_1}}+\|f\|_{L^{p_2}}\|(-\Delta)^{\frac{z}{2}}g\|_{L^{q_2}}.$$

Also,

$$\begin{aligned}
&\|Q_2(s,u_1,u_2)\|_{\dot{H}^r}\leq\int_0^t\|(-\Delta)^{\frac{r}{2}}e^{(\Delta-1)(t-\tau)}[\nabla\cdot(u_1\nabla u_2)]\|_{L^2}d\tau\\
&+\int_0^t\|(-\Delta)^{\frac{r}{2}}e^{(\Delta-1)(t-\tau)}[u_1s]\|_{L^2}d\tau+\int_0^t\|e^{\Delta(t-\tau)}[u_1u_2]\|_{L^2}d\tau\\
&\leq\int_0^t(t-\tau)^{-\frac{1}{2}-(\frac{3}{4}-\frac{1}{2})}\big[\|(-\Delta)^{\frac{r-1}{2}}u_1\|_{L^4}\|\nabla u_2\|_{L^2}+\|u_1\|_{L^4}\|(-\Delta)^{\frac{r}{2}}u_2\|_{L^2}\big]d\tau\\
&+\int_0^t(t-\tau)^{-(1-\frac{1}{2})}\Big[\|(-\Delta)^{\frac{r}{2}}s\|_{L^2}\|u_1\|_{L^2}+\|(-\Delta)^{\frac{r}{2}}u_1\|_{L^2}\|s\|_{L^2}\Big]d\tau\\
&+\int_0^t(t-\tau)^{-(1-\frac{1}{2})}\Big[\|(-\Delta)^{\frac{r}{2}}u_2\|_{L^2}\|u_1\|_{L^2}+\|(-\Delta)^{\frac{r}{2}}u_1\|_{L^2}\|u_2\|_{L^2}\Big]d\tau\\
&\leq T^{\frac{1}{4}}\Big[\sup_{0\leq t\leq T}\|u_1\|_X\sup_{0\leq t\leq T}\|u_2\|_X\Big]+T^{\frac{1}{2}}\Big[\sup_{0\leq t\leq T}\|s\|_X+\sup_{0\leq t\leq T}\|u_2\|_X\Big]\sup_{0\leq t\leq T}\|u_1\|_X.
\end{aligned}\tag{5.16}$$

Above, similar to (5.14), we made use of the Sobolev and Gagliardo-Nirenberg inequalities.

Moreover, similar to calculation for $\|Q_1(s, u_1, u_2)\|_{H^r}$

$$\|Q_3(s, u_1, u_2)\|_{\dot{H}^r} \leq T^{\frac{1}{2}} \left[\sup_{0\leq t\leq T} \|s\|_X + \sup_{0\leq t\leq T} \|u_1\|_X \right] \sup_{0\leq t\leq T} \|u_2\|_X.$$

5.3.4 Continuity of Q_1, Q_2 and Q_3

It is not difficult to follow the estimates in the previous sections and show the following estimates

$$\begin{aligned}
&\|Q_1(s, u_1, u_2) - Q_1(\tilde{s}, \tilde{u_1}, \tilde{u_2})\|_X \leq T\|u_2 - \tilde{u_2}\|_X \\
&+ \left[T^{\frac{1}{2}} + T^{1-\frac{1}{p}}\right] \left[\sup_{0\leq t\leq T} \|(s, u_1, u_2)\|_X + \sup_{0\leq t\leq T} \|(\tilde{s}, \tilde{u_1}, \tilde{u_2})\|_X \right] \\
&\left[\sup_{0\leq t\leq T} \|(s, u_1, u_2) - (\tilde{s}, \tilde{u_1}, \tilde{u_2})\|_X \right] \|Q_2(s, u_1, u_2) - Q_2(\tilde{s}, \tilde{u_1}, \tilde{u_2})\|_X \leq T \sup_{0\leq t\leq T} \|u_1 - \tilde{u_1}\|_X \\
&+ \left[T^{\frac{1}{4}} + T^{\frac{1}{2p}}\right] \left[\sup_{0\leq t\leq T} \|(s, u_1, u_2)\|_X + \sup_{0\leq t\leq T} \|(\tilde{s}, \tilde{u_1}, \tilde{u_2})\|_X \right] \\
&\left[\sup_{0\leq t\leq T} \|(s, u_1, u_2) - (\tilde{s}, \tilde{u_1}, \tilde{u_2})\|_X \right] + \left[T^{\frac{3}{4}} + T^{1-\frac{1}{2p}}\right] \left[\sup_{0\leq t\leq T} \|(s, u_1, u_2)\|_X + \right. \\
&\left. \sup_{0\leq t\leq T} \|(\tilde{s}, \tilde{u_1}, \tilde{u_2})\|_X \right] \left[\sup_{0\leq t\leq T} \|(s, u_1, u_2) - (\tilde{s}, \tilde{u_1}, \tilde{u_2})\|_X \right] \|Q_3(s, u_1, u_2) - Q_3(\tilde{s}, \tilde{u_1}, \tilde{u_2})\|_X \\
&\leq T\|u_2 - \tilde{u_2}\|_X + \left[T^{\frac{1}{2}} + T^{1-\frac{1}{p}}\right] \left[\sup_{0\leq t\leq T} \|(s, u_1, u_2)\|_X + \sup_{0\leq t\leq T} \|(\tilde{s}, \tilde{u_1}, \tilde{u_2})\|_X \right] \\
&\left[\sup_{0\leq t\leq T} \|(s, u_1, u_2) - (\tilde{s}, \tilde{u_1}, \tilde{u_2})\|_X \right].
\end{aligned} \tag{5.17}$$

Noting that $T < 1$, the appropriate estimates hold for the differences, whence the integral equations provide a contraction mapping in the space $\mathbb{Y}$, provided

$$T < \left[2Ce \sup_{0\leq t\leq T} \|(s^0, u_1^0, u_2^0)\|_X + 2Ce \sup_{0\leq t\leq T} \|(\tilde{s}^0, \tilde{u_1}^0, \tilde{u_2}^0)\|_X \right]^{-4}, \tag{5.18}$$

Therefore, the non-linear map given by (5.1.2) has a fixed point (s, u_1, u_2) in the space X, hence the existence of local solutions. □

5.4 Global Existence of the solutions (s, u_1, u_2) in the space of $L^p \cap H^r$

In this section we show that system of equations (5.1) admit strong global solutions in the space of $L^p \cap H^r$, $p \geq 2, r \geq 1$. The proof follows bootstraping process. We start by showing that given any $p \geq 2$, the solutions (s, u_1, u_2) have aprior estimates in these stimates, and the blow up is not happening at any given finite time. We then proceed and present similar conclusion for Hilbert spaces H^r, $r \geq 1$.

5.4.1 *Apriori* bounds in L^p spaces

We start by showing that the function $s(t,x)$ remains in any L^p spaces $2 \leq p \leq \infty$.

Lemma 5.4.1 *Let $2 \leq p \leq \infty$ and $T > 0$. Then for any $t \in [0,T]$ there exists $C = C(\|s_0(t)\|)$ so that*

$$\sup_{0\leq t\leq T} \|s(t,\cdot)\|_{L^p}^p + \int_0^t \|\partial[s^{\frac{p}{2}}]\|_{L^2}^2 d\tau \leq \|s_0\|_{L^p}^p e^t. \tag{5.19}$$

Proof We assume that $p = 2n$, and multiply both sides of the first equation of (5.1) in $s|s|^{p-2} = s^{p-1}$

$$\frac{1}{p}\partial_t \|s\|_{L^p}^p - \int (\Delta s) s^{p-1} dx + \|s\|_{L^{p+1}}^{p+1} + \int u_1 s^p dx + \int u_2 s^p dx = \|s\|_{L^p}^p,$$

where we moved the positive terms to the left hand side. Then (with some abuse of notations)

$$-\int (\Delta s) s^{p-1} dx = \int (\nabla s)^2 s^{\frac{p-2}{2}} = \|\nabla[s^{\frac{p}{2}}]\|_{L^2}^2.$$

We drop some of the positive terms in the left hand side and rewrite the energy estimate in the form of

$$\frac{1}{p}\partial_t \|s\|_{L^p}^p + \|\nabla[s^{\frac{p}{2}}]\|_{L^2}^2 \leq \|s\|_{L^p}^p,$$

The Granwall's inequality results in

$$\|s\|_{L^p}^p + \int_0^t \|\partial[s^{\frac{p}{2}}]\|_{L^2}^2 d\tau \leq \|s_0\|_{L^p}^p e^t.$$

The bounds for the L^p estimates, $p \neq 2n$ is available by interpolation and the L^∞ norm is achieved in the limiting case, as we let $p \to \infty$. □

Our next attempt is to prove similar bounds for the u_1 and u_2. The presence of the term $\nabla \cdot [u_1 \nabla u_2]$ in the second equation of (5.1) as well as $u_1 u_2$ with positive coefficient in third equation make it difficult to conclude the desired estimates. However, by adding the positivity condition on the initial value of ∇u_1^0 and ∇u_2^0 we get the desired result.

Lemma 5.4.2 *assume $T > 0$, and $2 \leq p \leq \infty$. Then for any $t \in [0,T]$ there exists $C = C(\|s_0(t)\|_{L^\infty}, \|u_1^0\|_{L^2})$ so that*

$$\sup_{0\leq t\leq T} \|u_1(t,\cdot)\|_{L^p}^p + \int_0^t \|\nabla[u_1^{\frac{p}{2}}]\|_{L^2}^2 d\tau \leq \|u_1^0\|_{L^p}^p e^{(\|s_0\|_{L^\infty}-1)t}. \tag{5.20}$$

Proof We assume $p = 2n$ and we find the inner product of the second equation in (5.1) with u_1^{p-1}

$$\begin{aligned} \frac{1}{p}\partial_t \|u_1\|_{L^2}^2 \quad - \quad & \int \Delta u_1 u_1^{p-1} dx + \|u_1\|_{L^p}^p + \int u_1^p u_2 dx \\ = \quad & \int \nabla \cdot (u_1 \nabla u_2) u_1^{p-1} dx + \int u_1^p s dx, \end{aligned}$$

$$\int \nabla \cdot (u_1 \nabla u_2) u_1 dx = -\int u_1^{p-1} \nabla u_2 \cdot \nabla u_1 dx \leq 0.$$

We also have

$$\left| \int s u_1^p dx \right| \leq \|s\|_{L^\infty} \|u_1\|_{L^p}^p \leq \|s_0\|_{L^\infty} \|u_1\|_{L^p}^p.$$

Then, since $-\int \Delta u_1 u_1^{p-1} dx = \int (\nabla u_1)^2 u_1^{p-2} dx = \|\nabla [u_1^{\frac{p}{2}}]\|_{L^2}^2$, we have

$$\frac{1}{2}\partial_t \|u_1\|_{L^p}^p + (1 - \|s_0\|_{L^\infty}) \|u_1\|_{L^p}^p + \|\nabla [u_1^{\frac{p}{2}}]\|_{L^2}^2 \leq 0, x$$

where we dropped positive term in the left hand side of the inequality. We then make use of the Granwall's inequality, which finishes the proof. The case L^∞ is available in the limiting case of $p \to \infty$, and L^p estimates, $p \neq 2n$, are available via interpolation between L^p norms, $p = 2n$. □

Similar argument leads to L^p bounds on the $u_2(t, x)$.

Lemma 5.4.3 *assume $T > 0$, and $2 \leq p \leq \infty$. Then for any $t \in [0, T]$ there exists C, C_1 and C_2 all depend on $\|s_0(t)\|_{L^\infty}$ and $\|u_2^0\|_{L^2}$, so that*

$$\sup_{0 \leq t \leq T} \|u_2(t, \cdot)\|_{L^p}^p + \int_0^t \|\nabla [u_2^{\frac{p}{2}}]\|_{L^2}^2 d\tau \leq C \|u_2^0\|_{L^p}^p e^{C\left(\|s_0\|_{L^\infty}, \|u_1^0\|_{L^\infty}\right) t}. \tag{5.21}$$

Proof We first find the inner product of the second equation in (5.1) with u_2^{p-1}

$$\frac{1}{p}\partial_t \|u_2\|_{L^p}^p - \int \Delta u_2 u_2^{p-1} dx + \|u_2\|_{L^p}^p = \int u_2^p s dx + \int u_2^p u_1 dx.$$

The right hand side of the equality is controlled as follows

$$\left| \int (s + u_1) u_2^p dx \right| \leq \left(\|s\|_{L^\infty} + \|u_1\|_{L^\infty}\right) \|u_2\|_{L^p}^p \leq C\left(\|s_0\|_{L^\infty}, \|u_1^0\|_{L^\infty}\right) \|u_2\|_{L^p}^p.$$

where we used the estimates in lemmas 5.4.2 and 5.4.3 with $p = \infty$. Then, considering the relation $-\int \Delta u_2 u^{p-1} dx = \|\nabla [u_1^{\frac{p}{2}}]\|_{L^2}^2$, we have

$$\frac{1}{2}\partial_t \|u_2\|_{L^p}^p + C_1\left(\|s_0\|_{L^\infty}, \|u_1^0\|_{L^\infty}\right) \|u_2\|_{L^p}^p + \|\nabla [u_2^{\frac{p}{2}}]\|_{L^2}^2 \leq 0.$$

We then make use of the Granwall's inequality, which finishes the proof. The case L^∞ is available in the limiting case of $p \to \infty$, and L^p estimates, $p \neq 2n$, are available via interpolation. □

5.4.2 *Apriori* bounds in Sobolev spaces

Our next attempt is to derive some upper bounds of the solutions in Sobolev spaces. We show that, given initial values in H^r, the solution s, u_1 and u_2 remain in in such spaces and the upper bounds are only depend on the initial values in the corresponding Sobolev spaces. With the L^p bounds (presented in the section 5.4) the proofs are quite straightforward, but here we bring them in details anyways.

Lemma 5.4.4 *Assume $T > 0$ is fixed and let $s_0 \in H^1$. Then for any $t \in [0, T]$ there exists $C = C(\|(s_0(t), u_1^0, u_2^0)\|_{L^\infty}, \|s_0(t)\|_{H^1})$ so that*

$$\sup_{0 \leq t \leq T} \|\partial s(t, \cdot)\|_{L^2}^2 + \int_0^t \|\Lambda^2 s\|_{L^2}^2 d\tau \leq \|s_0\|_{H^1}^2 e^t. \tag{5.22}$$

Proof We take ∂ derivative of the the first equation in (5.1) and find its inner product with ∂s. This leads to the energy estimates

$$\frac{1}{2}\partial_t\|\partial s\|_{L^2}^2 - \int(\partial\Delta s)\partial s dx = \|\partial s\|_{L^2}^2 + \int(\partial u_1 + \partial u_2)s\partial s dx + \int(u_1+u_2)(\partial s)^2 dx.$$

Then (with some abuse of notations)

$$-\int(\partial s)\partial s dx = \|\Lambda^2 s\|_{L^2}^2.$$

where we use the notation $\Lambda^2 = \nabla\partial$. The terms on the right hand side of the energy estimates are controlled as follows.

$$\begin{aligned}\int(\partial u_1 + \partial u_2)s\partial s dx &\leq C\|s\|_{L^\infty}\big(\|\partial u_1\|_{L^2} + \|\partial u_2\|_{L^2}\big)\|\partial s\|_{L^2}\\ &\leq \|\partial s\|_{L^2}^2 + C\|s\|_{L^\infty}^2\big(\|\partial u_1\|_{L^2}^2 + \|\partial u_2\|_{L^2}^2\big)\\ &\leq \|\partial s\|_{L^2}^2 + C\|s^0\|_{L^\infty}^2\big(\|\partial u_1\|_{L^2}^2 + \|\partial u_2\|_{L^2}^2\big)\\ &\leq \|\partial s\|_{L^2}^2 + C\|s^0\|_{L^\infty}^2\big(\|\partial u_1\|_{L^2}^2 + \|\partial u_2\|_{L^2}^2\big).\end{aligned}$$

In addition,

$$\begin{aligned}\int(u_1+u_2)(\partial s)dx &\leq C\big(\|u_1\|_{L^\infty} + \|u_2\|_{L^\infty}\big)\|\partial s\|_{L^4}^2\\ &\leq \big(\|u_1^0\|_{L^\infty} + \|u_2^0\|_{L^\infty}\big)\|\Lambda^{\frac{3}{2}}s\|_{L^2}^2\\ &\leq \big(\|u_1^0\|_{L^\infty} + \|u_2^0\|_{L^\infty}\big)\|s\|_{L^2}\|\Lambda^2 s\|_{L^2}\\ &\leq \frac{1}{100}\|\Lambda^2 s\|_{L^2} + C\|s^0\|_{L^2}^2\big(\|u_1^0\|_{L^\infty} + \|u_2^0\|_{L^\infty}\big)^2.\end{aligned}$$

$$\begin{aligned}\frac{1}{2}\partial_t\|\partial s\|_{L^2}^2 + C\|\Lambda^2 s\|_{L^2}^2 - \|\partial s\|_{L^2}^2 \leq{}& C\|s_0\|_{L^2}^2\big(\|u_1^0\|_{L^\infty} + \|u_2^0\|_{L^\infty}\big)^2\\ &+C\|s^0\|_{L^\infty}^2\big(\|\partial u_1\|_{L^2}^2 + \|\partial u_2\|_{L^2}^2\big).\end{aligned}$$

The Granwall's inequality completes the proof. Note that we used the fact that, from lemmas 5.4.2 and 5.4.3,

$$\int_0^t\big(\|\partial u_1\|_{L^2}^2 + \|\partial u_2\|_{L^2}^2\big)dt \leq C\big(\|u_1^0\|_{L^2}^2 + \|u_2^0\|_{L^2}^2\big)e^{Ct}.$$

□

We next prove the control on H^1 norm of the u_2. Note that, the presence of the term $\nabla\cdot[u_1\nabla u_2]$ does not allow similar result for $u_1(t,x)$. However, after establishing the $\|u_2\|_{H^1}$, we can treat this term.

Lemma 5.4.5 *Assume $T>0$ is fixed. Then for any $t\in[0,T]$ there exists $C = C(\|s_0\|_{H^1}, \|u_1^0\|_{L^2}, \|u_2^0\|_{L^2})$ so that*

$$\sup_{0\leq t\leq T}\|\partial u_2(t,\cdot)\|_{L^2}^2 + \int_0^t\|\Lambda^2 u_2\|_{L^2}^2 d\tau \leq Ce^t. \tag{5.23}$$

Proof We first find the inner product of the second equation in (5.1) with u_2^{p-1}

$$\frac{1}{p}\partial_t\|\partial u_2\|_{L^2}^2 - \int \Delta\partial u_2 \partial u_2 dx + \|\partial u_2\|_{L^2}^2 = \int (\partial u_2)^2(s+u_1)dx + \int u_2\partial u_2\,(\partial s + \partial u_1)dx,$$

The right hand side of the equality is controlled as follows

$$\Big|\int (\partial u_2)^2(s+u_1)dx\Big| \le \big(\|s\|_{L^\infty} + \|u_1\|_{L^\infty}\big)\|\partial u_2\|_{L^2}^2 \le C\big(\|s_0\|_{L^\infty}, \|u_1^0\|_{L^\infty}\big)\|\partial u_2\|_{L^2}^2,$$

and

$$\begin{aligned}\Big|\int u_2(\partial u_2)(\partial s + \partial u_1)dx\Big| &\le \|u_2\|_{L^\infty}\big(\|\partial s\|_{L^2} + \|\partial u_1\|_{L^2}\big)\|\partial u_2\|_{L^2} \\ &\le C\|\partial u_2\|_{L^2}^2 + C\big(\|\partial s\|_{L^2}^2 + \|\partial u_1\|_{L^2}^2\big)\|u_2^0\|_{L^\infty}^2.\end{aligned}$$

Then, considering the relation $-\int \Delta\partial u_2\partial u_2 dx = \|\nabla\partial u_2\|_{L^2}^2 = \|\Lambda^2 u_2\|_{L^2}^2$, we have

$$\frac{1}{p}\partial_t\|\partial u_2\|_{L^2}^2 + \|\Lambda^2 u_2\|_{L^2}^2 - C\|\partial u_2\|_{L^2}^2 \le C\big(\|\partial s\|_{L^2}^2 + \|\partial u_1\|_{L^2}^2\big)\|u_2^0\|_{L^\infty}^2.$$

In order to finish the proof, we then take the integral and use the fact that, from lemma 5.4.2,

$$\int_0^t \|\partial u_1\|_{L^2}^2 d\tau \le Ce^t.$$

□

We are now ready to prove similar H^1 bounds for the function $u_1(t,x)$.

Lemma 5.4.6 *Assume $T > 0$ is fixed. Then for any $t \in [0,T]$ there exists a constant $C = C(\|s_0(t)\|_{H^1\cap L^\infty}, \|u_1^0\|_{H^1}, \|u_2^0\|_{H^1\cap L^\infty})$ so that*

$$\sup_{0\le t\le T}\|\partial u_1(t,\cdot)\|_{L^2}^2 + \int_0^t \|\Lambda^2 u_1\|_{L^2}^2 d\tau \le Ce^{2t}. \tag{5.24}$$

Proof We take the ∂ derivative of the second equation in (5.1) and find its inner product with ∂u_1

$$\begin{aligned}\frac{1}{2}\partial_t\|\partial u_1\|_{L^2}^2 \quad &- \int(\Delta\partial u_1)\partial u_1 dx + \|\partial u_1\|_{L^2}^2 = \int \nabla\cdot\partial(u_1\nabla u_2)\partial u_1 dx \\ &+ \int(\partial u_1)^2(s-u_2)dx + \int(\partial s - \partial u_2)u_1\partial u_1 dx,\end{aligned}$$

We control the terms on the right hand side as it follows.

$$\begin{aligned}\Big|\int \nabla\cdot\partial(u_1\nabla u_2)\partial u_1 dx\Big| &= \Big|\int \partial(u_1\nabla u_2)\cdot\nabla\partial u_1 dx\Big| \le \|\Lambda^2 u_1\|_{L^2}\|\partial(u_1\nabla u_2)\|_{L^2} \\ &\le \|\Lambda^2 u_1\|_{L^2}\|\partial\nabla u_2\|_{L^2}\|u_1\|_{L^\infty} + \|\Lambda^2 u_1\|_{L^2}\|\partial u_1\|_{L^4}\|\nabla u_2\|_{L^4} \\ &\le \|\Lambda^2 u_1\|_{L^2}\|\partial\nabla u_2\|_{L^2}\|u_1\|_{L^\infty} + \|\Lambda^2 u_1\|_{L^2}\|u_1\|_{L^\infty}^{\frac12}\|\nabla\partial u_1\|_{L^2}^{\frac12}\|u_2\|_{L^\infty}^{\frac12}\|\nabla\partial u_2\|_{L^2}^{\frac12} \\ &\le \frac{1}{100}\|\Lambda^2 u_1\|_{L^2}^2 + C\Big(\|u_1\|_{L^\infty} + \|u_1\|_{L^\infty}\|u_2\|_{L^\infty}\Big)\|\nabla\partial u_2\|_{L^2}^2 \\ &\le \frac{1}{100}\|\Lambda^2 u_1\|_{L^2}^2 + C\Big(\|u_1^0\|_{L^\infty} + \|u_1^0\|_{L^\infty}\|u_2^0\|_{L^\infty}\Big)\|\nabla\partial u_2\|_{L^2}^2,\end{aligned} \tag{5.25}$$

Where we made use of the Gagliardo-Nirenberg inequality to make use of the bounds in lemma 5.4.5.

$$\|\partial u_1\|_{L^4} \leq \|\Lambda^2 u_1\|_{L^2}^{\frac{1}{2}} \|u_1\|_{L^\infty}^{\frac{1}{2}},$$

and similar bound for $\|\partial u_2\|_{L^4}$. We also have

$$\left| \int (\partial u_1)^2 (s - u_2) dx \right| \leq \left(\|s\|_{\|_{L^\infty}} \|u_2\|_{L^\infty} \right) \|\partial u_1\|_{L^2}^2 \leq \left(\|u_2^0\|_{L^\infty} + \|s_0\|_{L^\infty} \right) \|\partial u_1\|_{L^2}^2.$$

Moreover,

$$\begin{aligned} \left| \int (\partial s - \partial u_2) u_1 \partial u_1 dx \right| &\leq \|u_1\|_{L^\infty} \left(\|\partial s\|_{L^2} + \|\partial u_2\|_{L^2} \right) \|\partial u_1\|_{L^2} \\ &\leq \|\partial u_1\|_{L^2}^2 + \|u_1^0\|_{L^\infty}^2 \left(\|\partial s\|_{L^2}^2 + \|\partial u_2\|_{L^2}^2 \right), \end{aligned}$$

Then, since $-\int (\Delta \partial u_1) \partial u_1 dx = \|\Lambda^2 u_1\|_{L^2}^2$, we have

$$\frac{1}{2} \partial_t \|\partial u_1\|_{L^2}^2 + C \|\Lambda^2 u_1\|_{L^2}^2 \leq C \|\partial u_1\|_{L^2}^2 + C \|\Lambda^2 u_2\|_{L^2}^2. \tag{5.26}$$

We then take the integral and finish the argument. Note that, by lemma 5.4.5,

$$\int_0^t \|\Lambda^2 u_2\|_{L^2}^2 ds \leq C e^t,$$

and hence we can control the right hand side of (5.26). □

Remark 5.4.1 *The process of getting the H^1 norm in lemmas (5.4.4), 5.4.6 and 5.4.6 is easily applies recursively. In the next step, one can follow same process and use the result in these three lemmas to achieve the H^2 bounds, and the process goes on. Therefore, the bounds are available for any H^r space, $r \geq 0$, non integer r, are achieved via interpolation). Hence the following lemma is proved.*

Lemma 5.4.7 *Assume $T > 0$ is fixed and $r \geq 0$. Then there is a constant $C = C(t, \|(s^0, u_1^0, u_2^0)\|_{H^r \cap L^\infty})$ so that for any $t \in [0, T]$*

$$\sup_{0 \leq t \leq T} \left(\|s\|_{H^r} + \|u_1\|_{H^r} + \|u_2\|_{H^r} \right) + \int_0^t \left(\|s\|_{H^{r+1}} + \|u_1\|_{H^{r+1}} + \|u_2\|_{H^{r+1}} \right) dt \leq C \tag{5.27}$$

Remark 5.4.2 *Lemmas 5.4.3, 5.4.7 together states that the solutions (s, u_1, u_2) are not blowing up at any finite time $T > 0$. This observation guarantees that the solutions which were found locally (in section 5.3) are global in time.*

Conclusion

In this thesis generally two models of three species involved in ecology have been studied.

In the first model, we have presented a chemotaxis model of three species with intraguild predation (**IGP model**). We have investigated pattern formation and the existence of a global solution in 2D. Moreover, we have established a normal form of Turing-Hopf of the system. We perform chaotic behavior of **IGP Model** in the niche.

Further, stationary and oscillatory reaction-diffusion patterns, global in time solution of the model by rectangle invariant region method in the second model consist of two predators competing for one prey with Holling type II functional responses studied. We modified the model mentioned in (Ferreira, Silva, and Rao, 2019, Farkas, 1984).

In Chapter 2, we have proved **IGP Model** undergoes the Turing pattern due to the chemotaxis term. Some papers have mentioned a diffusive model of IG predation with Lotka- Volterra or Holling types. To the best of our knowledge, non of them investigated the formation of patterns due to chemotaxis. Therefore, this work is novel. We obtained instability regions and then proved necessary and sufficient conditions in which the system underlies Hopf, Turing, and Turing- Hopf instabilities. Roughly speaking, we have established chemotaxis parameter produces Turing instability. Also, the system oscillates in time due to Hopf bifurcation as the growth rate of IG predator concerning IG prey crosses its critical point. We have depicted that in the absence of self-diffusion of prey and IG predator, conditions do not ensure the formation of the Turing pattern. However, in the presence of one of the self-diffusion parameters, Turing patterns take place. We also demonstrated that if the death rate of prey concerning IG predator is zero, the system cannot perform Turing patterns. In addition, we have proved the necessary conditions in which the system undergoes or does not undergo Turing-Hopf instabilities.

We employed the spectral method to exhibit stationary Turing, time oscillations, chaotic, and spatiotemporal patterns. Moreover, a weakly nonlinear has been utilized to determine subcritical and supercritical Turing patterns. Our weakly nonlinear results are consistent with numerical simulations. We also have observed numerically that as the chemotaxis term increases, the system can transient from Turing patterns toward Turing-Hopf patterns. Indeed, a transition between different wave numbers can be predicted with linear analysis.

In addition, we have proved that wave instability cannot occur in this system in both the absence and presence of cross-diffusion parameter cases.

In Chapter 3, we have studied the normal form of **IGP Model**. Indeed, we employed a perturbation technique based on the multiple scales method to drive the normal form of **IGP Model**. Consequently, we have investigated the stationary solution of the reduced system. In particular, we have determined the regions in which Hopf, Turing, and Turing-Hopf occur, and then we have proved it numerically.

In Chapter 4, we have studied the model consisting of two predators competing for one prey with Holling type II functional response coupled with linear diffusion.

We have modified the model presented in (Ferreira, Silva, and Rao, 2019) and well-known reference (Farkas, 1984) to achieve a unique coexistence steady state instead of a line segment of stable equilibria. For this reason, we attached an intraspecific term to one of the predator's equations. In addition, we have supposed the strategy in which predators avoid each other. Thus, we have considered all self- and cross-diffusion parameters positive. Moreover, we performed linear analysis to determine the necessary condition of local stability and oscillation of the system due to the Hopf bifurcation parameter. We have then investigated Turing analysis for three different cases.

The first case states that the model does not undergo Turing instability in the absence of cross-diffusion parameters. While in two other cases (the presence of cross-diffusion parameters corresponding to predators and the presence of cross-diffusion parameters concerning predators and prey-predators), Turing patterns are formed. In particular, we have obtained the Turing region due to the positivity, stability, and Turing conditions of one case mentioned above.

Moreover, we have exhibited enhancement in which self- or cross-diffusion parameters increase or decrease the Turing region. We have numerically simulated Turing patterns. Then we applied the WNL method to determine the amplitude of patterns, and next, we compared them with numerical simulations. Indeed, we have used the finite element method equipped with $\theta - scheme$ and Lagrangian $\mathbb{P}_2$ polynomials. We next have surveyed the maximum growth rate of eigenvalues.

Finally, in this Chapter, we have established the global in time solution of the model by the invariant method in one case that the system contains only one cross-diffusion, which mentions the flux of the second predator in the opposite direction of the first predator, i.e., the second predator moves to the lower density of the first predator. To prove the global solution, first, we demonstrate that system admits a positive solution under positive initial values. Then according to the invariant method, we transformed the system into a diagonal one; next, by utilizing balance law and dissipativity conditions and providing a rectangle invariant region (described in the Chapter), we proved that system admits the global in time solutions.

In Chapter 5, we have studies the existence global solution of **IGP Model** in 2D. In order to prove that we followed two main steps. In the first step, we proved a time interval and space in which the solutions exist locally. Then we proved that in infinite time the solutions remain bounded. We proved that, under certain natural initial conditions, namely the positivity of the initial values s, u_1^0 and u_2^0, as well as the same sign condition on the gradients of u_1^0 and u_2^0 (i.e. $\nabla u_1^0 \cdot \nabla u_2^0 \geq 0$), the solutions exist globally in time in the spaces $L^p \cap H^r$, $r \geq 1$ and $2 \leq p \leq \infty$.

Finally, we suggest some open problems and directions for future work.

- Since in the **IGP Model**, the chemotaxis term $\nabla.(v\nabla w)$ is a subclass of cross-diffusion term $\nabla.(\nabla(vw))$. It would be intriguing to examine and compare the Turing region, stationary Turing, and oscillation of the model in time when both predators diffuse away from (or toward) the other specie's gradient.

- It would be interesting to study and exhibit the rich dynamics of both models mentioned in Chapters (4 and 2) theoretically and numerically in higher dimensions.

- Moreover, numerical and analytical investigation of Turing and Spatio-temporal patterns around diffusive degenerated Zip model with nonlinear cross-diffusion terms could also be of interest and challenging.

- In modified model (4.13), we applied the strategy which predators compete in different directions and avoid each other, therefore employing and comparing second strategy in which predators move toward prey in the same direction (cross- diffusion parameters corresponding to two predators are negative) could be considered.
- It would be the interest of applying finite element method for the model (4.13) in 2D and 3D in irregular domains.
- Finally, it would be of interest to work on the global solution of the **IGP Model** in a general case, and without considering any conditions on parameters or initial values.

Appendix A

Analysis of marginal stability of curve $F = 0$

In this Appendix we analyze the marginal stability curve $F = 0$, with F defined in (2.22), assuming $\alpha\eta \neq 0$. We have already proved that E^* is stable in all region $I(a)$, nevertheless, for the sake of completeness, we shall perform the analysis in all the plane (γ, δ). By substituting the coordinates of E^* given in (2.8), the function $F(\gamma, \delta)$ can be written as follows:

$$F(\gamma,\delta) = \frac{F_{s_u}(\gamma,\delta)(F_{s_v}(\gamma,\delta) + F_{s_w(\gamma,\delta)}) - F_s(\gamma,\delta)}{F_{s_d}^2}, \tag{A.1}$$

with:

$$\begin{aligned}
&F_{s_d}(\gamma,\delta) = (1+\alpha\eta)\delta - \gamma,\\
&F_{s_u}(\gamma,\delta) = \delta(1+n_1\eta) - n_2,\\
&F_{s_v}(\gamma,\delta) = \alpha(n_2(1+\alpha\eta) - \gamma(1+n_1\eta)),\\
&F_{s_w}(\gamma,\delta) = \gamma\eta((\alpha-n_1)\delta + n_1\gamma - \alpha n_2),\\
&F_s(\gamma,\delta) = [(\alpha-n_1)\delta + n_1\gamma - \alpha n_2](\alpha\delta\eta - \gamma)[n_2(1+\alpha\eta) - \gamma(1+n_1\eta)],
\end{aligned} \tag{A.2}$$

We first investigate the behavior of the function $F(\gamma, \delta)$ along the lines s_i, given in (2.12) and (2.23), and in regions I_2 and I_1, as depicted in Figure A.1.

By direct inspection, it is easy to check:
1. $F_{sd}(\gamma,\delta)|_{s_d} = 0$,
2. $F_{s_i}(\gamma,\delta)|_{s_i} = 0$, for $i = v, w$;
3. $F_s(\gamma,\delta)|_{s_i} = 0$ for $i = v, w, t$.

Moreover, using conditions (2.11)) it follows:
4. $F_{s_i}(\gamma,\delta)|_{s_5} > 0$, with $i = u, v, w$ in region I.
5. $F_{s_i}(\gamma,\delta)|_{s_3} > 0$, with $i = u, w$ in region I.
6. $F_{s_i}(\gamma,\delta)|_{s_4} > 0$, with $i = u, v$ in region I.
7. $F_{s_i}(\gamma,\delta) > 0$, with $i = u, v, w$ and $F_s(\gamma,\delta) < 0$, within region I_2.

By 2., 3., 5. and 6. it follows that:
8. $F(\gamma,\delta)|_{s_i} > 0$, with $i = v, w$.

By 3., 4. it follows that:
9.$F(\gamma,\delta)|_{s_t} > 0$.

Therefore, the curve $F(\gamma, \delta) = 0$ has the following properties:
P1. it is not defined on the line s_d, see 1.;
P2. it does not intersect the lines s_v and s_w see 8.;
P3. it does not intersect the line s_t, see 9.;
P4. no branches of the curve $F(\gamma, \delta) = 0$ stay within the region I_2, see 7.;

Moreover, in region I_1 the function $F(\gamma, \delta)$ attains either signs: it is positive along the

boundaries of the region, see 8. and 9. and also $F(\gamma, \delta)$ begin quadratic in δ, becomes negative when $\gamma \approx 0$ and $\delta \gg 1$.

Being $F(\gamma, \delta)$ a continuous function, it follows that:

P5. a branch of curve $F(\gamma, \delta) = 0$ lines in the region I_1.

In order to carry out an analytical study if $F(\gamma, \delta) = 0$, we rewrite F as follows:

$$F(\gamma, \delta) = \frac{A(\gamma)\delta^2 + B(\gamma)\delta + C(\gamma)}{F_{s_d}}, \tag{A.3}$$

where:

$$\begin{aligned}
&A(\gamma) = \eta(\alpha - n_1)((\alpha+1)(1+\eta n_1)\gamma - \alpha n_2(1+\alpha\eta)),\\
&B(\gamma) = \gamma^2(n_1(\eta+1)(1+\eta n_1) + \alpha(\eta^2 n_1^2 - 1))\\
&+ \gamma(-n_1 n_2 - \alpha + n_2\alpha + n_1 n_2\eta - 2(n_1 + n_2 + n_1 n_2)\alpha\eta - n_1\alpha(n_1 + n_2 + 2n_2\alpha)\eta^2)\\
&+ \alpha n_2(\alpha\eta + 1)(\alpha n_2\eta + \eta n_1 + 1),\\
&C(\gamma) = -\gamma^3 n_1(\eta n_1 + 1) + \gamma^2 n_2(n_1(2\alpha\eta - \eta + 1) + \alpha)
\end{aligned} \tag{A.4}$$

The roots of (A.3), given by the functions:

$$\delta^+(\gamma) = \frac{-B(\gamma) + \sqrt{B^2(\gamma) - 4A(\gamma)C(\gamma)}}{2A(\gamma)}, \text{ and } \delta^-(\gamma) = \frac{-B(\gamma) - \sqrt{B^2(\gamma) - 4A(\gamma)C(\gamma)}}{2A(\gamma)}, \tag{A.5}$$

are the branches of the curve $F(\gamma, \delta) = 0$.

The denominator $A(\gamma)$ of $\delta^\pm$ in (A) is zero at :

$$\gamma = \bar{\gamma} := \frac{\alpha}{\alpha+1}\frac{n_2(1+\alpha\eta)}{1+n_1\eta}, \tag{A.6}$$

In order to analyze the behavior of $\delta^\pm$ in a neighborhood of $\bar{\gamma}$, we must compute the following limits:

$$lim_{\gamma\to\bar{\gamma}^\pm}\delta^-, \quad lim_{\gamma\to\bar{\gamma}^\pm}\delta^+, \tag{A.7}$$

whose values depend on $B(\bar{\gamma})$, where

$$B(\bar{\gamma}) = \frac{\alpha n_2(1+\alpha\eta)((1+\alpha)(1+\eta n_1)^2 - n_2(\alpha - n_1)(\eta - 1))}{(1+\alpha)^2(1+\eta n_2)}, \tag{A.8}$$

Notice that $B(\bar{\gamma})$ is non zero unless

$$n_2 = \bar{n_1} := \frac{(1+\alpha)(1+\eta n_1)^2}{(\alpha - n_1)(1-\eta)}, \tag{A.9}$$

thus, when $n_2 \neq \bar{n_1}$, $B^2(\bar{\gamma}) - 4A(\bar{\gamma})C(\bar{\gamma}) = B^2(\bar{\gamma}) > 0$ and

$$\sqrt{B^2(\gamma) - 4A(\gamma)C(\gamma)},$$

is well defined in a neighborhood of $\bar{\gamma}$.

The polynomial $B(\bar{\gamma})$ is positive in the following two cases:

case 1: $\eta < 1$,

case 2: $\eta > 1$, $n_2 < \bar{n}_1$.
Both in *Case 1* and *Case 2*, the limits in (A.7) can be computed as follows:

$$\lim_{\gamma\to\bar{\gamma}^{\pm}} \delta^{-} = \lim_{\gamma\to\bar{\gamma}^{\pm}} \frac{-B(\bar{\gamma})}{A(\gamma)} = \pm\infty, \quad \lim_{\gamma\to\bar{\gamma}^{\pm}} \delta^{+} = \lim_{\gamma\to\bar{\gamma}^{\pm}} -\frac{2C(\gamma)}{B(\gamma)+\sqrt{B^2(\gamma)-4A(\gamma)C(\gamma)}} = -\frac{C(\bar{\gamma})}{B(\bar{\gamma})}, \tag{A.10}$$

where

$$-\frac{C(\bar{\gamma})}{B(\bar{\gamma})} = \frac{n_2((1+\alpha)^2(1+\eta n_1)^2) - \alpha(\eta-1)(1+\alpha+(\eta-1)n_1)n_2}{(1+\alpha)(1+\eta n_1)((1+\alpha)(1+\eta n_1)^2-(\eta-1)(\alpha-n_1)n_2)}, \tag{A.11}$$

From the first limit in (A.7), we observe that

$$s_a := \gamma = \bar{\gamma}, \tag{A.12}$$

is a vertical asymptotic for $\bar{\delta}$, which has at least two branches. Moreover, by Properties P2 and P4. of $F(\gamma,\delta) = 0$, one branch of $\bar{\delta}$ lies within region I_1, while the other one is outside region I From the second limit in (A.7), we see that the point $S \equiv (\gamma, \frac{\bar{C}(\bar{\gamma})}{B(\bar{\gamma})})$ is a removable discontinuity for δ^+. Since direct computations show that the point S lies below the line s_w in both *Case 1.* and *Case 2.*, then there is a branch of δ^+ outside region I (see Figure A.1A, Figure A.1B). Let us now analyze the behavior of $\delta^{\pm}$ in a neighborhood of $\bar{\gamma}$ when $B(\bar{\gamma}) < 0$, namely under the following constraints for the parameter.

Case 3. $\eta > 1$ and $n_2 > \bar{n}_2$:

$$\lim_{\gamma\to\bar{\gamma}^{\pm}} \delta^{-} = -\frac{2C(\gamma)}{B(\gamma)+\sqrt{B(\gamma)^2-4A(\gamma)C(\gamma)}} = -\frac{C(\bar{\gamma})}{B(\bar{\gamma})}, \quad \lim_{\gamma\to\bar{\gamma}^{\pm}} \delta^{+} = -\frac{B(\gamma)}{A(\gamma)} = \pm\infty, \tag{A.13}$$

where $-\frac{C(\bar{\gamma})}{B(\bar{\gamma})}$ is given in (A.11).

From the first limit in (A.13), we see that the point S is a removable discontinuity for δ^-. In *Case 3.* it is easy to check that the point S lies within I_1. Using Properties *P2* and *P4.* of $F(\gamma,\delta) = 0$, we can conclude that one branch of δ^- lies within region I_1 (see Figure A.1C).
From the second limit in (A.13), we observe that s_a is a vertical asymptotic for δ^+, which has at least two branches. Moreover, using again Properties P2 and P4. of $F(\gamma,\delta) = 0$, we observe that one branch of δ^+ lies within region I_1, while the other one is outside region I (see Figure A.1C).

Now, let us analyze $B^2(\gamma) - 4A(\gamma)C(\gamma) = \mathcal{P}_1(\gamma)\mathcal{P}_2(\gamma)$, where

$$\begin{aligned}
&\mathcal{P}_1 = (-\gamma(1+\eta n_1) + n_2(1+\alpha\eta))^2,\\
&\mathcal{P}_2 = \gamma^2(\alpha + n_1(\alpha\eta+\eta-1))^2\\
&+\gamma(-2\alpha(-\alpha+\alpha\eta n_2(\alpha+n_1(\alpha\eta+\eta-1)) + n_1(\eta+\eta n_1(\alpha\eta+\eta+1)+1)))\\
&+\alpha^2(2\eta n_1(n_2(\alpha\eta+2)+1) + (\alpha\eta n_2-1)^2 + \eta^2 n_1^2).
\end{aligned} \tag{A.14}$$

Notice that $\mathcal{P}_1(\gamma)$ is always nonnegative. Moreover, it is easy to check that $\mathcal{P}_1(\gamma_Q) = 0$, therefore the curves δ^+ and δ^- intersect at the point Q, given in (2.13). However, Q belongs to the line s_d, where the curve $F(\gamma,\delta) = 0$ is not defined. We

thus compute

$$\lim_{\gamma\to\gamma_Q^{\pm}} \delta^+ = \lim_{\gamma\to\gamma_Q^{\pm}} \delta^- = -\frac{B(\gamma_Q)}{2A(\gamma_Q)} = \delta_Q, \tag{A.15}$$

which means that the point Q is a removable discontinuity of $\delta^{\pm}$.
The discriminant of the polynomial $\mathcal{P}_2(\gamma)$ reads:

$$\Delta_{\mathcal{P}_2} = \alpha^2\eta n_1(\alpha - n_1)(n_2(\eta-1)(\alpha - n_1 + \eta(1+\alpha)n_1) - (\alpha+1)(\eta n_1+1)^2). \tag{A.16}$$

In *case 1.* $\Delta_{\mathcal{P}_2} < 0$, then $\mathcal{P}_2(\gamma)$ is always positive. Therefore, $B^2(\gamma) - 4A(\gamma)C(\gamma) > 0$ and $\delta^{\pm}(\gamma)$ are defined for all $\gamma \neq \bar{\gamma}$.

$\Delta_{\mathcal{P}_2}$ is zero at

$$n_2 = \bar{\bar{n}}_2 := \frac{(1+\alpha)(1+\eta n_1)^2}{(\alpha - n_1 + \eta(1+\alpha)n_1)(\eta-1)} < \bar{n}_2. \tag{A.17}$$

If the parameters are chosen as follows
case 2.1. $\eta > 1$ and $n_2 < \bar{\bar{n}}_2$
then, as in *Case 1.*, $\mathcal{P}_2(\gamma)$ is always positive. Therefore, $B^2(\gamma) - 4A(\gamma)C(\gamma) > 0$ and $\delta^{\pm}(\gamma)$ are defined for all $\gamma \neq \bar{\gamma}$. Choosing the parameters as in *Case 3.* or as follows:
case 2.2. $\eta > 1$ and $\bar{\bar{n}}_2 < n_2 < \bar{n}_2$ then $\mathcal{P}_2(\gamma)$ admits two roots;

$$\gamma_{\pm} = \frac{\alpha(-\alpha + \alpha\eta n_2(\alpha + n_1(\alpha\eta+\eta-1)) + n_1(\eta+\eta n_1(\alpha\eta+\eta+1)+1)) \pm \sqrt{\Delta_{\mathcal{P}_2}}}{(\alpha + n_1(\alpha\eta+\eta-1))^2}, \tag{A.18}$$

One can easily check that when $n_2 < \bar{\bar{n}}_2$ by the Cartesian rule of signs the two roots $\gamma_{1,2}$ are both positive. Therefore, $B^2(\gamma) - 4A(\gamma)C(\gamma) < 0$ for all $\gamma_- < \gamma < \gamma_+$ and in this range the curves $\delta^{\pm}$ are not defined. In particular:

$$\delta^+(\gamma_{\pm}) = \delta^-(\gamma_{\pm}) = -\frac{B(\gamma_{\pm})}{2A(\gamma_{\pm})}. \tag{A.19}$$

Lengthy but straightforward calculations show that $\bar{\gamma} < \gamma_- < \gamma_+ < \gamma_Q$.

From the properties P1-P5 of $F(\gamma,\delta) = 0$ and the above discussion on the branches $\delta^{\pm}$, we can conclude that there exists only one branch of the curve $F(\gamma,\delta) = 0$ lying on the region I_1. In particular, in *Case 1.* and *Case 2.1* it is the continuous branch of δ^- lying within I_1 (see Figure A.1A, where the parameters are chosen as in *Case 1.*, because *Case 2.1* is qualitatively equivalent). In *Case 2.2.*, the unique branch of $F(\gamma,\delta) = 0$ lying on the region I_1 is still given by the branch of the curve δ^- (see Figure A.1B). Finally, in *Case 3.* the unique branch of $F(\gamma,\delta) = 0$ lying on the region I_1 is given by the branch of the curve δ^- with a removable discontinuity in S, which is connected in γ_- with the continuous branch of δ^+ lying within I_1 (see Figure A.1C).

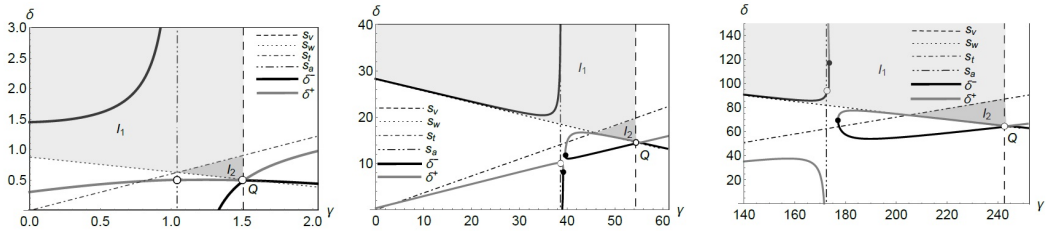

(A) (B) (C)

FIGURE A.1: Graph of the curve $F(\gamma, \delta) = 0$. (a) $B(\bar{\gamma}) > 0$ and $B^2(\gamma) - 4A(\gamma)C(\gamma) > 0$, which corresponds to *Case 1.* and *Case 2.1.* Here, the parameters are fixed as $n_1 = 0.5$, $n_2 = 0.7$, $\alpha = 2.5$, $\eta = 0.8$, $d_u = d = d_w = 0$, corresponding to *Case 1.*. (b) $B(\bar{\gamma}) > 0$ and $B^2(\gamma) - 4A(\gamma)C(\gamma) < 0$ when $\gamma_- < \gamma < \gamma_+$, where $\gamma_{1,2}$ are drawn in black dots. The parameters are fixed as $n_1 = 0.5$; $n_2 = 22.5$, $\alpha = 2.5$, $\eta = 1.1$, $d_u = d = d_w = 0$, which corresponds to *Case 2.2.*. (c) $B(\bar{\gamma}) > 0$ and $B^2(\gamma) - 4A(\gamma)C(\gamma) < 0$ when $\gamma_- < \gamma < \gamma_+$ where $\gamma_{1,2}$ are drawn in black dots. The parameters are fixed as $n_1 = 0.5$, $n_2 = 100$; $\alpha = 2.5$, $\eta = 1.1$, $d_u = d = d_w = 0$, which corresponds to *Case 3.*

Appendix B

Weakly nonlinear analysis

Here we continue calculation of **WNL** in higher orders.

B.1 Drivation of quintic- Stuart- Landau equation IGP system

Hence, the amplitude is considered with new time scale $A(T, T_1)$ as

$$t = \frac{T}{\varepsilon^2} + \frac{T_1}{\varepsilon^4} + \cdots,$$

and bifurcation parameter is expanded as

$$d = d_c + \varepsilon^2 d^{(2)} + \varepsilon^4 d^{(4)} + \cdots,$$

therefore $T = \varepsilon^2 t, T_1 = \varepsilon^4 t$ and consequently $\partial_t \to \partial_t + \varepsilon^2 \partial_T + \varepsilon^4 \partial_{T_1}$.
Since, at order three, the solution is given by

$$\mathbf{w}_3 = \mathbf{A}\mathbf{w}_{31}\cos(k_c x) + \mathbf{A}^3\mathbf{w}_{32}\cos(k_c x) + \mathbf{A}^3\mathbf{w}_{33}\cos(3k_c x)$$

, the terms $\mathbf{w}_{3i},\ i = 1, 2, 3$ can be determined by

$\mathbf{L}_1^{d_c}\mathbf{w}_{31} = \sigma\rho + \mathbf{G}_1^{(1)}$

$\mathbf{L}_2^{d_c}\mathbf{w}_{32} = -\mathbf{L}\rho + \mathbf{G}_1^{(3)}$, such that $\mathbf{L}_1 = \mathbf{L}_2 = K - k_c^2 D^{d_c}$, and

$\mathbf{L}_3^{d_c}\mathbf{w}_{33} = \mathbf{G}_3$, where $\mathbf{L}_3 = K - 9k_c^2 D^{d_c}$,

At $O(\varepsilon^4)$, calculation states that the system works with time scale $A(T)$ so we continue sorting order and coefficients which illustrates that

$$\mathcal{L}^{d_c}\mathbf{w}_4 = \mathbf{H}, \tag{B.1}$$

where

$$\mathbf{H} = 2A\frac{\partial A}{\partial T}\mathbf{w}_{20} + A^2\mathbf{H}_0^{(2)} + A^4\mathbf{H}_0^{(4)} + \left(2A\frac{\partial A}{\partial T}\mathbf{w}_{22} + A^2\mathbf{H}_2^{(2)} + A^4\mathbf{H}_2^{(4)}\right)\cos(2k_c x) + A^4\mathbf{H}_4\cos(4k_c x). \tag{B.2}$$

and
$\mathbf{H}_0^{(2)} = -\frac{1}{2}\mathcal{Q}_K(\rho, \mathbf{w}_{31})$,

$$\mathbf{H}_0^{(4)} = -\mathcal{Q}_K(\mathbf{w}_{20},\mathbf{w}_{20}) - \frac{1}{4}\mathcal{Q}_K(\mathbf{w}_{22},\mathbf{w}_{22}) - \frac{1}{2}\mathcal{Q}_K(\rho,\mathbf{w}_{32}),$$
$$\mathbf{H}_2^{(2)} = -\frac{1}{2}\mathcal{M}_2(\rho,\mathbf{w}_{31}) + 4k_c^2 d^{(2)}\begin{bmatrix}0&0&0\\0&0&v^*\\0&0&0\end{bmatrix}\mathbf{w}_{22},$$
$$\mathbf{H}_2^{(4)} = -\frac{1}{2}\mathcal{M}_2(\rho,\mathbf{w}_{32}) - \frac{1}{2}\mathcal{M}_2(\rho,\mathbf{w}_{33}) - \mathcal{M}_2(\mathbf{w}_{20},\mathbf{w}_{22})$$
$$\mathbf{H}_4 = -\frac{1}{2}\mathcal{M}_4(\rho,\mathbf{w}_{33}) - \frac{1}{2}\mathcal{M}_4(\mathbf{w}_{22},\mathbf{w}_{22})$$

Again solvability condition of the system (B.1) - $\langle \mathbf{H}, \psi \rangle = 0$- is satisfied and confirms the existence of the solution, hence

$$K\mathbf{w}_{40} = 2\sigma\mathbf{w}_{20} + \mathbf{H}_0^2,$$
$$K\mathbf{w}_{41} = -2\mathbf{L}\mathbf{w}_{20} + \mathbf{H}_0^4,$$
$$(K - 4k_c^2 D^{d_c})\mathbf{w}_{42} = 2\sigma\mathbf{w}_{22} + \mathbf{H}_2^2,$$
$$(K - 4k_c^2 D^{d_c})\mathbf{w}_{43} = -2\mathbf{L}\mathbf{w}_{22} + \mathbf{H}_2^4,$$
$$(K - 16k_c^2 D^{d_c})\mathbf{w}_{44} = \mathbf{H}_4,$$

At $O(\varepsilon^5)$, the equation is

$$\mathcal{L}^{d_c}\mathbf{w}_5 = \mathbf{P}, \tag{B.3}$$

in which

$$\mathbf{P} = \left(\frac{\partial A}{\partial T_1}\rho + \frac{\partial A}{\partial T}\mathbf{w}_{31} + 3A^2\frac{\partial A}{\partial T}\mathbf{w}_{32} + A\mathbf{P}_1^{(1)} + A^3\mathbf{P}_1^{(3)} + A^5\mathbf{P}_1^{(5)}\right)\cos(k_c x) \tag{B.4}$$
$$+ \left(3A^2\frac{\partial A}{\partial T}\mathbf{w}_{33} + A^3\mathbf{P}_3^{(3)} + A^3\mathbf{P}_3^{(5)}\right)\cos(3k_c x) + A^5\mathbf{P}_5\cos(5k_c x).$$

such that

$$\begin{aligned}\mathbf{P}_1^{(1)} &= d^{(2)}k_c^2\begin{bmatrix}0&0&0\\0&0&v^*\\0&0&0\end{bmatrix}\mathbf{w}_{31} + d^{(4)}k_c^2\begin{bmatrix}0&0&0\\0&0&v^*\\0&0&0\end{bmatrix}\rho,\\ \mathbf{P}_1^{(3)} &= d^{(2)}k_c^2\begin{bmatrix}0&0&0\\0&0&v^*\\0&0&0\end{bmatrix}\mathbf{w}_{32} - \mathcal{M}_1(\mathbf{w}_{20},\mathbf{w}_{31}) - \frac{1}{2}\mathcal{M}_1(\mathbf{w}_{22},\mathbf{w}_{31})\\ &- \mathcal{M}_1(\rho,\mathbf{w}_{40}) - \frac{1}{2}\mathcal{M}_1(\rho,\mathbf{w}_{42}),\end{aligned}$$

$$\begin{aligned}\mathbf{P}_1^{(5)} &= -\mathcal{M}_1(\mathbf{w}_{20},\mathbf{w}_{32}) - \frac{1}{2}\mathcal{M}_1(\mathbf{w}_{22},\mathbf{w}_{32}) - \mathcal{M}_1(\rho,\mathbf{w}_{41}) - \frac{1}{2}\mathcal{M}_1(\rho,\mathbf{w}_{43})\\ &- \frac{1}{2}\mathcal{M}_1(\mathbf{w}_{22},\mathbf{w}_{33}),\end{aligned}$$

$$\mathbf{P}_3^{(3)} = 9d^{(2)}k_c^2\begin{bmatrix}0&0&0\\0&0&v^*\\0&0&0\end{bmatrix}\mathbf{w}_{33} - \frac{1}{2}\mathcal{M}_3(\mathbf{w}_{22},\mathbf{w}_{31}) - \frac{1}{2}\mathcal{M}_3(\rho,\mathbf{w}_{42}),$$

$$\mathbf{P}_3^{(5)} = \frac{1}{2}\mathcal{M}_3(\mathbf{w}_{22}, \mathbf{w}_{32}) - \mathcal{M}_3(\mathbf{w}_{20}, \mathbf{w}_{33}) - \frac{1}{2}\mathcal{M}_3(\rho, \mathbf{w}_{43}) - \frac{1}{2}\mathcal{M}_3(\rho, \mathbf{w}_{44}),$$

$$\mathbf{P}_5 = -\frac{1}{2}\mathcal{M}_5(\mathbf{w}_{22}, \mathbf{w}_{33}) - \frac{1}{2}\mathcal{M}_5(\rho, \mathbf{w}_{44}),$$

Thus by applying the solvability criterion, we obtain the quintic Stuart- Landau equation

$$\frac{\partial A}{\partial T_1} = \tilde{\sigma} A - \tilde{L} A^3 + \tilde{Q} A^5,$$

whose coefficient are determined by

$$\tilde{\sigma} = -\frac{\langle \sigma \mathbf{w}_{31} + \mathbf{P}_1^{(1)}, \psi \rangle}{\langle \rho, \psi \rangle},$$

$$\tilde{\mathbf{L}} = \frac{\langle 3\sigma \mathbf{w}_{32} + \mathbf{L}\mathbf{w}_{31} + \mathbf{P}_1^{(3)}, \psi \rangle}{\langle \rho, \psi \rangle},$$

$$\tilde{\mathbf{Q}} = \frac{\langle 3\mathbf{L}\mathbf{w}_{32} - \mathbf{P}_1^{(5)}, \psi \rangle}{\langle \rho, \psi \rangle},$$

Finally, the coefficients of the quintic Landau- Stuart equation in time scale T is obtained by

$$\frac{\partial A}{\partial T} = \bar{\sigma} A - \bar{\mathbf{L}} A^3 + \bar{Q} A^5,$$

where

$$\bar{\sigma} = \sigma + \varepsilon^2 \tilde{\sigma}, \ \bar{\mathbf{L}} = \mathbf{L} + \varepsilon^2 \tilde{\mathbf{L}}, \ \bar{Q} = \tilde{Q} \varepsilon^2,$$

Therefore, asymptotic solution of the ODE system provides that

$$A_\infty = \frac{\bar{\mathbf{L}} - \sqrt{\bar{\mathbf{L}}^2 - 4\bar{\sigma}\bar{\mathbf{Q}}}}{2\bar{\mathbf{Q}}}$$

which requires that $\bar{\mathbf{Q}} < 0$.

B.2 Weakly nonlinear analysis of the system (4.13)

Consider perturbed bifurcation parameter $\epsilon^2 = \dfrac{k_{32} - k_{32}^c}{k_{32}^c}$,

$$\mathbf{W}^{\cdot} = \mathcal{L}\mathbf{W} + \frac{1}{2}\mathcal{Q}k(\mathbf{W}, \mathbf{W}) + \frac{1}{6}\mathcal{C}_k(\mathbf{W}, \mathbf{W}, \mathbf{W}), \tag{B.5}$$

$$\mathcal{L} = \mathcal{L}^{k_{32}^c} + \epsilon^2 k_{32}^1 \begin{bmatrix} 0 & 0 & 0 \\ 0 & 0 & 0 \\ 0 & 1 & 0 \end{bmatrix} \Delta, \ \mathbf{W}^{k_{32}^c} = K + \nabla^2 D^{k_{32}^c}, \tag{B.6}$$

$$\mathbf{W} = \epsilon \mathbf{W}_1 + \epsilon^2 \mathbf{W}_2 + \epsilon^3 \mathbf{W}_3 + O(\epsilon^4), \tag{B.7}$$

where quadratic and cubic terms in (B.5) are defined as :

$$\mathcal{Q}_k(x, y) = \begin{bmatrix} \mathcal{Q}_{11}(x^s y^s) + \mathcal{Q}_{12}(x^s y^{u_1} + x^{u_1} y^s) + \mathcal{Q}_{13}(x^s y^{u_2} + x^{u_2} y^s) \\ \mathcal{Q}_{21}(x^s y^s) + \mathcal{Q}_{22}(x^s y^{u_1} + x^{u_1} y^s) + \mathcal{Q}_{23}(x^{u_1} y^{u_1}) \\ \mathcal{Q}_{31}(x^s y^s) + \mathcal{Q}_{33}(x^s y^{u_2} + x^{u_2} y^s) \end{bmatrix}, \tag{B.8}$$

and

$$\mathcal{Q}_{11} = \frac{-2\gamma}{K} + \frac{2m_1u_1^*a_1}{(a_1+s^*)^3} + \frac{2m_2u_2^*a_2}{(a_2+s^*)^3},\ \mathcal{Q}_{12} = \frac{-m_1a_1}{(a_1+s^*)^2},\ \mathcal{Q}_{13} = \frac{-m_2a_2}{(a_2+s^*)^2},$$
$$\mathcal{Q}_{21} = \frac{-2m_1u_1^*a_1}{(a_1+s^*)^3},\ \mathcal{Q}_{22} = -\mathcal{Q}_{12},\ \mathcal{Q}_{23} = -2\epsilon,\ \mathcal{Q}_{31} = \frac{-2m_2u_2^*a_2}{(a_2+s^*)^3},\ \mathcal{Q}_{32} = -\mathcal{Q}_{13},$$

$$\mathcal{C}_k(x,y,z) = \begin{bmatrix} \mathcal{C}_{11}(x^sy^sz^s) + \mathcal{C}_{12}(x^{u_1}y^sz^s + x^sy^{u_1}z^s + x^sy^sz^{u_1}) + \mathcal{C}_{13}(x^{u_2}y^sz^s + x^sy^{u_2}z^s + x^sy^sz^{u_2}) \\ \mathcal{C}_{21}(x^sy^sz^s) + \mathcal{C}_{22}(x^{u_1}y^sz^s + x^sy^{u_1}z^s + x^sy^sz^{u_1}) \\ \mathcal{C}_{31}(x^sy^sz^s) + \mathcal{C}_{32}(x^{u_2}y^sz^s + x^sy^{u_2}z^s + x^sy^sz^{u_2}) \end{bmatrix}, \tag{B.9}$$

$$\mathcal{C}_{11} = (\frac{-6m_1a_1u_1^*}{(a_1+s^*)^4} - \frac{6m_2a_2u_2^*}{(a_2+s^*)^4}),\ \mathcal{C}_{12} = \frac{2m_1a_1}{(a_1+s^*)^3},\ \mathcal{C}_{13} = \frac{2m_2a_2}{(a_2+s^*)^3};$$

$$\mathcal{C}_{21} = \frac{6m_1a_1u_1^*}{(a_1+s^*)^4},\ \mathcal{C}_{22} = -\mathcal{C}_{12},\ \mathcal{C}_{13} = \frac{6m_2a_2u_2^*}{(a_2+s^*)^4},\ \mathcal{C}_{32} = -\mathcal{C}_{13},$$

By considering solution for orders ϵ , ϵ^2 and ϵ^3, $\mathbf{w}_i$ will be found.

$$\epsilon^2\partial_T(\epsilon\mathbf{W}_1 + \epsilon^2\mathbf{W}_2 + \epsilon^3\mathbf{W}_3 + \cdots) = L(\epsilon\mathbf{W}_1 + \epsilon^2\mathbf{W}_2 + \epsilon^3\mathbf{W}_3 + \cdots) + \frac{1}{2}\{\epsilon^2\mathcal{Q}_k(\mathbf{W}_1,\mathbf{W}_1) + 2\epsilon^3\mathcal{Q}_k(\mathbf{W}_1,\mathbf{W}_2) + \cdots\} + \frac{1}{6}\epsilon^3\mathcal{C}_k(\mathbf{W}_1,\mathbf{W}_1,\mathbf{W}_1), \tag{B.10}$$

Hence, for $O(\epsilon)$:

$$\mathcal{L}^{k_{32}^c}\mathbf{W}_1 = 0,$$

where $\mathbf{W}_1 = A(T)\rho cos(\delta_c x)$ and ρ belongs to the $\ker(K - \delta_c^2 D^{k_{32}^c})$, it is important to mention that in this case when the system $(K - \delta_c^2 D^{k_{32}^c})$ is computed for marginal value of critical bifurcation parameter k_{32}^c and critical mode δ_c^2 that is why the system is not full rank and we can find ρ. for $O(\epsilon^2)$: we have

$$\mathcal{L}^{k_{32}^c}\mathbf{W}_2 = -\frac{1}{2}\mathcal{Q}_k(\mathbf{W}_1,\mathbf{W}_1),$$

where $\mathcal{Q}_k(\mathbf{W}_1,\mathbf{W}_1)$ is computed as below

$$\mathcal{Q}_k(\mathbf{W}_1,\mathbf{W}_1) = \frac{A^2}{2}(1 + cos(2\delta_c x))\mathcal{Q}_k(\rho,\rho),$$

According Fredholm Alternative there there is $\psi \in ker(K - \delta_c^2 D^{k_{32}^c})^\dagger$ such that $< -\frac{1}{2}\mathcal{Q}_k(\mathbf{W}_1,\mathbf{W}_1), \psi >= 0$ that $(K - \delta_c^2 D^{k_{32}^c})^\dagger$ is conjugate transport of that$(K - \delta_c^2 D^{k_{32}^c})$. Finally, $\mathbf{W}_2 = A^2(\mathbf{W}_{20} + \mathbf{W}_{22}cos(2\delta_c))$ that $\mathbf{W}_{2i},\ i = 0, 2$, are obtained by

$$\begin{cases} K\mathbf{W}_{20} = -\frac{1}{4}\mathcal{Q}_k, \\ (K - 4\delta_c^2 D^{k_{32}^c})\mathbf{W}_{22} = -\frac{1}{4}\mathcal{Q}_k, \end{cases}$$

Moreover in higher order $O(\epsilon^3)$ $\mathcal{L}^{k_{32}^c}\mathbf{W}_3 = G$ that

$$G = (\frac{\partial A}{\partial T})\rho cos(\delta_c x) - k_{32}^{(1)} \begin{bmatrix} 0 & 0 & 0 \\ 0 & 0 & 0 \\ 0 & 1 & 0 \end{bmatrix} A\rho(\delta_c^2)cos(\delta_c x) - \mathcal{Q}_k(\mathbf{W}_1, \mathbf{W}_2) - \frac{1}{6}\mathcal{C}_k(\mathbf{W}_1, \mathbf{W}_1, \mathbf{W}_1),$$

such that $\frac{\partial A}{\partial T}$ is replaced by Stuart-Landau Equation i.e $\frac{\partial A}{\partial T} = \sigma A - LA^3$.

$$\mathcal{Q}_k(\mathbf{W}_1, \mathbf{W}_2) = A^3 cos(\delta x)\mathcal{Q}_k(\rho, \mathbf{W}_{20}) + A^3\frac{1}{2}(cos(\delta_c x) + cos(3\delta_c x))\mathcal{Q}_k(\rho, \mathbf{W}_{22}),$$

and $\mathcal{C}_k(\mathbf{W}_1, \mathbf{W}_1, \mathbf{W}_1)$ is calculated as

$$\mathcal{C}_k(\mathbf{W}_1, \mathbf{W}_1, \mathbf{W}_1) = A^3 cos^3(\delta_c x) = A^3(\frac{3}{4}cos(\delta_c x) + \frac{1}{4}cos(3\delta_c x))\mathcal{C}_k(\rho, \rho, \rho),$$

similarly , since the operator for order three still is $\mathcal{L}^{k_{32}^c}$ so due to Fredholm alternative $< G, \psi >= 0$. therefore we can find σ and L in Stuart- Landau Equation $\frac{\partial A}{\partial T} = \sigma A - LA^3$ and consequently we have

$$\sigma = -\frac{< k_{32}^{(1)} \begin{bmatrix} 0 & 0 & 0 \\ 0 & 0 & 0 \\ 0 & 1 & 0 \end{bmatrix} \rho(\delta_c^2), \psi >}{< \rho, \psi >},$$

and

$$L = -\frac{< \mathcal{Q}_k(\rho, \mathbf{W}_{20}) + 0.5\mathcal{Q}_k(\rho, \mathbf{W}_{22}) + \frac{1}{8}\mathcal{C}_k(\rho, \rho, \rho), \psi >}{< \rho, \psi >}.$$

Appendix C

Normal form calculations

In this Appendix we continue calculation of the normal form of **IGP** model.

C.1 Calculation of coefficients of $O(\varepsilon^2)$

Here we continue the calculation of the system (3.8).

$$\begin{aligned} &e^{i\Omega_c T_0}\left(\frac{-\partial\varphi_1}{\partial T_1}\mathbf{e_1}+\delta^{(1)}K^{\delta^{(1)}}\mathbf{e_1}\varphi_1\right)\\ &+e^{ik_cX_0}\left(-\frac{\partial\varphi_2}{\partial T_1}\mathbf{e_2}+\delta^{(1)}K^{\delta^{(1)}}\mathbf{e_2}\varphi_2-k_c^2\varphi_2D^{d^{(1)}}\mathbf{e_2}+ik_cD^{d_c}\frac{\partial\varphi_2}{\partial X_1}\varphi_2\right)+c.c+\mathbf{F}^*, \end{aligned} \tag{C.1}$$

where the vector $\mathbf{F}^*$ whose expression is obtained by below terms contained of orthogonal terms:

$$\begin{aligned} \mathbf{F}^* &= \varphi_1\bar{\varphi}_1\mathbf{F_0^{(1)}}+\varphi_2\bar{\varphi}_2\mathbf{F_0^{(2)}}+\varphi_1^2\mathbf{F_{20}}e^{2i\Omega_cT_0}+\bar{\varphi}_1{}^2\bar{\mathbf{F}}_{\mathbf{20}}e^{-2i\Omega_cT_0}\\ &+\varphi_2^2\mathbf{F_{02}}e^{2i\delta_cX_0}+\bar{\varphi}_2^2\bar{\mathbf{F}}_{\mathbf{02}}e^{-2i\delta_cX_0}+\varphi_1\varphi_2\mathbf{F_{11}}e^{i(\Omega_cT_0+\delta_cX_0)}+\bar{\varphi}_1\varphi_2\mathbf{F_{-11}}e^{i(-\Omega_cT_0+\delta_cX_0)}\\ &+\varphi_1\bar{\varphi}_2\mathbf{F_{1-1}}e^{i(\Omega_cT_0-\delta_cX_0)}+\bar{\varphi}_1\bar{\varphi}_2\mathbf{F_{-1-1}}e^{-i(\Omega_cT_0+\delta_cX_0)}, \end{aligned} \tag{C.2}$$

$$\mathbf{F_0^{(1)}}=\begin{pmatrix}-2\mathbf{e_1}(1)\bar{\mathbf{e}}_1(1)-(\mathbf{e_1}(1)\bar{\mathbf{e}}_1(2)+\mathbf{e_1}(2)\bar{\mathbf{e}}_1(1))-\eta(\mathbf{e_1}(1)\bar{\mathbf{e}}_1(3)+\mathbf{e_1}(3)\bar{\mathbf{e}}_1(1))\\ \alpha(\mathbf{e_1}(1)\bar{\mathbf{e}}_1(2)+\mathbf{e_1}(2)\bar{\mathbf{e}}_1(1))-(\mathbf{e_1}(2)\bar{\mathbf{e}}_1(3)+\mathbf{e_1}(3)\bar{\mathbf{e}}_1(2))\\ \gamma(\mathbf{e_1}(1)\bar{\mathbf{e}}_1(3)+\mathbf{e_1}(3)\bar{\mathbf{e}}_1(1))+\delta^c(\mathbf{e_1}(2)\bar{\mathbf{e}}_1(3)+\mathbf{e_1}(3)\bar{\mathbf{e}}_1(2))\end{pmatrix},$$

$$\mathbf{F_0^{(2)}}=\begin{pmatrix}-2\mathbf{e_2}(1)\bar{\mathbf{e}}_2(1)-(\mathbf{e_2}(1)\bar{\mathbf{e}}_2(2)+\mathbf{e_2}(2)\bar{\mathbf{e}}_2(1))-\eta(\mathbf{e_2}(1)\bar{\mathbf{e}}_2(3)+\mathbf{e_2}(3)\bar{\mathbf{e}}_2(1))\\ \alpha(\mathbf{e_2}(1)\bar{\mathbf{e}}_2(2)+\mathbf{e_2}(2)\bar{\mathbf{e}}_2(1))-(\mathbf{e_2}(2)\bar{\mathbf{e}}_2(3)+\mathbf{e_2}(3)\bar{\mathbf{e}}_2(2))\\ \gamma(\mathbf{e_2}(1)\bar{\mathbf{e}}_2(3)+\mathbf{e_2}(3)\bar{\mathbf{e}}_2(1))+\delta^c(\mathbf{e_2}(2)\bar{\mathbf{e}}_2(3)+\mathbf{e_2}(3)\bar{\mathbf{e}}_2(2))\end{pmatrix}$$

$$\mathbf{F_{20}}=\begin{pmatrix}-\mathbf{e_1^2}(1)-(\mathbf{e_1}(1)\mathbf{e_1}(2))-\eta(\mathbf{e_1}(1)\mathbf{e_1}(3))\\ \alpha(\mathbf{e_1}(1)\mathbf{e_1}(2))-(\mathbf{e_1}(2)\mathbf{e_1}(3))\\ \gamma(\mathbf{e_1}(1)\mathbf{e_1}(3))+\delta^c(\mathbf{e_1}(2)\mathbf{e_1}(3))\end{pmatrix},$$

$$\bar{\mathbf{F}}_{\mathbf{20}}=\begin{pmatrix}-\bar{\mathbf{e}}_1(1)\bar{\mathbf{e}}_1(1)-(\bar{\mathbf{e}}_1(1)\bar{\mathbf{e}}_1(2))-\eta(\bar{\mathbf{e}}_1(1)\bar{\mathbf{e}}_1(3))\\ \alpha(\bar{\mathbf{e}}_1(1)\bar{\mathbf{e}}_1(2))-(\bar{\mathbf{e}}_1(2)\bar{\mathbf{e}}_1(3))\\ \gamma(\bar{\mathbf{e}}_1(1)\bar{\mathbf{e}}_1(3))+\delta^c(\bar{\mathbf{e}}_1(2)\bar{\mathbf{e}}_1(3))\end{pmatrix},$$

$$\mathbf{F_{02}}=\begin{pmatrix}-\mathbf{e_2^2}(1)-(\mathbf{e_2}(1)\mathbf{e_2}(2))-\eta(\mathbf{e_2}(1)\bar{\mathbf{e}}_2(3))\\ \alpha(\mathbf{e_2}(1)\mathbf{e_2}(2))-(\mathbf{e_2}(2)\mathbf{e_2}(3))\\ \gamma(\mathbf{e_2}(1)\mathbf{e_2}(3))+\delta^c(\mathbf{e_2}(2)\mathbf{e_2}(3))\end{pmatrix}+4d_ck_c^2\begin{pmatrix}0\\ (\mathbf{e_2}(2)\mathbf{e_2}(3))\\ 0\end{pmatrix},$$

$$\bar{\mathbf{F}}_{\mathbf{02}} = \begin{pmatrix} -\bar{\mathbf{e}}_{\mathbf{2}}(\mathbf{1})\bar{\mathbf{e}}_{\mathbf{2}}(\mathbf{1}) - (\bar{\mathbf{e}}_{\mathbf{2}}(\mathbf{1})\bar{\mathbf{e}}_{\mathbf{2}}(\mathbf{2})) - \eta(\bar{\mathbf{e}}_{\mathbf{2}}(\mathbf{1})\bar{\mathbf{e}}_{\mathbf{2}}(\mathbf{3})) \\ \alpha(\bar{\mathbf{e}}_{\mathbf{2}}(\mathbf{1})\bar{\mathbf{e}}_{\mathbf{2}}(\mathbf{2})) - (\bar{\mathbf{e}}_{\mathbf{2}}(\mathbf{2})\bar{\mathbf{e}}_{\mathbf{2}}(\mathbf{3})) \\ \gamma(\bar{\mathbf{e}}_{\mathbf{2}}(\mathbf{1})\bar{\mathbf{e}}_{\mathbf{2}}(\mathbf{3})) + \delta^c(\bar{\mathbf{e}}_{\mathbf{2}}(\mathbf{2})\bar{\mathbf{e}}_{\mathbf{2}}(\mathbf{3})) \end{pmatrix} + 4d_c k_c^2 \begin{pmatrix} 0 \\ (\bar{\mathbf{e}}_{\mathbf{2}}(\mathbf{2})\bar{\mathbf{e}}_{\mathbf{2}}(\mathbf{3})) \\ 0 \end{pmatrix},$$

$$\mathbf{F}_{\mathbf{11}} = \begin{pmatrix} -2\mathbf{e}_{\mathbf{1}}(\mathbf{1})\mathbf{e}_{\mathbf{2}}(\mathbf{1}) - (\mathbf{e}_{\mathbf{1}}(\mathbf{1})\mathbf{e}_{\mathbf{2}}(\mathbf{2}) + \mathbf{e}_{\mathbf{1}}(\mathbf{2})\mathbf{e}_{\mathbf{2}}(\mathbf{1})) - \eta(\mathbf{e}_{\mathbf{1}}(\mathbf{1})\mathbf{e}_{\mathbf{2}}(\mathbf{3}) + \mathbf{e}_{\mathbf{1}}(\mathbf{3})\mathbf{e}_{\mathbf{2}}(\mathbf{1})) \\ \alpha(\mathbf{e}_{\mathbf{1}}(\mathbf{1})\mathbf{e}_{\mathbf{2}}(\mathbf{2}) + \mathbf{e}_{\mathbf{1}}(\mathbf{2})\mathbf{e}_{\mathbf{2}}(\mathbf{1})) - (\mathbf{e}_{\mathbf{1}}(\mathbf{2})\mathbf{e}_{\mathbf{2}}(\mathbf{3}) + \mathbf{e}_{\mathbf{1}}(\mathbf{3})\mathbf{e}_{\mathbf{2}}(\mathbf{2})) \\ \gamma(\mathbf{e}_{\mathbf{1}}(\mathbf{1})\mathbf{e}_{\mathbf{2}}(\mathbf{3}) + \mathbf{e}_{\mathbf{1}}(\mathbf{3})\mathbf{e}_{\mathbf{2}}(\mathbf{1})) + \delta^c(\mathbf{e}_{\mathbf{1}}(\mathbf{2})\mathbf{e}_{\mathbf{2}}(\mathbf{3}) + \mathbf{e}_{\mathbf{1}}(\mathbf{3})\mathbf{e}_{\mathbf{2}}(\mathbf{2})) \end{pmatrix}$$
$$- k_c^2 d_c \begin{pmatrix} 0 \\ (\mathbf{e}_{\mathbf{1}}(\mathbf{2})\mathbf{e}_{\mathbf{2}}(\mathbf{3})) \\ 0 \end{pmatrix},$$

$$\mathbf{F}_{\mathbf{-11}} = \begin{pmatrix} -2\bar{\mathbf{e}}_{\mathbf{1}}(\mathbf{1})\mathbf{e}_{\mathbf{2}}(\mathbf{1}) - (\bar{\mathbf{e}}_{\mathbf{1}}(\mathbf{1})\mathbf{e}_{\mathbf{2}}(\mathbf{2}) + \bar{\mathbf{e}}_{\mathbf{1}}(\mathbf{2})\mathbf{e}_{\mathbf{2}}(\mathbf{1})) - \eta(\bar{\mathbf{e}}_{\mathbf{1}}(\mathbf{1})\mathbf{e}_{\mathbf{2}}(\mathbf{3}) + \bar{\mathbf{e}}_{\mathbf{1}}(\mathbf{3})\mathbf{e}_{\mathbf{2}}(\mathbf{1})) \\ \alpha(\bar{\mathbf{e}}_{\mathbf{1}}(\mathbf{1})\mathbf{e}_{\mathbf{2}}(\mathbf{2}) + \bar{\mathbf{e}}_{\mathbf{1}}(\mathbf{2})\mathbf{e}_{\mathbf{2}}(\mathbf{1})) - (\bar{\mathbf{e}}_{\mathbf{1}}(\mathbf{2})\mathbf{e}_{\mathbf{2}}(\mathbf{3}) + \bar{\mathbf{e}}_{\mathbf{1}}(\mathbf{3})\mathbf{e}_{\mathbf{2}}(\mathbf{2})) \\ \alpha(\bar{\mathbf{e}}_{\mathbf{1}}(\mathbf{1})\mathbf{e}_{\mathbf{2}}(\mathbf{3}) + \bar{\mathbf{e}}_{\mathbf{1}}(\mathbf{3})\mathbf{e}_{\mathbf{2}}(\mathbf{1})) + \delta^c(\bar{\mathbf{e}}_{\mathbf{1}}(\mathbf{2})\mathbf{e}_{\mathbf{2}}(\mathbf{3}) + \bar{\mathbf{e}}_{\mathbf{1}}(\mathbf{3})\mathbf{e}_{\mathbf{2}}(\mathbf{2})) \end{pmatrix}$$
$$- k_c^2 d_c \begin{pmatrix} 0 \\ (\bar{\mathbf{e}}_{\mathbf{1}}(\mathbf{2})\mathbf{e}_{\mathbf{2}}(\mathbf{3})) \\ 0 \end{pmatrix},$$

$$\mathbf{F}_{\mathbf{1-1}} = \begin{pmatrix} -2\mathbf{e}_{\mathbf{1}}(\mathbf{1})\bar{\mathbf{e}}_{\mathbf{2}}(\mathbf{1}) - (\mathbf{e}_{\mathbf{1}}(\mathbf{1})\bar{\mathbf{e}}_{\mathbf{2}}(\mathbf{2}) + \mathbf{e}_{\mathbf{1}}(\mathbf{2})\bar{\mathbf{e}}_{\mathbf{2}}(\mathbf{1})) - \eta(\mathbf{e}_{\mathbf{1}}(\mathbf{1})\bar{\mathbf{e}}_{\mathbf{2}}(\mathbf{3}) + \mathbf{e}_{\mathbf{1}}(\mathbf{3})\bar{\mathbf{e}}_{\mathbf{2}}(\mathbf{1})) \\ \alpha(\mathbf{e}_{\mathbf{1}}(\mathbf{1})\bar{\mathbf{e}}_{\mathbf{2}}(\mathbf{2}) + \mathbf{e}_{\mathbf{1}}(\mathbf{2})\bar{\mathbf{e}}_{\mathbf{2}}(\mathbf{1})) - (\mathbf{e}_{\mathbf{1}}(\mathbf{2})\bar{\mathbf{e}}_{\mathbf{2}}(\mathbf{3}) + \mathbf{e}_{\mathbf{1}}(\mathbf{3})\bar{\mathbf{e}}_{\mathbf{2}}(\mathbf{2})) \\ \gamma(\mathbf{e}_{\mathbf{1}}(\mathbf{1})\bar{\mathbf{e}}_{\mathbf{2}}(\mathbf{3}) + \mathbf{e}_{\mathbf{1}}(\mathbf{3})\bar{\mathbf{e}}_{\mathbf{2}}(\mathbf{1})) + \delta^c(\mathbf{e}_{\mathbf{1}}(\mathbf{2})\bar{\mathbf{e}}_{\mathbf{2}}(\mathbf{3}) + \mathbf{e}_{\mathbf{1}}(\mathbf{3})\bar{\mathbf{e}}_{\mathbf{2}}(\mathbf{2})) \end{pmatrix}$$
$$- k_c^2 d_c \begin{pmatrix} 0 \\ (\mathbf{e}_{\mathbf{1}}(\mathbf{2})\bar{\mathbf{e}}_{\mathbf{2}}(\mathbf{3})) \\ 0 \end{pmatrix},$$

$$\mathbf{F}_{\mathbf{-1-1}} = \begin{pmatrix} -2\bar{\mathbf{e}}_{\mathbf{1}}(\mathbf{1})\bar{\mathbf{e}}_{\mathbf{2}}(\mathbf{1}) - (\bar{\mathbf{e}}_{\mathbf{1}}(\mathbf{1})\bar{\mathbf{e}}_{\mathbf{2}}(\mathbf{2}) + \bar{\mathbf{e}}_{\mathbf{1}}(\mathbf{2})\bar{\mathbf{e}}_{\mathbf{2}}(\mathbf{1})) - \eta(\bar{\mathbf{e}}_{\mathbf{1}}(\mathbf{1})\bar{\mathbf{e}}_{\mathbf{2}}(\mathbf{3}) + \bar{\mathbf{e}}_{\mathbf{1}}(\mathbf{3})\bar{\mathbf{e}}_{\mathbf{2}}(\mathbf{1})) \\ \alpha(\bar{\mathbf{e}}_{\mathbf{1}}(\mathbf{1})\bar{\mathbf{e}}_{\mathbf{2}}(\mathbf{2}) + \bar{\mathbf{e}}_{\mathbf{1}}(\mathbf{2})\bar{\mathbf{e}}_{\mathbf{2}}(\mathbf{1})) - (\bar{\mathbf{e}}_{\mathbf{1}}(\mathbf{2})\bar{\mathbf{e}}_{\mathbf{2}}(\mathbf{3}) + \bar{\mathbf{e}}_{\mathbf{1}}(\mathbf{3})\bar{\mathbf{e}}_{\mathbf{2}}(\mathbf{2})) \\ \gamma(\bar{\mathbf{e}}_{\mathbf{1}}(\mathbf{1})\bar{\mathbf{e}}_{\mathbf{2}}(\mathbf{3}) + \bar{\mathbf{e}}_{\mathbf{1}}(\mathbf{3})\bar{\mathbf{e}}_{\mathbf{2}}(\mathbf{1})) + \eta(\bar{\mathbf{e}}_{\mathbf{1}}(\mathbf{2})\bar{\mathbf{e}}_{\mathbf{2}}(\mathbf{3}) + \bar{\mathbf{e}}_{\mathbf{1}}(\mathbf{3})\bar{\mathbf{e}}_{\mathbf{2}}(\mathbf{2})) \end{pmatrix}$$
$$- k_c^2 d_c \begin{pmatrix} 0 \\ (\bar{\mathbf{e}}_{\mathbf{1}}(\mathbf{2})\bar{\mathbf{e}}_{\mathbf{2}}(\mathbf{3})) \\ 0 \end{pmatrix},$$

We notice that calculation of F_0^1, $F_{20}, \bar{F}_{20}$ do not contain the second order expansion of chemotaxis term. So the solution of (3.8) can be then computed as:

$$\begin{aligned} \mathbf{W}_{\mathbf{2}} = {} & \varphi_1\bar{\varphi}_1\mathbf{W}_{\mathbf{200}}^{(\mathbf{1})} + \varphi_2\bar{\varphi}_2\mathbf{W}_{\mathbf{200}}^{(\mathbf{2})} + \varphi_1^2\mathbf{W}_{\mathbf{220}}e^{2i\Omega_c T_0} + \bar{\varphi}_1{}^2\bar{\mathbf{W}}_{\mathbf{220}}e^{-2i\Omega_c T_0} \\ & + \varphi_2^2\mathbf{W}_{\mathbf{202}}e^{2ik_c X_0} + \bar{\varphi}_2^2\bar{\mathbf{W}}_{\mathbf{202}}e^{-2ik_c X_0} + \varphi_1\varphi_2\mathbf{W}_{\mathbf{211}}e^{i(\Omega_c T_0 + k_c X_0)} \\ & + \bar{\varphi}_1\varphi_2\mathbf{W}_{\mathbf{2-11}}e^{i(-\Omega_c T_0 + k_c X_0)} + \varphi_1\bar{\varphi}_2\mathbf{W}_{\mathbf{21-1}}e^{i(\Omega_c T_0 - k_c X_0)} + \bar{\varphi}_1\bar{\varphi}_2\mathbf{W}_{\mathbf{2-1-1}}e^{-i(\Omega_c T_0 + k_c X_0)} \\ & + \frac{\partial\varphi_2}{\partial X_1}\mathbf{W}_{\mathbf{201}}e^{ik_c X_0} + \frac{\partial\bar{\varphi}_2}{\partial X_1}\bar{\mathbf{W}}_{\mathbf{201}}e^{-ik_c X_0} \end{aligned} \tag{C.3}$$

where the coefficients $\mathbf{W}_{\mathbf{2ij}}, i, j = -1, 0, 1, 2$ are found by

$$\begin{aligned} & L(0,0)\mathbf{W}_{\mathbf{200}}^{(\mathbf{j})} = \mathbf{F_0}^{(j)}, \quad L(2,0)\mathbf{W}_{\mathbf{220}} = \mathbf{F}_{\mathbf{20}}, \quad L(-2,0)\bar{\mathbf{W}}_{\mathbf{200}} = \bar{\mathbf{F}}_{\mathbf{20}}, \\ & L(0,2)\mathbf{W}_{\mathbf{202}} = \mathbf{F}_{\mathbf{02}}, \quad L(0,-2)\bar{\mathbf{W}}_{\mathbf{202}} = \bar{\mathbf{F}}_{\mathbf{02}}, \\ & L(1,1)\mathbf{W}_{\mathbf{211}} = \mathbf{F}_{\mathbf{11}}, \quad L(1,-1)\mathbf{W}_{\mathbf{21-1}} = \mathbf{F}_{\mathbf{1-1}}, \\ & L(-1,1)\mathbf{W}_{\mathbf{2-11}} = \mathbf{F}_{\mathbf{-11}}, \quad L(-1,-1)\mathbf{W}_{\mathbf{2-1-1}} = \mathbf{F}_{\mathbf{-1-1}}, \\ & \mathbf{W}_{\mathbf{201}} = 2ik_c D^{c_2^c}\mathbf{e}_{\mathbf{2}}, \quad \bar{\mathbf{W}}_{\mathbf{201}} = -2ik_c D^{c_2^c}\mathbf{e}_{\mathbf{2}}, \end{aligned} \tag{C.4}$$

such that

$$\mathcal{L}e^{i(r\Omega_c T_0 + s\delta_c X_0)} = L(r,s)e^{i(r\Omega_c T_0 + s\delta_c X_0)} = (ir\Omega_c + D^{d_c}s^2k_c^2 - K^{\delta^c})e^{i(r\Omega_c T_0 + s\delta_c X_0)},$$

C.2 Calculation of coefficients of $O(\varepsilon^3)$

The calculations of $H^{(i)}$ in (3.19) are investigated here:

$$\mathbf{H^{(1)}} = -\frac{\partial \varphi_1}{\partial T_2}\mathbf{R_0} + \mathbf{H_0^{(1)}}\varphi_1 + \mathbf{H_1^{(1)}}|\varphi_1|^2\varphi_1 + \mathbf{H_2^{(1)}}|\varphi_2|^2\varphi_1 + \mathbf{H_3^{(1)}}\frac{\partial^2 \varphi_1}{\partial X_1^2}, \tag{C.5}$$

$$\mathbf{H^{(2)}} = -\frac{\partial \varphi_1}{\partial T_2}\mathbf{S_0} + \mathbf{H_0^{(2)}}\varphi_2 + \mathbf{H_1^{(2)}}|\varphi_2|^2\varphi_2 + \mathbf{H_2^{(2)}}|\varphi_1|^2\varphi_2 + \mathbf{H_3^{(2)}}\frac{\partial^2 \varphi_2}{\partial X_1^2}, \tag{C.6}$$

so that

$$\begin{aligned} \mathbf{R_0} = \mathbf{e_1}, \quad \mathbf{S_0} = \mathbf{e_2}, \\ \mathbf{H_0^{(1)}} = \delta^{(2)} \begin{pmatrix} 0 & 0 & 0 \\ 0 & 0 & 0 \\ 0 & 1 & 0 \end{pmatrix} \mathbf{e_1}, \end{aligned} \tag{C.7}$$

$$\mathbf{H_0^{(2)}} = \delta^{(2)} \begin{pmatrix} 0 & 0 & 0 \\ 0 & 0 & 0 \\ 0 & 1 & 0 \end{pmatrix} \mathbf{e_2} - k_c^2 d^{(2)} \begin{pmatrix} 0 & 0 & 0 \\ 0 & 0 & 1 \\ 0 & 0 & 0 \end{pmatrix} \mathbf{e_2} \tag{C.8}$$

$$\mathbf{H_1^{(1)}} = \begin{bmatrix} -2({h_1^{(1)}}_{11}) - ({h_1^{(1)}}_{12}) - \eta({h_1^{(1)}}_{13}) \\ \alpha({h_1^{(1)}}_{21}) - ({h_1^{(1)}}_{22}) \\ \gamma({h_1^{(1)}}_{31}) + \delta^c({h_1^{(1)}}_{32}) \end{bmatrix}, \tag{C.9}$$

where
${h_1^{(1)}}_{11} = \mathbf{e_1}(1)\mathbf{W_{200}}(1) + \bar{\mathbf{e}}_1(1)\mathbf{W_{220}}(1)$,
${h_1^{(1)}}_{12} = \mathbf{e_1}(1)\mathbf{W_{200}}(2) + \mathbf{e_1}(2)\mathbf{W_{200}}(1) + \bar{\mathbf{e}}_1(2)\mathbf{W_{220}}(1) + \bar{\mathbf{e}}_1(1)\mathbf{W_{220}}(2)$,
${h_1^{(1)}}_{13} = \mathbf{e_1}(1)\mathbf{W_{200}}(3) + \mathbf{e_1}(3)\mathbf{W_{200}}(1) + \bar{\mathbf{e}}_1(1)\mathbf{W_{220}}(3) + \bar{\mathbf{e}}_1(3)\mathbf{W_{220}}(1)$,
${h_1^{(1)}}_{21} = \mathbf{e_1}(1)\mathbf{W_{200}}(2) + \mathbf{e_1}(2)\mathbf{W_{200}}(1) + \bar{\mathbf{e}}_1(2)\mathbf{W_{220}}(1) + \bar{\mathbf{e}}_1(1)\mathbf{W_{220}}(2)$,
${h_1^{(1)}}_{22} = \mathbf{e_1}(2)\mathbf{W_{200}}(3) + \mathbf{e_1}(3)\mathbf{W_{200}}(2) + \bar{\mathbf{e}}_1(2)\mathbf{W_{220}}(3) + \bar{\mathbf{e}}_1(3)\mathbf{W_{220}}(2)$,
${h_1^{(1)}}_{31} = \mathbf{e_1}(1)\mathbf{W_{200}}(3) + \mathbf{e_1}(3)\mathbf{W_{200}}(1) + \bar{\mathbf{e}}_1(1)\mathbf{W_{220}}(3) + \bar{\mathbf{e}}_1(3)\mathbf{W_{220}}(1)$,
${h_1^{(1)}}_{13} = \mathbf{e_1}(2)\mathbf{W_{200}}(3) + \mathbf{e_1}(3)\mathbf{W_{200}}(2) + \bar{\mathbf{e}}_1(2)\mathbf{W_{220}}(3) + \bar{\mathbf{e}}_1(3)\mathbf{W_{220}}(2)$,

$$\mathbf{H_2^{(1)}} = \begin{bmatrix} -2({h_1^{(1)}}_{11}) - ({h_1^{(1)}}_{12}) - \eta({h_1^{(1)}}_{13}) \\ \alpha({h_1^{(1)}}_{21}) - ({h_1^{(1)}}_{22}) \\ \gamma({h_1^{(1)}}_{31}) + \delta_c({h_1^{(1)}}_{32}) \end{bmatrix}, \tag{C.10}$$

such that
${h_2^{(1)}}_{11} = \mathbf{e_1}(1)\mathbf{W_{200}^{(2)}}(1) + \bar{\mathbf{e}}_2(1)\mathbf{W_{211}}(1) + \mathbf{e_2}(1)\mathbf{W_{21-1}}(1)$,
${h_2^{(1)}}_{12} = \mathbf{e_1}(1)\mathbf{W_{200}^{(2)}}(2) + \mathbf{e_1}(2)\mathbf{W_{200}^{(2)}}(1) + \bar{\mathbf{e}}_2(1)\mathbf{W_{211}}(1) + \bar{\mathbf{e}}_2(1)\mathbf{W_{211}}(2)$
$+ \mathbf{e_2}(1)\mathbf{W_{21-1}}(2) + \mathbf{e_2}(2)\mathbf{W_{21-1}}(1)$,

$h_2^{(1)}{}_{13} = \mathbf{e_1(1)W^{(2)}_{200}(3)} + \mathbf{e_1(3)W^{(2)}_{200}(1)} + \mathbf{\bar{e}_2(1)W_{211}(3)} + \mathbf{\bar{e}_2(3)W_{211}(1)}$
$+ \mathbf{e_2(1)W_{21-1}(3)} + \mathbf{e_2(3)W_{21-1}(1)},$
$h_2^{(1)}{}_{21} = \mathbf{e_1(1)W^{(2)}_{200}(2)} + \mathbf{e_1(2)W^{(2)}_{200}(1)} + \mathbf{\bar{e}_2(1)W_{211}(1)} + \mathbf{\bar{e}_2(1)W_{211}(2)}$
$+ \mathbf{e_2(1)W_{21-1}(2)} + \mathbf{e_2(2)W_{21-1}(1)},$
$h_2^{(1)}{}_{22} = \mathbf{e_1(2)W^{(2)}_{200}(3)} + \mathbf{e_1(3)W^{(2)}_{200}(2)} + \mathbf{\bar{e}_2(3)W_{211}(2)} + \mathbf{\bar{e}_2(2)W_{211}(3)}$
$+ \mathbf{e_2(2)W_{21-1}(3)} + \mathbf{e_2(3)W_{21-1}(2)},$
$h_2^{(1)}{}_{31} = \mathbf{e_1(1)W^{(2)}_{200}(3)} + \mathbf{e_1(3)W^{(2)}_{200}(1)} + \mathbf{\bar{e}_2(1)W_{211}(3)} + \mathbf{\bar{e}_2(3)W_{211}(1)}$
$+ \mathbf{e_2(1)W_{21-1}(3)} + \mathbf{e_2(3)W_{21-1}(1)},$
$h_2^{(1)}{}_{32} = \mathbf{e_1(2)W^{(2)}_{200}(3)} + \mathbf{e_1(3)W^{(2)}_{200}(2)} + \mathbf{\bar{e}_2(3)W_{211}(2)} + \mathbf{\bar{e}_2(2)W_{211}(3)}$
$+ \mathbf{e_2(2)W_{21-1}(3)} + \mathbf{e_2(3)W_{21-1}(2)},$

$$\mathbf{H}_1^{(2)} = \begin{bmatrix} -2(h_1^{(2)}{}_{11}) - (h_1^{(2)}{}_{12}) - \eta(h_1^{(2)}{}_{13}) \\ \alpha(h_1^{(2)}{}_{21}) - (h_1^{(2)}{}_{22}) \\ \gamma(h_1^{(2)}{}_{31}) + \delta^c(h_1^{(2)}{}_{32}) \end{bmatrix} - d_c k_c^2 \begin{bmatrix} 0 \\ \mathbf{e_2(3)\bar{W}_{200}(2)} + \mathbf{\bar{e}_2(3)W_{202}(2)} \\ 0 \end{bmatrix}, \tag{C.11}$$

where
$h_1^{(2)}{}_{11} = \mathbf{e_2(1)W^{(2)}_{200}(1)} + \mathbf{\bar{e}_2(1)W_{202}(1)},$
$h_1^{(2)}{}_{12} = \mathbf{e_2(1)W^{(2)}_{200}(2)} + \mathbf{e_2(2)W^{(2)}_{200}(1)} + \mathbf{\bar{e}_2(2)W_{202}(1)} + \mathbf{\bar{e}_2(1)W_{202}(2)},$
$h_1^{(2)}{}_{13} = \mathbf{e_2(1)W^{(2)}_{200}(3)} + \mathbf{e_2(3)W^{(2)}_{200}(1)} + \mathbf{\bar{e}_2(3)W_{202}(1)} + \mathbf{\bar{e}_2(1)W_{202}(3)},$
$h_1^{(2)}{}_{21} = \mathbf{e_2(1)W^{(2)}_{200}(2)} + \mathbf{e_2(2)W^{(2)}_{200}(1)} + \mathbf{\bar{e}_2(2)W_{202}(1)} + \mathbf{\bar{e}_2(1)W_{202}(2)},$
$h_1^{(2)}{}_{22} = \mathbf{e_1(2)W^{(2)}_{200}(3)} + \mathbf{e_2(3)W^{(2)}_{200}(2)} + \mathbf{\bar{e}_2(2)W_{202}(3)} + \mathbf{\bar{e}_2(3)W_{202}(2)},$
$h_1^{(2)}{}_{31} = \mathbf{e_2(1)W^{(2)}_{200}(3)} + \mathbf{e_2(3)W^{(2)}_{200}(1)} + \mathbf{\bar{e}_2(3)W_{202}(1)} + \mathbf{\bar{e}_2(1)W_{202}(3)},$
$h_1^{(2)}{}_{32} = \mathbf{e_1(2)W^{(2)}_{200}(3)} + \mathbf{e_2(3)W^{(2)}_{200}(2)} + \mathbf{\bar{e}_2(2)W_{202}(3)} + \mathbf{\bar{e}_2(3)W_{202}(2)},$

$$\mathbf{H}_2^{(2)} = \begin{bmatrix} -2(h_2^{(2)}{}_{11}) - (h_2^{(2)}{}_{12}) - \eta(h_2^{(2)}{}_{13}) \\ \alpha(h_2^{(2)}{}_{21}) - (h_2^{(2)}{}_{22}) \\ \gamma(h_2^{(2)}{}_{31}) + \delta^c(h_2^{(2)}{}_{32}) \end{bmatrix} - d_c k_c^2 \begin{bmatrix} 0 \\ \mathbf{\bar{e}_1(3)W_{211}(2)} + \mathbf{e_1(3)W_{2-11}(2)} + \mathbf{e_2(3)W^{(1)}_{200}(2)} \\ 0 \end{bmatrix}, \tag{C.11}$$

$h_2^{(2)}{}_{11} = \mathbf{e_2(1)W^{(1)}_{200}(1)} + \mathbf{\bar{e}_1(1)W_{211}(1)} + \mathbf{e_1(1)W_{2-11}(1)},$
$h_2^{(2)}{}_{12} = \mathbf{e_2(1)W^{(1)}_{200}(2)} + \mathbf{e_2(2)W^{(1)}_{200}(1)} + \mathbf{\bar{e}_1(1)W_{211}(2)} + \mathbf{\bar{e}_1(2)W_{211}(1)}$
$+ \mathbf{e_1(1)W_{2-11}(2)} + \mathbf{e_1(2)W_{2-11}(1)},$
$h_2^{(2)}{}_{13} = \mathbf{e_2(1)W^{(1)}_{200}(3)} + \mathbf{e_2(3)W^{(1)}_{200}(1)} + \mathbf{\bar{e}_1(1)W_{211}(3)} + \mathbf{\bar{e}_1(3)W_{211}(1)}$
$+ \mathbf{e_1(1)W_{2-11}(3)} + \mathbf{e_1(3)W_{2-11}(1)},$
$h_2^{(2)}{}_{21} = \mathbf{e_2(1)W^{(1)}_{200}(2)} + \mathbf{e_2(2)W^{(1)}_{200}(1)} + \mathbf{\bar{e}_1(1)W_{211}(2)} + \mathbf{\bar{e}_1(2)W_{211}(1)}$
$+ \mathbf{e_1(1)W_{2-11}(2)} + \mathbf{e_1(2)W_{2-11}(1)},$
$h_2^{(2)}{}_{22} = \mathbf{e_2(2)W^{(1)}_{200}(3)} + \mathbf{e_2(3)W^{(1)}_{200}(2)} + \mathbf{\bar{e}_1(3)W_{211}(2)} + \mathbf{\bar{e}_1(2)W_{211}(3)}$
$+ \mathbf{e_1(2)W_{2-11}(3)} + \mathbf{e_2(3)W_{2-11}(2)},$
$h_2^{(2)}{}_{31} = \mathbf{e_2(1)W^{(1)}_{200}(3)} + \mathbf{e_2(3)W^{(1)}_{200}(1)} + \mathbf{\bar{e}_1(1)W_{211}(3)} + \mathbf{\bar{e}_1(3)W_{211}(1)}$
$+ \mathbf{e_1(1)W_{2-11}(3)} + \mathbf{e_1(3)W_{21-1}(1)},$
$h_2^{(2)}{}_{32} = \mathbf{e_2(2)W^{(1)}_{200}(3)} + \mathbf{e_2(3)W^{(1)}_{200}(2)} + \mathbf{\bar{e}_1(3)W_{211}(2)} + \mathbf{\bar{e}_1(2)W_{211}(3)}$

$+ \mathbf{e_1}(\mathbf{2})\mathbf{W_{2-11}}(\mathbf{3}) + \mathbf{e_2}(\mathbf{3})\mathbf{W_{2-11}}(\mathbf{2})$,

$$\mathbf{H_3^{(1)}} = d_c \begin{pmatrix} 0 & 0 & 0 \\ 0 & 0 & v^* \\ 0 & 0 & 0 \end{pmatrix} \mathbf{e_1} \tag{C.12}$$

$$\mathbf{H_3^{(2)}} = d_c \begin{pmatrix} 0 & 0 & 0 \\ 0 & 0 & v^* \\ 0 & 0 & 0 \end{pmatrix} \mathbf{e_2} + 2ik_c d_c \begin{pmatrix} 0 & 0 & 0 \\ 0 & 0 & v^* \\ 0 & 0 & 0 \end{pmatrix} \mathbf{W_{201}} \tag{C.13}$$

By imposing the compatibility condition for the equation (3.12) one obtains the system

$$\frac{\partial \varphi_1}{\partial T_2} = \tilde{\sigma_1}\varphi_1 - \tilde{L_1}|\varphi_1|^2\varphi_1 + \tilde{\Omega_1}|\varphi_2|^2\varphi_1 + \tilde{\delta_1}\frac{\partial^2 \varphi_1}{\partial X_1^2}, \tag{C.14}$$

$$\frac{\partial \varphi_2}{\partial T_2} = \tilde{\sigma_2}\varphi_2 - \tilde{L_2}|\varphi_2|^2\varphi_2 + \tilde{\Omega_2}|\varphi_1|^2\varphi_2 + \tilde{\delta_2}\frac{\partial^2 \varphi_2}{\partial X_1^2}, \tag{C.15}$$

for the fields φ_1 and φ_2, where the coefficients are easily calculated as follows:

$$\tilde{\sigma_i} = -\frac{\langle \mathbf{H_0^{(i)}}, \mathbf{e_i^*} \rangle}{\langle \mathbf{e_i}, \mathbf{e_i^*} \rangle}, \quad \tilde{L_i} = -\frac{\langle \mathbf{H_1^{(i)}}, \mathbf{e_i^*} \rangle}{\langle \mathbf{e_i}, \mathbf{e_i^*} \rangle}, \tag{C.16}$$

$$\tilde{\Omega_i} = -\frac{\langle \mathbf{H_0^{(i)}}, \mathbf{e_i^*} \rangle}{\langle \mathbf{e_i}, \mathbf{e_i^*} \rangle} \quad \tilde{\delta_i} = -\frac{\langle \mathbf{H_3^{(i)}}, \mathbf{e_i^*} \rangle}{\langle \mathbf{e_i}, \mathbf{e_i^*} \rangle} \tag{C.17}$$

where $\mathbf{e_1^*} \in Ker(i\Omega - K^{\delta^c})^\dagger$ and $\mathbf{e_2^*} \in Ker(K^{\delta^c} - k_c^2 D^{d_c})^\dagger$ .Notice that coefficients of the (C.14) are complex while the coefficients of the (C.15) are real. Moreover, the coefficients of the $\tilde{\sigma_1}$ is linearly dependent on $\delta^{(2)}$ due to (C.7), and $\tilde{\sigma_2}$ is linearly dependent on $\delta^{(2)}$ and $d^{(2)}$ due to (C.8). Other coefficients are not dependent on $\delta^{(2)}$and $d^{(2)}$.

References

Ahmed, E, AMA El-Sayed, and Hala AA El-Saka (2007). "Equilibrium points, stability and numerical solutions of fractional-order predator–prey and rabies models". In: *Journal of Mathematical Analysis and Applications* 325.1, pp. 542–553.

Akjouj, Imane and Jamal Najim (2021). "Feasibility of sparse large Lotka-Volterra ecosystems". In: *arXiv preprint arXiv:2111.11247*.

Anjos, Lucas dos, Michel Iskin da S Costa, and Regina C Almeida (2021). "Rapid spread agents may impair biological control in a tritrophic food web with intraguild predation". In: *Ecological Complexity* 46, p. 100926.

Armstrong, Robert A and Richard McGehee (1980). "Competitive exclusion". In: *The American Naturalist* 115.2, pp. 151–170.

Ayala, Francisco J (1969). "Experimental invalidation of the principle of competitive exclusion". In: *Nature* 224.5224, pp. 1076–1079.

Baek, Hunki (2008). "Extinction and permanence of a three-species Lotka-Volterra system with impulsive control strategies". In: *Discrete Dynamics in Nature and Society* 2008.

Bai, Dingyong et al. (2021). "Dynamics of an intraguild predation food web model with strong Allee effect in the basal prey". In: *Nonlinear analysis: real world applications* 58, p. 103206.

Bocsó, A and M Farkas (2003). "Political and economic rationality leads to velcro bifurcation". In: *Applied mathematics and computation* 140.2-3, pp. 381–389.

Brooks, Bernard P (2006). "The coefficients of the characteristic polynomial in terms of the eigenvalues and the elements of an n$\times$ n matrix". In: *Applied mathematics letters* 19.6, pp. 511–515.

Butler, GJ and Paul Waltman (1981). "Bifurcation from a limit cycle in a two predator-one prey ecosystem modeled on a chemostat". In: *Journal of Mathematical Biology* 12.3, pp. 295–310.

Cai, Liying et al. (2010). "Bifurcation and chaos of a three-species Lotka-Volterra food-chain model with spatial diffusion and time delays". In: *Scientific Research and Essays* 5.24, pp. 4068–4076.

Cantrell, Robert Stephen and Chris Cosner (2004). *Spatial ecology via reaction-diffusion equations*. John Wiley & Sons.

Cantrell, Robert Stephen, Chris Cosner, and Shigui Ruan (2004). "Intraspecific interference and consumer-resource dynamics". In: *Discrete & Continuous Dynamical Systems-B* 4.3, p. 527.

Cantrell, Robert Stephen et al. (2017). "A PDE model of intraguild predation with cross-diffusion". In: *Discrete & Continuous Dynamical Systems-B* 22.10, p. 3653.

Chang, Chueh-Hsin and Chiun-Chuan Chen (2021). "Existence of Front–Back-Pulse Solutions of a Three-Species Lotka–Volterra Competition–Diffusion System". In: *Journal of Dynamics and Differential Equations*, pp. 1–36.

Chattopadhyay, J, AK Sarkar, and PK Tapaswi (1996). "Effect of cross-diffusion on a diffusive prey-predator system—a nonlinear analysis". In: *Journal of Biological Systems* 4.02, pp. 159–169.

Chauvet, Erica et al. (2002). "A Lotka-Volterra three-species food chain". In: *Mathematics magazine* 75.4, pp. 243–255.

Chen, Yu-Shuo and Jong-Shenq Guo (2021). "Traveling wave solutions for a three-species predator–prey model with two aborigine preys". In: *Japan Journal of Industrial and Applied Mathematics* 38.2, pp. 455–471.

Cong, Pingping, Meng Fan, and Xingfu Zou (2021). "Dynamics of a three-species food chain model with fear effect". In: *Communications in Nonlinear Science and Numerical Simulation* 99, p. 105809.

Conway, Edward, David Hoff, and Joel Smoller (1978). "Large time behavior of solutions of systems of nonlinear reaction-diffusion equations". In: *SIAM Journal on Applied Mathematics* 35.1, pp. 1–16.

Coste, J, J Peyraud, and P Coullet (1979). "Asymptotic behaviors in the dynamics of competing species". In: *SIAM Journal on Applied Mathematics* 36.3, pp. 516–543.

Council, National Research et al. (2000). *Professional Societies and Ecologically Based Pest Management: Proceedings of a Workshop*. National Academies Press.

Cushing, JM (1984). "Periodic two-predator, one-prey interactions and the time sharing of a resource niche". In: *SIAM Journal on Applied Mathematics* 44.2, pp. 392–410.

Dang, Fei et al. (2021). "Transfer and toxicity of silver nanoparticles in the food chain". In: *Environmental Science: Nano* 8.6, pp. 1519–1535.

Deng, Hang et al. (2019). "Dynamic behaviors of Lotka–Volterra predator–prey model incorporating predator cannibalism". In: *Advances in Difference Equations* 2019.1, pp. 1–17.

Diehl, Sebastian and Margit Feißel (2000). "Effects of enrichment on three-level food chains with omnivory". In: *The American Naturalist* 155.2, pp. 200–218.

Du, Yanke and Rui Xu (2012). "Traveling wave solutions in a three-species food-chain model with diffusion and delays". In: *International Journal of Biomathematics* 5.01, p. 1250002.

Durant, Sarah M (2000). "Living with the enemy: avoidance of hyenas and lions by cheetahs in the Serengeti". In: *Behavioral ecology* 11.6, pp. 624–632.

Echeverri, Luis F, Óscar I Giraldo, and Edwin Zarrazola (2017). "A model of competing species that exhibits zip bifurcation". In: *Revista Integración* 35.1, pp. 127–141.

Elettreby, Mohammed Fathy, Ahlam Abdullah Al-Raezah, and Tamer Nabil (2017). "Fractional-order model of two-prey one-predator system". In: *Mathematical Problems in Engineering* 2017.

Ermentrout, Bard and Mark Lewis (1997). "Pattern formation in systems with one spatially distributed species". In: *Bulletin of mathematical biology* 59.3, pp. 533–549.

Farivar, F and F Hadadifard (submitted). "A chemotaxis Model of Three Species Lotka-Volterra Type with Intraguild Predation: Existence of Unique Global Solutions". In: *Journal of Mathematical Biology*.

Farkas, M (1987). "Competitive exclusion by zip bifurcation". In: *Dynamical Systems*. Springer, pp. 165–178.

Farkas, Miklós (1984). "Zip bifurcation in a competition model". In: *Nonlinear Analysis: Theory, Methods & Applications* 8.11, pp. 1295–1309.

Fedriani, Jose M et al. (2000). "Competition and intraguild predation among three sympatric carnivores". In: *Oecologia* 125.2, pp. 258–270.

Ferreira, Jocirei D and Luiz Augusto F de Oliveira (2009). "Zip bifurcation in a competitive system with diffusion". In: *Differential Equations and Dynamical Systems* 17.1, pp. 37–53.

Ferreira, Jocirei D, Severino Horácio da Silva, and V Sree Hari Rao (2019). "Stability analysis of predator–prey models involving cross-diffusion". In: *Physica D: Nonlinear Phenomena* 400, p. 132141.

Flynn, Kelly E and Daniel C Moon (2011). "Effects of habitat complexity, prey type, and abundance on intraguild predation between larval odonates". In: *Hydrobiologia* 675.1, pp. 97–104.

Freedman, Herbert I (1980). *Deterministic mathematical models in population ecology*. Vol. 57. Marcel Dekker Incorporated.

Freedman, HI and Shigui Ruan (1992). "Hopf bifurcation in three-species food chain models with group defense". In: *Mathematical biosciences* 111.1, pp. 73–87.

Freedman, HI and Paul Waltman (1977). "Mathematical analysis of some three-species food-chain models". In: *Mathematical Biosciences* 33.3-4, pp. 257–276.

Fuller, JM Fedriani TK and RM Sauvajotand EC York (2000). "Competition and intraguild predation among three sympatric carnivores". In: *Oecologia* 125, pp. 258–270.

Gajewski, Herbert, Klaus Zacharias, and Konrad Gröger (1998). "Global behaviour of a reaction-diffusion system modelling chemotaxis". In: *Mathematische Nachrichten* 195.1, pp. 77–114.

Gambino, G et al. (Preprinting). "Turing patterns in an intraguild predation model with nonlinear diffusion terms". In.

Gambino, Gaetana, Maria Carmela Lombardo, and Marco Sammartino (2012). "Turing instability and traveling fronts for a nonlinear reaction–diffusion system with cross-diffusion". In: *Mathematics and Computers in Simulation* 82.6, pp. 1112–1132.

— (2013). "Pattern formation driven by cross-diffusion in a 2D domain". In: *Nonlinear Analysis: Real World Applications* 14.3, pp. 1755–1779.

Gan, Qintao et al. (2010). "Travelling waves of a three-species Lotka–Volterra food-chain model with spatial diffusion and time delays". In: *Nonlinear Analysis: Real World Applications* 11.4, pp. 2817–2832.

Gause, GF (1934). "The struggle for existence Williams and Wilkins". In: *Baltimore, Maryland*.

Gilpin, Michael E (1975). "Limit cycles in competition communities". In: *The American Naturalist* 109.965, pp. 51–60.

Goh, BS (1976). "Global stability in two species interactions". In: *Journal of Mathematical Biology* 3.3, pp. 313–318.

Goodman, Maurice C et al. (2022). "Shifting fish distributions impact predation intensity in a sub-Arctic ecosystem". In: *Ecography*, e06084.

Gopalsamy, K (1982). "Exchange of equilibria in two species Lotka-Volterra competition models". In: *The ANZIAM Journal* 24.2, pp. 160–170.

Guin, Lakshmi Narayan, Debdeep Roy, and Salih Djilali (2021). "Dynamic analysis of a three-species food chain system with intra-specific competition". In: *Journal of Environmental Accounting and Management* 9.02, pp. 127–143.

Gurtin, Morton E (1974). "Some mathematical models for population dynamics that lead to segregation". In: *Quarterly of Applied Mathematics* 32.1, pp. 1–9.

Haile, Dawit and Zhifu Xie (2015). "Long-time behavior and Turing instability induced by cross-diffusion in a three species food chain model with a Holling type-II functional response". In: *Mathematical biosciences* 267, pp. 134–148.

Han, Renji and Binxiang Dai (2016). "Spatiotemporal dynamics and Hopf bifurcation in a delayed diffusive intraguild predation model with Holling II functional response". In: *International Journal of Bifurcation and Chaos* 26.12, p. 1650197.

Han, Renji, Binxiang Dai, and Yuming Chen (2019). "Pattern formation in a diffusive intraguild predation model with nonlocal interaction effects". In: *AIP Advances* 9.3, p. 035046.

Han, Renji, Binxiang Dai, and Lin Wang (2018). "Delay induced spatiotemporal patterns in a diffusive intraguild predation model with Beddington-DeAngelis functional response". In: *Mathematical Biosciences & Engineering* 15.3, p. 595.

Hardin, Garrett (1960). "The Competitive Exclusion Principle: An idea that took a century to be born has implications in ecology, economics, and genetics." In: *science* 131.3409, pp. 1292–1297.

Harrison, Gary W (1979). "Global stability of food chains". In: *The American Naturalist* 114.3, pp. 455–457.

Hastings, Alan and Thomas Powell (1991). "Chaos in a three-species food chain". In: *Ecology* 72.3, pp. 896–903.

Hazelbauer, Gerald L (1979). *Taxis and behavior*. Chapman and Hall.

Hoai Nguyen, Linh Thi, Quang Hong Ta, and Ton Viet Ta (2015). "Stability of a one-predator two-prey system governed by nonautonomous differential equations". In: *arXiv e-prints*, arXiv–1508.

Hofbauer, Josef, Karl Sigmund, et al. (1998). *Evolutionary games and population dynamics*. Cambridge university press.

Holt, Robert D and JH Lawton (1994). "The ecological consequences of shared natural enemies". In: *Annual review of Ecology and Systematics*, pp. 495–520.

Holt, Robert D and Gary A Polis (1997). "A theoretical framework for intraguild predation". In: *The American Naturalist* 149.4, pp. 745–764.

Hsu, SB, SP Hubbell, and Paul Waltman (1978a). "A contribution to the theory of competing predators". In: *Ecological Monographs* 48.3, pp. 337–349.

— (1978b). "Competing predators". In: *SIAM Journal on Applied Mathematics* 35.4, pp. 617–625.

Hsu, Sze-Bi, Shigui Ruan, and Ting-Hui Yang (2013). "On the dynamics of two-consumers-one-resource competing systems with Beddington-DeAngelis functional response". In: *Discrete & Continuous Dynamical Systems-B* 18.9, p. 2331.

— (2015). "Analysis of three species Lotka–Volterra food web models with omnivory". In: *Journal of Mathematical Analysis and Applications* 426.2, pp. 659–687.

Huang, Huey-Wen and Harold J Morowitz (1972). "A method for phenomenological analysis of ecological data". In: *Journal of theoretical biology* 35.3, pp. 489–503.

Hutchinson, G Evelyn (1964). "The lacustrine microcosm reconsidered". In: *American Scientist* 52.3, pp. 334–341.

Irigoien, Xabier and André de Roos (2011). "The role of intraguild predation in the population dynamics of small pelagic fish". In: *Marine Biology* 158.8, pp. 1683–1690.

Ji, Juping and Lin Wang (2022). "Competitive exclusion and coexistence in an intraguild predation model with Beddington–DeAngelis functional response". In: *Communications in Nonlinear Science and Numerical Simulation* 107, p. 106192.

Ji, Juping et al. (2022). "Spatiotemporal dynamics induced by intraguild predator diffusion in an intraguild predation model". In: *Journal of Mathematical Biology* 85.1, pp. 1–28.

Ji, Ruihong, Li Yan, and Jiahong Wu (2022). "Optimal decay for the 3D anisotropic Boussinesq equations near the hydrostatic balance". In: *Calculus of Variations and Partial Differential Equations* 61.4, pp. 1–34.

Kanel, Jacob Isaac and Mokhtar Kirane (1998). "Pointwise a priori bounds for a strongly coupled system of reaction–diffusion equations with a balance law". In: *Mathematical methods in the applied sciences* 21.13, pp. 1227–1232.

Kang, Yun and Lauren Wedekin (2013). "Dynamics of a intraguild predation model with generalist or specialist predator". In: *Journal of mathematical biology* 67.5, pp. 1227–1259.

Kerner, Edward H (1957). "A statistical mechanics of interacting biological species". In: *The bulletin of mathematical biophysics* 19.2, pp. 121–146.

Khalighi, Moein et al. (2021). "Three-species Lotka-Volterra model with respect to Caputo and Caputo-Fabrizio fractional operators". In: *Symmetry* 13.3, p. 368.

Kidachi, Hideyuki (1980). "On mode interactions in reaction diffusion equation with nearly degenerate bifurcations". In: *Progress of Theoretical Physics* 63.4, pp. 1152–1169.

Kirlinger, Gabriela (1986). "Permanence in Lotka-Volterra equations: linked prey-predator systems". In: *Mathematical Biosciences* 82.2, pp. 165–191.

Kishimoto, K, M Mimura, and K Yoshida (1983). "Stable spatio-temporal oscillations of diffusive Lotka-Volterra system with three or more species". In: *Journal of Mathematical Biology* 18.3, pp. 213–221.

Kishimoto, Kazuo (1982). *The diffusive Lotka-Volterra system with three species can have a stable non-constant equilibrium solution*.

Koch, Arthur L (1974). "Coexistence resulting from an alternation of density dependent and density independent growth". In: *Journal of Theoretical Biology* 44.2, pp. 373–386.

Kouachi, Said (2016). "A balance law for some strongly coupled reaction-diffusion systems and an invariance Theorem". In.

Krikorian, Nishan (1979). "The Volterra model for three species predator-prey systems: boundedness and stability". In: *Journal of mathematical biology* 7.2, pp. 117–132.

Křivan, Vlastimil (2007). "The Lotka-Volterra predator-prey model with foraging–predation risk trade-offs". In: *The American Naturalist* 170.5, pp. 771–782.

Kuiper, Hendrik J (1980). "Invariant sets for nonlinear elliptic and parabolic systems". In: *SIAM Journal on Mathematical Analysis* 11.6, pp. 1075–1103.

— (2000). "Positively Invariant Regions for Strongly Coupled Reaction–Diffusion Systems with a Balance Law". In: *Journal of mathematical analysis and applications* 249.2, pp. 340–350.

Kumar, Vikas and Nitu Kumari (2020). "Controlling chaos in three species food chain model with fear effect". In: *AIMS Mathematics* 5.2, pp. 828–842.

Kuwamura, Masataka (2015). "Turing instabilities in prey–predator systems with dormancy of predators". In: *Journal of mathematical biology* 71.1, pp. 125–149.

Leung, Margaret-Rose et al. (2015). "A symmetric intraguild predation model for the invasive lionfish and native grouper". In: *Commun. Math. Biol. Neurosci.* 2015, Article–ID.

Levin, SA (1981). "Mechanisms for the generation and maintenance of diversity in ecological communities". In: *The mathematical theory of the dynamics of biological populations*, pp. 173–194.

Levin, Simon A (1970). "Community equilibria and stability, and an extension of the competitive exclusion principle". In: *The American Naturalist* 104.939, pp. 413–423.

— (1974). "Dispersion and population interactions". In: *The American Naturalist* 108.960, pp. 207–228.

— (1976). "Population dynamic models in heterogeneous environments". In: *Annual review of ecology and systematics*, pp. 287–310.

Levin, Simon A and Lee A Segel (1985). "Pattern generation in space and aspect". In: *SIAM Review* 27.1, pp. 45–67.

Levins, Richard (2020). "Evolution in changing environments". In: *Evolution in Changing Environments*. Princeton University Press.

Li, Chenglin, Xiuqing Guo, and Dongmei He (2013). "An impulsive diffusion predator-prey system in three-species with Beddington-DeAngelis response". In: *Journal of Applied Mathematics and Computing* 43.1, pp. 235–248.

Li, YP et al. (2013). *Mathematical modeling for resources and environmental systems*.

Liang, Yuyong et al. (2022). "Flower provision reduces intraguild predation between predators and increases aphid biocontrol in tomato". In: *Journal of Pest Science* 95.1, pp. 461–472.

Lin, Jian-Jhong and Ting-Hui Yang (2018). "Traveling wave solutions for a diffusive three-species intraguild predation model". In: *International Journal of Biomathematics* 11.02, p. 1850022.

Loladze, Irakli et al. (2004). "Competition and stoichiometry: coexistence of two predators on one prey". In: *Theoretical Population Biology* 65.1, pp. 1–15.

Lou, Yuan, Salomé Martínez, and Wei-Ming Ni (2000). "On 3×3 Lotka-Volterra competition systems with cross-diffusion". In: *Discrete & Continuous Dynamical Systems* 6.1, p. 175.

Lucas, Éric, Daniel Coderre, and Jacques Brodeur (2000). "Selection of molting and pupation sites by Coleomegilla maculata (Coleoptera: Coccinellidae): avoidance of intraguild predation". In: *Environmental Entomology* 29.3, pp. 454–459.

Lv, Songjuan and Min Zhao (2008). "The dynamic complexity of a three species food chain model". In: *Chaos, Solitons & Fractals* 37.5, pp. 1469–1480.

Lv, Yunfei, Rong Yuan, and Yongzhen Pei (2013). "Turing pattern formation in a three species model with generalist predator and cross-diffusion". In: *Nonlinear Analysis: Theory, Methods & Applications* 85, pp. 214–232.

Ma, Zhan-Ping, Wan-Tong Li, and Yu-Xia Wang (2017). "Spatiotemporal patterns induced by cross-diffusion in a three-species food chain model". In: *International Journal of Bifurcation and Chaos* 27.01, p. 1750011.

Ma, Zhan-Ping, Wan-Tong Li, and Xiang-Ping Yan (2012). "Stability and Hopf bifurcation for a three-species food chain model with time delay and spatial diffusion". In: *Applied Mathematics and Computation* 219.5, pp. 2713–2731.

Ma, Zhaohai, Xin Wu, and Rong Yuan (2017). "Nonlinear stability of traveling wavefronts for competitive-cooperative Lotka–Volterra systems of three species". In: *Applied Mathematics and Computation* 315, pp. 331–346.

Majda, Andrew J, Andrea L Bertozzi, and A Ogawa (2002). "Vorticity and incompressible flow. Cambridge texts in applied mathematics". In: *Appl. Mech. Rev.* 55.4, B77–B78.

Makler-Pick, Vardit et al. (2017). "Intraguild predation dynamics in a lake ecosystem based on a coupled hydrodynamic-ecological model: The example of Lake Kinneret (Israel)". In: *Biology* 6.2, p. 22.

Martínez, Salomé (2003). "The effect of diffusion for the multispecies Lotka-Volterra competition model". In: *Nonlinear analysis: real world applications* 4.3, pp. 409–436.

May, Robert M and Warren J Leonard (1975). "Nonlinear aspects of competition between three species". In: *SIAM journal on applied mathematics* 29.2, pp. 243–253.

Mccann, Kevin and Peter Yodzis (1995). "Bifurcation structure of a three-species food-chain model". In: *Theoretical population biology* 48.2, pp. 93–125.

Mishra, Purnedu and Dariusz Wrzosek (2022). "Indirect taxis drives spatio-temporal patterns in an extended Schoener's intraguild predator–prey model". In: *Applied Mathematics Letters* 125, p. 107745.

Mortuja, Md Golam, Mithilesh Kumar Chaube, and Santosh Kumar (2021). "Dynamic analysis of a predator-prey system with nonlinear prey harvesting and square root functional response". In: *Chaos, Solitons & Fractals* 148, p. 111071.

Moser, Susan E and John J Obrycki (2009). "Competition and intraguild predation among three species of coccinellids (Coleoptera: Coccinellidae)". In: *Annals of the Entomological Society of America* 102.3, pp. 419–425.

Mukherjee, Nayana, S Ghorai, and Malay Banerjee (2019). "Detection of turing patterns in a three species food chain model via amplitude equation". In: *Communications in Nonlinear Science and Numerical Simulation* 69, pp. 219–236.

Murray, James D (2001). *Mathematical biology II: spatial models and biomedical applications*. Vol. 3. Springer New York.

Naji, Raid Kamel and Alla Tariq Balasim (2007). "Dynamical behavior of a three species food chain model with Beddington–DeAngelis functional response". In: *Chaos, solitons & fractals* 32.5, pp. 1853–1866.

Namba, Toshiyuki, Kumi Tanabe, and Naomi Maeda (2008). "Omnivory and stability of food webs". In: *Ecological Complexity* 5.2, pp. 73–85.

Novick, Aaron and Leo Szilard (1950). "Description of the chemostat". In: *Science* 112.2920, pp. 715–716.

Ohba, Shin-ya, Yasuhide Terazono, and Sho Takada (2022). "Interspecific competition amongst three species of large-bodied diving beetles: is the species with expanded distribution an active swimmer and a better forager?" In: *Hydrobiologia* 849.5, pp. 1149–1160.

Okubo, Akira and Simon A Levin (2001). *Diffusion and ecological problems: modern perspectives*. Vol. 14. Springer.

Paine, Robert T and Simon A Levin (1981). "Intertidal landscapes: disturbance and the dynamics of pattern". In: *Ecological monographs* 51.2, pp. 145–178.

Pang, Peter YH and Mingxin Wang (2004). "Strategy and stationary pattern in a three-species predator–prey model". In: *Journal of Differential Equations* 200.2, pp. 245–273.

Pang, PYH and MX Wang (2008). "Existence of global solutions for a three-species predator-prey model with cross-diffusion". In: *Mathematische Nachrichten* 281.4, pp. 555–560.

Panja, Prabir (2019). "Dynamics of a fractional order predator-prey model with intraguild predation". In: *International Journal of Modelling and Simulation* 39.4, pp. 256–268.

Parshad, Rana D et al. (2017). "On the explosive instability in a three-species food chain model with modified Holling type IV functional response". In: *Mathematical Methods in the Applied Sciences* 40.16, pp. 5707–5726.

Pekalski, Andrzej and Dietrich Stauffer (1998). "Three Species Lotka–Volterra Model". In: *International Journal of Modern Physics C* 9.05, pp. 777–783.

Polis, Gary A and Robert D Holt (1992). "Intraguild predation: the dynamics of complex trophic interactions". In: *Trends in ecology & evolution* 7.5, pp. 151–154.

Polis, Gary A, Christopher A Myers, and Robert D Holt (1989). "The ecology and evolution of intraguild predation: potential competitors that eat each other". In: *Annual review of ecology and systematics* 20.1, pp. 297–330.

Polis, Gary A and Donald R Strong (1996). "Food web complexity and community dynamics". In: *The American Naturalist* 147.5, pp. 813–846.

Raw, Sharada Nandan and Barsa Priyadarsini Sarangi (2022). "Dynamics of a diffusive food chain model with fear effects". In: *The European Physical Journal Plus* 137.1, pp. 1–36.

Raychaudhuri, S, DK Sinha, and J Chattopadhyay (1996). "Effect of time-varying cross-diffusivity in a two-species Lotka-Volterra competitive system". In: *Ecological modelling* 92.1, pp. 55–64.

Recalde, Fátima C, Crasso PB Breviglieri, and Gustavo Q Romero (2020). "Allochthonous aquatic subsidies alleviate predation pressure in terrestrial ecosystems". In: *Ecology* 101.8, e03074.

Reddy, Junuthula Narasimha (2014). *An Introduction to Nonlinear Finite Element Analysis Second Edition: with applications to heat transfer, fluid mechanics, and solid mechanics*. OUP Oxford.

Rescigno, Aldo and Irvin W Richardson (1965). "On the competitive exclusion principle". In: *The bulletin of mathematical biophysics* 27.1, pp. 85–89.

Rihan, Fathalla A and Hebatallah J Alsakaji (2022). "Stochastic delay differential equations of three-species prey-predator system with cooperation among prey species". In: *Discrete & Continuous Dynamical Systems-S* 15.2, p. 245.

Rosenzweig, Michael L and Robert H MacArthur (1963). "Graphical representation and stability conditions of predator-prey interactions". In: *The American Naturalist* 97.895, pp. 209–223.

Roy, Banani and Sankar Kumar Roy (2015). "Analysis of prey-predator three species models with vertebral and invertebral predators". In: *International Journal of Dynamics and Control* 3.3, pp. 306–312.

Roy, Sankar Kumar and Banani Roy (2016). "Analysis of prey-predator three species fishery model with harvesting including prey refuge and migration". In: *International Journal of Bifurcation and chaos* 26.02, p. 1650022.

Ruan, Shigui et al. (2007). "Coexistence in competition models with density-dependent mortality". In: *Comptes rendus biologies* 330.12, pp. 845–854.

Ryan, Daniel and Robert Stephen Cantrell (2015). "Avoidance behavior in intraguild predation communities: a cross-diffusion model". In: *Discrete & Continuous Dynamical Systems* 35.4, p. 1641.

Sabir, Zulqurnain (2022). "Stochastic numerical investigations for nonlinear three-species food chain system". In: *International Journal of Biomathematics* 15.04, p. 2250005.

Saeedian, Meghdad et al. (2021). "Effect of delay on the emergent stability patterns in Generalized Lotka-Volterra ecological dynamics". In: *arXiv preprint arXiv:2110.11914*.

Sáez, Eduardo, Eduardo Stange, and Iván Szántó (2006). "Simultaneous zip bifurcation and limit cycles in three dimensional competition models". In: *SIAM Journal on Applied Dynamical Systems* 5.1, pp. 1–11.

Samardzija, Nikola and Larry D Greller (1988). "Explosive route to chaos through a fractal torus in a generalized Lotka-Volterra model". In: *Bulletin of Mathematical Biology* 50.5, pp. 465–491.

Santra, PK (2021). "Fear effect in discrete prey-predator model incorporating square root functional response". In: *Jambura Journal of Biomathematics* 2.2, pp. 51–57.

Savitri, Dian and Hasan S Panigoro (2020). "Bifurkasi Hopf pada model prey-predator-super predator dengan fungsi respon yang berbeda". In: *Jambura Journal of Biomathematics (JJBM)* 1.2, pp. 65–70.

Segel, Lee A (1984). *Modeling dynamic phenomena in molecular and cellular biology*. Cambridge University Press.

Segel, Lee A and Julius L Jackson (1972). "Dissipative structure: an explanation and an ecological example". In: *Journal of theoretical biology* 37.3, pp. 545–559.

Segel, Lee A and Simon A Levin (1976). "Application of nonlinear stability theory to the study of the effects of diffusion on predator-prey interactions". In: *AIP conference proceedings*. Vol. 27. 1. American Institute of Physics, pp. 123–152.

Shen, Jianhe, Cheng-Hsiung Hsu, and Ting-Hui Yang (2020). "Fast–slow dynamics for intraguild predation models with evolutionary effects". In: *Journal of Dynamics and Differential Equations* 32.2, pp. 895–920.

Shigesada, Nanako, Kohkichi Kawasaki, and Ei Teramoto (1979). "Spatial segregation of interacting species". In: *Journal of theoretical biology* 79.1, pp. 83–99.

Shu, Hongying et al. (2015). "Delay induced stability switch, multitype bistability and chaos in an intraguild predation model". In: *Journal of mathematical biology* 71.6, pp. 1269–1298.

Smith, Hal L (1982). "The interaction of steady state and Hopf bifurcations in a two-predator–one-prey competition model". In: *SIAM Journal on Applied Mathematics* 42.1, pp. 27–43.

Smoller, Joel (2012). *Shock waves and reaction—diffusion equations*. Vol. 258. Springer Science & Business Media.

Spagnolo, B, A Fiasconaro, and D Valenti (2003). "Noise induced phenomena in Lotka-Volterra systems". In: *Fluctuation and Noise Letters* 3.02, pp. L177–L185.

Sunaryo, Mada Sanjaya Waryano, Zabidin Salleh, and Mustafa Mamat (2013). "Mathematical model of three species food chain with Holling type-III functional response". In: *Int J Pure Appl Math* 89.5, pp. 647–657.

Switalski, T Adam (2003). "Coyote foraging ecology and vigilance in response to gray wolf reintroduction in Yellowstone National Park". In: *Canadian Journal of Zoology* 81.6, pp. 985–993.

Tanabe, Kumi and Toshiyuki Namba (2005). "Omnivory creates chaos in simple food web models". In: *Ecology* 86.12, pp. 3411–3414.

Tian, Canrong, Zhi Ling, and Zhigui Lin (2011). "Turing pattern formation in a predator–prey–mutualist system". In: *Nonlinear Analysis: Real World Applications* 12.6, pp. 3224–3237.

— (2014). "Spatial patterns created by cross-diffusion for a three-species food chain model". In: *International Journal of Biomathematics* 7.02, p. 1450013.

Tuckett, Quenton M et al. (2021). "Unstable intraguild predation causes establishment failure of a globally invasive species". In: *Ecology* 102.8, e03411.

Turing, A. M. (1952). "The chemical basis of morphogensis". In: *Phil. Trans. Roy. Soc.* B.237, pp. 37–72.

Upadhyay, Ranjit Kumar and Raid Kamel Naji (2009). "Dynamics of a three species food chain model with Crowley–Martin type functional response". In: *Chaos, solitons & fractals* 42.3, pp. 1337–1346.

Upadhyay, Ranjit Kumar and Sharada Nandan Raw (2011). "Complex dynamics of a three species food-chain model with Holling type IV functional response". In: *Nonlinear Analysis: Modelling and Control* 16.3, pp. 553–374.

Vance, Richard R (1984). "Interference competition and the coexistence of two competitors on a single limiting resource". In: *Ecology* 65.5, pp. 1349–1357.

— (1985). "The stable coexistence of two competitors for one resource". In: *The American Naturalist* 126.1, pp. 72–86.

Wang, Chang-you et al. (2010). "Global asymptotic stability of positive equilibrium of three-species Lotka–Volterra mutualism models with diffusion and delay effects". In: *Applied Mathematical Modelling* 34.12, pp. 4278–4288.

Wang, Maoxiang et al. (2021). "Keep, break and breakout in food chains with two and three species". In: *Mathematical Biosciences and Engineering* 18.1, pp. 817–836.

Wang, Mingxin (2004). "Stationary patterns for a prey–predator model with prey-dependent and ratio-dependent functional responses and diffusion". In: *Physica D: Nonlinear Phenomena* 196.1-2, pp. 172–192.

Wang, Mingxin (2006). "Stationary patterns caused by cross-diffusion for a three-species prey-predator model". In: *Computers & Mathematics with Applications* 52.5, pp. 707–720.

Wang, Shaopeng, Ulrich Brose, and Dominique Gravel (2019). "Intraguild predation enhances biodiversity and functioning in complex food webs". In: *Ecology* 100.3, e02616.

Wangersky, Peter J (1978). "Lotka-Volterra population models". In: *Annual Review of Ecology and Systematics* 9, pp. 189–218.

Wei, Hsiu-Chuan (2019). "A mathematical model of intraguild predation with prey switching". In: *Mathematics and Computers in Simulation* 165, pp. 107–118.

Whittaker, RH and SA1 Levin (1977). "The role of mosaic phenomena in natural communities". In: *Theoretical population biology* 12.2, pp. 117–139.

Wilken, DR (1982). "Some remarks on a competing predators problem". In: *SIAM Journal on Applied Mathematics* 42.4, pp. 895–902.

Xie, Zhifu (2012). "Cross-diffusion induced Turing instability for a three species food chain model". In: *Journal of Mathematical Analysis and Applications* 388.1, pp. 539–547.

Yan, Xiang-Ping (2007). "Stability and Hopf bifurcation for a delayed prey–predator system with diffusion effects". In: *Applied Mathematics and Computation* 192.2, pp. 552–566.

Yang, Fang and Shengmao Fu (2008). "Global solutions for a tritrophic food chain model with diffusion". In: *The Rocky Mountain Journal of Mathematics*, pp. 1785–1812.

Zhang, Dawei and Binxiang Dai (2019). "A free boundary problem for the diffusive intraguild predation model with intraspecific competition". In: *Journal of Mathematical Analysis and Applications* 474.1, pp. 381–412.

Zhao, Min and Songjuan Lv (2009). "Chaos in a three-species food chain model with a Beddington–DeAngelis functional response". In: *Chaos, Solitons & Fractals* 40.5, pp. 2305–2316.

Zou, Xiaoling et al. (2022). "Dynamic properties for a stochastic food chain model". In: *Chaos, Solitons & Fractals* 155, p. 111713.